

VOLUME 77 OCTOBER 25, 1973 NUMBER 22

JPCHAX

THE JOURNAL OF
**PHYSICAL
CHEMISTRY**

PUBLISHED BIWEEKLY BY THE AMERICAN CHEMICAL SOCIETY

THE JOURNAL OF PHYSICAL CHEMISTRY

BRYCE CRAWFORD, Jr., *Editor*

STEPHEN PRAGER, *Associate Editor*

ROBERT W. CARR, Jr., FREDERIC A. VAN-CATLEDGE, *Assistant Editors*

EDITORIAL BOARD: A. O. ALLEN (1970-1974), C. A. ANGELL (1973-1977), J. R. BOLTON (1971-1975), M. FIXMAN (1970-1974), H. S. FRANK (1970-1974), R. R. HENTZ (1972-1976), J. R. HUIZENGA (1969-1973), W. J. KAUFMANN (1969-1973), R. L. KAY (1972-1976), W. R. KRIGBAUM (1969-1973), W. J. MOORE (1969-1973), R. M. NOYES (1973-1977), J. A. POPLE (1971-1975), B. S. RABINOVITCH (1971-1975), H. REISS (1970-1974), S. A. RICE (1969-1975), F. S. ROWLAND (1973-1977), R. L. SCOTT (1973-1977), W. A. ZISMAN (1972-1976)

AMERICAN CHEMICAL SOCIETY, 1155 Sixteenth St., N.W., Washington, D. C. 20036

Books and Journals Division

JOHN K CRUM *Director*

RUTH REYNARD *Assistant to the Director*

CHARLES R. BERTSCH *Head, Editorial Processing Department*

D. H. MICHAEL BOWEN *Head, Journals Department*

BACIL GUILLEY *Head, Graphics and Production Department*

SELDON W. TERRANT *Head, Research and Development Department*

©Copyright, 1973, by the American Chemical Society. Published biweekly by the American Chemical Society at 20th and Northampton Sts., Easton, Pa. 18042. Second-class postage paid at Washington, D. C., and at additional mailing offices.

All manuscripts should be sent to *The Journal of Physical Chemistry*, Department of Chemistry, University of Minnesota, Minneapolis, Minn. 55455.

Additions and Corrections are published once yearly in the final issue. See Volume 76, Number 26 for the proper form.

Extensive or unusual alterations in an article after it has been set in type are made at the author's expense, and it is understood that by requesting such alterations the author agrees to defray the cost thereof.

The American Chemical Society and the Editor of *The Journal of Physical Chemistry* assume no responsibility for the statements and opinions advanced by contributors.

Correspondence regarding accepted copy, proofs, and reprints should be directed to Editorial Processing Department, American Chemical Society, 20th and Northampton Sts., Easton, Pa. 18042. Head: CHARLES R. BERTSCH. Assistant Editor: EDWARD A. BORGER. Editorial Assistant: JOSEPH E. YURVATI.

Advertising Office: Centcom, Ltd., 142 East Avenue, Norwalk, Conn. 06851.

Business and Subscription Information

Send all new and renewal subscriptions *with payment to:* Office of the Controller, 1155 16th Street, N.W., Washington, D. C. 20036. Subscriptions should be renewed promptly to avoid a break in your series. All correspondence and telephone calls regarding changes of

address, claims for missing issues, subscription service, the status of records, and accounts should be directed to Manager, Membership and Subscription Services, American Chemical Society, P.O. Box 3337, Columbus, Ohio 43210. Telephone (614) 421-7230.

On changes of address, include both old and new addresses with ZIP code numbers, accompanied by mailing label from a recent issue. Allow four weeks for change to become effective.

Claims for missing numbers will not be allowed (1) if loss was due to failure of notice of change in address to be received before the date specified, (2) if received more than sixty days from date of issue plus time normally required for postal delivery of journal and claim, or (3) if the reason for the claim is "issue missing from files."

Subscription rates (1973): members of the American Chemical Society, \$20.00 for 1 year; to nonmembers, \$60.00 for 1 year. Those interested in becoming members should write to the Admissions Department, American Chemical Society, 1155 Sixteenth St., N.W., Washington, D. C. 20036. Postage to Canada and countries in the Pan-American Union, \$5.00; all other countries, \$6.00. Single copies for current year: \$3.00. Rates for back issues from Volume 56 to date are available from the Special Issues Sales Department, 1155 Sixteenth St., N.W., Washington, D. C. 20036.

Subscriptions to this and the other ACS periodical publications are available on microfilm. Supplementary material not printed in this journal is now available in microfiche form on a current subscription basis. For information on microfilm or microfiche subscriptions, write Special Issues Sales Department at the address above.

THE JOURNAL OF
PHYSICAL CHEMISTRY

Volume 77, Number 22 October 25, 1973

JPCA_x 77(22) 2587-2712 (1973)

ISSN 0022-3654

- Ion-Molecule Reactions in Monosilane-Methane Mixtures
..... **T. M. H. Cheng, Tung-Yang Yu, and F. W. Lampe*** 2587
- A Study of the Formation of Negative Ions in Nitric Oxide and the Interaction of NO with H⁻ and O⁻ from Water
..... **Satish K. Gupta and Charles E. Melton*** 2594
- On Abstraction or Stripping of CH₂ as a Route to Acetylene Formation in Hot Carbon Atom Reactions
..... **Timothy Rose* and Colin MacKay** 2598
- Heterogeneous Loss Reaction of Carbon Monosulfide
..... **R. J. Richardson,* H. T. Powell, and J. D. Kelley** 2601
- Kinetics and Mechanism for the Photolysis of Nitrogen Dioxide in Air
..... **D. H. Stedman* and H. Niki** 2604
- Photochemistry of Phenylcyclobutane. II
..... **Shih Yeng Ho, Robert A. Gorse, and W. Albert Noyes, Jr.** 2609
- Quenching of the Tris(ethylenediamine)chromium(III) Phosphorescence by Some Transition Metal Ions in Aqueous Solutions
..... **H. F. Wasgestian, R. Ballardini, G. Varani, L. Moggi,* and V. Balzani** 2614
- Kinetics of Electron Transfer from Aromatic Radical Anions to Alkyl Halides in Tetrahydrofuran. Effects of Sodium Cation Pairing
..... **Bradley Bockrath and Leon M. Dorfman*** 2618
- An Electron Paramagnetic Resonance Study of Hydrogen Atoms Trapped in γ -Irradiated Lithium Phosphates
..... **Y. P. Virmani, John D. Zimbrick,* and E. J. Zeller** 2622
- An Investigation of the Dynamic Equilibrium between Chemisorbed and Adsorbed Hydrogen in the Palladium/Hydrogen System
..... **J. F. Lynch and Ted B. Flanagan*** 2628
- The Nature of Molecular Hydrogen Adsorbed on Zinc Oxide
..... **C. C. Chang, L. T. Dixon, and R. J. Kokes*** 2634
- The Nature of Molecular Nitrogen Adsorbed over Zinc Oxide
..... **C. C. Chang and R. J. Kokes*** 2640
- Electron Spin Resonance Spectra of Sulfanyl Radicals in Solution
..... **J. R. Morton and K. F. Preston*** 2645
- Equilibrium Studies by Electron Spin Resonance. V. The Role of the Cation in Hydrogen Bonding to the Nitrobenzene Anion Radical
..... **Luis Echegoyen, Hector Hidalgo, and Gerald R. Stevenson*** 2649
- New Aromatic Anions. IX. Anion Radicals of the Monocyclic Oxocarbons
..... **Elizabeth V. Patton and Robert West*** 2652
- Raman Spectra of Thorium(IV) Fluoride Complex Ions in Fluoride Melts
..... **L. M. Toth* and G. E. Boyd** 2654
- Vibrational Transitions in Anharmonic Oscillators
..... **Hyung Kyu Shin** 2657
- Reactions of Hydroxyl Radicals with Unsaturated Aliphatic Alcohols in Aqueous Solution. A Spectroscopic and Electron Spin Resonance Radiolysis Study
..... **M. Simic, P. Neta, and E. Hayon*** 2662

ห้องสมุด คณะวิทยาศาสตร์
3 ต.ค. 2517

Combining Rules for Intermolecular Potential Parameters. III. Application to the Exp 6 Potential	Chang Lyoul Kong* and Manoj R. Chakrabarty	2668
The Effective Molecular Quadrupole Moment of Water	P. T. Eubank	2670
Application of the Quasilattice Model to Association in Dilute Reciprocal Molten Salt Mixtures. The System Silver Sulfate-Potassium Nitrate	C. E. Vallet* and J. Braunstein	2672 ■
Photoconductive Properties of Arylethynylcopper Polymers. Effects of Structure and Oxygen	Yoshiyuki Okamoto* and Samar K. Kundu	2677
Acidity Scales in Mixed Water-Acetonitrile Buffer Solutions	Frank Jordan	2681
Self-Diffusion Coefficients of Sodium Ion in Aqueous Sodium Polyacrylate Solutions Containing Sodium Chloride	Daniel S. Dixler and Paul Ander*	2684 ■
Pressure Dependence of Weak Acid Ionization in Aqueous Buffers	Robert C. Neuman, Jr.,* Walter Kauzmann, and Adam Zipp	2687 ■
Prehydration Scavenging of e_{aq}^- and the Yields of Primary Reducing Products in Water γ -Radiolysis	Z. D. Draganić and I. G. Draganić*	2691
Thermodynamic Group Contributions from Ion Pair Extraction Equilibria for Use in the Prediction of Partition Coefficients. Correlation of Surface Area with Group Contributions	Sister Marie Joan Harris, Takeru Higuchi,* and J. Howard Rytting	2694 ■
Surface Tension of Saturated Anhydrous Hydrogen Sulfide and the Effect of Hydrogen Sulfide Pressure on the Surface Tension of Water	Carlyle S. Herrick* and George L. Gaines, Jr.	2703
Thermochemistry of the Bromination of Carbon Tetrachloride and the Heat of Formation of Carbon Tetrachloride	G. D. Mendenhall, D. M. Golden, and S. W. Benson*	2707

COMMUNICATIONS TO THE EDITOR

Definition of Volume Flow in the Kedem-Katchalsky Formulation of Electroosmosis	John N. Weinstein and S. Roy Caplan*	2710
Comments on the Paper by Weinstein and Caplan on the Definition of Volume Flow in the Kedem-Katchalsky Formulation of Electroosmosis	O. Kedem	2711
Electron Spin Resonance Study of Photoinduced Triplet States from Organic Dye Solutions	F. R. Antonucci* and L. G. Tolley	2712

■ Supplementary material for this paper is available separately, in photocopy or microfiche form. Ordering information is given in the paper.

*In papers with more than one author, the asterisk indicates the name of the author to whom inquiries about the paper should be addressed.

AUTHOR INDEX

Ander, P., 2684	Eubank, P. T., 2670	Kundu, S. K., 2677	Rytting, J. H., 2694
Antonucci, F. R., 2712	Flanagan, T. B., 2628	Lampe, F. W., 2587	Shin, H. K., 2657
Ballardini, R., 2614	Gaines, G. L., Jr., 2703	Lynch, J. F., 2628	Simic, M., 2662
Balzani, V., 2614	Golden, D. M., 2707	MacKay, C., 2598	Stedman, D. H., 2604
Benson, S. W., 2707	Gorse, R. A., 2609	Melton, C. E., 2594	Stevenson, G. R., 2649
Bockrath, B., 2618	Gupta, S. K., 2594	Mendenhall, G. D., 2707	Tolley, L. G., 2712
Boyd, G. E., 2654	Harris, M. J., 2694	Moggi, L., 2614	Toth, L. M., 2654
Braunstein, J., 2672	Hayon, E., 2662	Morton, J. R., 2645	Vallet, C. E., 2672
Caplan, S. R., 2710	Herrick, C. S., 2703	Neta, P., 2662	Varani, G., 2614
Chakrabarty, M. R., 2668	Hidalgo, H., 2649	Neuman, R. C., Jr., 2687	Virmani, Y. P., 2622
Chang, C. C., 2634, 2640	Higuchi, T., 2694	Niki, H., 2604	Wasgestian, H. F., 2614
Cheng, T. M. H., 2587	Ho, S. Y., 2609	Noyes, W. A., Jr., 2609	Weinstein, J. N., 2710
Dixler, D. S., 2684	Jordan, F., 2681	Okamoto, Y., 2677	West, R., 2652
Dixon, L. T., 2634	Kauzmann, W., 2687	Patton, E. V., 2652	Yu, T.-Y., 2587
Dorfman, L. M., 2618	Kedem, O., 2711	Powell, H. T., 2601	Zeller, E. J., 2622
Draganić, I. G., 2691	Kelley, J. D., 2601	Preston, K. F., 2645	Zimbrick, J. D., 2622
Draganić, Z. D., 2691	Kokes, R. J., 2634, 2640	Richardson, R. J., 2601	Zipp, A., 2687
Echegoyen, L., 2649	Kong, C. L., 2668	Rose, T., 2598	

THE JOURNAL OF PHYSICAL CHEMISTRY

Registered in U. S. Patent Office © Copyright, 1973, by the American Chemical Society

VOLUME 77, NUMBER 22 OCTOBER 25, 1973

Ion-Molecule Reactions in Monosilane-Methane Mixtures¹

T. M. H. Cheng, Tung-Yang Yu, and F. W. Lampe*

Davey Laboratory, Department of Chemistry, The Pennsylvania State University, University Park, Pennsylvania 16802 (Received March 13, 1973)

Publication costs assisted by the U.S. Atomic Energy Commission

High-pressure mass spectrometry and tandem mass spectrometry have been used to study the collision reactions of primary ions of methane with monosilane and of primary ions of monosilane with methane. All primary ions of each constituent undergo at least one ion-molecule reaction with the opposite molecule, but by far the most predominant such "cross" reaction is hydride transfer from monosilane to the primary ions of methane, producing the SiH_3^+ ion. Reaction cross sections and rate constants for the various processes are presented.

Introduction

In a previous study² of ion-molecule reactions in monosilane-methane mixtures we reported the occurrence of a large number of reactions of SiH_2^+ with CH_4 and of CH_3^+ and CH_4^+ with SiH_4 in which product ions containing the Si-C bond were formed. This study was limited to ion-source pressures below 5μ and reaction identification was made principally on the basis of the appearance potentials of the product ions. A subsequent study³ of the electron-impact ionization and dissociation of methylsilane showed that several of the ion-molecule reactions proposed² were quite endothermic and, therefore, very improbable under the experimental conditions obtaining. Accordingly, we initiated a further investigation of the monosilane-methane system employing considerably higher ion-source pressures and tandem mass spectrometry. During the course of this investigation, an ion cyclotron resonance study by Stewart, Henis, and Gaspar⁴ confirmed the incorrectness of some of the reaction identifications made in the previous report.² The results of our present investigation confirm a number of those of Stewart, Henis, and Gaspar.⁴ In addition, we have observed a large number of reactions in the monosilane-methane system not reported by them.

Experimental Section

The tandem mass spectrometer, which consists of two quadrupole mass filters separated by a collision chamber and ion lenses, has been described previously.⁵ All experiments described in this work were carried out with the mass filters mounted in the in-line configuration. Relative

reaction cross sections were measured for reactant ion energies in the range of 1-6 eV in the laboratory systems. Retarding field measurements indicate an ion-energy spread of about 1 eV. In all experiments the gas pressure in the collision chamber (nominally 10^{-3} Torr) was measured with a capacitance manometer.

Measurements of the dependence of ionic abundances on ion-source pressure up to about 0.23 Torr were carried out in a Nuclide Associates 12-90G sector-field mass spectrometer, an instrument which has been described previously.^{2,5-8} The energy of the ionizing electron beam was 100 eV, the trap current was very small and not measured, and the ion-accelerating voltage was 2500 V. In all experiments the repeller field was 6.25 V/cm leading to an ion-exit energy of 2.1 eV. The temperature of the ion source was 70° in all experiments.

Ion-source pressures in the Nuclide mass spectrometer were measured by a McCleod gauge that was connected via $\frac{5}{16}$ -in. diameter tubing to the ion source. The pressure-dependent formation of CH_5^+ , which occurs in $\text{CH}_4^+-\text{CH}_4$ collisions with a known specific reaction rate,⁹⁻¹² indicated the pressure readings to be accurate to within $\pm 10\%$.

Monosilane was purchased from the J. T. Baker Chemical Co. and was also prepared in the laboratory by the action of lithium aluminum hydride on silicon tetrachloride in di-*n*-butyl ether solution. Research Grade methane, stated to have a purity of 99.54%, was obtained from the Phillips Petroleum Co. All gases were fractionated on a vacuum line and checked mass spectrometrically for satisfactory purity before use.

Results and Discussion

Examination of the pressure dependence of ion intensities in monosilane-methane mixtures up to ion-source pressure of 0.23 Torr indicates that the system is extremely complex with regard to ion-molecule reaction. In addition to the reactions that are known to occur in the one-component systems of methane¹³⁻¹⁶ and monosilane,^{5,17,18} it is evident that numerous reactions between primary ions of methane with monosilane and between primary ions of monosilane with methane (called here "cross reactions") also take place. Comparison of the primary ion-intensity dependence on pressure for a methane-rich mixture with that for a monosilane-rich mixture indicates that all primary ions of methane react with monosilane and that SiH_2^+ , at least, reacts with methane. This complexity precludes, from pressure-variation studies alone, a complete elucidation of the reactions occurring and would appear to account for the failure of the earlier low-pressure investigation² ($P_{\text{source}} \leq 0.005$ Torr) to identify correctly all the processes involved. Since an understanding of this complex pressure dependence requires a knowledge of the elementary processes taking place, we discuss first our tandem mass-spectrometric results which permit unambiguous identification of the bimolecular cross reactions taking place in this gaseous mixture.

1. *Tandem Mass Spectrometric Studies.* With the tandem mass spectrometer in the in-line configuration,⁵ we have examined the reactions of all the primary ions of methane with monosilane and of all the primary ions of monosilane with methane. In addition, the reaction of CH_5^+ with monosilane has been investigated. Relative reaction cross sections, computed from the ratios of secondary-ion intensity to the product of primary-ion intensity and target gas pressure, were determined for reactant-ion energies in the range of 1-6 eV in the laboratory system.

Relative cross sections at 1-eV (lab) reactant-ion energy for all the cross sections are shown in Table I. Correction of the cross section for the reaction $m/e\ 17 \rightarrow m/e\ 31$ for the isotopic contribution from $^{13}\text{CH}_4^+$ has been made. The other cross sections in Table I have not been corrected for isotopic contributions. With the exceptions of processes $m/e\ 13 \rightarrow m/e\ 43$, $m/e\ 14 \rightarrow 30$, and $m/e\ 31 \rightarrow 45$, these isotopic corrections to the cross sections in Table I are all less than 5% and were not deemed necessary. For the three reactions noted, however, corrections due to isotopic contributions were made in the subsequent computation of reaction rate constants.

The data in Table I identify clearly the reactant ion, the reactant molecule, and the product ion. For a complete reaction identification one needs also to know the neutral product(s). Thermochemical considerations are of considerable value in choosing among the various stoichiometrically possible sets of neutral products of a reaction, particularly if one knows if the reaction producing the given ion is exothermic or endothermic. When plotted as a function of reactant-ion energy the cross sections of endothermic reactions generally rise from zero at the energy threshold to a broad maximum several eV above the threshold.¹⁹⁻²³ On the other hand, the cross sections of exothermic ion-molecule reactions generally decrease for all values of the reactant ion energy.^{19,24-28} Exceptions to this general behavior are exothermic reactions in which symmetry and spin properties of the molecular orbitals involved prevent the reaction from occurring on the lowest potential energy surfaces.^{29,30} In such cases, as exemplified by the formation of NO^+ from O^+-N_2 collisions,²⁹⁻³¹

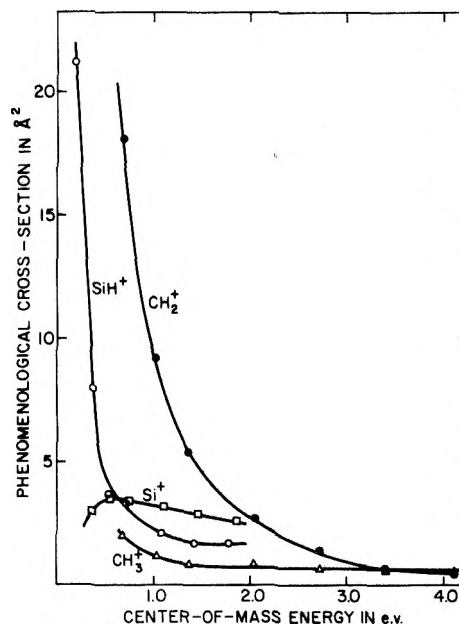


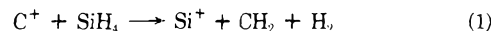
Figure 1. Reaction cross sections for SiCH_3^+ formation as a function of relative kinetic energy: reactant ions O, SiH^+ ; ●, CH_2^+ ; □, Si^+ ; △, CH_3^+ .

exothermic reaction cross sections may show the threshold and broad maximum in their dependence on reactant-ion energy that is characteristic of endothermic processes. However, endothermic reactions will not exhibit typical exothermic behavior. Therefore, while remaining alert to exceptions of the sort discussed, we have used the general shape of the dependence of reaction cross section on relative kinetic energy of reactants as an indication of the sign of the reaction enthalpy change. Typical such curves for the formation of SiCH_3^+ are shown in Figure 1.

In the remainder of this section we discuss the characteristics of the individual reactions whose relative cross sections for 1-eV (lab) ion energy are shown in Table I.

(a) $\text{C}^+ + \text{SiH}_4$. As shown in Table I, injection of 1-eV (lab) C^+ ions, produced by the impact of 100-eV electrons on methane, into monosilane produces ions at $m/e\ 28-31$, 41, and 42, which in this system can be only Si^+ , SiH^+ , SiH_2^+ , SiH_3^+ , SiCH^+ , and SiCH_2^+ , respectively. The dependence of the cross sections on relative kinetic energy indicates that all processes are exothermic, with the possible exception of SiH^+ formation.

Energetic considerations^{3,32} show that the only exothermic processes forming Si^+ involve complex formation or ionic dissociation subsequent to H_2^- transfer from SiH_4 to C^+ . Since, as will be seen, H_2^- transfer is a very dominant process, in the reactions of methane primary ions with monosilane, we conclude that (1) is the process producing Si^+ , viz.



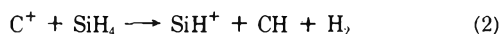
In the case of formation of SiH^+ , the thermochemical data^{3,32} available indicate that only a complex formation followed by dissociation to SiH^+ and CH_3 is exothermic. However, this reaction is so highly exothermic that one must expect that SiH^+ so formed would be prone to dissociate rapidly. Formation of SiH^+ by dissociative H^- transfer and dissociative H_2^- transfer is indicated to be endothermic by 11 and 15 kcal/mol, respectively. Although the dependence of cross section on kinetic energy that was observed suggests that SiH^+ formation may be endothermic, this is based on only one point and is in it-

TABLE I: Relative Cross Sections^{a,c} for Secondary Ion Formation

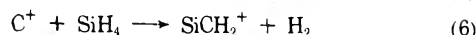
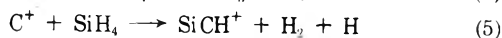
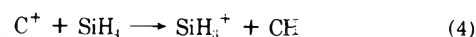
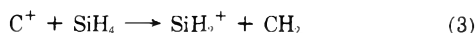
Reactant ion <i>m/e</i>	Major reactant ion	Reactant molecule	Relative cross section for formation of secondary ion at given <i>m/e</i>									
			28	29	30	31	41	42	43	44	45	
12	¹² C ⁺ (100%)	SiH ₄	5.2	7.8	13.0	54.6	2.7 ^b	7.1 ^b				
13	¹² CH ⁺ (>99%)	SiH ₄	5.0	9.8	9.1	42.5		18.6	13.4			
14	¹² CH ₂ ⁺ (>99%)	SiH ₄	2.3	7.3	2.3	47.2		2.5	15.1			
15	¹² CH ₃ ⁺ (>99%)	SiH ₄				52.5			1.7			1.6
16	¹² CH ₄ ⁺ (99%)	SiH ₄			10.9	35.2					1.0	1.5
17	¹² CH ₅ ⁺ (74%)	SiH ₄				49.5						
28	²⁸ Si ⁺ (100%)	CH ₄							2.5			
29	²⁸ SiH ⁺ (96%)	CH ₄							6.7	10.4		
30	²⁸ SiH ₂ ⁺ (98%)	CH ₄								4.4	2.6	
31	²⁸ SiH ₃ ⁺ (94%)	CH ₄										0.5

^a Reactant ion energy of 1 eV (laboratory) unless otherwise indicated. ^b Reactant ion energy of 1.5 eV (laboratory). ^c To convert to units of Å² the data in table should be multiplied by 1.2.

self not very convincing. Actually, the combined uncertainties in the enthalpies of formation^{3,32} of SiH⁺, CH₂, CH, and SiH₄, coupled with the possibility of excited states of C⁺ being present in the reactant beam, are sufficient for an exothermic reaction to be occurring by dissociative H⁻ or even H₂⁻ transfer. Accordingly, we rather arbitrarily choose between the two and ascribe SiH⁺ formation to the dissociative H⁻ transfer shown in (2), *viz.*

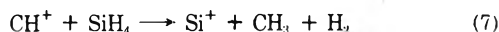


Thermochemical calculations show very convincingly that SiH₂⁺ and SiH₃⁺ can be formed in C⁺-SiH₄ collisions *only* by H₂⁻ transfer and H⁻ transfer, respectively. In the case of SiCH⁺ and SiCH₂⁺ ions, enthalpies of formation are not known and we ascribe their formation to reactions of lowest enthalpy change possible. Thus we write for the remainder of the reactions of C⁺ with SiH₄, (3)-(6), *viz.*



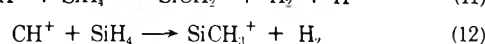
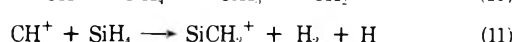
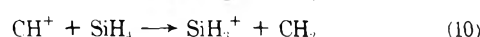
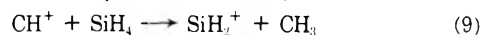
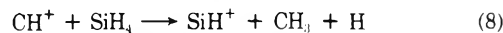
Neither of the earlier reports of ion-molecule reactions in monosilane-methane mixtures^{2,4} reported the occurrence of reactions of C⁺.

(b) CH⁺ + SiH₄. When CH⁺ ions react with monosilane, the product ions observed are Si⁺, SiH⁺, SiH₂⁺, SiH₃⁺, SiCH₂⁺, and SiCH₃⁺. All reactions producing these ions appear to be exothermic as indicated by the dependence of the cross sections on ion energy. Of the possible reactions producing Si⁺, only (1) complex formation, followed by dissociation to the neutral products CH₄ + H; and (2) dissociative H₂⁻ transfer, leading to the neutral products CH₃ + H₂, are feasible. We choose the latter and write (7), *viz.*



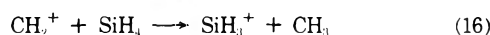
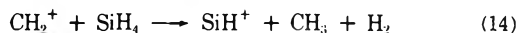
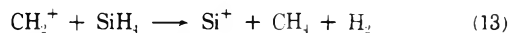
Thermochemical data^{3,32} indicate that SiH⁺ may be formed by either dissociative H⁻ transfer or dissociative H₂⁻ transfer, while SiH₂⁺ formation in an exothermic process is possible only by H₂⁻ transfer and SiH₃⁺ must be formed in an H⁻ transfer process. The neutral products formed along with SiCH₂⁺ have to be 3H or H₂ + H and, since the enthalpy of formation of SiCH₂⁺ is not known, we cannot choose except arbitrarily. Formation of SiCH₃⁺ is exothermic^{3,32} whether the neutral products are H₂ or

2H, and again we can here make only an arbitrary choice. In view of the above discussion the reactions assigned are given in (8)-(12).

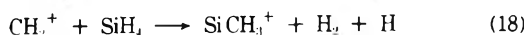


Of the above reactions observed to occur in collisions of CH⁺ with monosilane, only (11) has been reported⁴ previously. This ion cyclotron resonance study⁴ reported (11) to be exothermic which is in accord with the cross-section dependence on ion energy that we have observed.

(c) CH₂⁺ + SiH₄. Although different cross sections are observed (Table I), reaction of CH₂⁺ with SiH₄ produces the same product ions as when CH⁺ is the reactant ion, namely, Si⁺, SiH⁺, SiH₂⁺, SiH₃⁺, SiCH₂⁺, and SiCH₃⁺. All reactions are found to exhibit exothermic (or thermo-neutral) behavior with respect to cross-section dependence on kinetic energy. Thermochemical considerations^{3,32} then lead to the conclusion that Si⁺ must be formed by dissociative H₂⁻ transfer, SiH⁺ must be formed by either dissociative H₂⁻ or dissociative H⁻ transfer (or both), SiH₂⁺ must be formed by H₂⁻ transfer, and SiH₃⁺ must be formed by H⁻ transfer. Thus for formation of the product ions of *m/e* 28-31, we have the processes shown in (13)-(16), *viz.*



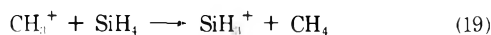
The only exothermic reaction yielding SiCH₃⁺ must produce H₂ + H as the neutral products. In the case of SiCH₂⁺, we cannot compute enthalpy changes but we write for the reaction the neutral products that give the smallest Δ*H* and are thus led to the reactions shown in (17) and (18). Only (18), of the reactions observed be-



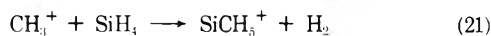
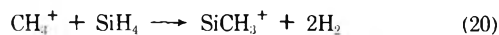
tween CH₂⁺ and SiH₄, has been reported previously.⁴

(d) CH₃⁺ + SiH₄. Table I shows that 1-eV CH₃⁺ ions react with monosilane to produce only three product ions,

namely, SiH_3^+ , SiCH_3^+ , and SiCH_5^+ . All reactions were found to exhibit exothermic dependence of cross section on kinetic energy. Energetic calculations show that SiH_3^+ must be formed in an H^- transfer, as shown by (19), *viz.*



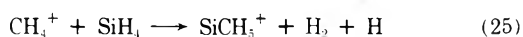
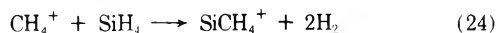
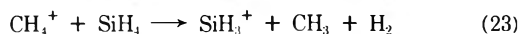
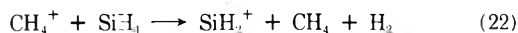
Reactions 20 and 21, which describe the observed forma-



tion of SiCH_3^+ and SiCH_5^+ have enthalpy changes of +4 and -48 kcal, respectively, when reported^{3,32} enthalpies of formation are used. The combined uncertainties in the enthalpies of formation^{3,32} of SiH_4 and SiCH_3^+ exceed 4 kcal/mol and so it is possible that (20) is actually exothermic for ground-state reactants. Another possibility is that (20) is actually endothermic as calculated but that the CH_3^+ ions contain sufficient internal energy (>4 kcal/mol) for the process being observed to be exothermic or thermoneutral. It is noteworthy that SiH_2^+ , SiH^+ , and Si^+ are not observed in CH_3^+ - SiH_4 collisions at these energies, a fact undoubtedly due to their formation being endothermic by +47, +22, and +84 kcal/mol, respectively.

Reaction 19 was reported by Stewart, Henis, and Gaspar.⁴ These latter authors also reported that (20) was observed as an endothermic reaction. Reaction 21 was not reported but the tandem mass spectrometric experiment shows clearly that this exothermic reaction occurs. Beggs and Lampe² reported the occurrence of (20).

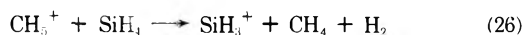
(e) $\text{CH}_4^+ + \text{SiH}_4$. When CH_4^+ ions collide with SiH_4 , the ionic products, as shown in Table I, are SiH_2^+ , SiH_3^+ , SiCH_4^+ , and SiCH_5^+ . All processes producing these ions, moreover, show exothermic dependence of cross section on kinetic energy. Thermochemical computations then show that the reactions responsible for formation of these product ions must be those shown by (22)-(25), *viz.*



Reaction 22 cannot be H^- transfer from SiH_4 followed by dissociation of SiH_3^+ to SiH_2^+ and H , because it would then be 85 kcal endothermic. It must be as written and is perhaps best pictured as H_2^- transfer to CH_4^+ with dissociation of the CH_6 neutral intermediate to CH_4 and H_2 . Reaction 23 is clearly an H^- transfer and although we have written the neutral products as $\text{CH}_3 + \text{H}_2$, we cannot distinguish them from $\text{CH}_4 + \text{H}$.

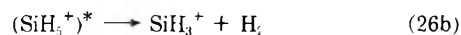
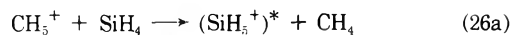
Reactions 23-25 were also reported by Stewart, Henis, and Gaspar⁴ in their ion cyclotron resonance study and (24) and (25) were reported by Beggs and Lampe² in their low-pressure mass spectrometric study.

(f) $\text{CH}_5^+ + \text{SiH}_4$. In agreement with observations from ion cyclotron resonance investigations,⁴ Table I shows that only one product ion is produced in collisions of CH_5^+ with SiH_4 , namely, SiH_3^+ . The process shows exothermic dependence of cross section on kinetic energy and therefore must be written as shown in (26), *viz.*



Proton transfer from CH_5^+ to SiH_4 with formation of SiH_5^+ is an energetically feasible process, since the pro-

ton affinity of monosilane is about 30 kcal/mol greater than that of methane,³³ which suggests that the mechanism involved in (26) might be as shown in (26a) and (26b), *viz.*



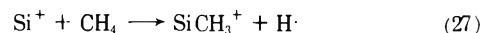
We believe, however, that (26) is more accurately described as a direct hydride ion abstraction from SiH_4 without intermediate formation of SiH_5^+ . The reasons for this conclusion are as follows.

(1) Substitution of CD_5^+ for CH_5^+ in (26) results, within experimental error, in the formation of only SiH_3^+ . No SiH_2D^+ ions were observed as products, whereas equivalence of all hydrogen species in an SiH_4D^+ intermediate would lead to a statistical yield of 60% SiH_2D^+ . This finding is in agreement with recent ion cyclotron resonance studies of CD_4 - SiH_4 mixtures.³⁴

(2) No appreciable amounts of SiH_5^+ were observed in the high-pressure mass-spectrometric studies of methane-rich mixtures, showing that collisional stabilization of $(\text{SiH}_5^+)^*$ was not occurring in pressure regions in which collisional stabilization of more energetic ion-molecule association products was observed.⁵

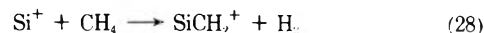
Thus while we cannot completely rule out a very rapid dissociation of an SiH_5^+ intermediate that occurs before randomization of hydrogenic species, we believe the evidence indicates strongly that (26) proceeds by a direct hydride ion transfer. Such a mechanism is in keeping with the polarity of the Si-H bond and the observed fact of predominance of hydride transfer from monosilane shown in Table I.

(g) $\text{Si}^+ + \text{CH}_4$. When 1-eV Si^+ ions react with methane, the only ion observed as a product is the SiCH_3^+ ion, as may be seen in Table I. The reaction involved can be only that shown in (27), *viz.*



The dependence of the reaction cross section on relative kinetic energy indicates the reaction to be an endothermic process with a threshold below 0.4 eV (9 kcal/mol). The enthalpy change of the reaction for ground-state Si^+ ions^{32,35} is +48 kcal, which is in accord with the qualitative observation of an endothermic process but not with the indicated location of the threshold energy. However, it is probable that the Si^+ beam, produced by the impact of 100-eV electrons on SiH_4 , contains a significant fraction of electronically excited ions. It is, therefore, plausible that it is the reaction of excited ions that yield the low threshold value.

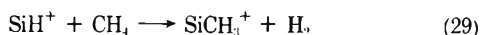
Although not shown in Table I because it does not occur at 1-eV (lab) reactant ion energy, the reaction shown in (28), *viz.*



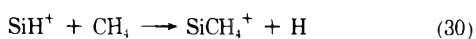
occurs as an endothermic process. The apparent threshold of 0.5 eV cannot be used to check for the presence of excited states of Si^+ in the beam because the enthalpy of formation of SiCH_2^+ is not known.

Neither reaction of Si^+ has been reported before.

(h) $\text{SiH}^+ + \text{CH}_4$. Table I shows that SiH^+ ions react with methane to yield two product ions, namely, SiCH_3^+ and SiCH_4^+ . The behavior of the reaction cross sections with relative kinetic energy indicates both reactions to be exothermic. Therefore, for the formation of SiCH_3^+ , we must have the reaction given in (29), *viz.*



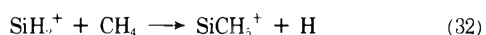
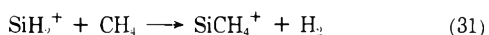
and stoichiometry demands that the reaction producing SiCH_4^+ be that shown in (30), namely



However, available thermochemical data^{3,32,35} indicate that, while (29) is exothermic by 18 kcal, (30) should be endothermic by 26 kcal. We can only suggest that either a considerable fraction of the SiH^+ beam is in excited states or that the heat of formation of SiCH_4^+ , determined by electron impact on SiH_3CH_3 ,³ is grossly in error. In view of a similar need to invoke the presence of excited states in the reactant ion beam in order to explain the low threshold observed for the endothermic reaction (27), and in view of the likelihood of this occurrence when using 100-eV electrons, we prefer the first suggestion. Of course, because of the fact that the energy spread of our ion beam is about 1 eV, we cannot rule out the possibility that, at energies lower than we could obtain experimentally, a maximum in the cross section could occur and endothermic behavior would thus be exhibited. However, the cross section observed is quite large for an endothermic process and this fact, coupled with the observed cross-section dependence on kinetic energy, leads us to conclude that the actual process producing SiCH_4^+ from SiH^+ under our conditions is exothermic; this in turn most likely demands the participation of excited states of SiH^+ .

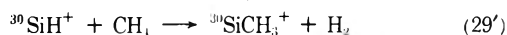
Although (29) was reported by Stewart, Henis, and Gaspar,⁴ these authors did not report the occurrence of (30).

(i) $\text{SiH}_2^+ + \text{CH}_4$. Two product ions appear when SiH_2^+ ions are injected into methane, namely, SiCH_4^+ and SiCH_5^+ , products which were also reported by Stewart, Henis, and Gaspar.⁴ The reactions producing these products can hardly be anything except what is shown in (31) and (32), *viz.*

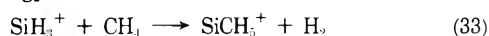


Available thermochemical data^{3,32,35} show (31) to be thermoneutral while (32) is endothermic by 8 kcal; the dependence of the cross sections on relative kinetic energy indicates both reactions to be exothermic. Since the combined uncertainties in the reported enthalpies of formation^{3,35} of SiCH_5^+ and SiH_2^+ exceed 8 kcal/mol, we feel it most probable that (32) is actually exothermic even for ground-state ions. This is confirmed by the observation of both (31) and (32) by Gaspar, Henis, and Stewart⁴ even at low electron-impact energies. Reaction 31 was also reported by Beggs and Lampe.²

(j) $\text{SiH}_3^+ + \text{CH}_4$. When ions of m/e 31 from monosilane are injected into methane a small product ion peak at m/e 45 is observed. While the major fraction of these product ions (0.7) is due to the interfering reactions of the minor isotopic constituents of the m/e 31 beam, *viz.*



extensive examination of the isotopic contributions as a function of energy lead us to conclude that (33) does in-



deed occur as an exothermic process, although with very small cross section. This is contrary to the conclusion of Stewart, Henis, and Gaspar,⁴ who reported that (29') and

(31') account for all of the m/e 45 produced when m/e 31 impinges on methane.

2. *High-Pressure Mass Spectra of Monosilane-Methane Mixtures.* It is quite clear from the data in Table I and from the above discussion that by far the predominant reaction of all methane primary ions with monosilane is hydride abstraction to produce SiH_3^+ . Since this is also the principal process in pure monosilane,^{5,13,14} a rapid growth and large abundance of SiH_3^+ in both methane-rich and monosilane-rich mixtures is to be expected. As shown in Figure 2, which depicts the abundance of major ions as a function of ion-source pressure for a 90% methane-10% monosilane mixture, this expectation is born out. Thus SiH_3^+ , produced principally in this mixture by reaction of methane primary ions with monosilane, rises from a zero-pressure limit of ~4% to a broad maximum near 50% abundance. The broad maximum in SiH_3^+ for this methane-rich mixture results from the fact that, as shown in Table I, SiH_3^+ reacts only very slowly if at all with methane; its depletion is due in this case almost exclusively to the slow three-body association with monosilane to form Si_2H_7^+ .

The formation of CH_5^+ *via* the well-known reaction of CH_4^+ with methane¹³ is also to be seen in Figure 2. The abundance of CH_5^+ rises to a maximum of 22.5% at a source pressure of ~0.025 Torr and then decreases with further increase in pressure. This decrease is clearly due to (26), since in pure methane CH_5^+ is unreactive and attains an abundance plateau¹⁶ of ~48%. Although not shown in Figure 2, C_2H_5^+ behaves quite similarly to CH_5^+ , including reaction³⁶ with monosilane to produce SiH_3^+ .

Ion abundance *vs.* pressure curves for silicon-containing ions in a monosilane-rich mixture are very similar to those in pure monosilane.⁵ This is quite expected because, according to Table I, methane primary ions, which in this mixture react mainly with monosilane, are quickly converted to predominantly SiH_3^+ ions. Very little CH_5^+ is formed in a monosilane-rich mixture since the precursor CH_4^+ is intercepted by monosilane *via* (22)-(25).

The high-pressure mass spectra of both methane-rich and monosilane-rich mixtures is very complex, including, in addition to the known reactions in the two pure gases, the cross reactions listed in Table I. Nonetheless, it is possible to account quantitatively for nearly all behavioral details for secondary ions in the mixtures on the basis of the results in Table I. Mechanistic descriptions of tertiary and higher ions (*i.e.*, Si_2CH_x^+ , SiC_2H_x^+ , Si_3H_x^+) are still a matter of conjecture.

3. *Reaction Rate Constants and Cross Sections.* The relative cross sections shown in Table I refer to a reactant-ion energy of 1 eV in the laboratory system. In the pressure studies carried out in the single-source mass spectrometer the ion-exit energy was 2.1 eV. For the purpose of evaluating phenomenological rate constants (or cross sections) from the pressure studies we use initial slopes of abundance *vs.* source pressure. For this zero-pressure limiting situation the space-average energy of the reactant ions in the source is 1.05 eV and their time-average energy in the source is 0.7 eV, both in the laboratory system. We thus assume that the reactant energies in the pressure studies, exemplified by the data of Figure 2, are comparable to the 1-eV ion energy applying to the data of Table I. With this assumption, we may combine *initial* slopes of pressure plots with the relative cross-section data at 1 eV to evaluate rate constants for all the cross-reactions found.

TABLE II: Reaction Rate Constants in Monosilane-Methane Mixtures

Reaction	ΔH , kcal	$10^{10}k$, cm ³ /sec		
		Ref 2	Ref 4	This work
$C^+ + SiH_4 \rightarrow Si^+ + CH_2 + H_2$	-48			2.5 ± 0.5
$C^+ + SiH_4 \rightarrow SiH^+ + CH_2 + H$	+15			3.7 ± 0.7
$C^+ + SiH_4 \rightarrow SiH_2^+ + CH_2$	-63			6.3 ± 1.2
$C^+ + SiH_4 \rightarrow SiH_3^+ + CH$	-58			26.4 ± 5.3
$C^+ + SiH_4 \rightarrow SiCH^+ + H_2 + H$	<0			1.3 ± 0.2
$C^+ + SiH_4 \rightarrow SiCH_2^+ + H_2$	<0			3.4 ± 0.7
$CH^+ + SiH_4 \rightarrow Si^+ + CH_3 + H_2$	-77			2.3 ± 0.5
$CH^+ + SiH_4 \rightarrow SiH^+ + CH_3 + H$	-14			4.6 ± 0.9
$CH^+ + SiH_4 \rightarrow SiH_2^+ + CH_3$	-92			4.2 ± 0.7
$CH^+ + SiH_4 \rightarrow SiH_3^+ + CH_2$	-74			19.7 ± 3.9
$CH^+ + SiH_4 \rightarrow SiCH_2^+ + H_2 + H$	<0		1.56 ± 0.4	3.6 ± 1.7
$CH^+ + SiH_4 \rightarrow SiCH_3^+ + H_2$	-135			6.2 ± 1.2
$CH_2^+ + SiH_4 \rightarrow Si^+ + CH_4 + H_2$	-62			1.0 ± 0.2
$CH_2^+ + SiH_4 \rightarrow SiH^+ + CH_3 + H_2$	0			3.3 ± 0.7
$CH_2^+ + SiH_4 \rightarrow SiH_2^+ + CH_4$	-77			1.0 ± 0.2
$CH_2^+ + SiH_4 \rightarrow SiH_3^+ + CH_3$	-69			21.6 ± 4.5
$CH_2^+ + SiH_4 \rightarrow SiCH_2^+ + 2H_2$	<0			1.1 ± 0.3
$CH_2^+ + SiH_4 \rightarrow SiCH_3^+ + H_2 + H$	-17		2.91 ± 0.53	6.9 ± 1.4
$CH_3^+ + SiH_4 \rightarrow SiH_3^+ + CH_4$	-47		11.1 ± 1.8	22.5 ± 4.5
$CH_3^+ + SiH_4 \rightarrow SiCH_3^+ + 2H_2$	+4	0.12	^a	0.73 ± 0.15
$CH_3^+ + SiH_4 \rightarrow SiCH_5^+ + H_2$	-48			0.69 ± 0.14
$CH_4^+ + SiH_4 \rightarrow SiH_2^+ + CH_4 + H_2$	-18			4.6 ± 1.1
$CH_4^+ + SiH_4 \rightarrow SiH_3^+ + CH_3 + H_2$	-10		25 ± 10	14.7 ± 3.0
$CH_4^+ + SiH_4 \rightarrow SiCH_4^+ + 2H_2$	-18	7.47	0.35 ± 0.23	0.42 ± 0.08
$CH_4^+ + SiH_4 \rightarrow SiCH_5^+ + H_2 + H$	-10	2.20	0.30 ± 0.18	0.63 ± 0.12
$CH_5^+ + SiH_4 \rightarrow SiH_3^+ + CH_4 + H_2$	-8		17.8 ± 2.5	19.9 ± 4.0
$Si^+ + CH_4 \rightarrow SiCH_3^+ + H$	+48			0.77 ± 0.15
$SiH^+ + CH_4 \rightarrow SiCH_3^+ + H_2$	-18		0.82 ± 0.28	2.1 ± 0.4
$SiH^+ + CH_4 \rightarrow SiCH_4^+ + H$	+26			3.5 ± 0.8
$SiH_2^+ + CH_4 \rightarrow SiCH_4^+ + H_2$	0		3.07 ± 0.61	1.3 ± 0.3
$SiH_2^+ + CH_4 \rightarrow SiCH_5^+ + H$	+8	0.18	0.52 ± 0.15	0.80 ± 0.17
$SiH_3^+ + CH_4 \rightarrow SiCH_5^+ + H_2$	-1			0.05 ± 0.03

^a Reported as endothermic reaction with no rate constant or cross section given.

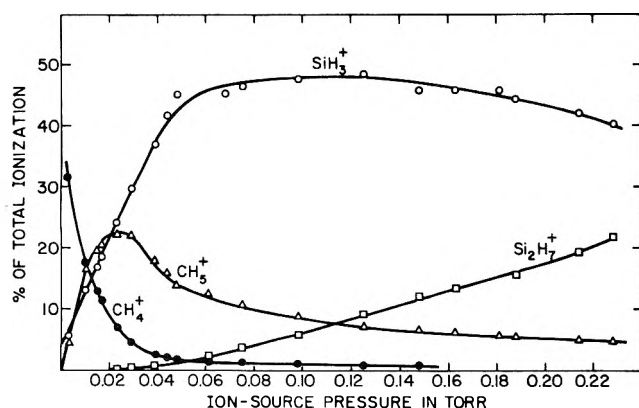


Figure 2. Pressure dependence of relative intensities of major ions in a 90% CH₄-10% SiH₄ mixture: ●, CH₄⁺; △, CH₅⁺; ○, SiH₃⁺; □, Si₂H₇⁺.

For example, we may from ion abundance *vs.* pressure data in the single mass spectrometer evaluate an *initial* slope for SiCH₅⁺ formation, *e.g.*, $(dX_{SiCH_5^+}/dP)_{P=0}$. Since the precursors to SiCH₄⁺ are known from Table I to

be CH₄⁺, SiH⁺, and SiH₂⁺, it is easily shown that this initial slope is given by

$$\lim_{P \rightarrow 0} (dX_{SiCH_4^+}/dP) = 2.83 \times 10^{16} L \{ X_{CH_4^+}^0 \sigma_{24} \gamma_{SiH_4} + X_{SiH^+}^0 \sigma_{30} \gamma_{CH_4} + X_{SiH_2^+}^0 \sigma_{31} \gamma_{CH_4} \} \quad (34)$$

where *L* is the travel distance of the ions in the source, *X_i⁰* is the zero-pressure limit of the percentage of the *i*th ion, *σ_i* the cross section of reaction *i*, *γ_i* is the mole fraction of neutral substance *i*, and 2.83×10^{16} is the conversion factor between molecular number density and pressure in Torr. Since the relative cross sections are known from Table I we may use (34) and the pressure data to evaluate the absolute phenomenological cross sections *σ₂₄*, *σ₃₀*, and *σ₃₁*. We obtain phenomenological rate constants by the general relationship (35), where *k_i* is the rate con-

$$k_i t_i = \sigma_i L \quad (35)$$

stant corresponding to the cross section *σ_i* and *t_i* is the residence time of the reactant ion in the source. Since we deal only with slopes in the limit of zero pressure, the residence time *t_i* is well defined. Knowing any one absolute

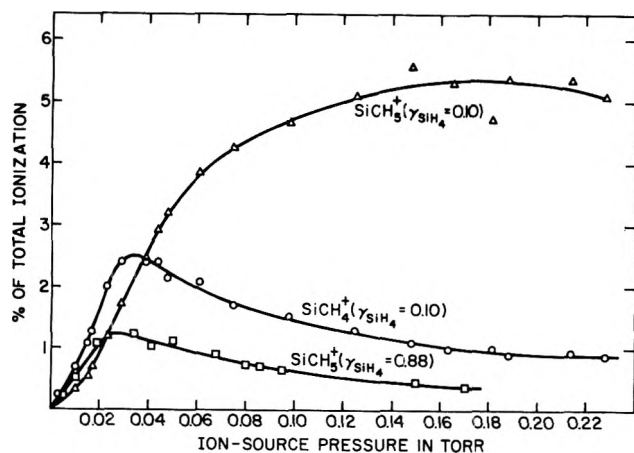
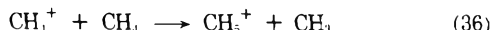


Figure 3. Pressure dependence of relative intensities of SiCH_4^+ and SiCH_5^+ in monosilane-methane mixtures: O, SiCH_4^+ in 90% CH_4 -10% SiH_4 ; Δ , SiCH_5^+ in 90% CH_4 -10% SiH_4 ; \square , SiCH_5^+ in 12% CH_4 -88% SiH_4 .

cross section or rate constant we may further use the data in Table I and eq 35 to evaluate the rate constants of all secondary reactions observed.

We have evaluated all the rate constants using the pressure data in the manner just described for (1) the formation of SiH_3^+ in the methane-rich mixture; (2) the formation of SiCH_4^+ in both mixtures; (3) the formation of SiCH_5^+ in both mixtures. Figure 2 shows the pressure data for SiH_3^+ while typical data for SiCH_4^+ and SiCH_5^+ are depicted in Figure 3. From these data and the treatment described we obtained a value of $14.9 \pm 3.2 \times 10^{-10} \text{ cm}^3/\text{sec}$ for reaction 23, the hydride abstraction from monosilane by CH_4^+ . To compare this result with an independent measurement in the tandem mass spectrometer we measured the cross section for reaction 23 relative to that for the well-known reaction, *viz.*



by simply interchanging methane and monosilane in the collision chamber. Taking the accepted value⁹⁻¹² of $12.0 \times 10^{-10} \text{ cm}^3/\text{sec}$ for the rate constant of (27), we obtain $k_{23} = 13.3 \pm 1.0 \times 10^{-10}$, a value in excellent agreement with the average obtained from Table I and the pressure data.

Rate constants for all reactions observed are collected in Table II, where the uncertainties indicated are average deviations from the average. Also shown in Table II are the enthalpy changes for the reactions and the rate constants reported by Stewart, Henis, and Gaspar⁴ in their ion cyclotron resonance study and by Beggs and Lampe² in their low-pressure mass-spectrometric study. In computing enthalpy changes, standard enthalpies of formation were taken from the general tabulation of Franklin, *et al.*,³² and from recent electron-impact studies in this laboratory.^{3,35}

The use of tandem mass spectrometry in our work has permitted us to identify unambiguously many more elementary reactions in this complex system than was possible in the ion cyclotron resonance studies of Stewart, Henis, and Gaspar,⁴ particularly reactions of the low-intensity primary ions, C^+ , CH^+ , CH_2^+ , Si^+ , and SiH^+ . For the ten reactions shown in Table II in which comparison of the rate constants determined in this study with

those from ion cyclotron resonance⁴ is possible, all but one agree within a factor of ~ 2.5 , with our values generally being the larger. The agreement is somewhat better for the major reactions, namely, those involving H^- transfer. Considering the different ionizing electron energies, different relative kinetic energies of reactants, and different pressures involved in the two studies the agreement between rate constants from our work and those of Stewart, Henis, and Gaspar⁴ should be considered as satisfactory. On the other hand the agreement with the low-pressure studies of Beggs and Lampe² is quite poor, which no doubt is a result of the complete inadequacy of low-pressure, single mass spectrometer studies (using appearance potentials for reactant identification) as a method for the detailed elucidation of such a complex system of ion-molecule reactions.

Acknowledgment. This work was supported by the U. S. Atomic Energy Commission under Contract No. AT(11-1)-3416. We also wish to thank the National Science Foundation for providing funds to assist in the original purchase of the Nuclide mass spectrometer.

References and Notes

- U. S. Atomic Energy Commission Document No. COO-3416-8.
- D. P. Beggs and F. W. Lampe, *J. Phys. Chem.*, **73**, 4194 (1969).
- P. Potzinger and F. W. Lampe, *J. Phys. Chem.*, **74**, 587 (1970).
- G. W. Stewart, J. M. S. Henis, and P. P. Gaspar, *J. Chem. Phys.*, **57**, 1990 (1972).
- T.-Y. Yu, T. M. H. Cheng, V. Kempter, and F. W. Lampe, *J. Phys. Chem.*, **76**, 3321 (1972).
- P. Potzinger and F. W. Lampe, *J. Phys. Chem.*, **74**, 719 (1970).
- J. J. DeCorpo and F. W. Lampe, *J. Phys. Chem.*, **74**, 3939 (1970).
- P. Potzinger and F. W. Lampe, *J. Phys. Chem.*, **75**, 13 (1971).
- V. L. Tal'roze and E. L. Frankevich, *Zh. Fiz. Khim.*, **34**, 2709 (1960).
- C. W. Hand and H. Von Weysenhoff, *Can. J. Chem.*, **42**, 195 (1964).
- J. L. Franklin, Y. Wada, P. Natalis, and P. M. Hierl, *J. Phys. Chem.*, **70**, 2353 (1966).
- S. K. Gupta, E. G. Jones, A. G. Harrison, and J. J. Myher, *Can. J. Chem.*, **45**, 3107 (1967).
- V. E. Tal'roze and A. K. Lyubimova, *Dokl. Akad. Nauk SSSR*, **86**, 909 (1952).
- D. O. Schissler and D. P. Stevenson, *J. Chem. Phys.*, **24**, 926 (1956).
- S. Wexler and N. Jesse, *J. Amer. Chem. Soc.*, **84**, 3425 (1962).
- F. H. Field and M. S. B. Munson, *J. Amer. Chem. Soc.*, **87**, 3289 (1965).
- G. G. Hess and F. W. Lampe, *J. Chem. Phys.*, **44**, 2257 (1966).
- J. M. S. Henis, G. W. Stewart, M. K. Tripodi, and P. P. Gaspar, *J. Chem. Phys.*, **57**, 389 (1972).
- C. F. Giese and W. B. Maier, *J. Chem. Phys.*, **39**, 197 (1963).
- W. B. Maier, *J. Chem. Phys.*, **46**, 4991 (1967).
- J. D. Martin and T. L. Bailey, *J. Chem. Phys.*, **49**, 1977 (1968).
- P. S. Wilson, R. W. Rozett, and W. S. Koski, *J. Chem. Phys.*, **52**, 5321 (1970).
- E. Lindemann, L. C. Frees, R. W. Rozett, and W. S. Koski, *J. Chem. Phys.*, **56**, 1003 (1972).
- G. Gioumoussis and D. P. Stevenson, *J. Chem. Phys.*, **29**, 294 (1958).
- W. B. Maier, *Planet. Space Sci.*, **16**, 477 (1968).
- J. Sayers and D. Smith, *Discuss. Faraday Soc.*, **37**, 167 (1964).
- T. F. Moran and L. Friedman, *J. Chem. Phys.*, **45**, 3837 (1966).
- C. F. Giese and W. B. Maier, *J. Chem. Phys.*, **39**, 739 (1963).
- J. J. Kaufman and W. S. Koski, *J. Chem. Phys.*, **50**, 1942 (1969).
- A. Pipano and J. J. Kaufman, *J. Chem. Phys.*, **56**, 5258 (1972).
- C. F. Giese, *Advan. Chem. Ser.*, **No. 58**, 20 (1966).
- J. L. Franklin, J. G. Dillard, H. M. Rosenstock, J. T. Herron, K. Draxl, and F. H. Field, *Nat. Stand. Ref. Data Ser.*, *Nat. Bur. Stand.*, **No. 26** (1969).
- T. M. H. Cheng and F. W. Lampe, *Chem. Phys. Lett.*, **19**, 532 (1973).
- G. W. Stewart, J. M. S. Henis, and P. P. Gaspar, *J. Chem. Phys.*, **57**, 2247 (1972).
- P. Potzinger and F. W. Lampe, *J. Phys. Chem.*, **73**, 3912 (1969).
- T. M. H. Cheng and F. W. Lampe, unpublished results.

A Study of the Formation of Negative Ions in Nitric Oxide and the Interaction of NO with H^- and O^- from Water¹

Satish K. Gupta and Charles E. Melton*

Chemistry Department, University of Georgia, Athens, Georgia 30602 (Received June 21, 1973)

Publication costs assisted by the University of Georgia

A comprehensive study on the formation of negative ions in nitric oxide, primary as well as secondary, has been made. Three ions, O^- , NO^- , and NO_2^- , were observed. The appearance potential of O^- is 7.0 eV. A maximum cross section of $1.2 \times 10^{-18} \text{ cm}^2 \text{ molecule}^{-1}$ was observed at 8.0 eV. The ions NO^- and NO_2^- are produced by termolecular reactions of the type $(NO)_2 + e \rightarrow NO^- + NO$ and $O^- + (NO)_2 \rightarrow NO_2^- + NO$. An unusually large rate constant of $7.6 \times 10^{-27} \text{ cc}^3 \text{ sec}^{-1}$ was observed for the termolecular reaction producing NO_2^- . Mixtures of NO and H_2O were studied to determine the mechanism of the action of NO in radiolysis reactions. In addition to the O^- -NO reaction, a charge transfer reaction $H^- + NO \rightarrow H + NO^-$ was observed with a rate constant of $k = 4.0 \times 10^{-9} \text{ cc molecule}^{-1} \text{ sec}^{-1}$. The experimental value of the rate constant is in excellent agreement with the theoretical value derived on the assumption of locked-dipole ion-molecule interactions. This study shows that the scavenger NO is actually a source of H atoms produced by the reaction of NO with H^- .

Introduction

Small quantities of nitric oxide have been known for many years to change the yield of chemical reactions produced by ionizing radiation. The theory for the effect was almost always interpreted from a phenomenological or semiphenomenological point of view. Specifically the molecule was assumed to scavenge some intermediate in the reaction. The effect of a scavenger can be interpreted on the basis of three different elementary processes. They are (1) a reduction or increase in the population of a specific positive ion, (2) a reduction or increase in the population of specific free radicals, and (3) a reduction or increase in the population of specific negative ions produced in the system.

One purpose of this study was to determine the effect of small quantities of NO on the elementary reactions in water subjected to ionizing radiation.

In the study, we planned to restrict our attention to process 3 the effect of NO on the population of negative ions produced in water by ionizing radiation (electrons). Positive ions in the NO- H_2O system have been studied by other investigators.^{2a}

Before investigating the effect of a system, the behavior of each of the one component systems must be known accurately. In a series of papers^{2b-4} we have described the formation and subsequent reactions of negative ions produced in water by ionizing electrons. The negative ions formed in nitric oxide, on the other hand, have not been studied in detail. Some aspects of the formation of primary negative ions have been studied,⁵⁻⁷ but the subsequent reactions of these ions with the system has not been reported. Consequently, a detailed study of negative ionization in NO was necessary for a proper interpretation of the results.

Locht and Momigny⁷ have reported two possible processes leading to the production of O^- from NO. Other workers^{4,5} have indicated only one process. In view of these different interpretations, a careful study of the ionization efficiency curve for O^- from NO might tend to resolve the differences.

In a study of the total ionization cross section, Rapp and Briglia⁸ observe two maxima of about equal magnitude in the ionization efficiency curve for O^- from NO. Since mass analysis was not made by these investigators, the results are suspect. Furthermore, all other investigators⁷ reporting two maxima indicate the second maxima has a much lower intensity than the first. Thus, another purpose of the present study was to determine using mass analysis the absolute cross section for the dissociative attachment process in NO for comparison with the results reported by Rapp and Briglia.

Experimental Section

The experiments were carried out with a 6-in. radius, 90° sector type research mass spectrometer constructed at this laboratory. The instrument,³ experimental technique, and necessary calibration procedures have been described elsewhere.⁴ A 3-l. borosilicate glass expansion reservoir was used as a sample holder for pure NO and for mixtures of NO and H_2O . The reservoir was connected to the ionization chamber by a molecular leak 0.001 in. in diameter which maintained a constant pressure in the ionization chamber over fairly long periods of time. The pressure in the ionization chamber was determined by an MKS Baratron pressure gauge. The gauge was calibrated by introducing argon into the system and comparing the measured pressure with the calculated value. The calculated value was obtained from a knowledge of experimental parameters and the relationship

$$N^+ = \sigma N_0 N_e x \quad (1)$$

where N^+ and N_e are the ion and electron currents, respectively, N_0 is the density of neutral molecules, x is the path length for the electrons, and σ is the cross section for ionization. A value of $2.79 \times 10^{-16} \text{ cm}^2$ was used for the cross section for the production of $^{40}\text{Ar}^+$ with 100-eV electrons.^{9,10} The agreement between the measured and the calculated pressures was within $\pm 10\%$. To further test the apparatus and the pressure determination, the cross section for dissociative electron capture by O_2 to form O^-

was measured with 6.6-eV electrons. A measured value of $1.32 \times 10^{-18} \text{ cm}^2 \text{ molecule}^{-1}$ was obtained. The value is in excellent agreement with some recent experimental values of $1.3 \times 10^{-18} \text{ cm}^2 \text{ molecule}^{-1}$. The electron energy scale was calibrated with O⁻ from CO, AP (O⁻/CO) = 9.5 eV⁷, and O⁻ from O₂, AP (O⁻/O₂) = 4.5 eV.¹¹

Absolute cross sections for the production of O⁻ from NO by dissociative electron capture were obtained with the high transmission ion source described in ref 4. Ion-molecule reactions were studied with a high-pressure ion source described elsewhere.¹² By using a "tight" ionization chamber with circular apertures of 0.007 in. diameter for admission of the electron beam and exit of the ions, pressures as high as 1.0 Torr could be maintained in the chamber. However, the normal operation pressure was in the range of from 0.01 to 0.5 Torr.

Ions were detected by means of either a Faraday cup or a 14-stage electron multiplier used in conjunction with a vibrating capacitor amplifier. The detector circuit was checked for linearity by measuring the isotopic abundance of neon or three different scales and comparing the experimental values with the known values.¹³⁻¹⁵ The linearity was better than 0.25% over all ranges.

The nitric oxide gas used in these experiments was obtained from Matheson Company, Inc. It was further purified to remove H₂O, O₂, and other oxides of nitrogen. To remove H₂O, N₂O, NO₂, and higher oxides of nitrogen by condensation, a sample of NO was submerged in a Dry Ice-acetone bath (-90°) for several hours. The uncondensed sample was then transferred to another sample bottle immersed in liquid N₂ whence pure NO liquified in the second sample bottle. Finally, the liquid NO was pumped for a short while to remove possible uncondensed gases such as N₂ and O₂. A positive ion mass spectrum of the purified NO showed no impurities with an abundance greater than a few ppm. For experiments involving H₂O, a triply distilled¹⁶ sample of water was used.

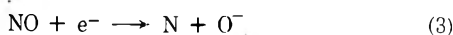
Ion-molecule reactions were identified by "standard" appearance potential and pressure techniques.¹⁷ The cross section, Q , for the ion-molecule reactions were computed by substituting experimental data in the expression

$$Q = (I_s/I_p)[dN_0p]^{-1} \quad (2)$$

where I_p and I_s are the mass spectral currents of the primary and the secondary ions respectively, d is the length of the path of the primary ions through the reactant gas at the pressure, p , and N_0 is the ideal gas number density of the neutral molecules at 1-Torr pressure and at 87°, the ion source temperature. This expression for Q is based on the assumption of (a) equal ion collection efficiencies of the primary and the secondary ions, and, (b) that the fraction of the primary ions lost by reaction is negligibly small. The conditions are approximately fulfilled in a well-designed ion source operated at relatively low pressure.

Results and Discussion

Pure Nitric Oxide. At low pressures ($\sim 10^{-4}$ Torr) of NO in the ion source and low-energy ionizing electrons, the only negative ion detected was O⁻ probably formed by the dissociative attachment reaction



The ionization efficiency curve for this process is shown in Figure 1 where the intensity of O⁻ is shown as a function of electron energy. The maximum of the cross section occurs at 8.0 ± 0.2 eV. This value of the position of the

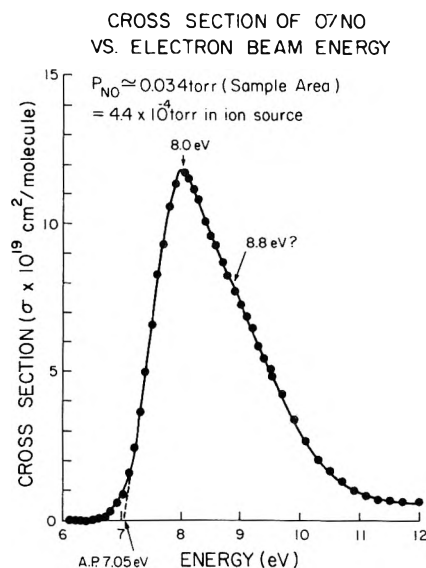


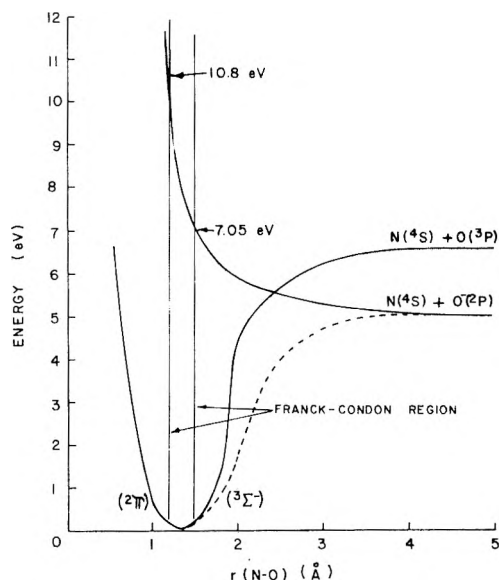
Figure 1. Ionization efficiency curve for the production of O⁻ from NO by electron impact. Pressure in the ion chamber was 4.4×10^{-4} Torr.

maximum is in very good agreement with a recently determined value of 8.1 ± 0.2 eV by Locht and Momigny.⁷ The threshold of the dissociative attachment process determined by linear extrapolation of the low-energy side of the ionization efficiency curve, 7.0 ± 0.2 eV, is somewhat lower than the value of 7.43 ± 0.2 eV obtained by the same workers.⁷ The value for the threshold energy of O⁻ observed in the present study agrees well, however, with an earlier determination of 6.99 ± 0.05 eV by Frost and McDowell.¹⁸ The present value of 7.0 eV is about 2 eV higher than the calculated value of 5.01 eV. No excess kinetic energy is permitted in the calculation using electron affinity of O = 1.48 eV¹⁹ and $D(\text{NO}) = 6.49$ eV.²⁰

Heirl and Franklin, on the other hand, report an experimental value of appearance potential O⁻ from NO in agreement with the calculated value. We have no conclusive explanation for the much lower value reported by these workers. We did observe, however, that the value obtained in the present study was a strong function of the purity of the sample. A trace of NO₂ in the sample caused a marked decrease in the appearance potential of O⁻.

If O⁻ is produced by two different processes, one with a maximum cross section at 8.0 eV and the other with a maximum at about 8.8 eV, the cross section for the higher energy process is about 50% lower than that for the lower energy process. This observation is qualitatively in agreement with the results reported by Locht and Momigny,⁷ but in complete disagreement with the results reported by Rapp and Briglia.⁸ These workers reported about equal cross sections for the two processes. It should be pointed out, however, that the work of Rapp and Briglia was done without mass analysis. Consequently, negative ions produced from any possible impurity would have been interpreted as O⁻ ions from NO. The absolute value of the cross section for the process with a maximum at about 8.0 eV is in good agreement with that reported by Rapp and Briglia,⁸ 1.2 vs. $1.3 \times 10^{-18} \text{ cm}^2 \text{ molecule}^{-1}$.

The results from this study have been combined to give the hypothetical potential energy diagram shown in Figure 2. Intercepts of the potential curves with the Frank-Condon region are obtained from appearance potential data, Figure 1. Ionization may actually occur from the X³Σ⁻ state with an electronic configuration²¹ of

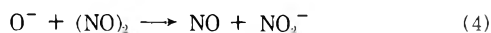


HYPOTHETICAL POTENTIAL ENERGY DIAGRAM FOR NO

Figure 2. Qualitative dissociation curves for NO^- . The intercepts of the potential curves with the Frank-Condon region are obtained from the data of Figure 1. These results suggest that O^- from NO is formed with excess kinetic energy.

$\text{KK}\cdots(5\sigma)^2(1\pi)^4(2\pi)^2(6\sigma)$. This mechanism assumes a transition to the excited state of NO during the electron capture process.²¹ These curves indicate that the O^- ion would have about 1 eV excess kinetic energy.

At ion source pressures $<10^{-3}$ Torr in addition to O^- , ion currents corresponding to the species NO^- and NO_2^- were also observed. Experimental plots of the intensities of the three ions, O^- , NO^- , and NO_2^- , as function of the NO pressure in the source are shown in Figure 2. The data were taken at an electron beam energy of 8.0 eV. The ionization efficiency curve for NO_2^- has the same shape as that for O^- (Figure 1), with the maximum occurring at identical position (8.0 eV). Thus O^- is the precursor for NO_2^- . Since no NO_2^- ion current could be detected at NO pressures $<10^{-3}$ Torr, NO_2^- must be produced by the termolecular reaction



the second molecule of NO being needed to remove the excess energy.

Smoothed data from Figure 3 are tabulated in Table I. From these data the termolecular rate constant for the reaction 4 can be calculated. The relationship is

$$k_{\text{term}} = 6.95 \times 10^5 \frac{[I_{\text{NO}_2^-}]}{[I_{\text{O}^-}][N_{\text{NO}}]^2 x} \left(\frac{Ex}{M_{\text{O}^-}} \right)^{1/2} \quad (5)$$

where E is the repeller field in volts cm^{-1} , x is the reaction path length in cm, N_{NO} is the number density of the neutral NO molecules, and M_{O^-} is the mass of O^- in atomic mass units. The termolecular rate constants calculated with above expression are also listed in Table I. It is seen from Table I that, except for the lowest pressure, the rate constants for the reaction 4 at various pressures are practically identical, giving an average value of $k_{\text{term}} = 7.6 \times 10^{-27} \text{ cc}^3 \text{ sec}^{-1}$. The low value of $k_{\text{term}} = 6.5 \times 10^{-27} \text{ cc}^3 \text{ sec}^{-1}$ at 2×10^{-2} Torr NO pressure indicates probably the effect of decreased probability of termolecular collisions at this pressure. On the other hand, it just may reflect the scatter of the experimental data. In any case, the rate constant for the reaction 4 is relatively

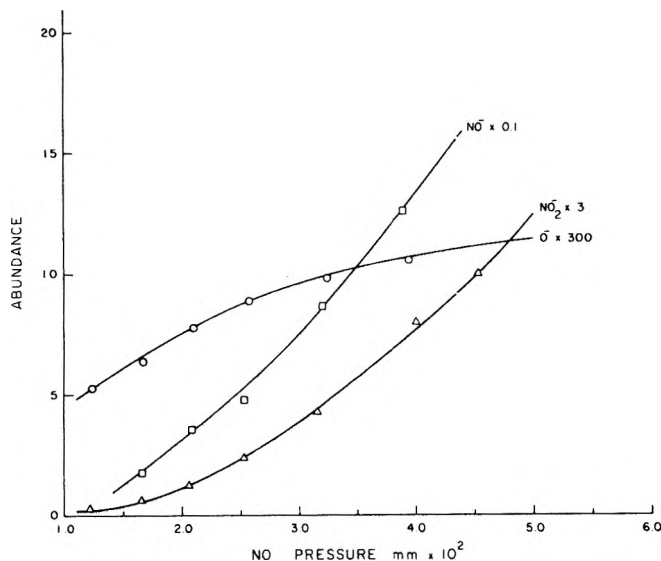


Figure 3. Intensities of the ions, O^- , NO^- , and NO_2^- as a function of NO pressure in the ion chamber. The electron beam energy was 8.0 eV.

TABLE I: Intensities of O^- , NO^- , and NO_2^- at Various NO Pressures and Termolecular Rate Constants for the Reaction $\text{NO} + \text{O}^- + \text{NO} \rightarrow \text{NO} + \text{NO}_2^-$

NO pressure, mm $\times 10^2$	I_{O^-}	I_{NO^-}	$I_{\text{NO}_2^-}$	k termolecular, $\text{cc}^3 \text{ sec}^{-1} \times 10^{27}$
4.0	3210	1.31	23.1	0.77
3.5	3060	1.03	17.1	0.78
3.0	2865	0.76	11.7	0.77
2.5	2610	0.52	7.05	0.74
2.0	2250	0.35	3.45	0.65

large, suggesting that this process may be playing an important role in the chemistry of NO in the atmosphere.

The small ion current due to NO^- was found to be independent of the energy of the electron beam through a wide range and no discrete process could be assigned to explain the production of NO^- . The plot of the variation of NO^- ion current with NO pressure is very similar to that for NO_2^- . Also, since NO^- current is not detected at lower pressures, we believe that NO^- is formed by the scattered electrons in a termolecular collision represented by



It was not possible to calculate the rate constants for this reaction from the data contained in Table I.

$\text{NO}-\text{H}_2\text{O}$ Mixtures. In $\text{NO}-\text{H}_2\text{O}$ mixtures of compositions ranging from a few per cent up to 50% of H_2O , significantly large ion currents corresponding to the species NO^- were observed. In H_2O , three primary ions, H^- , O^- , and OH^- , are formed by dissociative attachment processes at 6.4, 8.4, and 11.2 eV energy.³ The NO^- ion current shows a maximum at 6.4-eV energy and its ionization efficiency curve is identical in shape with that for H^- produced by dissociative attachment in H_2O . The cross sections for O^- and OH^- formation by dissociative attachment in H_2O are smaller than that for H^- by about 2 and 4 orders of magnitude, respectively. It is apparent thus, that in $\text{NO}-\text{H}_2\text{O}$ mixture, NO^- is produced by the charge-transfer reaction

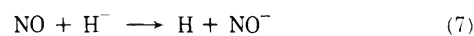


TABLE II: Cross Sections and Rate Constants for the Reaction H⁻ + NO → H + NO⁻

Repeller field <i>E</i> , V cm ⁻¹	H ⁻ ion energy, eV	Cross section <i>Q</i> , cm ² mole- cule ⁻¹ × 10 ¹⁸	Rate constant <i>k</i> , cm ³ mole- cule ⁻¹ sec ⁻¹ × 10 ⁹
1.25	0.25	4.18	2.50
2.50	0.50	3.99	3.38
3.75	0.75	3.43	3.56
5.00	1.00	3.90	4.19
7.50	1.50	2.90	4.26
10.00	2.00	2.35	3.98
12.50	2.50	2.13	4.04
15.00	3.00	1.88	3.90
17.50	3.50	1.80	4.04
20.00	4.00	1.48	3.55
22.50	4.50	1.60	4.07
25.00	5.00	1.32	3.54
30.00	6.00	1.50	4.40

^a Average rate constant (excluding first two values) = 3.96×10^{-9} cm³ molecule⁻¹ sec⁻¹.

In order for this reaction to proceed, the electron affinity of NO must be greater than that of H. In the past various values have been assigned to the lower limit for the electron affinity of NO.²²⁻²⁴ From the above charge transfer reaction the lower limit to the electron affinity of NO would be set at 0.75 eV, the electron affinity of H.²⁵

The experimental cross sections, *Q*, for the reaction 7 at a series of repeller field strengths, *E*, are listed in Table II. These cross sections are plotted as a function of *E*^{-1/2} in Figure 4. According to theory,²⁶ the phenomenological cross section for the ion-molecule reaction is given by

$$Q = 2\pi \left(\frac{2Me^2\alpha}{\mu} \right)^{1/2} \frac{1}{(eEd)^{1/2}} \quad (8)$$

where *M* is the mass of the ion, *e* is the electronic charge, *μ* is the reduced mass, *α* is the average electric polarizability of the neutral molecule, and *d* is the reaction path length. This expression predicts an *E*^{-1/2} dependence for the reaction cross section. From Figure 3 it is seen that, except for very low potential fields, the cross sections for the reaction indeed shows an *E*^{-1/2} dependence. The small cross sections at low repeller fields can be accounted for by the fact that at low repeller potentials the ion collection efficiency for NO⁻ is low; consequently, the experimental ratio *I*(NO⁻)/*I*(H⁻) (eq 2) is too small. No data on the reaction 7 could be found in literature, to compare with the present results.

The Langevin rate constant²⁶ for an ion molecule reaction is given by

$$k = 2\pi(e^2\alpha/\mu)^{1/2} \quad (9)$$

so that the relationship between the rate constant and the cross section is expressed, by combining eq 8 and 9, as

$$k = (eEd/2M)^{1/2}Q \quad (10)$$

The rate constants for reaction 7, calculated from the experimental cross sections by the above expression, are listed in Table II. Within experimental errors, it is seen from Table II that the rate constant is independent of the repeller field strength. Neglecting the first two values at very low repeller fields, the average value of *k* is obtained as 3.96×10^{-9} cm³ molecule⁻¹ sec⁻¹. Using a value of 1.86×10^{-24} cc for the electric polarizability,²⁷ *α*, of NO in eq 10, the theoretical value of *k* for reaction 7 is calcu-

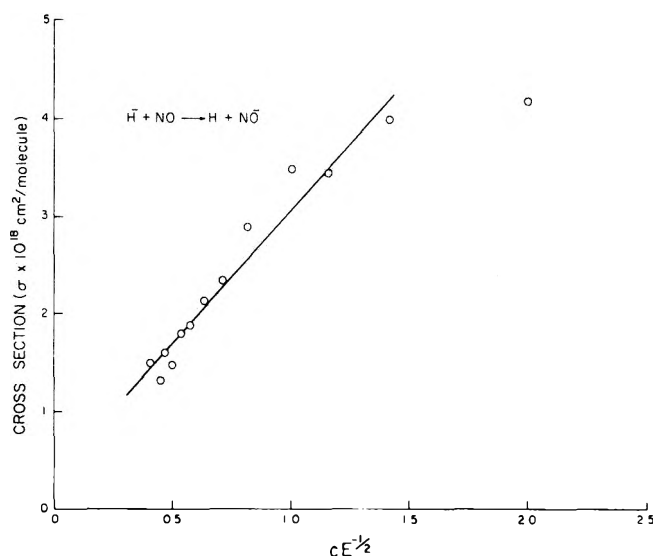


Figure 4. Cross sections for the reaction H⁻ + NO → H + NO⁻ as a function of *cE*^{-1/2}, *E* being the repeller field and *c* is a constant.

lated to be 2.99×10^{-9} cm³ molecule⁻¹ sec⁻¹. This is about 25% smaller than the experimental average value. However, the expression (9) for *k* is derived on the assumption that the reactant molecule is nonpolar. The dipole moment of 0.16 esu²⁸ for NO is small but not insignificant. Gupta and coworkers²⁹ have derived the following expression for the rate constant for reaction between an ion and a dipolar molecule

$$k_{ld} = 2\pi \left(\frac{e^2\alpha}{\mu} \right)^{1/2} + 2\pi e\mu_D \left(\frac{2}{\pi kT\mu} \right) \quad (11)$$

where *μ_D* is the dipole moment of the neutral molecule, *k* is the Boltzmann constant, and *T* is the temperature; other symbols have the same meaning as before. In deriving this expression it was assumed that the molecular dipole "lock-in" as the reacting ion approaches.³⁰ The "locked-dipole" rate constant for the charge transfer reaction between H⁻ and NO⁻ is calculated to be 4.30×10^{-9} cm³ molecule⁻¹ sec⁻¹ at 360°K, the temperature of the ion source. This value is only about 10% larger than the average experimental rate constant.

In conclusion, the species NO₂⁻ is produced by a termolecular collision between O⁻ and two NO molecules with a very large rate constant. Although NO has an unpaired electron, it does not form NO⁻ by the direct capture of an electron. It, however, does attract an electron from H⁻ to produce molecular negative ion, NO⁻. The experimental rate constant for this charge transfer reaction compares very well with the theoretical rate constant based upon locked-dipole interaction between the ion and the molecule.

This study shows also that NO reacts with H⁻ to produce H atoms and is thus a source of free radicals.

References and Notes

- (1) Supported by the U. S. Atomic Energy Commission under Contract No. AT-(38-1) 640 with the University of Georgia.
- (2) (a) M. J. McAdams and L. I. Bone, *J. Chem. Phys.*, **57**, 2173 (1972); (b) C. E. Melton, *J. Phys. Chem.*, **74**, 582 (1970).
- (3) C. E. Melton, *J. Chem. Phys.*, **57**, 4218 (1972).
- (4) C. E. Melton, *J. Phys. Chem.*, **76**, 3116 (1972).
- (5) H. D. Hagstrum, *Rev. Mod. Phys.*, **23**, 185 (1951).
- (6) P. M. Hierl and J. L. Franklin, *J. Chem. Phys.*, **47**, 3154 (1967).
- (7) R. Loch and J. Momigny, *Int. J. Mass Spectrom Ion Phys.*, **4**, 379 (1970).

- (8) D. Rapp and D. Briglia, *J. Chem. Phys.*, **43**, 1480 (1965).
 (9) C. E. Melton and P. S. Rudolph, *J. Chem. Phys.*, **47**, 1771 (1967).
 (10) G. J. Schulz, *Phys. Rev.*, **128**, 178 (1962).
 (11) J. A. D. Stockdale, R. N. Compton, and P. W. Reinhardt, *Phys. Rev. Lett.*, **21**, 664 (1968); *Phys. Rev.*, **184**, 81 (1969).
 (12) C. E. Melton and G. A. Neece, *J. Amer. Chem. Soc.*, **93**, 6757 (1971).
 (13) C. E. Melton, W. Massey, and B. N. Abels, *Z. Naturforsch. A*, **26**, 1241 (1971).
 (14) P. Eberhardt, O. Eugster, and K. Marti, *Z. Naturforsch. A*, **20**, 623 (1965).
 (15) J. R. Waton and A. E. Cameron, *Z. Naturforsch. A*, **21**, 115 (1966).
 (16) J. P. Chittum and V. K. Lamer, *J. Amer. Chem. Soc.*, **59**, 2424 (1937).
 (17) C. E. Melton, "Mass Spectra of Organic Ions," F. W. McLafferty, Ed., Academic Press, New York, N. Y., 1963, p 82.
 (18) D. C. Frost and C. A. McDowell, *J. Chem. Phys.*, **29**, 1424 (1958).
 (19) L. M. Branscomb and S. J. Smith, *Phys. Rev.*, **98**, 1127 (1955).
 (20) H. D. Hagstrum, *J. Chem. Phys.*, **23**, 1178 (1955).
 (21) F. R. Gilmore, *J. Quanta Spectrosc. Radium. Transfer*, **5**, 369 (1969).
 (22) J. A. D. Stockdale, R. N. Compton, G. S. Hurst, and P. W. Reinhardt, *J. Chem. Phys.*, **50**, 2176 (1969).
 (23) A. L. Farragher, F. M. Page, and R. C. Wheeler, *Discuss. Faraday Soc.*, **37**, 203 (1964).
 (24) J. Jortner and U. Sokolov, *Nature (London)*, **190**, 1003 (1961).
 (25) J. D. Weisner and B. H. Armstrong, *Proc. Phys. Soc.*, **83**, 13 (1964).
 (26) G. Giomousis and D. P. Stevenson, *J. Chem. Phys.*, **29**, 294 (1958).
 (27) H. A. Landolt and R. Börnstein, "Zahlenwerte und Functionen," Vol. 1, Part 1, 6th ed, Springer, Berlin, 1951, p 514.
 (28) "Handbook of Chemistry and Physics," 50th ed, The Chemical Rubber Publishing Company, Cleveland, Ohio, 1969, p E-72.
 (29) S. K. Gupta, E. G. Jones, A. G. Harrison, and J. J. Myher, *Can. J. Chem.*, **45**, 3107 (1967).
 (30) C. E. Melton, "Principles of Mass Spectrometry and Negative Ions," Marcel Dekker, New York, N. Y., 1970, p 233.

On Abstraction or Stripping of CH₂ as a Route to Acetylene Formation in Hot Carbon Atom Reactions

Timothy Rose*

Department of Chemistry, Texas A & M University, College Station, Texas 77843

and Colin MacKay

Department of Chemistry, Haverford College, Haverford, Pennsylvania 19041 (Received May 21, 1973)

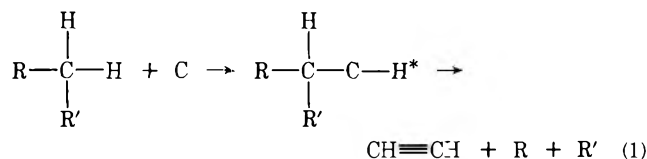
The yields of acetylene and the C₄ fragmentation products resulting from the reaction of carbon atoms with cyclopentene and cyclopentane show very different effects with changes in the experimental parameters. Analysis of the results shows that more than half of the acetylene is formed by a direct reaction of a hot atom rather than through an energy equilibrated intermediate which can lead to both acetylene and the C₄ products. These conclusions are consistent with the acetylene double tracer work reported previously.

Introduction

Studies of the hot atom chemistry of the monovalent tritium and halogen atoms have revealed completely new modes of reaction unavailable to species limited to thermal energies.¹⁻³ By contrast, for some time the multivalent carbon atom was thought to undergo the same primary modes of reaction as the thermal atom, with only the relative importance of these being altered.⁴ However, recently Lemmon, *et al.*, have pointed out that the experimental observations on acetylene formation in hot C atom systems do not rule out a contribution from a high-energy stripping mechanism,⁵ and Wolf, *et al.*, have discussed formation of C₂ and C₂H_n analogs by a stripping process as a possible source of the isotopically mixed acetylene fraction found in reactions with mixtures of hydrogenated and deuterated hydrocarbons.⁶ We wish to report evidence indicating that hot C atoms remove groups such as CH₂ as a single unit in a rapid reaction which does not involve formation of an equilibrated intermediate, and may well be a direct reaction such as stripping.⁷

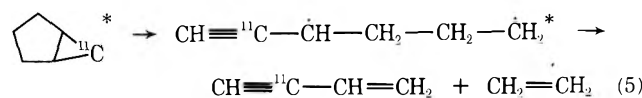
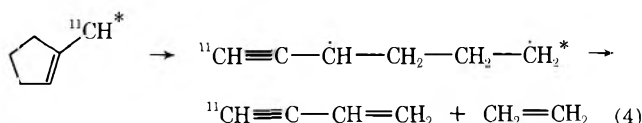
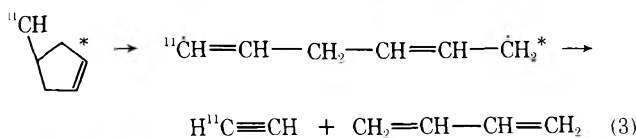
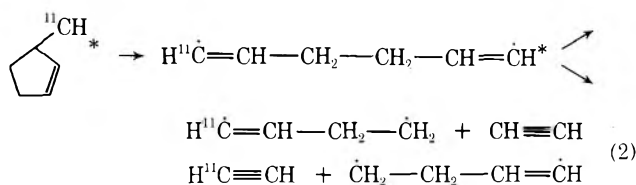
Acetylene is produced from hydrocarbons by both hot and thermal atoms.^{6,3,9} Flash photolytic experiments pro-

vide strong evidence that it is produced by the reaction of a C(¹D) atom with methane,⁹ and the production of acetylene in hot systems by two paths, one of which involves a single molecule, is well documented.^{4,6} This latter path has usually been explained as involving insertion of a C atom into a C-H bond followed by unimolecular decay of the resulting adduct.⁴



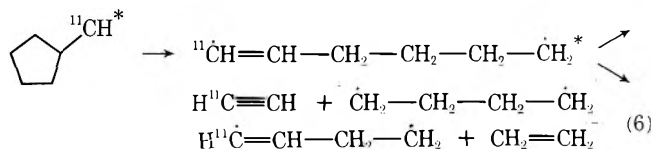
Evidence that the reaction may be more complex than indicated by this simple equation has been presented by Welch and Wolf.¹⁰

Reactions 2-4 represent some of the unimolecular decay processes expected to follow insertion of a C atom into C-H bonds of cyclopentene, and reaction 5 represents the sequence initiated by the π -bond attack which is also expected.^{4,11} Reactions 2, 3, and 4 are particularly signifi-



cant since they yield both ¹¹C-acetylene and labeled C₄ compounds from a set of very similar primary intermediates. Consequently in experiments such as those involving comparison of gas and condensed phase results in which the energy distribution of reacting ¹¹C atoms is unchanged, it seems required that with such energy equilibrated intermediates the yields of both ¹¹C-acetylene and labeled C₄ molecules be affected to about the same degree. For example, a reduction in the yield of labeled C₄ molecules from reaction 2 by a given factor should be accompanied by a reduction in the ¹¹CH≡CH yield from this reaction by about the same factor. Similarly, since (3) and (4) are quite similar, a reduction in the yield of labeled vinylacetylene from (4) should be accompanied by a roughly comparable reduction of ¹¹C-acetylene from (3).

Cyclopentane represents an even more straightforward situation. Here there is only a single primary intermediate.¹¹ Quenching of this intermediate should affect both



yields to about the same degree. Thus the *relative* yields of acetylene and C₄'s from (6) should not be greatly different in the gas and condensed phases.

Experimental Section

Standard nuclear recoil methods were used for generation of the radioactive carbon-11 atoms (20.5 min half-life).^{4,12} The details of the procedure are described elsewhere. All irradiations were done on the Yale electron accelerator (EAL) except those samples containing neon which were done on the Yale heavy ion accelerator (HILAC). The radiation damage on both accelerators has been determined to be less than 10⁻² eV/molecule.

Cyclopentene and cyclopentane were obtained commercially and had specified purities of 95–99%. Gas chromatographic analysis showed the principal impurity in the cyclopentane was cyclopentene (2–4%). Both hydrocarbons were degassed on the vacuum line before use. Matheson research grade neon and extra dry grade oxygen were used directly from the cylinders.

The separation and analysis of the labeled products of interest were carried out by standard techniques of radio gas chromatography using columns described previously.¹² Absolute yields of the gas-phase irradiations were determined using ethane as a monitor on the EAL¹³ and oxygen on the HILAC.¹⁴

Results

In Table I we show our results for gas-phase reactions of nucleogenic ¹¹C with cyclopentane and cyclopentene and compare them to the liquid-phase results of Jewett and Voigt.¹⁵ Since the addition of oxygen as scavenger has no effect on any yield,¹⁶ these data reflect primary processes which are not significantly modified by secondary reactions such as loss of C₄ radicals by reaction with radicals produced by the general radiation field.

First of all we call attention to the 95% neon moderator results. These represent a lower average energy of reaction than in the unmoderated system as is illustrated by the reduction in the yield of diacetylene relative to the unmoderated system. This is expected to be a high-energy product presumably formed by elimination of H₂ either from excited C₄H₄ formed in reactions 2, 4, and 5, or from the corresponding primary intermediates. More significant for the purposes of this paper is the marked decrease in the acetylene yield in the moderated samples relative to the unmoderated ones, indicating that most of the acetylene yield is formed in a hot reaction.

Comparison of the gas- and liquid-phase results is striking, particularly for cyclopentane. Contrary to our expectation based on formation of the energy equilibrated intermediate of (6) that in the gas and liquid phases the ratio of acetylene to butadiene should be about the same, we find it changing by a factor of about 10 in favor of acetylene. Examination of the cyclopentene data reveals the same general pattern. The yield of acetylene is barely quenched in the liquid, while that of butadiene is noticeably reduced.

Discussion

Qualitatively it seems clear from our results that most of the acetylene comes from a process or processes other than those involving the energy equilibrated intermediates of (2)–(6).¹⁷ Moreover, the process leading to acetylene must be sufficiently different from those leading to the C₄'s that it is barely quenched in the liquid phase whereas C₄ pathways are very effectively quenched. The intermediates of reactions 2–6 do not seem to meet these requirements.

The most plausible explanation of these results is that there are at least two important paths to acetylene formation. One involves unimolecular decay of energy equilibrated intermediates to either acetylene or C₄ compounds depending upon which is favored by the structure of a given intermediate. This route is effectively quenched in the liquid phase. The second type leads exclusively to acetylene formation *via* a reaction occurring on a time scale comparable to or faster than the time between collisions in solution (~10⁻¹² sec) and, therefore, is almost totally unaffected on going from gas to condensed phase. Such a reaction might better be described as a hot abstraction of CH₂ or as a stripping reaction^{1,3,5,6} rather than as an insertion into a C–H bond followed by unimolecular decay.¹⁹ As such, the mechanism resembles the type of rapid reaction at a single site which is such a

TABLE I: Yields of ^{11}C Labeled Fragmentation Products from ^{11}C Reactions with Cyclopentene and Cyclopentane

Product	Cyclopentene			Cyclopentane	
	30 cm ^a	4 cm, 76 cm Ne ^a	Liquid ^b	30 cm ^a	Liquid ^b
Ethylene	1.6 ± 0.2	nd	1.2 ± 0.07	3.8 ± 1.3	3.22 ± 0.13
Acetylene	15.2 ± 2.6	5.8	14.3 ± 0.3	22.0 ± 2.5	16.4 ± 0.5
Methylacetylene	} 0.9 ± 0.1	} 0.6	0.56 ± 0.02	} 1.6 ± 0.6	1.15 ± 0.05
Allene			0.86 ± 0.01		1.59 ± 0.08
1,3-Butadiene	2.9 ± 0.2	1.5 ± 1.0	1.79 ± 0.02	7.4 ± 0.3	0.53 ± 0.07
Vinylacetylene	11.6 ± 0.8	15.3 ± 1.4	nr	5.7 ± 0.2	nr
Diacetylene	3.4 ± 0.5	1.4	nr	0.8 ± 0.2	nr

^a Yields are per cent total ^{11}C atoms available for reaction. nd means not determined. Errors indicate the standard deviation of several measurements. Where no error is indicated only a single measurement was made and the estimated error is less than ±20%. ^b Data from ref 15. Yields are per cent of total ^{11}C atoms available for reaction. nr means not reported.

prominent feature of the chemistry of hot hydrogen atoms and which Wolfgang has classified as a direct reaction.¹

Relative Importance of the Two Routes. A natural question involves the relative importance of the two routes leading to acetylene formation. A rough estimate can be made for cyclopentane on the basis of two reasonable assumptions: (1) the yield, D , of acetylene from the fast, direct reaction is the same in the gas and liquid phases; (2) for the energy equilibrated intermediates the ratio of the yield of ^{11}C -acetylene to labeled butadiene, Y_A/Y_B , is the same in the two phases, which allows us to calculate from the butadiene yield the acetylene yield for this route. The first assumption seems justified by the small phase effect on the acetylene yield. The second seems consistent with the nature of reaction 6 as discussed above. These assumptions and the data lead to the following two equations

$$Y_G = D + (7.4 \pm 0.3)(Y_A/Y_B) = 22.0 \pm 2.5 \quad (7)$$

$$Y_L = D + (0.53 \pm 0.07)(Y_A/Y_B) = 16.4 \pm 0.5 \quad (8)$$

where Y_G and Y_L are the total gas- and liquid-phase yields of acetylene, and 7.4 ± 0.3 and 0.53 ± 0.7 are the butadiene yields in the two phases. These equations yield the values $D = 16.0 \pm 1.4$ and $Y_A/Y_B = 0.8 \pm 0.4$ which means that $73 \pm 10\%$ of the acetylene comes from direct reaction in the gas phase.²⁰ It thus appears that in the hot ^{11}C reaction with cyclopentane most of the acetylene formed arises from nonequilibrated intermediates.

The cyclopentene system is more complex than cyclopentane, and the data are not as tractable. Nevertheless we can use the above method in calculating the direct yield if we make an additional assumption. In addition, by using a previously developed empirical equation for correlating acetylene production in the C_5 molecules to the number and types of bonds, we will use the calculated direct yield from cyclopentane to estimate a value for cyclopentene. We will find that the results of the two calculations taken together imply strongly that most of the acetylene formed from cyclopentene also comes from the direct reaction.

In order to apply the cyclopentane method to cyclopentene we must make the additional assumption that the relative importance of reactions 2, 3, and 4 is not altered on going from gas to condensed phase. With this assumption we calculate $D = 12.9 \pm 4.2$, and $85 \pm 30\%$ of the acetylene is formed directly in the gas phase. While the error limits are large, this calculation does indicate that

direct production of acetylene is important in cyclopentene.

That the cyclopentane and cyclopentene results are consistent is shown by a different computation based on cyclopentane. The direct yield of acetylene from cyclopentane is $3.3 \pm 0.3\%$ per CH_2 group. Rose¹⁶ has shown for cyclopentane, cyclopentene, cyclopentadiene, and benzene that the yield of acetylene can be directly related to the number of CH_2 and $-\text{HC}=\text{CH}-$ groups, with the yield from the CH_2 group being 1.8 times from the $-\text{HC}=\text{CH}-$ group. The predicted direct yield of acetylene from cyclopentene on this basis is $11.7 \pm 0.8\%$, in good agreement with the value of D calculated above.

In summary, while we cannot make as reliable an estimate of the importance of the direct reaction from cyclopentene as we can for cyclopentane, estimates by two methods indicate strongly that for cyclopentene as for cyclopentane the direct reaction should account for at least half of the acetylene in the unmoderated systems.

Nature of the Direct Reaction. It seems reasonable to speculate on the identity of the group or groups removed in the direct reaction. Work with deuterium-labeled hydrocarbons indicates that characteristically 15–20% of the acetylene observed comes from an intermolecular reaction.⁶ For cyclopropane and benzene this rises to 35–40%, but no higher percentage of intermolecular reaction has been reported. The fact that more than half of the acetylene from cyclopentane and cyclopentene is formed directly implies that the direct reaction must have a significant intramolecular component. In other words, the CH_2 group must be removed as an entity at least part of the time. Conversion of translational energy to internal energy on subsequent collision by this translationally hot $\text{C}-\text{CH}_2$ entity can lead to bond rupture and account, at least in part, for formation of C_2 and C_2H fragments of the type discussed by Lemmon, *et al.*,⁵ and Wolf, *et al.*⁶ If a CH_2 group can be removed in a direct reaction it seems likely that a CH_3 group can be as well, and this provides an additional route to be considered in hot formation of ethylene from these groups.^{21–23}

Acknowledgment. This work was done at Yale University using the facilities of the Yale HILAC and electron accelerators. We thank the directors and staff for their cooperation. The support of this work by the Atomic Energy Commission and the Robert A. Welch Foundation is gratefully acknowledged.

References and Notes

- (1) R. L. Wolfgang, *Progr. React. Kinet.*, **3**, 99 (1965).
- (2) F. S. Rowland in "Chemical Kinetics," Vol. 9, J. C. Polanyi, Ed., Butterworths University Park Press, London, 1972, Chapter 4.
- (3) J. W. Dubrin, *Ann. Rev. Phys. Chem.*, **24**, in press.
- (4) R. F. Peterson, Jr., and R. L. Wolfgang, *Advan. High Temp. Chem.*, **4**, 43 (1971).
- (5) H. M. Pohlit, T.-H. Lin, and R. M. Lemmon, *J. Amer. Chem. Soc.*, **91**, 5425 (1969); H. M. Pohlit, W. Erwin, H. T. Lin, and R. M. Lemmon, *J. Phys. Chem.*, **75**, 2555 (1971).
- (6) R. N. Lambrecht, N. Furukawa, and A. P. Wolf, *J. Phys. Chem.*, **74**, 4605 (1970).
- (7) Evidence that high-energy stripping is a general reaction of hot species is accumulating both from studies of ion molecule reactions,³ and from theoretical studies. For a recent trajectory study on F + H₂ see J. T. Muckerman, *J. Chem. Phys.*, **57**, 3388 (1972).
- (8) J. Villaume and P. S. Skell, *J. Amer. Chem. Soc.*, **94**, 3455 (1972).
- (9) W. Braun, A. M. Bass, D. D. Davis, and J. D. Simons, *Proc. Roy. Soc., Ser. A*, **417** (1969); D. Husain and L. J. Kirsch, *Trans. Faraday Soc.*, **67**, 2025 (1971).
- (10) M. J. Welch and A. P. Wolf, *J. Chem. Soc. D*, 117 (1968); *J. Amer. Chem. Soc.*, **91**, 6584 (1969).
- (11) These representations are not meant to exclude the possibility of direct decomposition of the primary intermediate to a given product.
- (12) J. Dubrin, C. MacKay, and R. Wolfgang, *J. Amer. Chem. Soc.*, **86**, 4747 (1964).
- (13) G. Stocklin and A. P. Wolf, *J. Amer. Chem. Soc.*, **85**, 229 (1963).
- (14) J. Dubrin, C. MacKay, M. L. Pandow, and R. Wolfgang, *J. Inorg. Nucl. Chem.*, **26**, 2113 (1964).
- (15) G. L. Jewett and A. F. Voigt, *J. Phys. Chem.*, **75**, 3201 (1971).
- (16) T. Rose, Ph.D. Thesis, Yale University, 1967.
- (17) A possible explanation of these results is that we lose C₄ compounds by bimolecular reaction in the condensed phase, but do not do so in the gas. This seems unlikely. As already mentioned, gas-phase experiments with O₂ show no reduction in C₄ yield. This indicates that the processes which convert the radicals of (2) and (6) to molecules, which are probably primarily H atom shifts, are fast compared to the rate of addition of these radicals to O₂. In condensed phase, C₄ radicals can be removed by coupling to radiation produced radicals, or, in the cyclopentene, by addition to the double bond. However, under our conditions radical concentrations are too low to compete with the indicated rapid intramolecular process (ref 12). Addition of radicals to olefins also seems to be too slow to compete effectively (ref 18). Even if C₄ radicals were removed, in the cyclopentene experiments only sequence (2) would be affected. However, butadiene, the most likely product of (2), is least affected of all the C₄'s by the phase change.
- (18) J. A. Kerr and A. R. Trotman-Dickenson, *Progr. React. Kinet.*, **1**, 100 (1961); J. M. Tedder and J. C. Walton, *ibid.*, **4**, 37 (1967).
- (19) We have not discussed the possible consequences of the fact that our system contains both singlet and triplet atoms. For the purpose of this paper we need only note that the existence of a unique route to acetylene formation cannot be simply explained as involving energy equilibrated intermediates, whether singlet or triplet, since both types of intermediates should give C₄ and C₂ radioactive products in the way discussed above. We do not rule out the very reasonable possibility that the rapid hot formation of acetylene which we note involves a hot triplet atom as an abstracting reagent, while the path which involves insertion followed by unimolecular decay involves only a singlet.
- (20) Since this comparison involves results from two different laboratories, the question of the effect of a systematic difference in the two sets of results is of interest. The most drastic effect would occur if the condensed phase yields were systematically lower than those quoted here. As one example, if the condensed phase yields were reduced by a factor of 1.5, the direct yield in the gas phase would be 47 ± 7%. This is an extreme assumption, so it seems unlikely that such systematic differences would alter our general conclusion that the direct reaction accounts for more than half of the acetylene yield in the unmoderated system.
- (21) For discussions of ethylene production by insertion of a CH radical see the following: A. P. Wolf and G. Stocklin, Abstracts, 146th National Meeting of the American Chemical Society, Denver, Colo., Jan 1964, p 326; D. E. Clark and A. F. Voigt, *J. Amer. Chem. Soc.*, **87**, 5558 (1965); G. F. Palino and A. F. Voigt, *ibid.*, **91**, 242 (1969); and ref 15.
- (22) Hot abstraction of monovalent atoms by C atoms is known (ref 4).
- (23) Note Added in Proof. Professor A. F. Voigt, private communication, has recently informed us that later work in his laboratory showed that the yields reported in ref 15 should be divided by 1.23. With the corrected yields the direct yield for cyclopentane should be 12.5 ± 1.2, and from cyclopentene 8.0 ± 3.3. The direct yield for CH₂ group from cyclopentane is 2.5 and estimated direct yield from cyclopentene using the method of Rose¹⁶ is 8.9%. The main conclusion of the paper, that a hot reaction leading to nonequilibrated intermediates accounts for the bulk of the acetylene yield, is unchanged.

Heterogeneous Loss Reaction of Carbon Monosulfide¹

R. J. Richardson,* H. T. Powell, and J. D. Kelley

McDonnell Douglas Research Laboratories, McDonnell Douglas Corporation, St. Louis, Missouri 63166 (Received May 3, 1973)

Publication costs assisted by McDonnell Douglas Corporation

A mass spectrometer study of the loss of gas-phase carbon monosulfide is presented; the principal loss mechanism is found to be a heterogeneous wall reaction producing carbon disulfide and a carbon-rich wall deposit. Carbon monosulfide lifetimes are found to be of the order of minutes in a clean vessel but are reduced to seconds once a surface layer of the deposit is formed. The loss of gas-phase CS at room temperature does not appear to be accompanied by formation of a solid CS polymer as has been widely assumed.

Introduction

Carbon monosulfide (CS) can be produced in the gas phase from the electrical discharge^{2a} or thermal dissociation^{2b} of carbon disulfide (CS₂) vapor. The CS molecule is not a reactive free radical in that it has a singlet ground state³ and has been observed to persist at low pressures for times ranging from a few seconds to many minutes.⁴

The mechanism for CS disappearance involves reaction at the vessel surface; hence, the lifetime depends on surface to volume ratio.

Dewar and Jones^{2a} postulated that the principal surface reaction responsible for CS loss is a simple polymerization at the wall. In a later investigation, Hogg and Spice⁵ presented a qualitative argument that the formation of a (CS)_n polymer from CS would be exothermic. Although

reference to this polymer appears throughout the literature in studies of CS₂,⁵⁻⁸ the experimental evidence supporting polymer formation is inconclusive. Both Dewar and Jones and Hogg and Spice studied the behavior of solid CS condensed at 77 K. Upon warming, this condensate undergoes a rapid and sometimes explosive reaction leaving a nonvolatile solid residue. This residue was found to contain carbon and sulfur in the ratio of 3:1 by Hogg and Spice and 1:1 by Dewar and Jones; no attempt was made to identify any volatile products.

We have studied the loss of gaseous CS at room temperature using a mass spectrometer to monitor the contents of a closed CS sample bulb. Our results indicate that the loss of CS proceeds at the wall by a reaction which produces CS₂ and a carbon-rich solid rather than a CS polymer. In addition, we have studied the effect of various wall coatings on the CS loss rate.

Experimental Section

The apparatus used in this investigation is depicted schematically in Figure 1. The CS₂ vapor was introduced into the glass flow system through a needle valve; the backing pressure was supplied by degassed liquid CS₂ (reagent grade, Matheson Coleman and Bell) immersed in a water bath at room temperature. An Evenson microwave cavity⁹ was operated with about 40 W of incident power to decompose the CS₂.

Typically the CS₂ pressure at the microwave discharge was approximately 1 Torr and the CS₂ flow rate about 15 μmol/sec. A trap was placed between the discharge and the CS collection bulb and maintained at a temperature of 156 K by an ethanol slurry. Without the microwave discharge, the trap reduced the downstream CS₂ pressure to a few mTorr as measured with a capacitance manometer pressure gauge (MKS 90M-XRP Baratron equipped with a 90H-1SP head). A quadrupole mass spectrometer (Uthe Technology 100C) was used to monitor the CS and CS₂ concentrations in the glass sample bulb through a 0.05 mm diameter hole in the closed end of a glass tube.

With the discharge, a pressure rise was observed in the sample bulb accompanied by a rise in the mass 44 intensity which was attributed to the production of CS in the discharge. A search for other gaseous products in the sample bulb indicated that only CS and CS₂ were present downstream from the trap. When the sample bulb was valved off, the CS mass peak was observed to decay and the CS₂ peak to rise in direct correspondence to the CS decay. During subsequent runs the CS decay time decreased and the sample bulb darkened with a homogeneous solid deposit which could be removed by baking the glassware at 900 K in an annealing oven.

The carbon to sulfur ratio of the solid material deposited during the CS loss was determined in the following manner. A sealed Pyrex sample bulb containing the deposit from several runs plus 60 Torr of oxygen was heated in a furnace at 900 K. The end products of this oxidation procedure were found to be carbon dioxide and sulfur dioxide, and they were separated from the remaining oxygen with a liquid nitrogen trap. Their concentration was then measured by the previously calibrated mass spectrometer to determine the molar carbon to sulfur ratio of the original deposit.

Results and Interpretation

Experimental curves for a 5-l. sample bulb which had been twice previously filled with CS are shown in Figure

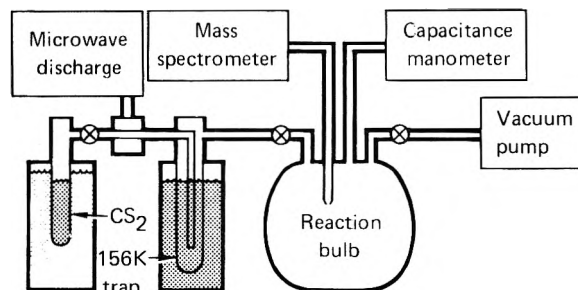
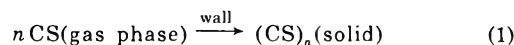


Figure 1. Apparatus used to study CS loss in a closed system. The CS₂ is removed from the flow stream by the trap at 156 K and the contents of the reaction bulb are monitored by the mass spectrometer.

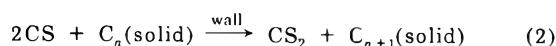
2. The mass 76 peak is proportional to CS₂ concentration, and the mass 44 peak is proportional to CS concentration plus a cracking peak from CS₂. When the microwave discharge was initiated at time A, the discharge extended on either side of the cavity for several centimeters. At time B the discharge collapsed to the size of the microwave cavity and produced a sharp rise in the CS production. At time C the sample bulb was valved off with a total pressure of 68 mTorr above the background level,¹⁰ 64 mTorr of CS and 4 mTorr of CS₂. The CS₂ contribution to the total pressure at point C was calculated from the 76 peak height and the measured sensitivity of the mass spectrometer to CS₂.

These data show the CS concentration decaying exponentially in the isolated bulb. This decay was accompanied by an increase in CS₂ pressure and a decrease in the total pressure, both with the same time constant as the CS decay. The bulb leak rate and the pump-out rate resulting from the mass spectrometer sampling hole were negligible on the time scale of Figure 2. The portion of the final CS₂ pressure attributable to the decay of CS was 24 mTorr. During successive runs the decay constant for the CS loss became progressively shorter and was accompanied by the formation of the homogeneous solid deposit on the walls mentioned previously. However, the conversion ratio of original CS pressure to final CS₂ pressure remained at about 35% for each run.

Previous investigators have generally attributed the primary removal mechanism of CS from the gas phase to a wall reaction



in which energy is released. Since we have observed the decay of CS to be accompanied by the production of CS₂, we propose the simplest alternative reaction that produces CS₂. The stoichiometry of this reaction at the deposited carbon surface is



This reaction as written is exothermic by 50 to 100 kcal/mol. The upper limit of 100 kcal/mol can be obtained from the following ΔH_f° values: CS, 65 kcal/mol;¹¹ CS₂, 28 kcal/mol;¹² C₅, 230 kcal/mol;¹² C₆, 230 kcal/mol.¹² The values used for C₅ and C₆ are those for the molecules in the gas phase; their use is equivalent to assuming that a C-C_n bond energy of about 170 kcal/mol is appropriate in reaction 2. If a C-C_n bond energy as low as 120 kcal/mol is assumed, the lower limit of 50 kcal/mol is obtained for the exothermicity of reaction 2.

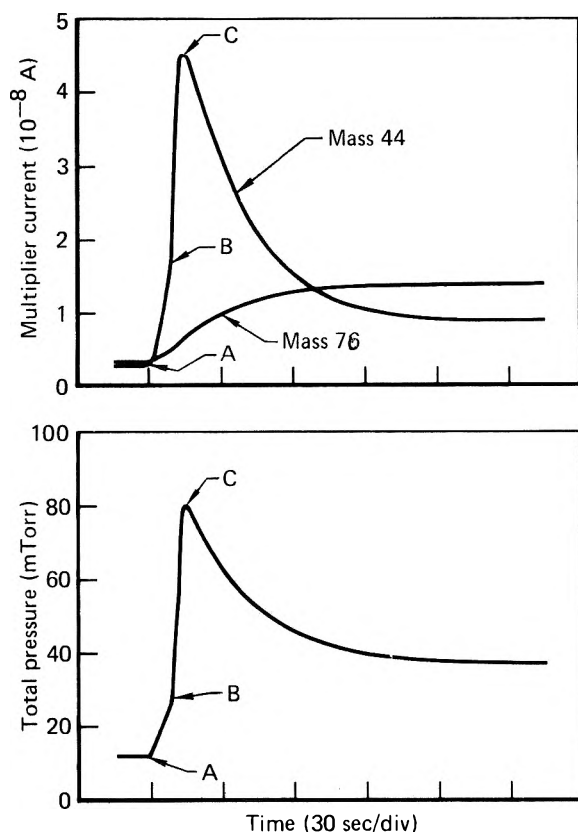


Figure 2. The upper figure illustrates the loss of mass 44 and increase of mass 76 as a function of time. The total pressure is plotted on the same time scale in the lower figure. At time A the discharge is turned on, collapses (see text) at time B, and is isolated from the sample bulb at time C.

Since the stoichiometry of the reaction is such that one CS_2 molecule is created for every two CS molecules destroyed, the final total pressure attained in a closed system containing pure CS should be 50% of the starting pressure. The observed final percentage is about 35%. Part of the missing CS_2 is likely adsorbed by the carbon deposited on the walls by the reaction itself; in a separate experiment a small amount of CS_2 was released from this deposit when the evacuated sample bulb was warmed.

The observed ratio of the final pressure of CS_2 , produced by the decay, to the initial pressure of CS requires by stoichiometry that the carbon to sulfur ratio of the wall deposit for a single run be about 2 to 1. Numerous analyses of the wall coatings produced by several runs yielded molar carbon to sulfur ratios from 1.5:1 to 5:1. This variability in the carbon to sulfur ratio is probably caused by absorption and desorption of CS_2 as the deposits were alternately exposed to CS_2 vapor and vacuum in the deposition procedure. Nevertheless, the carbon to sulfur ratio is always appreciably greater than unity and is, therefore, like the gas-phase data, inconsistent with simple CS polymerization.

These experiments do not reveal the nature of the induction process by which the first carbonaceous layer is deposited on a clean surface. A calculation of the quantity of material available indicates that approximately one monolayer is deposited during each run. At the beginning of the first run in a clean vessel the CS loss proceeded quite slowly with an apparent decay time of many minutes. However, the loss rate increased markedly during the run and a clear deviation from exponential decay was

observed. After the first three or four runs, simple exponential decays with decay constants of about 20 sec were observed. A possible mechanism consistent with the stoichiometry of reaction 2 and the apparent first-order kinetics is a reaction at the carbon surface between gas-phase CS and previously adsorbed CS.

To investigate the reactivity of CS with carbon surfaces, a 1-l. side bulb was attached to the main bulb and coated with charcoal powder. After the main bulb was filled with CS and isolated, the side arm was opened and the effect of the powder on decay time and gaseous end products was observed. The charcoal powder reduced the decay time to about 10 sec, and a negligible amount of CS_2 was released. However, when the charcoal-covered side bulb was filled with CS_2 vapor at about 1 Torr and the experiment repeated, the CS_2 was produced as the CS decayed in approximately the same proportion as in a clean bulb. In addition to the increased surface area, the same mechanism appears to be operating here as in the case of a "dirty" system except that fresh charcoal is able to adsorb all of the CS_2 released by the reaction.

The effect of coating the surfaces exposed to CS in the sample bulb with various oils was also investigated. In the case of the highly viscous Santovac 5 (a polyphenyl ether diffusion pump fluid, manufactured by Monsanto Co.) the decay constant changed slowly from 1 min to 30 sec during many successive runs. The liquid surface coating apparently retards the surface reaction and should have practical application for maintaining substantial CS concentrations.

Conclusion

This investigation indicates that CS loss from the gas phase proceeds by a wall reaction which produces CS_2 and a carbon-rich solid. The observed rate depends upon surface condition and is markedly slower in a clean glass bulb than in one with walls coated by the carbon deposit. The data are not consistent with the assumption of simple CS polymerization as the loss mechanism although the chemical incorporation of some sulfur in the solid reaction product cannot be excluded. The polymerization mechanism, mentioned previously, was suggested by Dewar and Jones and supported by Hogg and Spice on the basis of studies of CS condensed at 77 K and subsequently warmed, while our experiments were performed at room temperature. However, their observations can also be interpreted in terms of reaction 2 accompanied by adsorption of CS_2 and/or chemical incorporation of some sulfur in the residue.

Acknowledgment. The authors wish to acknowledge the able assistance of D. L. Panter and M. A. Grayson in the analysis of the carbon deposit. We would also like to thank W. Q. Jeffers for providing the impetus to consider this problem.

References and Notes

- (1) This research was supported by the Office of Naval Research.
- (2) (a) J. Dewar and H. Jones, *Proc. Roy. Soc., Ser. A*, **85**, 574 (1911); (b) T. C. Peng, *J. Phys. Chem.*, submitted for publication.
- (3) F. H. Crawford and W. A. Shurcliff, *Phys. Rev.*, **45**, 860 (1934).
- (4) See, for example, J. E. Wollrab and R. L. Rasmussen, *J. Chem. Phys.*, **58**, 4702 (1973).
- (5) M. A. F. Hogg and J. E. Spice, *J. Chem. Soc.*, 4196 (1958).
- (6) P. J. Dyne and D. A. Ramsay, *J. Chem. Phys.*, **20**, 1055 (1952).
- (7) M. de Sargo, A. J. Yarwood, O. P. Strausz, and H. E. Gunning, *Can. J. Chem.*, **43**, 1886 (1965).
- (8) W. P. Wood and J. Heicklen, *J. Phys. Chem.*, **75**, 854 (1971).
- (9) F. C. Fehsenfeld, K. M. Evenson, and H. P. Broida, *Rev. Sci. Instrum.*, **36**, 294 (1965).

- (10) Although the capacitance manometer indicates pressure changes to an accuracy greater than 1 mTorr, the initial background pressure, largely air, shown in Figure 2 is nominal.
- (11) Recent determinations of ΔH_f° (CS) range from ~ 63 to ~ 70 kcal/mol: (a) G. Hancock, C. Morley, and I. W. M. Smith, *Chem. Phys. Lett.*, **12**, 193 (1971); (b) S. Bell, T. L. Ng, and C. Suggitt, *J. Mol. Spectrosc.*, **44**, 267 (1972); (c) D. L. Hildebrand, *Chem. Phys. Lett.*, **12**, 193 (1971).
- (12) "JANAF Thermochemical Tables," 2nd ed, National Bureau of Standards, Washington, D. C., 1971.

Kinetics and Mechanism for the Photolysis of Nitrogen Dioxide in Air¹

D. H. Stedman*

Institute for Environmental Quality and Department of Chemistry, University of Michigan, Ann Arbor, Michigan 48104

and H. Niki

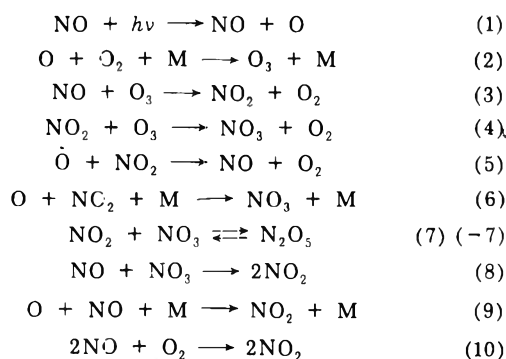
Ford Motor Company, Science Research Laboratory, Dearborn, Michigan 48121 (Received March 30, 1973)

Publication costs assisted by the Ford Motor Co.

The photolysis of low concentrations (0.9–100 ppm) of nitrogen dioxide in air was investigated using NO/O₃ chemiluminescence detectors. The rate constants of three of the elementary reactions were directly determined at 298°K: $2\text{NO} + \text{O}_2 \rightarrow 2\text{NO}_2$, $k_{10} = 4.0 \pm 0.2 \times 10^{-38} \text{ cm}^6 \text{ sec}^{-1}$; $\text{NO}_2 + \text{O}_3 \rightarrow \text{NO}_3 + \text{O}_2$, $k_4 = 6.5 \pm 0.8 \times 10^{-17} \text{ cm}^3 \text{ sec}^{-1}$; $\text{NO} + \text{O}_3 \rightarrow \text{NO}_2 + \text{O}_2$, $k_3 = 1.73 \pm 0.1 \times 10^{-14} \text{ cm}^3 \text{ sec}^{-1}$. The rate constant ratio for $\text{O} + \text{NO}_2 \rightarrow \text{O}_2 + \text{NO}$ to $\text{O} + \text{O}_2 + \text{M} \rightarrow \text{O}_3 + \text{M}$ was also determined.

Introduction

The reactions occurring in the photolysis of low concentrations of NO₂ in air are important in the chemistry of both photochemical smog and the upper atmosphere. Previous investigations of reactions occurring in this system are summarized in recent reviews.²⁻⁴ There is general agreement that the following reactions are involved in the mechanism of the photolysis of NO₂ in dry air.



In the present report, this system of reactions was studied using the high sensitivity and fast response speed of chemiluminescent NO/O₃ detectors.^{5,6} The results have provided some new rate constants for the individual reactions and a rapid method of measuring the effective light intensity (k_1) in a photochemical smog reactor.⁷

Experimental Section

In these experiments the concentration/time profiles of

NO, NO₂, and O₃ in a photochemical reactor were determined at atmospheric pressure and room temperature, 298 ± 2°K.

The gases used to make up the bulk of the air were ultra-high-purity nitrogen (American Cryogenics) and ultra-high-purity oxygen (Matheson), without further purification. The only hydrocarbon impurity detected was 4.2 ppm of methane. The relative humidity in these sample gases was less than 1.5%, which was the lowest detection limit of the electrical sensors used (Hewlett-Packard and Phys. Chem. Research Corp.). For the reactant gases, nitric oxide was trapped over liquid N₂ from cylinder gas (Matheson) and then distilled from liquid O₂ to liquid N₂, rejecting the first and last fractions. Nitrogen dioxide was prepared from this nitric oxide by adding an excess of oxygen in a 2-l. flask at room temperature and then trapping the product at 77°K. These oxides of nitrogen were stored as solids at 77°K. Known concentrations of ozone in oxygen were prepared by irradiating the O₂ by a mercury penlight in a flow system.

Nitric oxide and nitrogen dioxide were introduced into transfer vessels of known volume (10–1000 cc) by warming the traps to obtain the required vapor pressure, which was read using a pressure transducer (Pace Whittaker). The contents of the transfer vessels were then flushed first with nitrogen and then with oxygen, into the photochemical reactor, which was a 44-l. Pyrex bell jar. The first flush with N₂ was to minimize oxidation of NO to NO₂ in the transfer process. Most experiments were carried out at 760 Torr total pressure with 150 Torr of O₂. Mixing of the reactant gases was achieved in less than 1 min with a

multiperforated Pyrex inlet tube designed so as to direct incoming gas tangentially throughout the height of the bell jar.

The bell jar rested on the Teflon-coated stainless steel plate with Viton gasket. The vessel surface was 93% Pyrex and 7% Teflon with the surface-to-volume ratio 0.2 cm⁻¹. The vessel was pumped down between runs to 7–10 μ pressure by means of a liquid N₂ foreline trap and a mechanical pump.

Illumination was provided by a single air-cooled F40 BLHO black-light fluorescent tube mounted on the axis of the bell jar, or externally by twelve air-cooled black-light fluorescent lamps. The ultraviolet light intensity was qualitatively measured by a sodium salicylate-sensitized Cd/Se photocell which was mounted behind a Corning glass 7-60, 3000–4000 Å filter and diffuser. This light monitoring device indicated that it could take as long as 6 sec for the twelve lamps to all switch on. Furthermore, the total light output reached a stable level only after 20–30 min of warm-up. Therefore, in order to conduct experiments in a constant light intensity the lamps were warmed up for a period of 30–60 min, and the bell jar was covered with a black cloth shutter. This shutter could be lifted off in less than 1 sec for the purpose of observing the transient behavior of NO and O₃ under constant-illumination conditions. This arrangement was used for the majority of the experiments.

Two movable 10-μ diameter, 5-cm long capillaries inside the reaction vessel were used to sample nitric oxide and ozone into the chemiluminescent analyzers with flow rates of 35 cc min⁻¹ each. The chemiluminescent analyzers have been described previously.⁵ These analyzers were operated with a noise level ~1 ppb and overall response time <1 sec. The detector for NO was fitted with a converter which could be placed in the incoming sample stream. This converter consisted of a molybdenum impregnated carbon tube operated at 475°. In this device NO₂ was reduced to NO such that a total [NO_x] reading could be made. By reading [NO] independently, [NO₂] was obtained by subtraction. The construction and calibration of this converter have been described elsewhere.⁸ Some experimental results suggested that this converter might be sensitive to higher oxides of nitrogen and perhaps to HNO₃. A sample of N₂O₅ was prepared by the method described by Schott and Davidson.⁹ When 2 ppm of N₂O₅ was introduced into the vessel, a signal corresponding to <0.2 ppm NO_x was observed; but on repeating the experiment several times, a response comparable to [NO_x] equal to twice the initial [N₂O₅] was obtained. However, the reading tended to wander ±20% over a period of 3–4 min. A similarly variable response was observed for HNO₃, although the signal never exceeded one half that for a comparable [NO_x]. This effect made it impossible to measure the decay of NO₂ in excess O₃.

The NO detector was calibrated with 52 ppm of NO in N₂ (Scott Research Labs). A standard photolytic ozone source was constructed and calibrated by the titration with nitric oxide described elsewhere.⁵ The ozone detector was calibrated against this standard source.

Results

2NO + O₂. In this experiment the rate constant for reaction 10 was measured directly. The concentration of NO was followed as a function of time in the presence of known concentrations of O₂. Second-order decay of [NO]

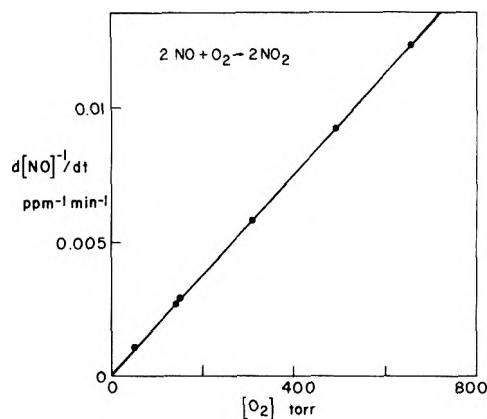


Figure 1. The effect of [O₂] on the second-order decay rate of NO at 298°K and 1 atm pressure of N₂.

was observed for the range between 1000 and 5 ppm,⁵ with no observable effect of [H₂O] between 1.5 and 60% humidity. Figure 1 shows the slopes of these second-order decays as a function of the oxygen concentration. From this figure a rate constant $k_{10}(-d[NO]/dt = k_{10}[NO]^2[O_2])$ was determined to be $4.0 \pm 0.2 \times 10^{-38}$ cm⁶ sec⁻¹ ($k[O_2] = 2.8 \times 10^{-4}$ ppm⁻¹ min⁻¹) under atmospheric conditions.

When the vessel was illuminated in the presence of 30 ppm of NO, the observed rate of NO oxidation was slower than the dark reaction 10. This was expected from the mechanism, since the product NO₂ is photolyzed back to NO. However, the dark reaction of 1 ppm of NO in air, which is very slow, was accelerated by uv illumination, such that a typical loss of 0.15 ppm was observed in the first 2 hr. The decay due to the dark reaction was ~0.04 ppm. Similar results have been described previously by Bufalini and Stephens.¹⁰ This observation cannot be explained on the basis of the earlier mechanism and is discussed later.

NO₂ + O₃. In an attempt to measure a rate constant for reaction 4, the experiments were carried out by adding small concentrations of O₃ in oxygen together with excess NO₂ and monitoring the decay of [O₃]. Figure 2 shows typical behavior of first-order decays of O₃ as a function of [NO₂]. The first-order decay slopes are plotted against [NO₂] in Figure 3, from which is derived a rate constant k_4 of $6.5 \pm 0.8 \times 10^{-17}$ cm³ sec⁻¹, or 9.5×10^{-2} ppm⁻¹ min⁻¹. The major sources of the measured uncertainty appear to be the measurement of [NO₂] and possible fluctuations of room temperature, since this reaction might have an activation energy¹¹ of as high as 7 kcal mol⁻¹.

Although these experiments were intentionally carried out in such a manner that the change in [O₃] should be $\ll [NO_2]_0$, some change in NO_x reading would be expected. No change was observed. An attempt was made to study the decay of NO₂ in excess [O₃]. However, the NO_x detector signal did not decay, but remained at the same magnitude as the initial signal with a slowly wandering intensity. This suggested that the converter could reduce the reaction product N₂O₅ to NO and hence give a signal. Such an effect was observed with pure N₂O₅ in separate experiments. Thus the overall stoichiometry of the NO₂ + O₃ system ($\Delta NO_2/\Delta O_3$) could not be determined by these experiments.

NO + O₃. Reaction 3 between NO and O₃ was too fast to be studied by mixing the gases in the reaction vessel. However, the reaction times of the order of 5–20 sec were easily within the response speed of the detector. There-

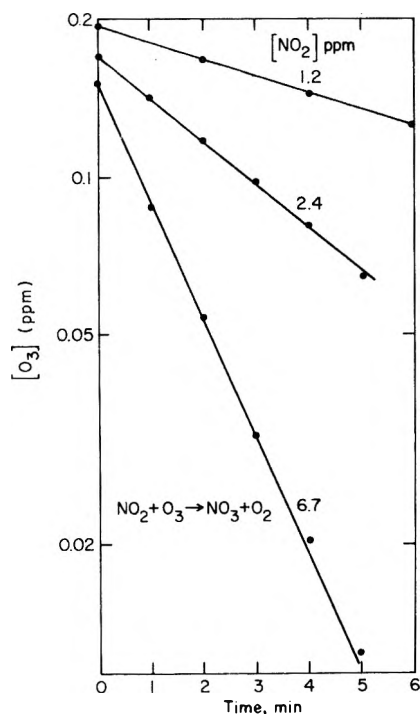


Figure 2. Some experimental logarithmic decays of O_3 in the presence of different concentrations of NO_2 at $298^\circ K$ in 1 atm of air.

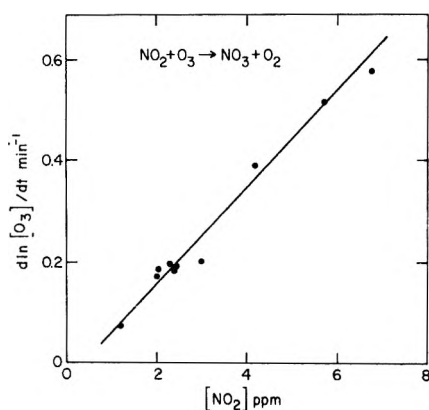


Figure 3. The effect of $[NO_2]$ on the first-order decay slopes of $[O_3]$ at $298^\circ K$ in 1 atm of air. The least-squares slope of this line gives a rate constant $k = 6.5 \pm 0.8 \times 10^{-17} \text{ cm}^3 \text{ sec}^{-1}$ ($9.5 \times 10^{-2} \text{ ppm}^{-1} \text{ min}^{-1}$).

fore, NO and O_3 were generated simultaneously in the reactor by photolyzing NO_2 in the presence of air. Subsequently, the reaction between NO and O_3 could be monitored by shutting off the light source. It was observed that in this photolysis, which is described later, there is an initial buildup of nearly equal concentrations of NO and O_3 , followed by a slow increase in [NO] and corresponding decrease in $[O_3]$. When NO reached $>10 \times [O_3]$, the lights were shut off and the decay of $[O_3]$ was measured. Typical logarithmic decays of $[O_3]$ are shown in Figure 4. After subtracting a correction ($<3\%$) for the previously determined rate of $NO_2 + O_3$, these rates were plotted in Figure 5 against the average [NO] during the decay. Another method was possible when NO_2 was photolyzed in the presence of olefinic hydrocarbons. In this $[O_3]$ increased over [NO]. Thus again by shutting off the lights with $[O_3] > 10 \times [NO]$, first-order decay of NO could be observed. The slopes of these lines are shown as a function of the

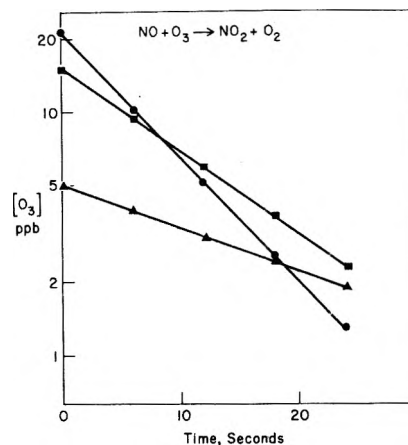


Figure 4. Some experimental logarithmic decays of $[O_3]$ after shutting off the lights during the photolysis of NO_2 . The concentrations of NO were 270, 180, and 88 ppb.

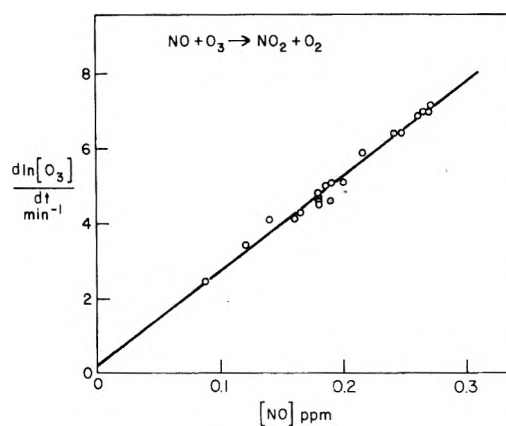


Figure 5. The effect of $[NO]$ on the first-order decay slopes of $[O_3]$ in excess $[NO]$. The least-squares slope of the line gives a rate constant $1.76 \pm 0.08 \times 10^{-14} \text{ cm}^3 \text{ sec}^{-1}$ ($26 \text{ ppm}^{-1} \text{ min}^{-1}$).

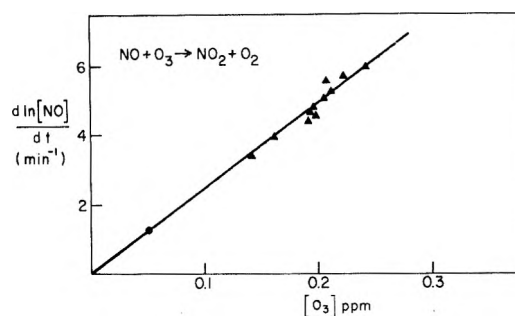


Figure 6. The effect of $[O_3]$ on the first-order decay slopes of $[NO]$ in excess $[O_3]$. The point indicated was measured as a second-order decay $[NO]_0 = [O_3]$. The least-squares slope of the line gives a rate constant of $1.69 \pm 0.13 \times 10^{-14} \text{ cm}^3 \text{ sec}^{-1}$ ($25 \text{ ppm}^{-1} \text{ min}^{-1}$).

average $[O_3]$ in Figure 6. The reaction was also measured when $[O_3]_0 = [NO]_0$. In this case $[NO]^{-1}$ was linear with time, and the observed rate is indicated in Figure 6. Thus the reaction was shown to follow a bimolecular rate law, and the rate constant obtained was $1.73 \pm 0.1 \times 10^{-14} \text{ cm}^3 \text{ sec}^{-1}$ or $25.5 \text{ ppm}^{-1} \text{ min}^{-1}$.

Photolysis of NO_2 in Air. The experimental NO and O_3 traces shown in Figure 7 were obtained during the photolysis of NO_2 between 0.9 and 8 ppm. The parallel rise of equal concentration of O_3 and NO in the first 30 sec is followed by an increase in [NO] and decrease in $[O_3]$. The

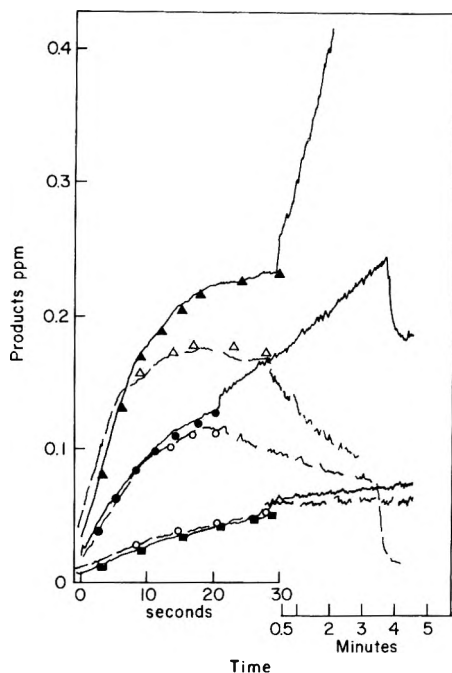


Figure 7. Experimental concentration/time profiles of NO and O₃ from the photolysis of NO₂ in air. The solid lines indicate [NO], dashed line [O₃]. The points are computed concentrations using the rate coefficients in Table II with $k_1 = 0.14 \text{ min}^{-1}$: \blacktriangle , \triangle [NO₂]₀ = 8.0 ppm, \bullet , \circ [NO₂]₀ = 3.7 ppm, \blacksquare , \square [NO₂]₀ = 0.9 ppm. The breaks halfway along are a change in chart speed from 0.1 in./sec to 0.5 in./min. The break at the end of the 3.7 ppm trace is the effect of turning off the lights.

points in Figure 7 are calculated from the mechanism and will be discussed later. The rate at which [NO] and [O₃] separated ($d[\text{NO}]/dt - d[\text{O}_3]/dt$) in the later stages of the reaction was investigated as a function of [NO₂]. The values of this parameter were plotted in Figure 8 against [NO₂] on a log-log scale. The data fall on a line of slope 2.

The initial parallel rise of [NO] and [O₃] shown in Figure 7 gives a direct method of estimating the light intensity; the details are discussed in a separate paper.⁷

Discussion

$2\text{NO} + \text{O}_2$. The rate constant of $4.0 \pm 0.2 \times 10^{-38} \text{ cm}^6 \text{ sec}^{-1}$ has been determined over a wider range of oxygen concentrations and down to lower concentrations of NO than previous work. The observed kinetics were always second order in [NO] and were first order in [O₂], as shown in Figure 1. This value is in agreement with previous studies.²⁻⁴

The result that the thermal oxidation of high concentrations of NO is inhibited by uv irradiation is expected on the basis of the mechanism. However, at low [NO] ~ 1 ppm the thermal oxidation was enhanced by uv light. This can only be accounted for in terms of a photochemical chain oxidation process for $\text{NO} \rightarrow \text{NO}_2$ conversion. This implies the presence of some unobserved impurity. This behavior has been commonly observed;¹² however, it is not frequently reported. This is a very important feature if one is to obtain reliable smog chamber data. Therefore, the decay of 1 ppm NO under illumination in clean air is a useful indicator of the state of contamination of either the surface or the inlet air of a photochemical smog reactor. We were unable to completely remove this effect by prolonged heating of the chamber to 50° under vacuum.

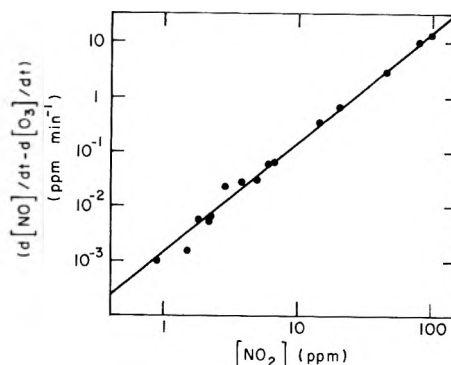
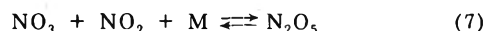
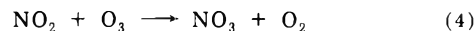


Figure 8. The dependence of $(d[\text{NO}]/dt - d[\text{O}_3]/dt)$ on [NO₂] in the photolysis of NO₂ in air on a log-log chart. A line of slope 2 is drawn over the data points.

$\text{NO}_2 + \text{O}_3$. In this study a rate constant of $6.5 \pm 0.8 \times 10^{-17} \text{ cm}^3 \text{ molecule}^{-1} \text{ sec}^{-1}$ was obtained for this reaction. The most extensive previous data on the rate constant are by Johnston and Yost.¹¹ Using $[\text{NO}_2] \sim [\text{O}_3] = 1\text{--}10 \text{ Torr}$, they obtained a rate constant of $6.3 \pm 1.7 \times 10^{-17} \text{ cm}^3 \text{ sec}^{-1}$ at 25° and an activation energy of $7.0 \pm 0.6 \text{ kcal mol}^{-1}$. Johnston and Yost¹¹ did not determine the stoichiometry of the reaction but used a previous value of 2NO₂ removed per O₃.¹³ Ford, Doyle, and Endow¹⁴ determined a rate constant in a flow reactor at concentration ~ 1 ppm. Their average rate constant is 2.98×10^{-17} , but their data spread over a factor of 2. Their stoichiometry $\Delta\text{NO}_2/\Delta\text{O}_3$ varies between 4.75 and 0.88 NO₂ removed per O₃ removed. In our system the stoichiometry could not be determined, for reasons mentioned earlier. However, the calculated rate constant is based on the equation $-d[\text{O}_3]/dt = k[\text{NO}_2][\text{O}_3]$, since $[\text{NO}_2] \gg [\text{O}_3]$ the stoichiometry does not enter directly into the evaluation of the rate constant. The expected second-order nature of the reaction is shown in Figures 2 and 3.

Wulf, Daniels, and Karrer in 1922¹³ showed that the stepwise addition of 2.3–7.3% [O₃] in ozonized oxygen to NO₂–N₂O₄ removed 2.04 ± 0.05 equivalents of NO₂. At 8.15, 11.89, and 17.04% [O₃] their stoichiometry increased to 2.5, 3.1, and 2.8, respectively. They suggested that this might have been caused by errors in their analytical procedure for determining the larger [O₃]. If the stoichiometry of 2 is accepted, then the mechanism would seem to be



as suggested by Johnston and Yost.¹¹ Reaction 4 is $25.5 \text{ kcal mol}^{-1}$ exothermic.⁹ Another possible exothermic pathway is $\text{NO}_2 + \text{O}_3 \rightarrow \text{NO} + 2\text{O}_2$, which is exothermic by $20.4 \text{ kcal mol}^{-1}$. This reaction would be followed by $\text{NO} + \text{O}_3 \rightarrow \text{NO}_2 + \text{O}_2$ and would result in lowering of the stoichiometry. This second mechanism may be related to the first in terms of the fact that two possible structures for NO₃ exist, and that some of the NO₃ produced in reaction 4 may decompose before being sufficiently stabilized. In order to determine if this mechanism is important, a study of the stoichiometry of the NO₂ + O₃ reaction under varying conditions is necessary. It is worth noting that reaction $\text{O} + \text{NO}_2$ going *via* some form of NO₃, which is $45.9 \text{ kcal mol}^{-1}$ exothermic, leads to stabilized NO₃ at atmospheric pressure at $\frac{1}{3}$ of the rate at which it decomposes to NO and O₂.^{2a}

TABLE I: Rate Constants at 298°K for the Reaction $\text{NO} + \text{O}_3 \rightarrow \text{NO}_2 + \text{O}_2$

Author	Ref	Excess	Concn range, ppm	Rate constant, $\text{cm}^3 \text{sec}^{-1} \times 10^{14}$	Estimated errors	Activation energy, kcal mol^{-1}
Johnston, <i>et al.</i>	15	O_3	50–500	2.0	Factor of 2	
Phillips, <i>et al.</i>	16	O_3	4–11	2.1	± 0.5	2.5
Marte, <i>et al.</i>	17	NO	1000	2.9	Factor of 2.5	
Clyne, <i>et al.</i>	18	NO	2–4	1.56	± 0.16	2.46
This work		Both	0.05–0.27	1.73	± 0.1	

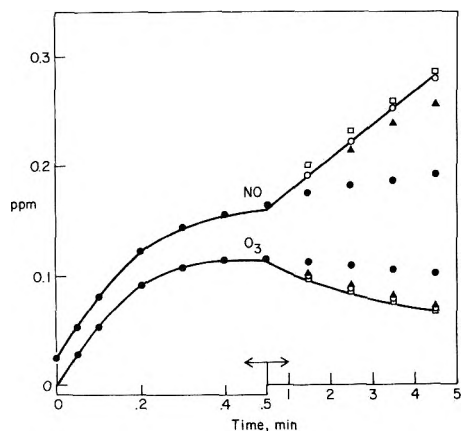


Figure 9. A computed fit to the O_3 and NO data in the photolysis of 4.2 ppm NO_2 in air using the reaction mechanism of Table II: (—) experimental; (●) calculated. Note the break in the time axis at 0.5 min.

$\text{NO} + \text{O}_3$. The dependence of $\ln [\text{O}_3]$ on time and on $[\text{NO}]$ is shown in Figures 4 and 5. Figure 6 shows the determination with O_3 in excess, and one data point at which $[\text{NO}] = [\text{O}_3]$ decayed as $[\text{NO}]^{-1} \propto \text{time}$. This is one of the three fast reactions setting up the photostationary state.^{2a,4,7} An accurate value for its rate constant is important for the determination of light intensity in photochemical reactors, or in the atmosphere. The largest systematic error in this rate determination is in the calibration of the NO and O_3 detectors. These are both calibrated using tanks of NO in N_2 , checked against standard mixtures in this laboratory and in the Analytical Services group at Ford by the Saltzmann technique. The error from this source is estimated to be less than 3%. The limits of error are derived from the least-squares analysis of the slopes of Figures 5 and 6, which combined with the calibration error lead to an overall value of $k_3 = 1.73 \pm 0.1 \times 10^{-14} \text{ cm}^3 \text{ sec}^{-1}$.

Table I^{15–18} shows that the present constant falls between the two most accurate previous studies.^{16,18} There is general agreement on an activation energy of 2.5 kcal mol^{-1} over the range from 198 to 330°K. Thus the expression $k_3 = 1.13 \times 10^{-12} \exp(-2500/RT)$ can be used to good accuracy over the range of temperatures likely to be encountered in the atmosphere. The O_3 detector was routinely calibrated against NO assuming a unit stoichiometry. This has been established in other studies.^{15,16}

The Photolysis of NO_2 in Air. This reaction was carried out at 10 ppm of NO_2 in air by Ripperton and Lillian,¹⁹ as a baseline experiment for a photochemical smog study. They observed rapid increase of NO and O_3 , as expected; but then $[\text{O}_3]$ increased slowly, and $[\text{NO}]$ decreased. This contrasts with the behavior observed here between 1 and 10 ppm NO_2 , shown in Figure 7. Ripperton and Lillian suggest that their observations may be indicative of the presence of an organic impurity.

TABLE II: Mechanism of Photolysis of NO_2 in Air

Reaction	Rate constant, $\text{ppm}^{-1} \text{ min}^{-1}$	Rate constant, $\text{cm}^3 \text{ sec}^{-1}$	Ref
1	0.15		This work ^a
2	20	1.37×10^{-14}	22 ^b
3	25.5	1.73×10^{-14}	This work
4	9.5×10^{-2}	6.5×10^{-17}	This work
5	1.25×10^4	8.3×10^{-12}	24
6	3.8×10^3	2.6×10^{-12}	7 ^b
7	4.5×10^3	3.06×10^{-12}	25
–7	14		25
8	3.2×10^4	2.2×10^{-11}	25
9	2.5×10^3	1.7×10^{-12}	23 ^b
10	2.8×10^{-4}	1.9×10^{-19}	This work ^b

^a Units min^{-1} . ^b Expressed as a bimolecular rate constant in 1 atm of air.

TABLE III: Ratio of Rate Constants $\text{O} + \text{O}_2 + \text{M} \rightarrow \text{O}_3 + \text{M}$ ($k_2[\text{M}]$) and $\text{O} + \text{NO}_2 \rightarrow \text{O}_2 + \text{NO}$ (k_5)

Author	$k_2[\text{M}]/k_5$	Ref
This work	$1.08 \pm 0.12 \times 10^{-3}$	
Schuck, <i>et al.</i>	$1.15 \pm 0.08 \times 10^{-3}$	21
Ford, <i>et al.</i>	1.33×10^{-3}	14
Bufalini, <i>et al.</i>	$\sim 6 \times 10^{-4}$	10
From Table II	$1.6 \pm 0.4 \times 10^{-3}$	
Davis, <i>et al.</i>	1.1×10^{-3}	26 ^a
Clyne, <i>et al.</i>	2.2×10^{-3}	27 ^a

^a Using the author's new values for k_5 , and $k_2[\text{M}]$ from Table II.

Experiments such as those shown in Figure 7 were conducted for the purpose of: (a) demonstrating that an analysis of $[\text{NO}]$ and $[\text{O}_3]$ in the first 30 sec of photolysis of NO_2 can lead to a direct measurement of the light intensity; and (b) understanding the details of the reactions in the NO_2 photolysis system.

The rapid buildup of equal concentrations of NO and O_3 is predicted by the first three equations in the mechanism. The slower increase of $[\text{NO}]$ and decrease of $[\text{O}_3]$ in the later stages, such that $(d[\text{NO}]/dt - d[\text{O}_3]/dt) \propto [\text{NO}_2]^2$ as shown in Figure 8 can only be interpreted with a more extensive mechanism. The best available rate constants were assigned to each step in the mechanism in Table II.

Assuming steady-state $[\text{NO}_3]$, $[\text{O}_3]$, $[\text{O}]$, and $[\text{N}_2\text{O}_5]$ in equilibrium, an analytical solution can be derived from the mechanism

$$(d[\text{NO}]/dt - d[\text{O}_3]/dt) = 2k_1k_5[\text{NO}_2]^2/k_2[\text{O}_2][\text{M}] \quad (\text{I})$$

Equation I has the correct functional dependence on $[\text{NO}]^2$ shown in Figure 8. A value of $k_2[\text{M}]/k_5 = 1.08 \pm 0.12 \times 10^{-3}$ is derived from the position of the line in Figure 8. This is compared with literature data in Table III.

The data of Table III are good evidence that the absolute rate constants are correct, and that the mechanism of Table II gives an adequate understanding of the photolysis of 1–10 ppm of NO₂. Further verification is provided by computer modeling using the experimental initial concentrations and the rate constants of Table II.²⁰ The points in Figure 8 show the results of these calculations over the first 30 sec of reaction. Figure 9 shows as solid circles the results of this calculation applied to 5 min of data from the photolysis of 4.2 ppm of NO₂. The agreement is within the errors of the absolute rate constants.

Acknowledgments. The authors acknowledge helpful discussions with Dr. E. E. Daby and other members of the Fuel Sciences Department at Ford Motor Co., where the experimental work was carried out.

References and Notes

- (1) Work performed at the Ford Motor Company.
- (2) (a) E. A. Schuck and E. R. Stephens, *Advan. Environ. Sci.*, **1**, 73 (1970); (b) H. S. Johnston, Project Clean Air 4, Task Force No. 7, Section 4, University of California, 1970.
- (3) J. Hecklen and N. Cohen, *Advan. Photochem.*, **5**, 157 (1968).
- (4) (a) P. A. Leighton, "The Photochemistry of Air Pollution," Academic Press, New York, N. Y., 1961; (b) A. P. Altshuler and J. J. Bufalini, *Environ. Sci. Technol.*, **5**, 39 (1971).
- (5) D. H. Stedman, E. E. Daby, F. Stuhl, and H. Niki, *J. Air Pollut. Contr. Ass.*, **22**, 260 (1972).
- (6) A. Fontijn, A. J. Sabadell, and R. J. Ronco, *Anal. Chem.*, **42**, 575 (1970).
- (7) D. H. Stedman and H. Niki, *Environ. Sci. Technol.*, in press.
- (8) L. P. Breitenbach and M. Shelef, *J. Air Pollut. Contr. Ass.*, **23**, 128 (1973).
- (9) G. Schott and N. Davidson, *J. Amer. Chem. Soc.*, **80**, 1841 (1958).
- (10) J. J. Bufalini and E. R. Stephens, *Int. J. Air Water Pollut.*, **9**, 123 (1965).
- (11) H. S. Johnston and D. M. Yost, *J. Chem. Phys.*, **17**, 386 (1949).
- (12) B. Dimitriades, *J. Air Pollut. Contr. Ass.*, **17**, 460 (1967).
- (13) O. R. Wulf, F. Daniels, and S. Karrer, *J. Amer. Chem. Soc.*, **44**, 2938 (1922).
- (14) (a) H. W. Ford, G. J. Doyle, and N. Endow, *J. Chem. Phys.*, **26**, 1336 (1957); (b) H. W. Ford and N. Endow, *ibid.*, **27**, 1156, 1277 (1957).
- (15) H. S. Johnston and H. J. Crosby, *J. Chem. Phys.*, **22**, 689 (1954).
- (16) L. F. Phillips and H. I. Schiff, *J. Chem. Phys.*, **36**, 1059 (1962).
- (17) J. E. Marte, E. Tschuikow-Roux, and H. W. Ford, *J. Chem. Phys.*, **39**, 3277 (1963).
- (18) M. A. A. Clyne, B. A. Thrush, and R. P. Wayne, *Trans. Faraday Soc.*, **60**, 359 (1964).
- (19) L. A. Ripperton and D. Lillian, *J. Air Pollut. Contr. Ass.*, **21**, 629 (1971).
- (20) T. E. Sharp and E. E. Daby adapted a chemical kinetics program (D. F. DeTar, *J. Chem. Educ.*, **44**, 193 (1967)) for use on the Philco-Ford timeshare system. Ford Motor Co. Scientific Lab Report No. SR 71-111.
- (21) E. A. Schuck, E. R. Stephens, and R. P. Schrock, *J. Air Pollut. Contr. Ass.*, **11**, 695 (1966).
- (22) F. Stuhl and H. Niki, *J. Chem. Phys.*, **55**, 3943 (1971), and references therein.
- (23) F. Stuhl and H. Niki, *Chem. Phys. Lett.*, **7**, 197 (1970), and references therein.
- (24) M. A. A. Clyne and H. W. Cruse, *Trans. Faraday Soc.*, **67**, 2869 (1971).
- (25) L. Zafonte, Project Clean Air 4, task Force No. 7, Section 4, University of California, 1970, and references therein.
- (26) D. D. Davis, J. T. Herron, R. E. Huie, Paper presented at the 164th National Meeting of the American Chemical Society, New York, N. Y., Aug 1972.
- (27) M. A. A. Clyne and H. W. Cruse, *J. Chem. Soc., Faraday Trans. 2*, **68**, 1281 (1972).

Photochemistry of Phenylcyclobutane. II¹

Shih Yeng Ho, Robert A. Gorse, and W. Albert Noyes, Jr.*

Department of Chemistry, The University of Texas at Austin, Austin, Texas 78712 (Received May 25, 1973)

Publication costs assisted by the University of Texas at Austin

The products of the photolysis of phenylcyclobutane have been confirmed but yields of styrene and of ethylene are somewhat higher than previously found as are yields of *cis*- and *trans*-1-methyl-2-phenylcyclopropane. The reason is probably to be ascribed to wall effects. Since fluorescence yields agree with earlier values, the effect is probably on the excited triplet state. The external heavy atom effect of added xenon is to increase somewhat the yields of styrene and of ethylene but to decrease markedly the yields of the cyclopropanes at 266 nm. Triplet sensitizers with high fluorescence yields tend to decrease product yields but others with high crossovers to triplet states have little effect. Without question styrene and ethylene must come partially but perhaps not solely from the triplet state. The source of the cyclopropanes is either the high vibrational levels of the ground state or of the triplet state. Neither state can be excluded or confirmed as the sole precursor of isomerization.

Recently Autard² has shown that phenylcyclobutane gives four principal products upon photolysis: (a) styrene; (b) ethylene; (c) *cis*-1-methyl-2-phenylcyclopropane; (d) *trans*-1-methyl-2-phenylcyclopropane. Styrene yields were always lower than ethylene yields and this was ascribed to polymerization of the styrene. All yields decreased with decrease in wavelength of the incident radiation as did

also the yield of fluorescent emission. Even at the longest wavelength used (266 nm) an energy balance was not achieved and only about 0.76 of the absorbed photons could be accounted for either by product formation or by light emission. By use of *cis*-2-butene which presumably quenches triplet but has little effect on singlet states, some evidence relating product formation to the triplet

state was adduced. Autard did not feel, however, that conclusions could be drawn with certainty which would relate the multiplicity of the excited state to a definite mode of reaction.

The present work was undertaken with a view to establishing more completely the detailed mechanism of the photochemistry of phenylcyclobutane. The external heavy atom effect to enhance crossover to the triplet state and photosensitization by other aromatic molecules have been used as aids to attempt to relate the various reactions to definite energy states. It is now apparent that either an impurity or the condition of the walls is responsible for the polymerization of the styrene and possibly also for reduction in the yields of c and d above. The photon accountability is brought up to about 0.90. The cause of the yield reduction is probably the walls since yields of fluorescence are little affected and the lifetime of the singlet excited state (probably about 50 nsec)³ is undoubtedly much shorter than that of the triplet. The present work was performed solely in the neighborhood of the (0,0) band at 266 nm. For many molecules both fluorescence and crossover to the triplet state are maxima under such conditions.

Experimental Section

Phenylcyclobutane was prepared by the reaction of phenylmagnesium bromide with cyclobutanone to give 1-phenylcyclobutan-1-ol which was subsequently reduced with sodium in liquid ammonia to give the phenylcyclobutane.⁴ The phenylcyclobutane was purified by vapor-phase chromatography on a 20% FFAP (free fatty acid phthalate) Chromasorb P column 6 m in length and 1.0 cm in diameter at 125°. The product was shown by vpc to be better than 99.95% pure.

Benzene, toluene, *o*- and *p*-xylene, *n*-hexane (all Phillips Research Grade), *n*-heptane (Matheson Spectroquality), and xenon (Union Carbide Research Grade) were used without further purification except for thorough degassing on the vacuum line.

A grease-free, mercury-free system was used for all experiments. A cold cathode vacuum gauge showed the pressure upon prolonged evacuation to be less than 3×10^{-7} Torr. The quartz photolysis cell was the same as used by Autard.² The cell and connecting Teflon stopcock (Delmar with Viton O-rings) were housed in an electrically heated asbestos oven with front and rear Supracil windows.

The light source was a Hanovia 977B-1 1000-W mercury-xenon high-pressure lamp. The light was focused on the entrance slit of a Bausch and Lomb Model 33-86-45 monochromator with a reciprocal linear dispersion of 1.6 nm per mm. The entrance slit was 2 mm in width and the exit slit 1 mm. A parallel beam about 2 cm² in cross section was passed centrally through the axis of the cell for the photochemical experiments. For measurements of fluorescence the diameter of the beam was about 5 mm. The incident light was monitored by placing a Supracil plate at 45° to the light path outside of the oven, thus reflecting part of the beam on an RCA 935 phototube. The transmitted light was also monitored by an RCA 935 phototube placed at the rear of the cell. The light entering the cell had an integrated intensity of about 3.49×10^{14} photons sec⁻¹. Fluorescence was measured by an IP28 photomultiplier tube operated on 700 V. The method of measurement of fluorescence has been described.² The integrated

intensity was measured by use of hydrogen iodide as an internal actinometer.⁵

Yields of fluorescence were made by use of benzene ($\Phi_f = 0.19$ at 253 nm)⁶ and toluene ($\Phi_f = 0.30$ at 266 nm)⁷ as standards. Light intensities were corrected for change in phototube sensitivity with wavelength.⁸

Butylcyclohexane (1%) was added to the phenylcyclobutane to serve as a convenient internal standard for the product analysis by gas chromatography. It was shown to have no effect either on the fluorescence or on the photochemistry. The use of butylcyclohexane tended to cancel out errors due to incomplete condensation of products.

A microliter syringe was used to introduce the phenylcyclobutane and other liquid reactants, following which they were thoroughly degassed.

The normal irradiation time was 30 min. Incident, transmitted, and emitted intensities were measured every 5 min.

Ethylene was determined as described previously.² The remainder of the mixture was condensed at -196° and then analyzed on a Perkin-Elmer gas chromatograph with a 15.2 m column of *m*-bis(*m*-phenoxyphenoxy)benzene-Apieszon L (MBMA) column at 70°. The three products (excluding ethylene) and the butylcyclohexane were well resolved. A planimeter was used to measure peak areas.

Xenon was expanded into the cell onto the phenylcyclobutane from a Wallace-Tiernan pressure gauge. After photolysis the mixture was cooled to -78° and the xenon pumped off. The rest of the mixture was analyzed as before.

Photopolymerization of the styrene formed during photolysis was shown to be unimportant under the present conditions by photolyzing 5 Torr of a mixture of styrene (2%), butylcyclohexane (2%), and benzene (96%) at 266 nm at 40°. Styrene recovery exceeded 98%. Ethylene was not normally determined because analysis for the styrene was more accurate.

The 30 min irradiations resulted in about 1% conversion of the phenylcyclobutane, except for the phenylcyclobutane-toluene mixtures where conversion may have reached 2%.

Results

Yields of fluorescence for pure phenylcyclobutane were determined and agree well with those obtained by Autard.² They are included in column 2 of Table I for completeness. The value obtained by Autard at 4.5 Torr at 40° was 0.28 ± 0.07 at 266 nm. The average deviation from the mean is given in Table I. It shows that there is no significant trend with pressure over the range studied.

Table II shows that xenon quenches significantly the fluorescence of phenylcyclobutane. The linear Stern-Volmer plot leads to the following equation

$$1/\Phi_f = 3.65 + 0.0201P_{Xe} \quad (1)$$

where P_{Xe} is in Torr. The slope is slightly greater than found by Autard, but agreement is good. Other foreign gases studied were *n*-hexane and *n*-heptane which give the following equations

$$1/\Phi_f = 3.70 + 0.0034P_{hex} \quad (2)$$

$$1/\Phi_f = 3.67 + 0.0092P_{hep} \quad (3)$$

The cross sections for quenching are about 0.05 and 0.14 $\times 10^{-16}$ cm², respectively. Since the data in Table III show that *n*-hexane causes a slight decrease in styrene yields while xenon causes a slight increase the quenching

TABLE I: Product Quantum Yields in the Photolysis of Phenylcyclobutane at 266 nm and 40°

[PCB] ₀ , ^a Torr	Φ _f ⁰	Φ(C ₂ H ₄)	Φ _{styrene}	Φ _{cis}	Φ _{trans}
0.5	0.260		0.472	0.048	0.071
1.0	0.267	0.520	0.503	0.060	0.077
1.0	0.261	0.509	0.497	0.053	0.070
1.0	0.271	0.499	0.480	0.052	0.068
1.0	0.266	0.518	0.505	0.048	0.068
2.0	0.270	0.512	0.498	0.050	0.061
Av	0.266	0.512	0.494	0.052	0.069
	±0.004	0.006	0.002	0.003	0.004

^a [PCB]₀ = initial pressure of phenylcyclobutane.

TABLE II: Product Quantum Yields in the Photolysis of Phenylcyclobutane-Xenon Mixtures at 266 nm and 40°

[PCB] ₀ , Torr	[Xe], Torr	Φ _f	Φ _{styrene}	Φ _{cis}	Φ _{trans}
1.0	0	0.270	0.494	0.052	0.069
1.0	50	0.205	0.504	0.012	0.014
1.0	110	0.173	0.533	0.009	0.012
1.0	216	0.132	0.566	0.005	0.007
1.0	423	0.081	0.534		

TABLE III: Product Quantum Yields in the Photolysis of Phenylcyclobutane-n-Hexane Mixtures at 266 nm and 40°

[PCB] ₀ , Torr	[n-Hexane], Torr	Φ _f	Φ _{styrene}
1.0	0	0.270	0.434
1.0	25	0.263	0.465
1.0	50	0.260	0.452
1.0	100	0.247	0.461

steps presumably are not identical. One might suggest that *n*-hexane and *n*-heptane cause a small amount of vibrational "heating" of molecules excited near the (0,0) band.⁹ Such small quenching effects are being actively studied in other laboratories and a better explanation may be forthcoming in the future.

Quenching by xenon is ascribed to an external heavy atom effect in promoting cross-over to the triplet state.⁷ No new products were identified, however. Yields are given in Table I for pure phenylcyclobutane and show no trend with pressure over the range studied.

Table II shows that the styrene yield increases by more than experimental error and may even go through a maximum. More data on this point are needed. Xenon is inefficient in causing vibrational relaxation and the hexane results (Table III) show that styrene yields are only slightly affected by vibrational relaxation. Thus the effect of the xenon on the styrene yields is best ascribed to enhanced intersystem crossing to the triplet state. This should be a near adiabatic process.

It should be noted from the data in Table I that fluorescence and products yields in these experiments conducted near the (0,0) band of phenylcyclobutane add as follows: 0.266 + 0.512 + 0.052 + 0.069 = 0.90 and 0.266 + 0.494 + 0.052 + 0.069 = 0.88. These sums differ from unity by about the limit of experimental error. In many mechanisms of photochemical isomerization it can be reasonable to postulate an intermediate which may either revert to the parent molecule or go over to an isomer. The data in

TABLE IV: Product Quantum Yields in the Photolysis of Phenylcyclobutane with Other Aromatic Molecules at 266 nm and 40°

[PCB] ₀ , Torr	[A], Torr	α	Φ _f ^T	Φ _{styrene}	Φ _{cis}	Φ _{trans}
A. Benzene (253 nm)						
1.0	0.0	1.000	0.118	0.530	0.028	0.036
1.0	5.0	0.477	0.156	0.517		
1.0	10.0	0.314	0.162	0.521		
0.5	10.0	0.186	0.171	0.521		
0.5	20.0	0.103	0.178	0.492		
B. Toluene						
1.0	0.0	1.000	0.270	0.494	0.052	0.069
1.0	2.0	0.383	0.285	0.499	0.017	0.019
1.0	5.0	0.197	0.289	0.482	0.007	0.008
1.0	10.0	0.110	0.284	0.440		
C. <i>o</i> -Xylene						
1.0	0.0	1.000	0.270	0.494	0.052	0.069
1.0	1.1	0.366	0.320	0.430	0.016	0.017
1.0	3.2	0.164	0.385	0.370		
1.0	5.4	0.104	0.401	0.330		
D. <i>p</i> -Xylene						
1.0	0.0	1.000	0.270	0.494	0.052	0.069
1.0	1.1	0.258	0.430	0.301	0.008	0.010
1.0	3.2	0.109	0.480	0.220	0.002	0.003
1.0	5.0	0.069	0.496	0.173		
1.0 ^a	0.0	1.000	0.190	0.499	0.053	0.070
1.0 ^a	5.3	0.065	0.365	0.178		
1.0 ^a	5.3	0.065	0.370	0.174		

^a Temperature = 60°.

the present experiments are not accurate enough to provide evidence for or against such an intermediate but it is quite possible that the fates of molecules of phenylcyclobutane excited to the first upper singlet state could be quantitatively accounted for in this way.

Benzene, toluene, and the three xylenes when excited near their (0,0) bands seem either to fluoresce or to cross over to their triplet states.¹⁰ Benzene may be a slight exception.¹⁰ Any of these molecules might be used as triplet sensitizers for phenylcyclobutane. Table IV shows results obtained with benzene, with toluene, with *o*-xylene, and with *p*-xylene, respectively. The fraction of the light absorbed by the phenylcyclobutane (α) is calculated from the equation

$$\alpha = \alpha_1 P_1 / (\alpha_1 P_1 + \alpha_2 P_2) \quad (4)$$

and the fluorescence yields were found to follow the relationship

$$\Phi_f^T = \alpha \Phi_f^0 + (1 - \alpha) \Phi_f' \quad (5)$$

where α₁ and α₂ are the absorption coefficients of phenylcyclobutane and of the sensitizer, respectively, and P₁ and P₂ are their corresponding pressures. The absorption coefficients were obtained experimentally using the equation I_{t,r} = I₀ exp(α_iP_i). The Φ_f^T, Φ_f⁰, and Φ_f['] are respectively the fluorescence yields of the mixture, of the pure phenylcyclobutane, and of the pure sensitizer.

With benzene and with toluene as the added gases (Table IV) styrene yields did not change much more than experimental error. Triplet yields for the two molecules seem to be about the same.¹⁰ With the two xylenes fluorescence increases because fluorescence yields for these

two molecules are higher than for phenylcyclobutane, but styrene yields are lowered possibly because triplet yields are lower.

Discussion

The results with added xenon indicate that since fluorescence of phenylcyclobutane is quenched, triplet yields should increase. If the principle products (styrene and ethylene) come from the singlet state their yields in the presence of xenon should decrease parallel to the fluorescence. If these products arise from the triplet state their yields should increase in the presence of xenon. The fluorescence yield of phenylcyclobutane drops from 0.27 to 0.081 with the addition of 423 Torr of xenon. Superficially the triplet yield might change from 0.73 to 0.92 and the styrene yield might change from 0.49 to $0.49 \times 0.92/0.73 = 0.62$. It actually increases to at most about 0.56.

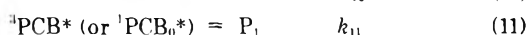
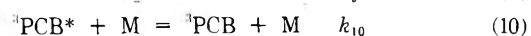
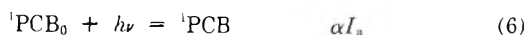
Adiabatic collision-induced intersystem crossing from excited singlet to the excited triplet state could also be accompanied by a secondary process of induced intersystem crossing from the triplet state to the upper levels of the ground singlet state. Therefore the net effect of high xenon pressures would be an apparent induced internal conversion from the excited singlet state to the ground-state singlet. This type of an effect would explain both the failure of the styrene yield to reach the theoretical value of 0.62 as well as the possible maximum in the styrene yield as the xenon pressure is increased.

Since the addition of *n*-hexane has very little effect on the styrene yield, it appears that vibrational energy in the triplet state plays only a minor role in the dissociation to give styrene and ethylene. Alternatively the dissociation from the triplet state may be very rapid (*e.g.*, the cross over might be to a repulsive triplet state most of the time, in which case dissociation would occur prior to bimolecular collisions).

The yields of the cyclopropanes decrease in the presence of xenon. They are also quenched totally in the presence of other gases. Earlier data showed these yields to decrease at short wavelengths where by analogy with other molecules cross over should be very low. It is evident that the cyclopropanes are formed from a vibrationally excited state such that rapid vibrational relaxation inhibits the isomerization reaction. Photolysis near the (0,0) band produces a singlet state with little or no vibrational energy content. The relative change in the dissociation yields to the isomerization yields in going from 266 to 254 nm (Table IV, lines 1 and 6) seems to indicate that these processes are occurring from different states. Alternatively this could be due to the onset of a contribution of the vibrationally excited singlet state to the dissociation process. The cyclopropanes are therefore most likely formed from vibrationally excited levels of the triplet state or the upper levels of the ground state populated from the triplet. There are some other cases²¹ in which conclusions of this type appear to be necessary but they are put forward here only tentatively.

The results with the triplet sensitizers require a more detailed treatment. The following mechanism is proposed and justification for the various steps will be made later.

I. Steps necessary to explain the photochemistry of phenylcyclobutane at 266 nm (near the (0,0) band) are



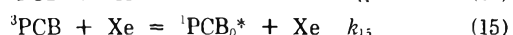
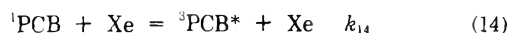
where ${}^1\text{PCB}_0$, ${}^1\text{PCB}_0^*$, ${}^1\text{PCB}$, ${}^3\text{PCB}$, and ${}^3\text{PCB}^*$ represent phenylcyclobutane in the normal ground state, in the vibrationally excited ground state, in the first excited singlet state, in the relaxed triplet state, and in the vibrationally excited triplet state, respectively. P_2 represents the dissociation products, styrene and ethylene, and P_1 represents the isomerization products, *cis*- and *trans*-1-methyl-2-phenylcyclopropane. M is anything capable of removing vibrational excitation on collision. The reaction ${}^3\text{PCB} = \text{P}_2$ is also a probable process. The ${}^1\text{PCB}_0^*$ could be formed either in a low yield internal conversion process from ${}^1\text{PCB}$ or by an intersystem crossing from ${}^3\text{PCB}$. Reaction 11 indicates the uncertainty as to which vibrationally excited molecule is the main precursor to the isomerization process.

II. Additional steps necessary at shorter wavelengths are

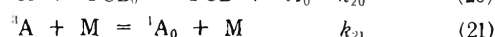
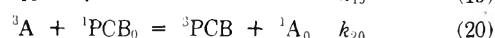


The primary products of these two states are not known but presumably both lead ultimately to ground state molecules.

III. In the presence of xenon additional steps must be introduced



IV. In the presence of aromatic sensitizers the following steps must be added



where A is a molecule of aromatic sensitizer and M is any molecule capable of producing relaxation electronically.

The nonproductive loss of singlet sensitizer molecules by (19) may only be necessary for benzene where the yields of fluorescence and of crossover to the triplet state do not seem to add to unity¹⁰ within the probable experimental error. Isomerization to benzvalene and possibly to other molecules could conceivably be responsible for this failure.¹² Collisional loss of electronic energy by (21) seems to be important in the case of the xylenes. This could lead to an excimer or to an exciplex. In any case for benzene and toluene it appears to be unimportant compared to triplet quenching by phenylcyclobutane. Triplet quenching in the case of the xylenes may be slow because of steric hindrance due to the methyl groups.

The styrene yield in pure cyclobutane is given by the product of the triplet yield, Φ_T^0 , and the fraction of the triplet state which dissociates by (9) to give P_2

$$\Phi_{\text{P}_2}^0 = [k_8/(k_7 + k_8)][k_9/(k_9 + k_{11})] \quad (22)$$

The triplet yield is at least approximately $1 - \Phi_T^0 = 0.73$ and $k_9/(k_9 + k_{11})$ is approximately $0.494/(0.494 + 0.052 + 0.069) = 0.80$ or $k_{11} = 0.25k_9$. This simple calculation neglects any possible reversion of an intermediate to the

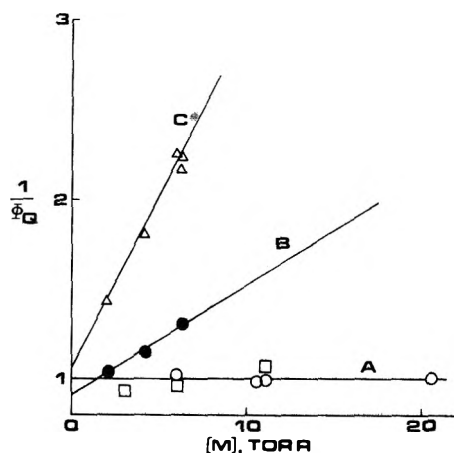


Figure 1. Plot of inverse quenching efficiency vs. total pressure for phenylcyclobutane sensitization by benzene (O), toluene (□), *o*-xylene (●), and *p*-xylene (Δ). Φ_Q is defined as the fraction of triplet sensitizer quenched by phenylcyclobutane. Curve A: $1/\Phi_Q = 1.000$; curve B: $1/\Phi_Q = 0.92 + 0.061[M]$; curve C: $1/\Phi_Q = 1.04 + 0.192[M]$; $P_{PCB} = 1.0$ Torr.

parent molecule. The styrene yield is independent of k_{10} because it is formed with equal efficiency from either 3PCB or from $^3PCB^*$.

In the presence of a sensitizer the styrene yields are given by (see Table IV)

$$\Phi_{p_2} = [k_9/(k_9 + k_{11})][(1 - \alpha)\Phi_Q\Phi_T^S + \alpha\Phi_T^0] \quad (23)$$

where Φ_Q is defined as the fraction of triplet sensitizer quenched by phenylcyclobutane. $\Phi_Q = [k_{20}(^1PCB_0)/k_{20}(^1PCB_0) + k_{21}(M)]$ and Φ_T^S is the triplet yield of the sensitizer = $k_{18}/(k_{17} + k_{18} + k_{19})$. The triplet yields used are as follows: benzene (0.72); toluene (0.70); *o*-xylene (0.60); *p*-xylene (0.50). From observed styrene yields and values of α from (4), the values of Φ_Q have been calculated. The results are plotted in Figure 1. Within experimental error $\Phi_Q = 1$ for benzene and for toluene. Thus for these two molecules all of the triplet state molecules are quenched by phenylcyclobutane, and $k_{20}(^1PCB)$ is much greater than $k_{21}(M)$ for all pressures studied. For the two xylenes Φ_Q is observed to be a function of pressure. Plots of $1/\Phi_Q$ vs. (M) give $k_{21}/k_{20} = 0.061$ and 0.192 for *o*- and *p*-xylene, respectively. In a system of 1 Torr of PCB and 10 Torr of sensitizer 38% of the *o*-xylene and 66% of the

p-xylene triplets are lost by bimolecular quenching, *i.e.*, these amounts do not form 3PCB . As stated above this may be due to a steric interaction between the methyls and the cyclobutyl ring. The validity of this assumption will be tested by CNDO-INDO calculations.

For all of the sensitizers the intercept of the plot of $1/\Phi_Q$ vs. concentration is unity, thus verifying that unimolecular loss of the triplet sensitizer is unimportant under the present conditions.

Conclusion

The data indicate that the photochemical formation of styrene and ethylene at 40° in the gaseous phase from phenylcyclobutane occurs from the triplet manifold and that the 1-methyl-2-phenylcyclopropanes are formed from a readily quenched vibrationally excited molecule which may be either the triplet state or the ground state of phenylcyclobutane. The results agree qualitatively with those of Autard. No other products are found and fluorescence is the only emission observed.

Ground-state phenylcyclobutane quenches the triplet states of benzene and of toluene quantitatively but the xylenes are quenched much less effectively. A tentative explanation for the difference is proposed.

References and Notes

- (1) The authors wish to thank the Robert A. Welch Foundation for support of this work as well as the Office of Scientific Research, Air Research and Development Command, United States Air Force.
- (2) P. Autard, *J. Phys. Chem.*, **76**, 3355 (1972). Part I of this series.
- (3) For a review of this matter see K. E. Al-Ani and W. A. Noyes, Jr., *Chem. Rev.*, submitted for publication.
- (4) S. Shabarov, N. A. Donskaya, and R. Ya Levina, *Zh. Obshch. Khim.*, **33**, 3434 (1963).
- (5) R. M. Martin and J. E. Willard, *J. Chem. Phys.*, **40**, 2999 (1964).
- (6) C. S. Parmenter, *Advan. Chem. Phys.*, **22**, 365 (1972).
- (7) C. S. Burton and W. A. Noyes, Jr., *J. Chem. Phys.*, **49**, 1705 (1968).
- (8) The response curves supplied by the manufacturer were used. Since the correction is small over the range used and was about the same as used for the standards, the errors introduced here should be negligible.
- (9) See W. A. Noyes, Jr., D. Anderson, and D. A. Harter, *J. Chim. Phys. Phys.-Biol.*, **204** (1970), special issue devoted to the 20th Reunion of the Societe de Chimie Physique, May 1969.
- (10) W. A. Noyes, Jr., and D. A. Harter, *J. Phys. Chem.*, **75**, 2741 (1971); J. B. Birks, "Photophysical Processes of Aromatic Molecules," Wiley, New York, N. Y., 1970, pp 301-371 and 420-433.
- (11) M. Comtet, *J. Amer. Chem. Soc.*, **92**, 5308 (1970).
- (12) K. E. Wilzbach, A. L. Harkness, and L. Kaplan, *J. Amer. Chem. Soc.*, **90**, 1116 (1968); L. Kaplan and K. E. Wilzbach, *ibid.*, **90**, 3291 (1968).

Quenching of the Tris(ethylenediamine)chromium(III) Phosphorescence by Some Transition Metal Ions in Aqueous Solutions

H. F. Wasgestian,^{1a} R. Ballardini,^{1b} G. Varani,^{1b} L. Moggi*^{1c} and V. Balzani^{1c}

Institut für physikalische Chemie der Universität, Frankfurt a.M., Germany; Istituto Chimico dell'Università, Centro di Studio sulla Fotochimica e Reattività degli Stati Eccitati dei Composti di Coordinazione del C.N.R., Ferrara, Italy; and Istituto Chimico "G. Ciamician" dell'Università, Bologna, Italy (Received June 8, 1973)

The intensity and lifetime quenchings of the $\text{Cr}(\text{en})_3^{3+}$ phosphorescence have been investigated in aqueous solution at room temperature. It has been found that $\text{Mn}_{\text{aq}}^{2+}$, whose lowest excited state is at 18.9 kK, does not exhibit any quenching effect, whereas $\text{Fe}_{\text{aq}}^{2+}$ and $\text{Co}_{\text{aq}}^{2+}$, which have very low lying excited states (<10 kK), do quench the $\text{Cr}(\text{en})_3^{3+}$ phosphorescence. The quenching action of CoCl_2 has been investigated under various experimental conditions. It has been found that (i) the emission intensity and lifetime are quenched in parallel, (ii) the Stern-Volmer plots (I^0/I or τ^0/τ against $[\text{CoCl}_2]$) show a positive curvature, and (iii) the quenching effect increases with increasing Cl^- concentration. The results obtained are quantitatively accounted for considering the relative abundances and the different quenching abilities of the various $\text{Co}(\text{II})$ species (e.g., $\text{Co}(\text{H}_2\text{O})_6^{2+}$, $\text{Co}(\text{H}_2\text{O})_5\text{Cl}^+$, etc.) that are present in aqueous solutions containing Co^{2+} and Cl^- ions.

Introduction

The quenching of the luminescence emission of coordination compounds in fluid solutions has been scarcely investigated. However, recent studies have pointed out that the nature of the ligands,² the charges of the complex and the quencher,²⁻⁵ and several parameters of the medium (ionic strength, viscosity, etc.^{5,6}) play important roles in determining the value of the quenching constants. The possibility of carrying out systematic investigations in this field is somewhat limited because of the difficulty of finding suitable quenchers. This is particularly true in the case of the $\text{Cr}(\text{III})$ complexes which have low absorption bands and emit at very low energies (12–15 kK). In this paper, we wish to report the results of an investigation on the quenching of the $\text{Cr}(\text{en})_3^{3+}$ phosphorescence by some transition metal ions in aqueous solution, under various experimental conditions. Some of these ions are very suitable for quenching experiments since they have low lying (<10 kK) excited states, low absorption, and high solubility in aqueous solutions. However, it will be shown that the quenching ability of these ions strongly depends on the actual nature of the species (e.g., $\text{M}(\text{H}_2\text{O})_6^{2+}$, $\text{M}(\text{H}_2\text{O})_5\text{Cl}^+$, etc.) that they are incorporated in.

Experimental Section

Materials. Tris(ethylenediamine)chromium(III) chloride dihydrate, $[\text{Cr}(\text{en})_3]\text{Cl}_3 \cdot 2\text{H}_2\text{O}$, was prepared following the procedure indicated in the literature.⁷ The corresponding perchlorate salt was obtained by adding concentrated perchloric acid to an aqueous solution of the chloride salt. $\text{FeCl}_2 \cdot 3\text{H}_2\text{O}$, $\text{CoCl}_2 \cdot 6\text{H}_2\text{O}$, $\text{MnCl}_2 \cdot 4\text{H}_2\text{O}$, and all the other chemicals used were of reagent grade.

Apparatus. The emission spectra were recorded by means of a Hitachi-Perkin-Elmer MPF-3 spectrofluorimeter equipped with a high sensitivity cell assembly and a red sensitive (R-446) photomultiplier. Luminescence lifetimes were obtained by exciting with a frequency doubled ruby laser (104 TRG/Control Data Corp.). The arrangement used has been described elsewhere.⁸

Procedures. A weighed amount of the complex was dissolved in the selected medium so as to obtain a $2.5 \times 10^{-2} M$ solution. This operation was carried out in red light. The media used were as follows: (i) aqueous solutions which contained the desired concentration of the quencher and which had been slightly acidified with HCl so as to have a pH of about 2.5; (ii) the same solutions as above, except that their total Cl^- concentration⁹ was adjusted to 2.0, 4.0, or 5.2 M by adding KCl or MgCl_2 ; (iii) aqueous solutions which contained the desired concentration of the quencher and whose total Cl^- concentration was adjusted to 2.0, 4.0, or 5.2 M by adding HCl. For the study of the intensity quenching, the excitation was carried out at 365 nm when using CoCl_2 or MnCl_2 and at 464 nm when using FeCl_2 , in order to minimize the fraction of exciting light absorbed by the quencher (see Figure 1). Because of the low phosphorescence quantum yield, large excitation and emission slits (~ 30 nm) had to be used. In order to obtain reliable I^0/I values (see Results), the measured emission intensities had to be corrected for each one of the following factors: (a) the fraction of the exciting light absorbed by the quencher (maximum values: 8% for CoCl_2 , 4% for FeCl_2 , and 5% for MnCl_2); (b) the change in the emission intensity due to the change of the total absorbance of the solution at the wavelength of irradiation (maximum changes of absorbance for 1 cm of optical path: from 1.16 to 1.26 for CoCl_2 , to 1.21 for FeCl_2 , and to 1.22 for MnCl_2); (c) the "trivial" reabsorption of the emission by the quencher (minimum transmittance for 1-cm optical path: 0.42 for CoCl_2 , 0.68 for FeCl_2 , and 0.94 for MnCl_2). The correction for point a is a simple one. The other corrections are much more complicated since they also depend on the optical geometry of the spectrofluorimeter. The methods used for such corrections were based on experimental calibration plots and they will be fully described elsewhere.¹⁰ No correction had to be made for the lifetime measurements since absorption by the quencher reduces the luminescence intensity but, obviously, does not affect the luminescence lifetime. All experiments were performed at room temperature ($\sim 20^\circ$).

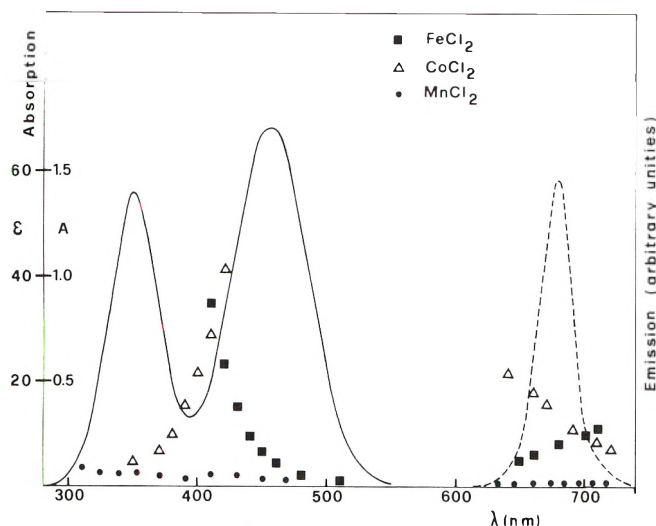


Figure 1. Molar extinction coefficients (solid line) and relative emission intensity (dotted line) of $\text{Cr}(\text{en})_3^{3+}$. The absorbances of 1.7 M FeCl_2 , 1.6 M CoCl_2 , and 2.0 M MnCl_2 are also shown.

Since it is known that under these conditions neither the intensity¹¹ nor the lifetime² of the $\text{Cr}(\text{en})_3^{3+}$ phosphorescence are affected by oxygen, all experiments were carried out in air equilibrated solutions.

Results

Quenching of the Phosphorescence Intensity. We found that the luminescence intensity of $\text{Cr}(\text{en})_3^{3+}$ in aqueous solution was not affected by the presence of KCl (up to 4 M) and MgCl_2 (up to 5.2 M), whereas HCl exhibited some quenching action ($I^0/I = 1.2$ for $[\text{HCl}] = 4$). We also found that MnCl_2 did not quench the $\text{Cr}(\text{en})_3^{3+}$ luminescence (see Figure 2). In contrast, CoCl_2 and FeCl_2 were found to exhibit a quenching effect. The Stern-Volmer plot for the quenching by CoCl_2 is shown in Figure 2. The quenching by FeCl_2 showed a very similar behavior.

Using CoCl_2 as a quencher, other experiments were carried out in order to find the reason for the positive curvature of the Stern-Volmer plot of Figure 2. It was found that the addition of Cl^- ions to solutions containing a fixed amount of $[\text{Co}^{2+}]_{\text{tot}}$ ⁹ strongly enhanced the intensity quenching. As is shown in Figure 3, for $[\text{Cl}^-]_{\text{tot}} = 2$ or 4⁹ this effect was the same regardless of whether HCl, KCl, or MgCl_2 was used for adjusting the Cl^- concentration. Some experiments were also carried out in solutions containing $[\text{Cl}^-]_{\text{tot}} = 5.2$ (adjusted with MgCl_2). Under these conditions, I^0/I was 1.9 and 4.1 for $[\text{Co}^{2+}]_{\text{tot}} = 0.1$ or 0.3, respectively.

Quenching of the Phosphorescence Lifetime. The emission lifetime of $\text{Cr}(\text{en})_3^{3+}$, τ^0 , was found to be 1.33 ± 0.03 μsec in aqueous solution at room temperature. This value is in agreement with a previously reported one¹² and is also similar to the values obtained in different media.^{2,8} We found that the presence of 1.1 M MnCl_2 or MgCl_2 (up to 5.2 M) did not affect the emission lifetime of $\text{Cr}(\text{en})_3^{3+}$. When the complex was dissolved in concentrated HCl solutions, only a very small decrease in lifetime was observed ($\tau = 1.26$ μsec for HCl 5.2 M). We found that the emission lifetime of $\text{Cr}(\text{en})_3^{3+}$ was quenched by CoCl_2 . The most important results obtained are shown in Figures 2 and 3. As one can see from Figure 2, the Stern-Volmer plot for the lifetime quenching coincided with that of the intensity quenching. Moreover, the effect of Cl^- addition was the same as that found for the

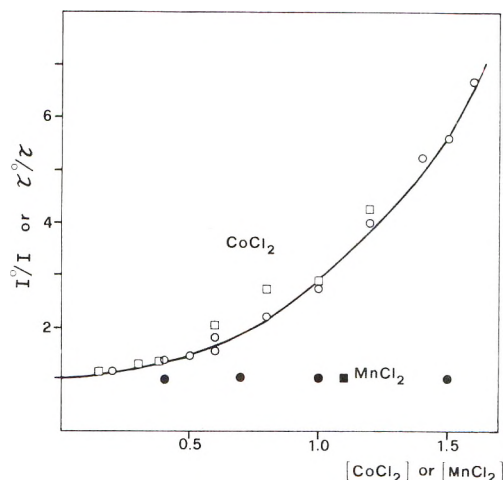


Figure 2. Quenching of the $\text{Cr}(\text{en})_3^{3+}$ phosphorescence intensity (O) and lifetime (□) by CoCl_2 . The curve represents the values calculated on the basis of eq 2 (see text). The lack of quenching by MnCl_2 (● and ■) is also shown.

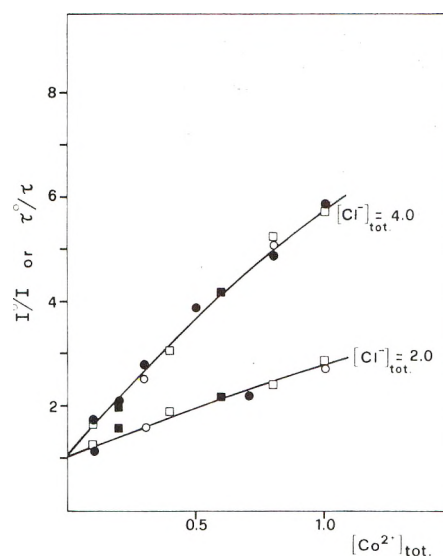


Figure 3. Quenching of the $\text{Cr}(\text{en})_3^{3+}$ phosphorescence intensity (O) and lifetime (□) by Co^{2+} for solutions having constant Cl^- concentration. Open symbols refer to solutions whose Cl^- concentration was adjusted with MgCl_2 or KCl; solid symbols refer to solutions whose Cl^- concentration was adjusted with HCl. The curves represent the values calculated on the basis of eq 2 (see text).

intensity quenching, at least for $[\text{Cl}^-]_{\text{tot}} = 2$ or 4 (Figure 3). A few experiments were also carried out at $[\text{Cl}^-]_{\text{tot}} = 5.2$. Using MgCl_2 to adjust the Cl^- concentration, the τ^0/τ values were 2.2 and 4.15 for $[\text{Co}^{2+}]_{\text{tot}} = 0.1$ and 0.3, respectively. Using HCl, τ^0/τ was 2.4 for $[\text{Co}^{2+}]_{\text{tot}} = 0.1$.

Discussion

The results obtained may be summarized as follows: (i) KCl, MgCl_2 , and MnCl_2 do not quench the $\text{Cr}(\text{en})_3^{3+}$ emission, whereas CoCl_2 and FeCl_2 exhibit a quenching effect; (ii) the Stern-Volmer plots for the quenching by CoCl_2 or FeCl_2 show a positive curvature; (iii) the quenching effect of CoCl_2 increases with increasing Cl^- concentration; (iv) at least for $[\text{Co}^{2+}]_{\text{tot}} \leq 1.0$, and $[\text{Cl}^-]_{\text{tot}} \leq 4.0$, the effect due to the increase in $[\text{Cl}^-]$ does not depend on whether MgCl_2 or HCl are used for adjusting the chloride ion concentration; (v) at least under the

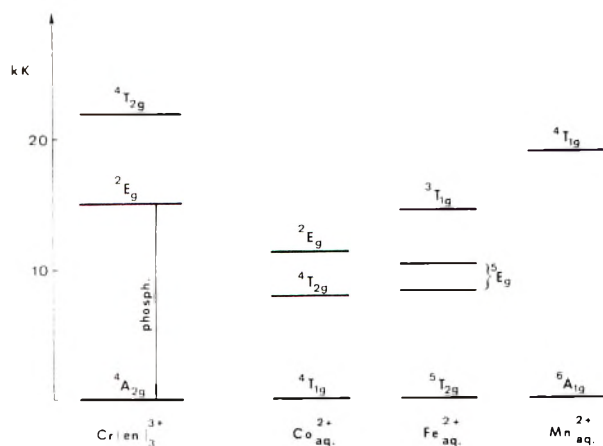


Figure 4. Energy level diagram for $\text{Cr}(\text{en})_3^{3+}$ and the hexaaqua ions used as quenchers. The $\text{Co}(\text{II})$ and $\text{Fe}(\text{II})$ species which are present in concentrated Cl^- solutions are also expected to exhibit energy levels lower than the 2E_g of $\text{Cr}(\text{en})_3^{3+}$.

experimental conditions given above, the emission intensity and lifetime are quenched in parallel.

The results mentioned in point i seem to indicate that the quenching of $\text{Cr}(\text{en})_3^{3+}$ emission involves electronic energy transfer to the low lying excited states of $\text{Co}_{\text{aq}}^{2+}$ and $\text{Fe}_{\text{aq}}^{2+}$ (or to some other $\text{Co}(\text{II})$ or $\text{Fe}(\text{II})$ species, see later). As shown in Figure 4, $\text{Mn}_{\text{aq}}^{2+}$ has no excited state lying at lower energy than that of the $\text{Cr}(\text{en})_3^{3+}$ emitting state. Of course, the same is true for KCl and MgCl_2 . It does not seem likely that the quenching by $\text{Co}_{\text{aq}}^{2+}$ and $\text{Fe}_{\text{aq}}^{2+}$ is due to electron transfer. The doublet state of $\text{Cr}(\text{en})_3^{3+}$ is not expected to exhibit remarkable redox properties. Moreover, if $\text{Co}_{\text{aq}}^{2+}$ acted as an electron donor toward excited $\text{Cr}(\text{en})_3^{3+}$, $\text{Mn}_{\text{aq}}^{2+}$ would exhibit a similar quenching action since the ionization and oxidation potential of $\text{Co}_{\text{aq}}^{2+}$ and $\text{Mn}_{\text{aq}}^{2+}$ are practically equal. The lack of quenching by $\text{Mn}_{\text{aq}}^{2+}$ also shows that the presence of a paramagnetic ion does not enhance the ${}^2E_g \rightarrow {}^4A_{2g}$ intersystem crossing of $\text{Cr}(\text{en})_3^{3+}$. As far as the small quenching action of HCl is concerned (see Results), the most plausible explanation is that of an acid catalysis on the $\text{Cr}(\text{en})_3^{3+}$ photolysis which is known to take place, at least in part, from the lowest quartet excited state.¹³

The positive curvature of the Stern-Volmer plots of Figure 2 cannot be due to the quenching of two excited states or to some static quenching.¹⁴ Such phenomena, in fact, could account for the curvature in the plot of the intensity quenching, but they cannot account for the non-linearity of the lifetime plot and for the fact that intensity and lifetime are quenched in parallel. For a dynamic quenching, when the excited state and the quencher have ionic charge of the same sign, a positive curvature of the Stern-Volmer plot is expected because of the ionic strength influence.¹⁵ However, for high ionic strengths ($0.4 < \mu < 3.4$, for the experiments plotted in Figure 2) this effect is expected to be very small,¹⁵ in agreement with the experimental results mentioned in point iv. Therefore, the most important cause for the observed behavior (Figure 2) seems to be a change in the nature of the quenching species with increasing CoCl_2 concentration. Actually, it is well known that different species may be present in CoCl_2 solutions, depending on its concentration and on the addition of other compounds which contain Co^{2+} or Cl^- ions. To our knowledge, the most complete investigation on this problem was that carried out by Zeltmann, *et al.*¹⁶ who identified the following impor-

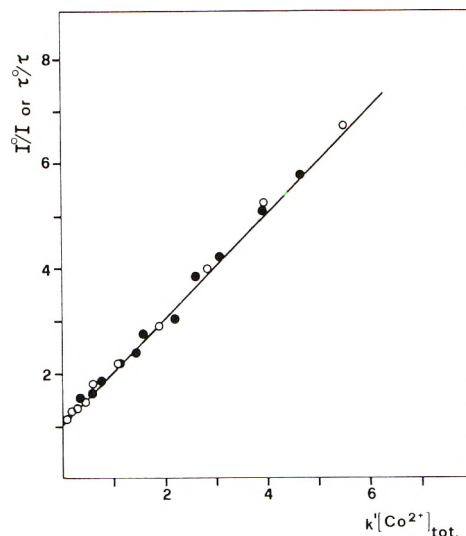


Figure 5. Quenching of the $\text{Cr}(\text{en})_3^{3+}$ phosphorescence by $\text{Co}(\text{II})$ species. Open and solid circles refer to the experiments previously shown in Figures 2 and 3, respectively. For the meaning of k' , see text.

tant species for Co^{2+} in hydrochloric acid solutions: $\text{Co}(\text{H}_2\text{O})_6^{2+}$, $\text{Co}(\text{H}_2\text{O})_5\text{Cl}^+$, $\text{Co}(\text{H}_2\text{O})_2\text{Cl}_2$, $\text{Co}(\text{H}_2\text{O})\text{Cl}_3^-$, and CoCl_4^{2-} .¹⁷ In diluted aqueous solutions of CoCl_2 , $\text{Co}(\text{H}_2\text{O})_6^{2+}$ is the dominant species. When the concentration of CoCl_2 or of added Cl^- increases, the chloride containing species become important. Then, the positive curvature of the plot in Figure 2 and the positive effect of added Cl^- on the quenching constant (Figure 3) may be qualitatively accounted for assuming that the Stern-Volmer quenching constant increases with increasing the number of Cl^- present in the $\text{Co}(\text{II})$ species. Since the substitution of water by Cl^- , which is a weaker ligand, is expected to decrease the reducing ability of $\text{Co}_{\text{aq}}^{2+}$, the positive effect of added Cl^- is another evidence against an electron-transfer quenching mechanism.

In order to consider the problem from a quantitative point of view, let us assume that all the above-mentioned $\text{Co}(\text{II})$ species can act as quenchers. The Stern-Volmer equation for the emission quenching can thus be written as follows

$$I^0/I = \tau^0/\tau = 1 + k_1[\text{Co}(\text{H}_2\text{O})_6^{2+}] + k_2[\text{Co}(\text{H}_2\text{O})_5\text{Cl}^+] + k_3[\text{Co}(\text{H}_2\text{O})_2\text{Cl}_2] + k_4[\text{Co}(\text{H}_2\text{O})\text{Cl}_3^-] + k_5[\text{CoCl}_4^{2-}] \quad (1)$$

or

$$I^0/I = \tau^0/\tau = 1 + (k_1\alpha_1 + k_2\alpha_2 + k_3\alpha_3 + k_4\alpha_4 + k_5\alpha_5)[\text{Co}^{2+}]_{\text{tot}} \quad (2)$$

where α_i are the relative abundances of the various $\text{Co}(\text{II})$ species. By means of a nmr study, Zeltmann, *et al.*,¹⁶ were able to obtain the α values for hydrochloric acid solutions. The results in point iv suggest that Zeltmann's α values can be used to discuss our experiments, at least for $[\text{Co}^{2+}]_{\text{tot}} \leq 1.0$ and $[\text{Cl}^-]_{\text{tot}} \leq 4.0$. Under such conditions, only $\text{Co}(\text{H}_2\text{O})_6^{2+}$, $\text{Co}(\text{H}_2\text{O})_5\text{Cl}^+$, and $\text{Co}(\text{H}_2\text{O})_2\text{Cl}_2$ are present, *i.e.* α_4 and α_5 are practically zero. By means of the least-squares method, we found that our experimental results are best explained by the following Stern-Volmer quenching constants: $k_1 = 0.2 \text{ M}^{-1}$, $k_2 = 7 \text{ M}^{-1}$, and $k_3 = 1 \times 10^2 \text{ M}^{-1}$. Using these values and eq 2, the curves shown in Figures 2 and 3 were obtained. As one can see,

the agreement with the experimental values is excellent. A more direct comparison between the results obtained under various experimental conditions and the proposed interpretation is given in Figure 5, where the line with unitary slope and intercept represents the plot of the first member of eq 2 against $k'[\text{Co}^{2+}]_{\text{tot}}$ (where $k' = k_1\alpha_1 + k_2\alpha_2 + k_3\alpha_3$). As one can see, the agreement with the experimental values (which are all those previously shown in Figures 2 and 3) is again excellent.¹⁹

For $[\text{Cl}^-]_{\text{tot}} = 5.2$, α_4 is still very small (0.005 for $[\text{Co}^{2+}]_{\text{tot}} = 0.1$) but, in eq 2, the term $k_4\alpha_4$ can no longer be neglected. By using the few results of the experiments carried out under such conditions, we obtained a value of about $3 \times 10^2 M^{-1}$ for k_4 .

Dividing each one of the above Stern-Volmer quenching constants by the lifetime of $\text{Cr}(\text{en})_3^{3+}$ in the absence of Co(II) ($\tau^0 = 1.33 \mu\text{sec}$), one may obtain the following values for the bimolecular quenching rate constants of the various Co(II) species: $k_{q1} = 1.5 \times 10^5 M^{-1} \text{sec}^{-1}$, $k_{q2} = 5 \times 10^6 M^{-1} \text{sec}^{-1}$, $k_{q3} = 8 \times 10^7 M^{-1} \text{sec}^{-1}$, and $k_{q4} \sim 2 \times 10^8 M^{-1} \text{sec}^{-1}$. As is expected for the quenching of a cationic species,³⁻⁵ these constants increase as the positive charge of the quencher is decreased. It can be noted that all these values are much lower than the diffusion rate constants calculated by means of the Debye equation.²⁰ As already observed, the energy transfer between complex ions seems to have a scarce efficiency especially when the ions have electric charge of the same sign.³⁻⁵ In this regard, it is to be noted that the ratio between the calculated diffusion rate constant²⁰ and the experimental quenching rate constant for our system progressively decreases as the charge of the quencher passes from +2 to -1 (e.g., such a ratio is 3000 for $\text{Co}(\text{H}_2\text{O})_6^{2+}$ and about 90 for $\text{Co}(\text{H}_2\text{O})\text{Cl}_3^-$). In line with this trend, it has recently been found⁶ that the $\text{Ru}(\text{bipy})_3^{2+}$ phosphorescence is quenched by $\text{Cr}(\text{CN})_6^{3-}$ with a rate constant very close to the diffusion controlled one.²¹ It should be noted, however, that the role played by the ionic charge in determining the quenching ability cannot be unequivocally established, since the change in the ionic charge is accompanied by a change in the nature of the ligands, which is also known to play an important role in this regard.^{2,23}

Acknowledgments. The authors express their appreciation to Professor V. Carassiti for his interest in this study.

This work was partly supported by the Deutsche Forschungsgemeinschaft and by the Consiglio Nazionale delle Ricerche.

References and Notes

- (1) (a) Frankfurt University; (b) Ferrara University; (c) Bologna University.
- (2) A. Pfeil, *J. Amer. Chem. Soc.*, **93**, 5395 (1971).
- (3) N. J. Demas and A. W. Adamson, *J. Amer. Chem. Soc.*, **93**, 1800 (1971).
- (4) N. J. Demas, Proceedings of the XIV International Conference on Coordination Chemistry, Toronto, June 1972, p 166.
- (5) I. Fujita and H. Kobayashi, *Ber. Bunsenges. Phys. Chem.*, **76**, 115 (1972).
- (6) F. Bolletta, M. Maestri, and L. Moggi, *J. Phys. Chem.*, **77**, 861 (1973).
- (7) M. Linhard and M. Weigel, *Z. Anorg. Allg. Chem.*, **271**, 115 (1953).
- (8) W. Geis, H. F. Wasgestian, and H. Kelm, *Ber. Bunsenges. Phys. Chem.*, **76**, 1093 (1972).
- (9) Hereafter, the symbols $[\text{Cl}^-]_{\text{tot}}$ and $[\text{Co}^{2+}]_{\text{tot}}$ will be used for indicating the total (i.e., free plus complexed) concentration of these species in the solution.
- (10) L. Moggi, R. Ballardini, and G. Varani, to be submitted for publication.
- (11) V. Balzani, R. Ballardini, M. T. Gandolfi, and L. Moggi, *J. Amer. Chem. Soc.*, **93**, 339 (1971).
- (12) S. N. Chen and G. B. Porter, Abstracts of the X Informal Conference on Photochemistry, Stillwater, Okla., May 1972, p 155.
- (13) R. Ballardini, G. Varani, H. F. Wasgestian, L. Moggi, and V. Balzani, *J. Phys. Chem.*, submitted for publication.
- (14) See, for example, (a) P. J. Wagner in "Creation and Detection of the Excited State," Vol. 1, Part A, A. A. Lamola, Ed., Marcel Dekker, New York, N. Y., 1971, p 173; (b) W. R. Ware, *loc. cit.*, Vol. 1, Part A, 1971, p 213.
- (15) R. W. Stoughton and G. K. Rollefson, *J. Amer. Chem. Soc.*, **61**, 2634 (1939); J. Q. Umberger and V.-K. LaMer, *ibid.*, **67**, 1099 (1945).
- (16) A. H. Zeltmann, N. A. Matwiyoff, and L. O. Morgan, *J. Phys. Chem.*, **72**, 121 (1968); **73**, 2689 (1969).
- (17) The conclusions of a more recent investigation¹⁸ are partly different in this regard.
- (18) U. Kraus and G. Lehmann, *Ber. Bunsenges. Phys. Chem.*, **76**, 1068 (1972).
- (19) As we have seen, in order to interpret our results there is no need to consider the change in the ionic strength of the solution. This is not surprising not only because the ionic strength is always very high (see above), but also because, when the CoCl_2 concentration is increased or Cl^- is added, the composition of the quenching system gradually evolves toward species that have lower ionic charge.
- (20) P. Debye, *Trans. Electrochem. Soc.*, **82**, 265 (1942).
- (21) The quenching of the $\text{Cr}(\text{NH}_3)_2(\text{NCS})_4^-$ phosphorescence by $\text{Cr}(\text{CN})_6^{3-}$ at -65° in fluid solution is close to diffusion controlled, although both ions are negative.²² Under such conditions, however, the diffusion rate is very low ($\sim 4 \times 10^6 M^{-1} \text{sec}^{-1}$) and the encounter lifetime is very long, so that the inefficiency in the energy transfer can be masked.
- (22) S. N. Chen and G. B. Porter, *J. Amer. Chem. Soc.*, **92**, 3196 (1970).
- (23) F. Bolletta, M. Maestri, L. Moggi, and V. Balzani, *J. Amer. Chem. Soc.*, submitted for publication.

Kinetics of Electron Transfer from Aromatic Radical Anions to Alkyl Halides in Tetrahydrofuran. Effects of Sodium Cation Pairing¹

Bradley Bockrath and Leon M. Dorfman*

Department of Chemistry, The Ohio State University, Columbus, Ohio 43210 (Received June 29, 1973)

Publication costs assisted by the U. S. Atomic Energy Commission

Absolute rate constants have been determined, by the pulse radiolysis method, for electron transfer from naphthalenide and biphenylide ions to *n*-butyl bromide and *n*-butyl iodide in tetrahydrofuran solution. The sodium cation-paired form of the radical anion, (Na⁺, A^{•-}), exhibits reactivity that is roughly two orders of magnitude lower than that of the free-radical anion, A^{•-}. The temperature coefficient for the reaction was interpreted in terms of an equilibrium of loose and tight ion pairs, the former exhibiting greater reactivity. A small effect of added salts upon the rate constants was observed.

Introduction

We have determined, by the pulse radiolysis method, the effect of sodium cation pairing on the rate constants for electron transfer from aromatic radical anions as donors to alkyl halides in tetrahydrofuran solution. Effects of metal cation pairing on the reactivity of aromatic radical anions in several types of reaction have been established²⁻⁷ earlier, although limited data pertaining to electron transfer are available.⁸ The pulse radiolysis method, which has been used extensively in the study of electron transfer kinetics,^{9,10} provides a convenient means of studying such cation-pairing effects since the reaction may be observed with metal cations present or absent, as one chooses.

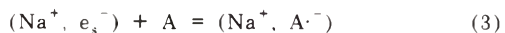
Pulse radiolysis of solutions of aromatic molecules in liquids such as tetrahydrofuran yields the radical anion⁹⁻¹¹ by attachment of the solvated electron



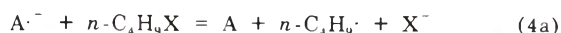
In the presence of free excess Na⁺, the ion pair¹¹ with the solvated electron, (Na⁺, e_s⁻), is formed ($k_2 = 7.9 \times 10^{11} M^{-1} \text{sec}^{-1}$ in THF)



This species will also attach, with a high rate constant,¹¹ to aromatic hydrocarbons to yield the ion-paired radical anion



Observation of either A^{•-} or (Na⁺, A^{•-}), by fast optical absorption spectrophotometry, with nanosecond time resolution when necessary, permits comparative kinetic studies of the two species to be easily made. We have obtained such data for naphthalene and biphenyl radical anions reacting with *n*-butyl bromide and *n*-butyl iodide in THF



Experimental Section

The source of the electron pulse, as in our earlier studies,¹² was a Varian V-7715A electron linear accelerator, delivering 3-4-MeV electrons at a pulse current of about 350 mA for pulse duration of 100-1500 nsec and about 600 mA for pulse duration less than 80 nsec. Electron pulses

for 20-80-nsec duration were used in this work. The transient optical absorptions were observed using an H.T.V. 196 detector with an S-1 response. A Bausch and Lomb grating monochromator, type 33-86-25, *f*/3.5 was used. Corning filters were used to eliminate second-order components from the analyzing light beam.

Our standard reaction cells,¹² with high-purity silica windows and a cell length of 20.0 mm, were used in most runs with a double pass of the analyzing light beam. Accordingly the optical path length was 40.0 mm. Temperature coefficients of the rate constants were obtained with a thermostatic box heated or cooled by a stream of nitrogen gas.

The THF was purified first by refluxing under argon, for several hours, a solution containing benzophenone and excess sodium metal. This was followed by distillation through a glass bead-packed column, the middle fraction being retained. It was then degassed and vacuum transferred into a bulb containing a mirror of freshly triple-distilled potassium. It was vacuum transferred from this bulb into the reaction cells just prior to the runs.

The aromatic compounds used were zone refined, commercially supplied, with a nominal purity of at least 99.9%. *n*-Butyl bromide (Fisher reagent grade) and *n*-butyl iodide (Matheson Coleman and Bell) were purified by washing with several portions of concentrated H₂SO₄, followed by several portions of 10% sodium carbonate, and finally distilled water. The washed materials were dried and distilled through a glass bead-packed column, and the middle fraction was retained. *n*-Butyl iodide was stored in the dark over mercury.

Sodium tetraphenylboron (Fisher reagent grade) was recrystallized as recommended,¹³ and stored *in vacuo* until used. Sodium iodide (either Baker analyzed grade, 99.08%, or Alfa Inorganics optronic grade) and sodium perchlorate (G. Fredrick Smith reagent) were used without further purification.

Results and Discussion

The reactions were observed by monitoring the decay of the aromatic radical anion at the maximum of the long wavelength absorption bands. Naphthalenide was monitored at 775 nm, biphenylide at 630 nm. The differential rate equation for the observed process, reaction 4a or 4b, is

$$-d[A^{\bullet-}]/dt = k_4[A^{\bullet-}][n\text{-C}_4\text{H}_9\text{X}] \quad (5)$$

Under our experimental conditions, with $[n\text{-C}_4\text{H}_9\text{X}]_0 \gg [\text{A}\cdot^-]_0$ or $[n\text{-C}_4\text{H}_9\text{X}]_0 \gg [(\text{Na}^+, \text{A}\cdot^-)]_0$, the reaction follows a first-order rate law, and k_4 is readily obtained by linearization of the data in accord with the integrated form of (5).

In a typical series of experiments, the decay of $\text{A}\cdot^-$ or $(\text{Na}^+, \text{A}\cdot^-)$ was monitored in the absence and in the presence of alkyl halide. In the absence of alkyl halide the decay of $\text{A}\cdot^-$ followed second-order kinetics, while that of $(\text{Na}^+, \text{A}\cdot^-)$ followed either second-order or, in some cases, mixed first- and second-order kinetics. With alkyl halide present the decay was shown to follow a first-order rate law over a range of alkyl halide concentrations of about one order of magnitude. The initial condition $[n\text{-C}_4\text{H}_9\text{X}]_0/[\text{A}\cdot^-]_0$ was such that the half-life of the radical anion in the absence of $n\text{-C}_4\text{H}_9\text{X}$ was at least ten times its half-life in the presence of the electron acceptor. The pseudo-first-order rate constants, k'_{4a} or k'_{4b} , obtained from first-order plots under these conditions, were then plotted against $[n\text{-C}_4\text{H}_9\text{X}]$ to determine k_{4a} or k_{4b} .

The data exhibited no dependency of the rates on the concentration of the aromatic molecule, indicating that there was no measurable back reaction. The kinetic order in butyl halide was unity, the slopes from plots of $\log k_4$ vs. $\log [n\text{-C}_4\text{H}_9\text{X}]$ falling in the range 0.94–1.08. As indicated, the rate of reaction of the donor anion with the solvent counterion was, in most cases, negligible relative to the rate of reaction 4. Where this was not the case it was taken into account in determining k_4 .

In the case of reactions involving biphenylide ion as donor, the following complication necessitated a modification in the method of determining k_4 from the observed rate curves. In the biphenylide systems the absorption at 630 nm did not decay to zero, but reached, instead, a weak residual plateau after the initial decay.

At 630 nm the residual plateau was typically about 5% of the absorption measured at time zero. Time resolved absorption spectra, Figure 1, taken at time zero and at the plateau region, show the absorption remaining after the decay of the aromatic radical anion. Several species might reasonably contribute to the residual absorption. The biphenyl radical cation,¹⁴ the biphenyl triplet,¹⁵ and the phenylcyclohexadienyl radical¹⁶ all have uv absorptions that could contribute to a composite spectrum. The long wavelength component may possibly be due to the radical cation, while the short wavelength component could be due to any one or a mixture of the three species.

Where such a plateau is formed, the pseudo-first-order rate constants, k'_{4a} , were obtained from plots of $\ln(D_t - D_\infty)$ vs. time. This method is valid if the residual absorption, D_∞ , does not change during the course of the reaction with butyl halide.

The D_∞ plateau shows negligible decay on the time scale of observation of reaction 4a. The possibility that the species responsible for the D_∞ absorption grows in during reaction 4a was also ruled out because plots of $\ln(D_t - D_\infty)$ were always linear and values of k_{4a} were constant over a wide range of butyl halide concentration. As a further check, values of k_{4a} obtained at 400 nm, where the residual absorption constitutes a higher percentage of the initial absorption, were found to be equal to those determined at 630 nm. Furthermore, there is no growth of absorption at these wavelengths after the end of a pulse in solutions of biphenyl without added butyl halide. The formation of the D_∞ absorption is therefore most likely complete by the end of pulse.

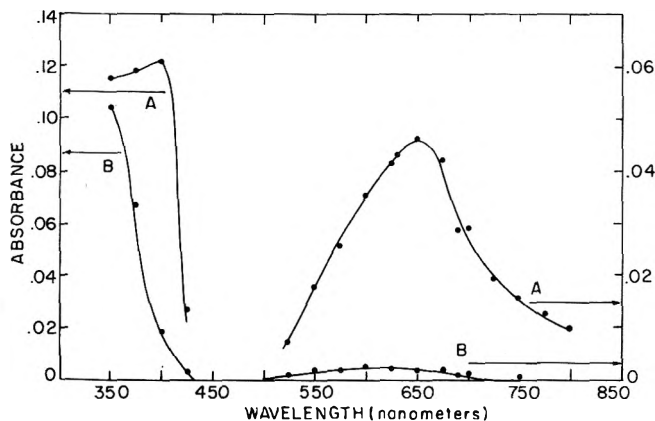


Figure 1. Spectra of THF solution $5.5 \times 10^{-2} M$ in biphenyl and $2.2 \times 10^{-3} M$ in n -butyl iodide showing absorption due to biphenylide and the residual absorption plateau after reaction 4a is complete. Curve A taken at time zero following an 80-nsec electron pulse. Curve B taken 300 nsec following the electron pulse at the plateau of residual absorption.

TABLE I: Rate Constants for Reaction 4a with n -Butyl Iodide and n -Butyl Bromide in THF

	Rate constant, $M^{-1} \text{sec}^{-1}$ at 298°K	
	n -Butyl iodide ^a	n -Butyl bromide ^a
Biphenylide	$(9.6 \pm 1.4) \times 10^9$	$(3.4 \pm 0.6) \times 10^7$
Naphthalenide	$(7.4 \pm 1.1) \times 10^9$	$(3.3 \pm 0.6) \times 10^7$

^a The range of concentration used in determining k_{4a} was 5×10^{-4} – $3 \times 10^{-3} M$ for n -butyl iodide and 0.02–0.2 M for n -butyl bromide.

It was necessary to use $\ln(D_t - D_\infty)$ plots only for the reactions of free biphenylide ion. In other cases, D_∞ is a negligible fraction of the initial absorption. In the former cases, a relatively high biphenyl concentration (0.06 to 0.3 M) was used in order to overcome the competition for e_s^- by the added butyl halide, whose electron-scavenging rate constants are very high.¹¹ This would undoubtedly favor a higher fractional yield of the intermediates responsible for the D_∞ absorption.

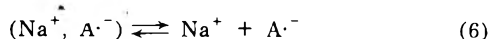
Rate Constants for Free Aromatic Radical Anion

Values for k_{4a} with both n -butyl iodide and n -butyl bromide as acceptor are shown in Table I. It is interesting to note that, whereas the electron transfer to n -butyl iodide is perhaps only slightly lower than the diffusion-controlled limit, the reaction with n -butyl bromide is some two orders of magnitude slower than diffusion controlled. Earlier studies¹⁰ of electron transfer from aromatic radical anions to a different neutral aromatic molecule, in solvents such as 2-propanol and ethylenediamine, had shown that the rate constants approached the diffusion-controlled limit when the reduction potential of the donor exceeded that of the acceptor by roughly 0.2 V. The results for the reaction with n -butyl bromide, which very likely involves a dissociative attachment, implies qualitatively that n -butyl bromide is more difficult to reduce than either biphenyl or naphthalene.

Rate Constants for the Cation-Paired Radical Anion

Values for k_{4b} were determined by monitoring the decay of $(\text{Na}^+, \text{A}\cdot^-)$ for naphthalenide and biphenylide in the presence of butyl halide in a THF solution containing sufficient free sodium ion to maintain the aromatic

radical anion in the cation-paired form. This was achieved by addition of dissociative sodium salts to the solution. Three salts were used in separate experiments: sodium tetraphenylboron (for which the dissociation constant in THF is known¹³), sodium iodide, and sodium perchlorate. The concentration of sodium ion was well in excess of the amount required to maintain the equilibrium¹⁷



overwhelmingly in the cation-paired form.

The decay of the ion-paired aromatic radical anion was monitored in the absence as well as the presence of butyl halide. In the absence of butyl halide the decay was of second order or under some conditions of mixed order, and presumably consisted mainly of reaction with the solvent counterion. This rate of decay was roughly an order of magnitude slower than in the case of the free aromatic radical anions, indicating a counterion recombination rate constant of about $10^{10} \text{ M}^{-1} \text{ sec}^{-1}$ for the cation-paired radical anion and $10^{11} \text{ M}^{-1} \text{ sec}^{-1}$ for the free aromatic radical anion. This seems reasonable since the counterion recombination for $(\text{Na}^+, \text{A}^{\cdot-})$ is an ion-dipole reaction rather than an ion-ion reaction.

The values obtained for k_{4b} in THF solutions containing $1-2 \times 10^{-2} F$ sodium tetraphenylboron are shown in Table II. Comparison of these values with the corresponding data in Table I reveals that the reactivity of the sodium cation paired aromatic ion in these electron transfers is fully one to two orders of magnitude lower than the reactivity of the free anion.

It is also interesting to compare our values of k_{4b} with the rate constant of $4.3 \times 10^{-4} \text{ M}^{-1} \text{ sec}^{-1}$ measured by Garst and Barton¹⁸ for the reaction of sodium naphthalenide with either hexyl or octyl fluoride in DME. The reactivity of the alkyl halides thus spans more than 12 orders of magnitude over the series from iodide to fluoride.

In presenting the data in Table II, it was essential to cite the particular added salt used, as well as its concentration, for the following reason. The value of the rate constant, as it turns out, is dependent upon both the choice of added salt and its concentration, showing an increase with increasing concentration. This may be seen very clearly in Figure 2 which shows the value of the observed rate constant for the electron transfer from sodium biphenylide to *n*-butyl iodide as a function of concentration for all three added salts.

The increase in the observed rate constant with increase in added salt concentration is not due to reaction of the donor radical anion with the added salt. This was shown by determining the lifetime of $(\text{Na}^+, \text{A}^{\cdot-})$ in the absence of butyl halide, at an increased concentration of added salt. It was found that the rate of decay of sodium biphenylide increased to the extent of only 50% for an increase in sodium perchlorate concentration from 0.025 to 0.31 *F*. Since the half-time for this decay is always more than ten times the half-time in the presence of butyl iodide (at all concentrations used), direct reaction of $(\text{Na}^+, \text{A}^{\cdot-})$ with the perchlorate, if it occurs at all, cannot be the cause of the increased rate constant in Figure 2.

The concentration of added salt does, however, affect the value of k_{4b} , as may be seen in Figure 2 which shows a nonlinear increase in the observed rate constant with increase in salt concentration. The sensitivity to salt concentration depends strongly on the nature of the anion of the salt, perchlorate showing the largest effect and tetraphenylboron a very small effect. The solid curves in this

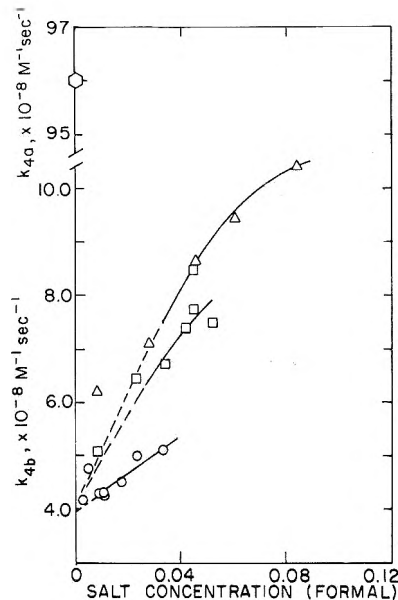


Figure 2. Effect of added salts on k_{4b} . Solid lines pertain to concentrations of added sodium salts sufficient to assure biphenylide is completely associated with sodium cation. Dashed lines represent extrapolation of k_{4b} to infinite dilution of added salt. The rate constant for reaction of free biphenylide, k_{4a} , has been added for comparison: Δ , sodium perchlorate; \square , sodium iodide; \circ , sodium tetraphenylboron; \circ , k_{4a} for reaction of free biphenylide without added salt.

TABLE II: Rate Constants for Reaction 4b with *n*-Butyl Iodide and *n*-Butyl Bromide in THF Solution Containing $1-2 \times 10^{-2} F$ of Sodium Tetraphenylboron

	Rate constant, $\text{M}^{-1} \text{ sec}^{-1}$, at 298°K	
	<i>n</i> -Butyl iodide ^a	<i>n</i> -Butyl bromide ^a
Na^+ , biphenylide	$(4.3 \pm 0.2) \times 10^8$	$(1.3 \pm 0.1) \times 10^6$
Na^+ , naphthalenide	$(9.3 \pm 0.5) \times 10^7$	$<4 \times 10^5$

^a The range of concentration used in determining k_{4b} was 8×10^{-4} – $2 \times 10^{-2} M$ for *n*-butyl iodide, and 0.13–0.58 *M* for *n*-butyl bromide.

figure represent values for the rate constant for the sodium cation-paired species only, since concentrations of salt above about 0.01–0.02 *F* are high enough, in view of the value of K_6 , to ensure that the aromatic ion is in the form $(\text{Na}^+, \text{A}^{\cdot-})$.

The increase in k_{4b} cannot be due to participation of the more reactive free aromatic anion, $\text{A}^{\cdot-}$, since the direction of the effect is opposite to expectations. Nor can the increase be attributed to any role of triple ions, $(\text{Na}_2^+, \text{Ar}^{\cdot-})$, since the most highly dissociative of the added salts, sodium tetraphenylboron, is least effective in changing k_{4b} .

It can be attributed to the effect of the added salt in producing, at increased concentration, deviation of the reacting species from ideal behavior in these solutions in THF, a solvent of low dielectric strength. The approximation, in equating nominal concentrations of the reactants with their activities, is not valid except, perhaps, at infinite dilution of the added salt. For the case of nonideal solutions, the rate constant, in terms of transition state theory, is given¹⁹ by

$$k_{4b} = \frac{kT}{h} \frac{C^\ddagger}{C^{(\text{Na}^+, \text{A}^{\cdot-})} C^{\text{BuI}}} \frac{\gamma^{(\text{Na}^+, \text{A}^{\cdot-})} \gamma^{\text{BuI}}}{\gamma^\ddagger} \quad (7)$$

where C represents the concentration and γ the activity

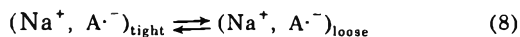
coefficient. Our results indicate that $\gamma(\text{Na}^+, \text{A}^{\cdot-})\gamma^{\text{BuI}}/\gamma^\ddagger$ increases with increasing salt concentration, and that the extent of this increase depends on the nature of added salt.

Our data are not sufficient to form the basis for any considerations of a molecular model for such effects, but it is interesting to note that salt effects upon the rate constants for ionic dissociation of organic solutes in THF solutions have been reported.^{20,21} These effects also depend strongly upon the nature of the added salt used in such solvolysis and rearrangement reactions. Specific interactions covering as much as six orders of magnitude have been observed²¹ for lithium perchlorate. These effects have been attributed to interaction of the ion pairs of the added salt with the transition state.^{21,22} Similarly, salt-induced effects upon activity coefficients of organic substrates in solution have been measured.²³ In reaction 4b, dipolar species are involved in the formation of the transition state, which must itself be dipolar. Such an effect of the added salt (the larger portion of which is in the ion paired form) must exist for the transition state and the sodium biphenylide itself, and to a lesser extent for the butyl iodide. It should be noted that there may, in general, be such kinetic effects even in the absence of added salts if the concentrations of the ion-paired aromatic radical anions are sufficiently high.

It would seem useful, in the face of such salt effects upon k_{4b} , to define to the extent that the data in Figure 2 permit a rate constant at infinite dilution of the added salt. The curves for all three salts appear to extrapolate to approximately the same value at infinite dilution, $k_{4b}^0 = (4.0 \pm 0.2) \times 10^8 \text{ M}^{-1} \text{ sec}^{-1}$. For sodium tetraphenylboron, in the concentration range used, k_{4b} is only very slightly larger than k_{4b}^0 , and the comparison we have made of data in Table II with those in Table I is justifiable.

Temperature Coefficient of the Rate Constants

The temperature coefficient for two of the foregoing reactions with *n*-butyl iodide as acceptor and two different added salts was determined in an attempt to obtain the activation energy. The most striking aspect of the data, shown in Figure 3, is the distinct nonlinear behavior of the plots of $\log k_{4b}$ as a function of $1/T$. Temperature dependence of this general form has been reported by Hirota⁷ for the electron exchange reaction of sodium naphthalenide with naphthalene in THF. Our interpretation of these observations for the reactions we have studied is the same as Hirota suggested for the electron exchange reactions. There is independent evidence^{2,3,24,25} that the sodium cation–aromatic anion pairs exist in different forms, exhibiting a different extent of pairing in the form of loose and tight ion pairs. The equilibrium



is temperature dependent, with lower temperatures favoring the loose ion pair. The loose ion pair exhibits the greater reactivity. Consequently, the shift in equilibrium with increasing temperature leads eventually to the decrease in the observed rate constant shown in Figure 3.

These effects lead to some curious results. For example, the observed rate constant for reaction of sodium biphenylide with *n*-butyl iodide has the same value at +60° as at -65°. Determination of an activation energy from the data in Figure 3 is valid only for that portion of the plot which clearly represents the reaction of one particular

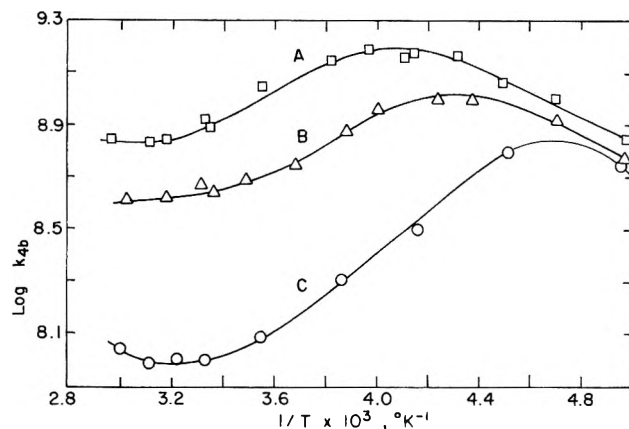
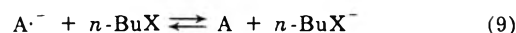


Figure 3. $\log k_{4b}$ vs. reciprocal temperature for reaction with *n*-butyl iodide: curve A, sodium biphenylide with $4.5 \times 10^{-2} F$ sodium iodide added; curve B, sodium biphenylide with $7.3 \times 10^{-3} F$ sodium tetraphenylboron added; curve C, sodium naphthalenide with $1.4 \times 10^{-3} F$ sodium tetraphenylboron added.

type of ion pair. It seems legitimate to conclude that the low-temperature portion of the curve for sodium biphenylide and *n*-butyl iodide, curve A, leads to $\Delta E_a \geq 2.1 \text{ kcal/mol}$, $\Delta H^* \geq 1.6 \text{ kcal/mol}$, and $\Delta S^* \geq -8.9 \text{ eu}$. These parameters pertain to the loose ion pairs. We, as well as Hirota,⁷ have been unable to determine the analogous data for the tight ion pairs by using the extrapolated portion from the low-temperature region together with the known value for K_8 . The physical nature of either of the two types of ion pairs may be modified by change in temperature over an extended range.

It should be noted, in Figure 3, that the salt effect is manifested over the entire temperature range in which the equilibrium of reaction 8 has been examined. It would therefore seem that the kinetic effect of the added salt is not to be attributed to its influence on this equilibrium.

The data obtained in the determination of both k_{4a} and k_{4b} permit us to draw the following conclusion about any equilibrium involving a metastable alkyl halide radical anion and the reactants



Since the observed rates for the decay of $\text{A}^{\cdot-}$ [or of $(\text{Na}^+, \text{A}^{\cdot-})$] were in all cases independent of the concentration of aromatic molecule, it is clear that this equilibrium plays no role in our kinetics, and that the values obtained for k_{4a} must therefore represent the rate constants for the forward reaction. The lifetime of $n\text{-BuX}^{\cdot-}$ with respect to dissociation is undoubtedly very short.

Summary

The relative order of reactivity for reaction 4 is free ion > loose ion pair > tight ion pair. This order is identical with that found for the electron exchange reaction of sodium naphthalenide and naphthalene,⁷ but opposite to the order found for protonation of sodium naphthalenide or anthracenide by water.⁴ Our results draw further attention to the importance of the relative ability of the reactant to enter the solvation shell of the metal cation of the ion pair. The relative order of reactivity seems dependent upon the extent to which reactant may displace solvent from this solvation shell. Obviously, theoretical treatments of such reactions must take these factors into account. For example, application of Marcus theory to such ion pairs may have to include an evaluation of W , the

work necessary to bring the reactants together, which may be important even if one of the reactants is uncharged.

Acknowledgment. We are indebted to Mr. John Richter and Mr. Amin Bishara for maintaining the effective operation of the linear accelerator and the detection equipment.

References and Notes

- (1) This work was supported by the U. S. Atomic Energy Commission under Contract No. AT(11-1)-1763.
- (2) M. Szwarc, "Carbanions, Living Polymers and Electron Transfer Processes," Interscience, New York, N. Y., 1968.
- (3) "Ions and Ion Pairs in Organic Reactions," Vol. 1, M. Szwarc, Ed., Wiley-Interscience, New York, N. Y., 1972.
- (4) S. Bank and B. Bockrath, *J. Amer. Chem. Soc.*, **93**, 430 (1971); **94**, 6076 (1972).
- (5) E. R. Minnich, L. D. Long, J. M. Ceraso, and J. L. Dye, *J. Amer. Chem. Soc.*, **95**, 1601 (1973).
- (6) A. Raines, R. Tung, and M. Szwarc, *J. Amer. Chem. Soc.*, **95**, 659 (1973).
- (7) N. Hirota, R. Carraway, and W. Schook, *J. Amer. Chem. Soc.*, **90**, 3611 (1968).
- (8) G. Rämme, M. Fisher, S. Claesson, and M. Szwarc, *Proc. Roy. Soc., Ser. A*, **327**, 475 (1972).
- (9) S. Arai, D. A. Grev, and L. M. Dorfman, *J. Chem. Phys.*, **46**, 2572 (1967).
- (10) J. R. Brandon and L. M. Dorfman, *J. Chem. Phys.*, **53**, 3849 (1970).
- (11) B. Bockrath and L. M. Dorfman, *J. Phys. Chem.*, **77**, 1002 (1973).
- (12) W. D. Felix, B. L. Gall, and L. M. Dorfman, *J. Phys. Chem.*, **71**, 384 (1967).
- (13) C. Carvajal, K. J. Toile, J. Smid, and M. Szwarc, *J. Amer. Chem. Soc.*, **87**, 5548 (1965).
- (14) S. Arai, H. Ueda, R. F. Firestone, and L. M. Dorfman, *J. Chem. Phys.*, **50**, 1072 (1969).
- (15) G. Porter and M. W. Windsor, *Proc. Roy. Soc., Ser. A*, **245**, 238 (1958).
- (16) S. Arai and L. M. Dorfman, *J. Chem. Phys.*, **41**, 2190 (1964).
- (17) P. Chang, R. V. Slates, and M. Szwarc, *J. Phys. Chem.*, **70**, 3180 (1966).
- (18) J. F. Garst and F. E. Barton, *Tetrahedron Lett.*, **No. 7**, 587 (1967).
- (19) L. P. Hammett, "Physical Organic Chemistry," 2nd ed, McGraw-Hill, New York, N. Y., 1970, p 111.
- (20) S. Winstein, S. Smith, and D. Darwish, *J. Amer. Chem. Soc.*, **81**, 5511 (1959).
- (21) S. Winstein, E. C. Friedrich, and S. Smith, *J. Amer. Chem. Soc.*, **86**, 305 (1964).
- (22) C. L. Perrin and J. Pressing, *J. Amer. Chem. Soc.*, **93**, 5705 (1971).
- (23) E. Grunwald and A. F. Butler, *J. Amer. Chem. Soc.*, **82**, 5647 (1960).
- (24) Y. Karasawa, G. Levin, and M. Szwarc, *Proc. Roy. Soc., Ser. A*, **326**, 53 (1971).
- (25) N. Hirota, *J. Amer. Chem. Soc.*, **90**, 3603 (1968).

An Electron Paramagnetic Resonance Study of Hydrogen Atoms Trapped in γ -Irradiated Lithium Phosphates

Y. P. Virmani, John D. Zimbrick,* and E. J. Zeller

Departments of Chemistry, Radiation Biophysics, Geology, and Physics, The University of Kansas, Lawrence, Kansas 66044

(Received April 12, 1973)

Epr studies were carried out on trapped H atoms (H_t) in ^{60}Co γ -irradiated lithium ortho-, meta-, and pyrophosphate polycrystals at room temperature. The radiation yields of H_t varied from $G(H_t) = 0.08$ for lithium orthophosphate to $G(H_t) = 0.01$ for lithium meta- and pyrophosphate. The H_t decayed slowly at room temperature with initial halftimes which varied from 14 hr for lithium orthophosphate to 48 hr for lithium pyrophosphate. The widths of the epr lines of H_t varied from 0.74 G for lithium orthophosphate to 3.2 G for lithium metaphosphate. Two sets of satellite lines were observed in the epr spectra of the H_t doublet in lithium orthophosphate and lithium pyrophosphate. These satellites were attributed to forbidden spin flips of adjacent H and P nuclei which populate the H atom traps. Paramagnetic relaxation time measurements *vs.* radiation dose were made on the H_t epr lines in lithium orthophosphate. These data when correlated with thermal decay and dose saturation data supported the hypothesis that the H_t are distributed uniformly in the polycrystalline matrix.

I. Introduction

The γ -radiolysis of acidic glasses and polycrystalline ices which contain oxyanion salts at 77°K produces hydrogen atom radicals (\dot{H}) which become trapped (H_t) and can be detected by epr.¹ The epr and radiation chemical properties of H_t in these matrices have been well summarized by Kevan² and by Ershov and Pikaev.³ The only materials reported thus far, in which H_t can be produced by γ -irradiation at room temperature, are calcium and lithium phosphates.^{4,5} We recently carried out a detailed study on the radiation yields, epr line widths, dose saturation, and paramagnetic relaxation characteristics of H_t in

irradiated calcium phosphate.⁶ In the present work we have extended these studies to H_t in irradiated lithium orthophosphate (Li_3PO_4), lithium metaphosphate (LiPO_3), and lithium pyrophosphate ($\text{Li}_4\text{P}_2\text{O}_7$). The results support the hypothesis that the H_t are located in shallow traps near hydrated phosphate anions and are distributed uniformly in the crystalline matrix.

II. Experimental Section

Reagent grade Li_3PO_4 , LiPO_3 , and $\text{Li}_4\text{P}_2\text{O}_7$ as polycrystalline powders were obtained from K & K Laboratories Inc. and they were examined without further purification.

The concentration of water in each of the above samples was measured by differential thermal analysis techniques. The results indicated that the water content in all the samples is essentially the same within experimental error.

Samples were irradiated in Pyrex vials at ambient temperatures in an Atomic Energy of Canada Model 200 ^{60}Co γ cell at a dose rate of 10^5 rads/hr as calibrated by ferrous sulfate dosimetry.

Epr analysis was carried out in a Varian V-4502 spectrometer system equipped with audio and 100 kHz modulation, and operated in the low-power bridge configuration. The slow passage power saturation measurements were done with a modulation frequency of 200 Hz. Fast passage measurement utilized a modulation frequency of 100 kHz. The modulation amplitude, H_m , was set at a value of 0.25 G for the H_t lines in Li_3PO_4 and $\text{Li}_4\text{P}_2\text{O}_7$ because of the small line widths of H_t doublet (0.74 and 0.96 G, respectively).

The microwave magnetic field, H_1 , in the Varian TE₁₀₂ single cavity was calculated from measurement of the microwave power entering the cavity by a formula recently developed by Bales and Kevan⁷ and adjusted to our experimental conditions. Microwave power measurements were made with a Hewlett-Packard X-487B thermistor connected to a Microlin 31A1 power meter and attached to the low-power sample cavity arm through a Hewlett-Packard precision attenuator.

G values for H_t production in the phosphate samples (no. of H_t produced per 100 eV radiation energy absorbed) were obtained by comparison of the area of the doubly integrated H_t high-field line with that obtained from glassy 8.7 M H_2SO_4 ice at 77°K irradiated and analyzed in the same fashion. The $G(H_t)$ in glassy 8.7 M H_2SO_4 was taken to be 1.66.⁸

III. Results and Discussion

A. Epr Spectral Characteristics of Irradiated Lithium Phosphates. The epr spectra of irradiated Li_3PO_4 , LiPO_3 , and $\text{Li}_4\text{P}_2\text{O}_7$ (^{60}Co γ dose = 1.4×10^6 rads) are shown in Figure 1. The doublet lines marked H_t and split by 503 G, are attributed to H_t and closely resemble those attributed to H_t in γ -irradiated calcium phosphate⁴⁻⁶ [$\text{Ca}_{10}(\text{PO}_4)_6(\text{OH})_2$] and acidic glasses.^{8,9} The width between points of maximum slope of the high-field H_t line for each phosphate studied is given in Table I. The line width for H_t in LiPO_3 is 3.2 G which is comparable with the line width observed in acidic glasses.^{8,9} However the line width of H_t in Li_3PO_4 and $\text{Li}_4\text{P}_2\text{O}_7$ is much smaller than in acidic ices but is larger than the line width of H_t in γ -irradiated calcium phosphate [$\text{Ca}_{10}(\text{PO}_4)_6(\text{OH})_2$].⁶

The line shape parameter of any epr line determined by the derivative curve slope method¹⁰ is 2.2 for an ideal gaussian line and 4.0 for an ideal Lorentzian line. The line shape parameter values are also given in Table I. The values of this parameter are 3.4 for the high-field H_t line in Li_3PO_4 and 3.5 for the corresponding line in LiPO_3 which indicates that the line shapes are intermediate between Gaussian and Lorentzian. This line shape parameter for the high-field H_t line in $\text{Li}_4\text{P}_2\text{O}_7$ is approximately 9 which is extra-Lorentzian.

The effects of variations in radiation dose on the H_t line shape parameter and line width for H_t in γ -irradiated LiPO_3 , Li_3PO_4 , and $\text{Li}_4\text{P}_2\text{O}_7$ were studied. It was found that the line widths and line shape parameters of the H_t lines in LiPO_3 and Li_3PO_4 do not change significantly throughout the entire γ dose range studied of 0–14 Mrad.

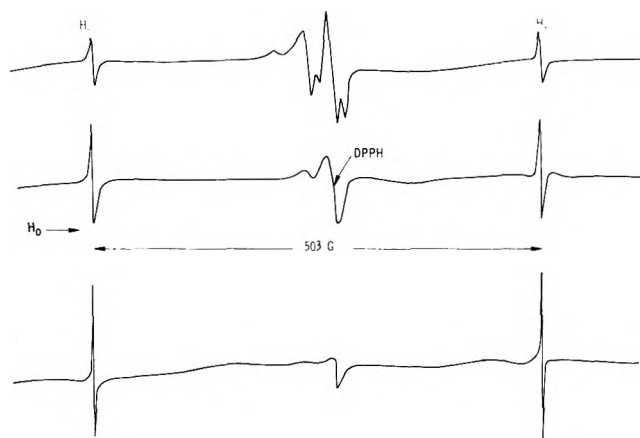


Figure 1. Epr spectra of H_t in irradiated lithium phosphates at room temperature: top spectrum, LiPO_3 ; center spectrum, $\text{Li}_4\text{P}_2\text{O}_7$; lower spectrum, Li_3PO_4 ; ^{60}Co γ dose = 1.4×10^6 rads; $H_1 = 0.011$ G; $H_m = 0.25$ G.

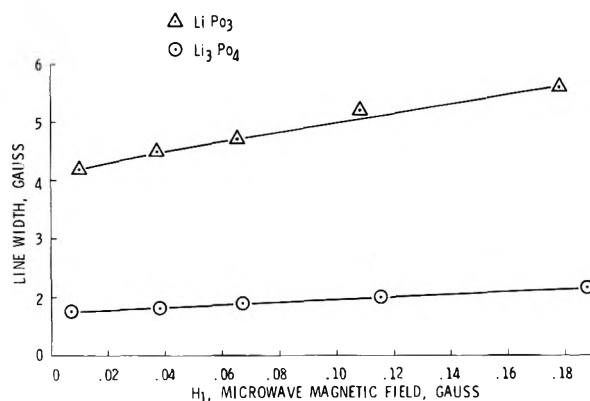


Figure 2. Variation of epr peak-to-peak line width of H_t . High-field line in LiPO_3 and Li_3PO_4 with increasing microwave magnetic field, H_1 ; ^{60}Co γ -dose = 1.4×10^6 rads; $H_m = 0.25$ G.

TABLE I

Compound	Line width, G	Line shape parameter
Lithium phosphate (Li_3PO_4)	0.74	3.4
Lithium pyrophosphate ($\text{Li}_4\text{P}_2\text{O}_7$)	0.96	10.0
Lithium metaphosphate (LiPO_3)	3.2	3.5
Calcium phosphate [$\text{Ca}_{10}(\text{PO}_4)_6(\text{OH})_2$]	0.35 ^a	3.1 ^a

^a Reference 6.

However, as shown in Figure 2, the high-field H_t line width in LiPO_3 and Li_3PO_4 increases with increasing microwave magnetic field, H_1 . The intensity of this H_t line saturates readily with increasing H_1 ; a representative slow passage progressive saturation curve is shown in Figure 3. After the onset of saturation the H_t signal intensity decreases sharply which is characteristic of an epr line broadened by significant homogeneous contributions. The line shape parameter of 3.4 and the broadening of H_t line with increasing H_1 also suggest that these lines are broadened predominantly by homogeneous mechanisms, with a much smaller contribution from inhomogeneous mechanisms.

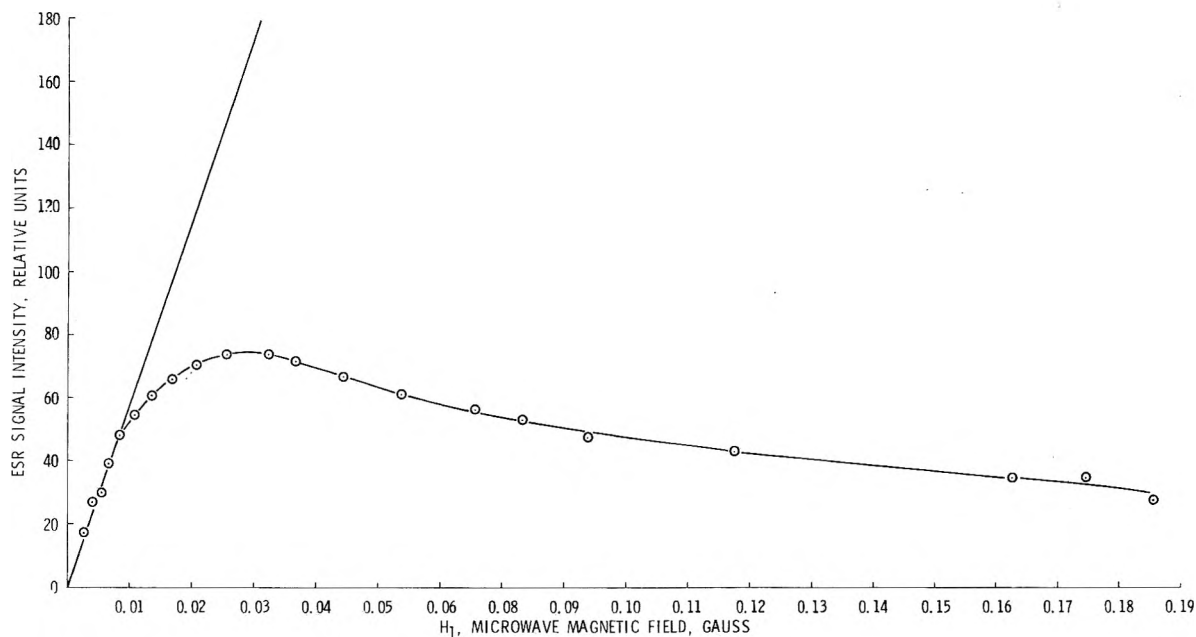


Figure 3. Slow-passage (200 Hz) microwave power saturation of the high-field epr line of H_t in Li_3PO_4 : ^{60}Co γ -dose = 1.4×10^6 rads; $H_m = 0.25$ G.

The line broadening characteristics of H_t in γ -irradiated $\text{Li}_4\text{P}_2\text{O}_7$ are different from those described above for Li_3PO_4 and LiPO_3 . The H_t line shape in $\text{Li}_4\text{P}_2\text{O}_7$ remains extra-Lorentzian up to the highest radiation dose studied. The unsaturated line width slowly increases from 0.96 G at low γ doses to 1.20 G at a dose of 14 Mrads. The line broadens significantly with increasing H_1 , and the shape of the microwave power saturation curve is very similar to that shown in Figure 3 for H_t in Li_3PO_4 . These data are consistent with the hypothesis that the H_t lines in $\text{Li}_4\text{P}_2\text{O}_7$ are broadened almost completely by homogeneous mechanisms and that inhomogeneous broadening mechanisms are negligible. Thus the increasing H_t concentrations produced by increasing radiation doses result in increased spin-spin relaxation which is observed as an increasing H_t line width at low values of H_1 . The increases in spin-spin relaxation with increasing H_t concentration suggest that the H_t are homogeneously distributed in the crystalline matrix; such interpretations have been described in detail previously by Zimbrick and Kevan¹ and Hase and Kevan.¹¹ (Also, see section E below.) The line shape, line broadening, and microwave power saturation characteristics of the H_t lines in the phosphates reported herein closely resemble the corresponding characteristics of H_t in low-temperature irradiated acidic glasses.^{1,2} However, the large difference between the unsaturated line width of H_t in acidic glass and the three types of phosphate (Table I) would not be expected *a priori* and this finding warrants further discussion. The differences in line width can be explained by one or a combination of the following hypotheses: (a) the great differences in yield of H_t between acidic glass and the phosphates, and among the phosphates, results in widely varying spin-spin relaxation which, in turn, controls the observed line width through its effect on homogeneous line broadening; or (b) the H_t trapping sites are populated with magnetic nuclei (P and H in the case of the phosphates) which result in varying amounts of unresolved hyperfine interaction with the unpaired electrons on the H_t . This unresolved hyperfine interaction affects the observed H_t line width through its contribution to inhomogeneous

TABLE II

Compound	$G(H_t)^a$	Water content, mg of $\text{H}_2\text{O/g}$ of solid ^b	amount of P/mol wt of compd
Li_3PO_4	0.080	29.40	2.67×10^{-1}
$\text{Li}_4\text{P}_2\text{O}_7$	0.012	29.60	3.07×10^{-1}
$\text{Ca}_{10}(\text{PO}_4)_6(\text{OH})_2$	0.0032 ^c	18.8 ^c	1.85×10^{-1}
LiPO_3	0.011	27.60	3.60×10^{-1}

^a Experimental error $\pm 15\%$. ^b Experimental error $\pm 5\%$. ^c Reference 6.

line broadening. It is evident that hypothesis a alone cannot explain the differences in line width, since the yields of H_t in the three types of phosphates (see section C and Table II) are all much lower than the yields in acidic glass; therefore, the line widths of H_t in the phosphates should be much more narrow than those in the acidic glass whereas in LiPO_3 they are almost as broad as in acidic glass (3.2 *vs.* ~ 4 G, respectively). Also, within the three types of phosphates, irradiated Li_3PO_4 exhibits the highest yield of H_t but the most narrow H_t lines, which is not predicted by hypothesis a alone. Hypothesis b must also be involved in the explanation of the line width variations since the satellite spectra associated with the H_t lines to be discussed in section B indicate clearly that the unpaired electron spins on the H_t are close to H and P nuclei. The data in Table II indicate that the bulk water content (and thus the number of protons) does not vary significantly among the three types of phosphates but that the relative amount of phosphorus varies as $\text{LiPO}_3 > \text{Li}_4\text{P}_2\text{O}_7 > \text{Li}_3\text{PO}_4$. The H_t line widths also vary in this sequence from broadest to most narrow. It is likely that a combination of factors from both hypotheses are operating to produce the observed line width variations.

B. Epr Satellite Lines and Local Environment of H_t . Zeldes and Livingston¹² and Trammell, *et al.*,¹³ have observed and studied the effect of surrounding magnetic nuclei on the satellite lines observed in the epr spectrum of H $_t$ in γ -irradiated H_2SO_4 and H_3PO_4 glasses. They as-

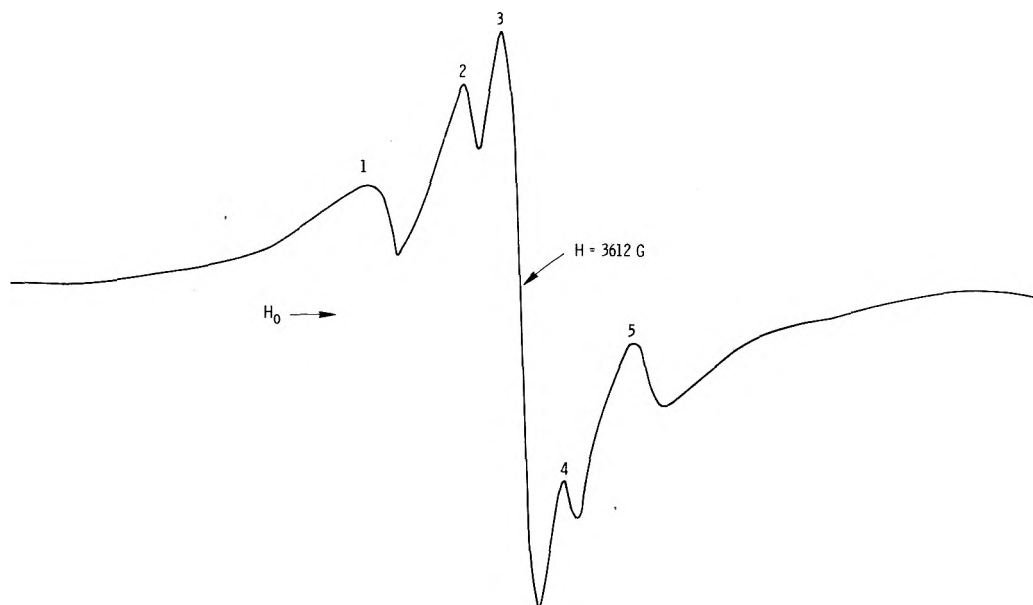


Figure 4. Epr spectrum of the high-field line of H_t in Li_3PO_4 : ^{60}Co γ -dose = 1.4×10^6 rads; $H_1 = 0.36$ G; $H_m = 0.25$ G.

cribed these satellite lines to the forbidden transitions of nearby proton spins in conjunction with the transitions of the electron spins as a consequence of a weak magnetic dipole-dipole coupling. Zimbrick and Myers¹⁴ have also observed satellites on both sides of the trapped electron line in γ -radiolysis of aqueous sugar ices.

The H_t epr spectrum in γ -irradiated Li_3PO_4 at high microwave power (shown in Figure 4) consists of five lines including the strong central (third line) H_t line. The outer lines numbered 1 and 5 appear to be a satellite pair with characteristics very close to those observed earlier for H_t in H_2SO_4 and H_3PO_4 . The separation of this satellite pair is ± 4.8 G for lower field H_t line at 3100 G and ± 5.6 G for the high-field H_t line at 3605 G. It is evident that the distance between the satellite pair is magnetic field dependent as observed earlier by Zeldes and Livingston.¹² The second and fourth lines constitute a second satellite pair separated from the central line by 4.76 MHz/sec or ± 1.7 G for H_t at 3100 G and 6.2 MHz/sec or ± 2.2 G for H_t at 3605 G. We have calculated the phosphorus resonant frequencies at 3100 and 3605 G and these are, respectively, ± 5.34 MHz/sec or ± 1.9 G and 6.21 MHz/sec or ± 2.2 G which are in good agreement with the observed spectra. Hence, it appears that these spectra are in fact due to the transitions of both adjacent phosphorus and proton spins in conjunction with the transitions of the H_t electron spins in Li_3PO_4 . A similar but somewhat less well-resolved spectrum of H_t is observed in the case of γ -irradiated $Li_4P_2O_7$ and is shown in Figure 5. In the same figure the effect of microwave power on the intensity of the satellite lines is shown. It is evident from the spectra that satellite lines are only observed at higher microwave powers. The outer lines marked 1 and 5 are separated from the central line by ± 5.0 G at 3100 G and ± 5.7 G at 3605 G which are typical distances for hydrogen satellites. The phosphorus satellite here is not quite as well resolved as in the case of Li_3PO_4 . These spectra present clear evidence that the trapping sites of H_t in Li_3PO_4 and $Li_4P_2O_7$ are populated with H and P nuclei. A careful study of the H_t lines in irradiated $LiPO_3$ failed to reveal the presence of either P or H satellite lines. The absence of satellite lines due to P transitions is not unexpected since they would be

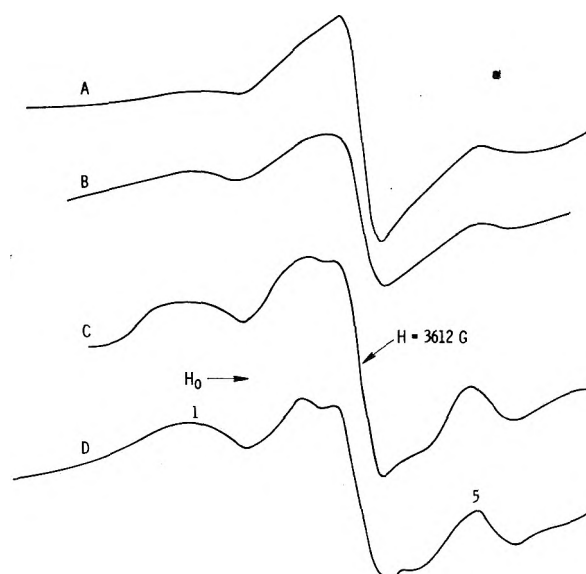


Figure 5. Epr spectra of the high-field line of H_t in $Li_4P_2O_7$ at various microwave powers: ^{60}Co γ -dose = 1.4×10^6 rads; $H_m = 0.25$ G, H_1 spectrum A = 0.011 G; H_1 spectrum B = 0.178 G; H_1 spectrum C = 0.263 G; H_1 spectrum D = 0.358 G.

obscured in the relatively large power saturated H_t line width in this phosphate (4.6 G). It is not clear at present why no proton satellite lines are observed in $LiPO_3$, but every other spectral characteristic of H_t in this matrix suggests that the P and H nuclei should be present at the trapping sites of H_t .

C. Radiation Induced Yields of H_t . The observed yields of H_t in Li_3PO_4 , $LiPO_3$, and $Li_4P_2O_7$ were determined by use of a radiation dose of 10^5 rads as described in the experimental section; the G values are given in Table II. This table also shows the water content for each of the phosphates studied. The $G(H_t)$ values in these lithium phosphates are much lower than those in other systems such as acidic ices but are larger than the $G(H_t)$ reported for calcium phosphate⁶ which, for comparison, is also shown in Table II. The $G(H_t)$ in Li_3PO_4 is about 7 times greater than in $Li_4P_2O_7$ and $LiPO_3$ although the water

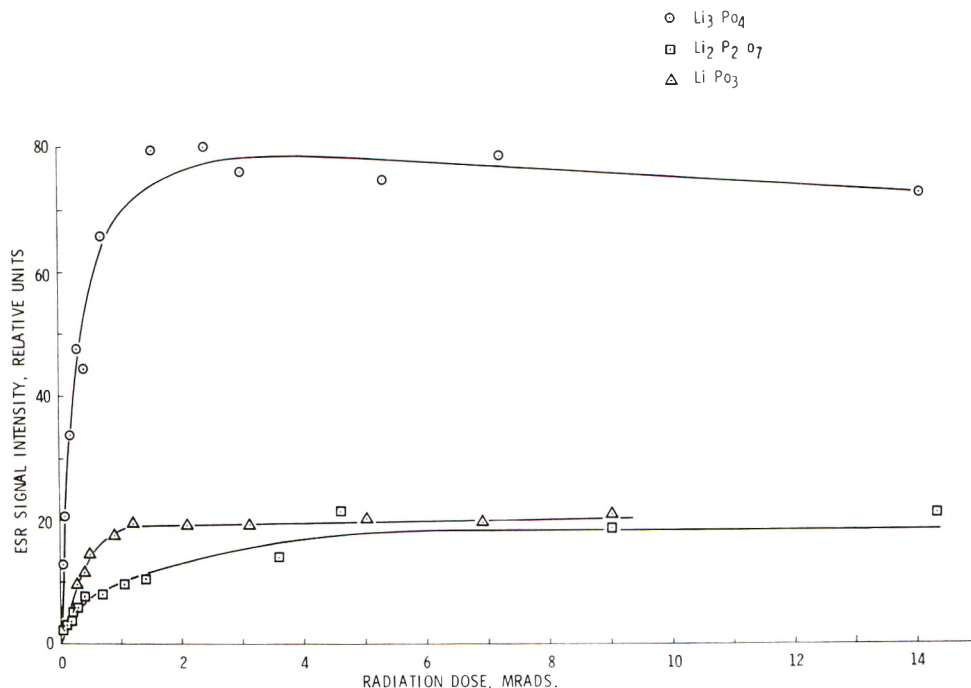
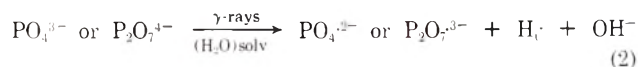
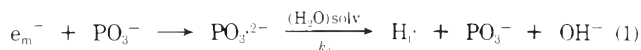


Figure 6. Relative concentration of H_1 vs. ^{60}Co γ -dose in lithium phosphates: $H_1 = 0.011$ G; $H_m = 0.25$ G.

content of each phosphate is similar to within experimental error. These data do not rule out the importance of the water of hydration for the formation of H_1 but they do indicate that other factors, such as the mobility of $H\cdot$ and local crystal structure, are important in determining the observed $G(H_1)$.

Since the data in the previous section indicate that the H_1 trapping site is populated with both H and P nuclei, it is proposed that the H_1 are formed according to reactions 1 and 2. This kind of reaction scheme was originally pro-



posed by Kevan¹⁵ as the mode of formation of H_1 in irradiated frozen polycrystalline oxyanion ices. In reaction 2, the radiation-produced mobile electron, e_m^- , cannot approach the polynegative phosphate anions close enough to react, due to charge repulsion, so that e_m^- is not directly involved in the production of H_1 in these cases.

D. Radiation Dose Saturation and Decay of H_1 at Room Temperature. The relative concentration of H_1 (as represented by $\Delta w^2/h$ in which Δw is the peak-to-peak line width and h is the peak-to-peak height of the first derivative absorption signal) was measured as a function of ^{60}Co radiation dose in the three types of phosphates. The results are shown graphically in Figure 6. The irradiated Li_3PO_4 contains about 7 times more H_1 than $\text{Li}_4\text{P}_2\text{O}_7$ or LiPO_3 at very low doses (up to 0.2 Mrad). The relative H_1 concentrations begin to saturate in the dose region 1–3 Mrads. At saturation, $\text{Li}_4\text{P}_2\text{O}_7$ and LiPO_3 contain approximately the same concentration of H_1 which is one-fourth the H_1 concentration in Li_3PO_4 .

Samples of the three types of phosphates which had been irradiated with a ^{60}Co dose of approximately 1.4 Mrads were studied to determine the amount of decay in

the H_1 signal intensity as a function of storage time at room temperature. These data are plotted in Figure 7. The relative rates of decay decrease in the order $\text{Li}_3\text{PO}_4 > \text{LiPO}_3 > \text{Li}_4\text{P}_2\text{O}_7$.

Upon comparison of the curves in Figures 6 and 7 it is evident that the phosphates in which the concentrations of H_1 are highest also yield the most rapid H_1 decay rates. The initial half-times for H_1 decay in Li_3PO_4 , LiPO_3 , and $\text{Li}_4\text{P}_2\text{O}_7$ are, respectively, 14, 32, and 48 hr, all of which are much shorter than the value of 96 hr measured previously for H_1 in calcium phosphate.⁶ Since the H_1 are not stable at room temperature, there will always be decay occurring during production. This in turn means that the dose region in which saturation occurs is dose-rate dependent at low dose rates, where irradiation times that are appreciable fractions of the H_1 half-time must be employed.

E. Paramagnetic Relaxation Characteristics of the Epr Doublet of H_1 . Numerous previous studies^{1,2,11,14,16} have used paramagnetic relaxation times to give information about the spatial distributions of trapped species. In these studies, the root of the relaxation time product $(T_1T_2)^{1/2}$ is measured as a function of radiation dose; T_1 is the spin-lattice relaxation time and T_2 is the spin-spin relaxation time which is controlled by the local concentration of trapped spins. Changes in $(T_1T_2)^{1/2}$ with dose are interpreted as being due to changes in T_2 which in turn indicate changes in local spin concentration. If $(T_1T_2)^{1/2}$ decreases in a dose region in which the sample-average concentration of trapped spins is increasing, this result supports the hypothesis that the trapped spins have a spatially uniform distribution. The opposite result (no change in $[T_1T_2]^{1/2}$ in the same dose region) supports the hypothesis that the spins have a nonuniform spatial distribution. Regardless of the uniformity or nonuniformity of the spatial distribution of spins, the choice of theoretical treatment to be used to calculate relaxation times depends on whether the epr line is broadened entirely by either homogeneous or inhomogeneous mechanisms or by a combination of both types of mechanisms. If the line

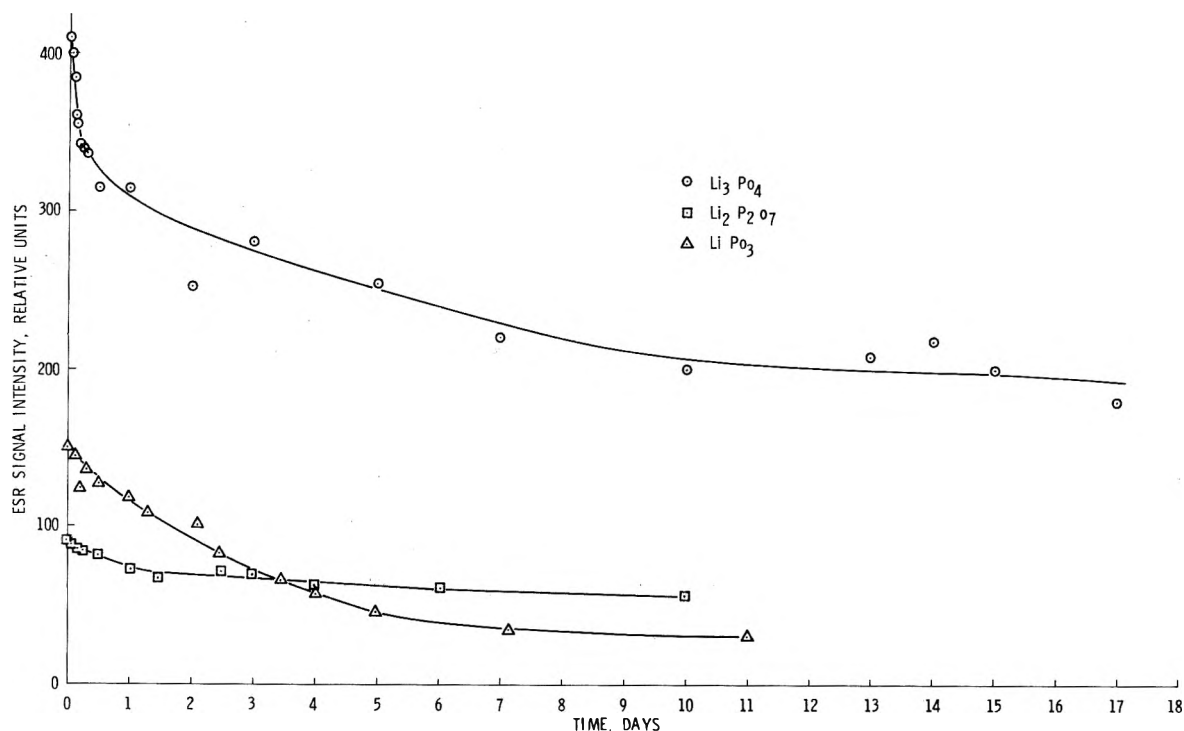


Figure 7. Thermal decay of H_t in irradiated lithium phosphates as a function of post-irradiation storage time at room temperature: ^{60}Co γ -dose = 1.4×10^6 rads; $H_m = 0.25$ G; $H_1 = 0.011$ G.

broadening is entirely homogeneous or inhomogeneous, then the Portis¹⁷ treatment is used; if a combination of broadening mechanisms exists, then the Castner¹⁸ treatment is applied.

In the present work, the relaxation characteristics of the high-field line of the H_t doublet from irradiated Li_3PO_4 were studied by means of slow-passage (200 Hz) progressive power saturation measurements. Li_3PO_4 was the only one of the three types of phosphate studied which exhibited yields of H_t sufficient to be detected by 200-Hz modulation over a wide dose region. Based on the spectral parameters discussed in previous sections (Lorentzian line shape, broadening of H_t lines at high microwave powers, and shape of the microwave power saturation curves) it was apparent that the Portis¹⁷ treatment of homogeneous line broadening should be applied to the power saturation curves to obtain values of $(T_1T_2)^{1/2}$. Figure 8 presents a plot of $(T_1T_2)^{1/2}$ vs. ^{60}Co radiation dose for H_t in Li_3PO_4 . $(T_1T_2)^{1/2}$ decreases from a value of 2.7×10^{-6} sec at the lowest dose studied to a value of 1.95×10^{-6} sec at a dose of 5.0 Mrads. A comparison of the data in Figures 7 and 8 shows that the decrease in relaxation time occurs in the same region of dose in which the concentration of H_t is increasing sharply. These data support the hypothesis that the H_t in Li_3PO_4 are distributed homogeneously in the polycrystalline matrix. A similar result was obtained earlier by Zimbrick and Kevan¹ for H in irradiated acidic glass at 77°K. However, it was reported previously that $(T_1T_2)^{1/2}$ of the H_t line in calcium phosphate actually increased with radiation dose in the same dose region in which the concentration of H_t increased.⁶ From these data it was hypothesized that the H_t were produced initially with an inhomogeneous spatial distribution but, due to their mobility, the distribution became more uniform with increasing radiation dose. In the present case of Li_3PO_4 it must be recalled that the initial half-time of the H_t is only 14 hr compared with 96 hr for H_t in calcium phos-

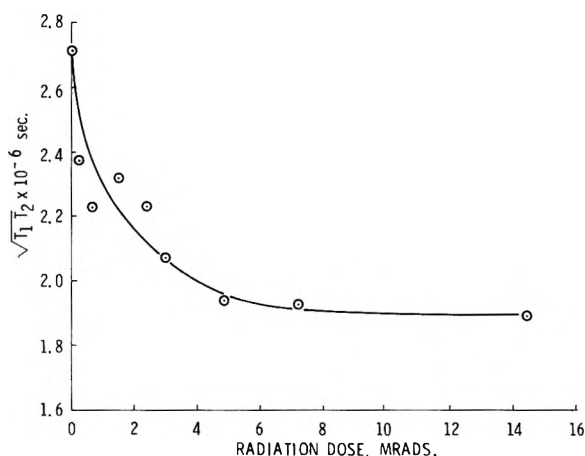


Figure 8. Variation of relaxation time with ^{60}Co γ -dose for the high-field epr line of H_t in Li_3PO_4 ; $H_m = 0.25$ G.

phate matrix. It is likely that although the H_t in Li_3PO_4 are mobile in the Li_3PO_4 matrix than in the calcium phosphate matrix. It is likely that although the H_t in Li_3PO_4 are produced with an initial inhomogeneous distribution, they will have moved to a sufficient extent to randomize their distribution by the time epr relaxation measurements have been made.

Acknowledgment. Partial financial support for this research was provided by United States Atomic Energy Commission, Contract No. AT(11-1)-1057-8, which furnished chemical supplies and provided partial salary for one of the investigators. National Aeronautics and Space Administration Grant No. NGR-17-002-050 provided partial salary for one of the investigators and a technical assistant. U. S. Air Force Contract No. F19628-69-C-0009 furnished funds for part of the epr apparatus. Thanks are also expressed to Professor Larry Kevan, Wayne State

University, Detroit, Mich., for valuable discussions and to Gisela Dreschhoff for her assistance in performing the data analyses.

References and Notes

- (1) J. D. Zimbrick and L. Kevan, *J. Chem. Phys.*, **47**, 5000 (1967).
- (2) L. Kevan in "Radiation Chemistry of Aqueous Systems," G. Stein, Ed., Wiley-Interscience, New York, N. Y., 1968, p 21.
- (3) B. G. Ershov and A. K. Pikaev, *Radiat. Res. Rev.*, **2**, 1 (1969).
- (4) P. W. Atkins, N. Keen, M. C. R. Symons, and H. W. Wardale, *J. Chem. Soc.*, 5594 (1963).
- (5) S. Ogawa and R. W. Fessenden, *J. Chem. Phys.*, **41**, 1516 (1964).
- (6) Y. P. Virmani, J. D. Zimbrick, and E. J. Zeller, *J. Phys. Chem.*, **75**, 1936 (1971).
- (7) B. L. Bales and L. Kevan, *J. Chem. Phys.*, **52**, 4644 (1970).
- (8) R. Livingston and A. Weinberger, *J. Chem. Phys.*, **33**, 499 (1960).
- (9) R. Livingston, H. Zeldes, and E. H. Taylor, *Discuss. Faraday Soc.*, **19**, 166 (1955).
- (10) R. A. Levy, *Phys. Rev.*, **102**, 31 (1956).
- (11) H. Hase and L. Kevan, *J. Chem. Phys.*, **52**, 3183 (1970).
- (12) H. Zeldes and R. Livingston, *Phys. Rev.*, **96**, 1702 (1954).
- (13) G. T. Trammell, H. Zeldes, and R. Livingston, *Phys. Rev.*, **110**, 630 (1958).
- (14) J. D. Zimbrick and L. S. Myers, Jr., *J. Chem. Phys.*, **54**, 2899 (1971).
- (15) L. Kevan in "Progress in Solid-State Chemistry," Vol. 2, H. Reiss, Ed., Pergamon Press, New York, N. Y., 1965, pp 304-329.
- (16) Y. P. Virmani, J. D. Zimbrick, and E. J. Zeller, *Mod. Geol.*, **3**, 43 (1971).
- (17) A. M. Portis, *Phys. Rev.*, **91**, 1971 (1953).
- (18) T. G. Castner, *Phys. Rev.*, **115**, 1501 (1959).

An Investigation of the Dynamic Equilibrium between Chemisorbed and Absorbed Hydrogen in the Palladium/Hydrogen System

J. F. Lynch and Ted B. Flanagan*

Chemistry Department, University of Vermont, Burlington, Vermont (Received May 14, 1973)

It is shown that the chemisorbed hydrogen which is the precursor to absorbed hydrogen in palladium is chemisorbed only after a strongly chemisorbed monolayer of hydrogen is formed. It is suggested that the weakly chemisorbed hydrogen is located in surface interstitial sites and is thus a natural precursor to interstitially absorbed hydrogen. The strongly chemisorbed hydrogen is not in equilibrium with absorbed hydrogen. Weak chemisorption can be extensive, *e.g.*, at 2 mm (0°), $\theta' = 0.34$ where θ' is based on chemisorbed hydrogen in excess of the strongly held monolayer. Isothermic heats of weak chemisorption vary from 44.8 kJ/mol of H_2 ($\theta' = 0.06$) to 36.4 kJ/mol of H_2 ($\theta' = 0.3$). Differential entropies of weak chemisorption are reported.

Introduction

The absorption of hydrogen by palladium has been investigated over a wide range of temperatures, pressures, and concentrations.¹ At small concentrations the dissolved hydrogen behaves ideally; *i.e.*, Sieverts' law is obeyed, n ($= H$ to Pd atomic ratio) $= K_s p^{1/2}$. In this region of small hydrogen solubilities, the α -phase, nonideal behavior commences as the hydrogen concentration increases until a second, hydrogen-rich, nonstoichiometric phase appears, β . The compositions of the α and β phases which coexist at 25° are $n = 0.015$ and 0.58 , respectively.¹ In both phases the palladium lattice is fcc with the hydrogen atoms located in the octahedral interstices.¹

Despite palladium's importance as a hydrogenation catalyst, there have been relatively few attempts to investigate the adsorption of hydrogen by palladium because of complications introduced by the occurrence of simultaneous absorption. On a palladium film, Beek² reported a value of $q = 108.8$ kJ/mol of H_2 for the calorimetric heat of adsorption at $\theta = 0$. Vert, Mosevitch, and Tverdovskii³ measured adsorption isotherms for the Pd/ H_2 system by a clever electrochemical technique. Heats of adsorption were found to be 113.0 kJ/mol of H_2 at $\theta = 0$ (remarkably close to Beek's value); the heats remained constant at this value to $\theta = 0.4$ and then declined to 54.4 kJ/mol of

H_2 as θ approached unity. This method suffers from a possible error if adsorption and absorption overlap.

Breger and Gileadi⁴ have recently determined electrochemically the equilibrium constant for the hydrogen absorption-adsorption equilibrium on bright palladium at room temperature. Over the range studied, the α phase, a greater value of θ was found for the surface than for the bulk; *e.g.*, at $\theta_{ads} = 0.5$, n ($= \theta_{abs}$) $= 7.5 \times 10^{-4}$. The Frumkin isotherm described the adsorption data over most of the θ range and a Langmuir isotherm applied at low coverages. Heats of adsorption were not measured.

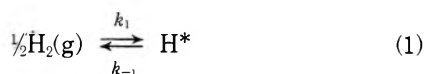
Gas-phase studies have been made recently under ultra-high vacuum (UHV) conditions by Tardy and Teicher⁵ and Aldag and Schmidt⁶ with palladium filaments. The former workers observed only one type of adsorbed hydrogen which desorbed at approximately 650° and did not correspond to a complete monolayer. In the other flash desorption study,⁶ three different adsorbed states of binding energies, 92, 104.6, and 146.4 kJ/mol of H_2 were found after the filament had been exposed to hydrogen at 200 or $300^\circ K$. However, when the filament was exposed to hydrogen at $100^\circ K$, an additional peak appeared in the desorption spectra corresponding to a binding energy of only 54 to 58 kJ/mol of H_2 . They attributed this to absorbed hydrogen because they concluded that at the temperatures

studied only at 100°K would the β phase of the Pd/H₂ system form at the pressures which they used. It is not clear however, why substantial hydrogen should not dissolve to form the α phase of the Pd/H₂ system at 200 or 300°K. This solubility can be readily estimated from the known Sieverts' constants for the Pd/H₂ system;^{7,8} e.g., at 300°K, 1.6×10^{16} molecules should be absorbed into the α phase at 5×10^{-5} mm pressure and this corresponds to approximately 10 times the monolayer capacity of their filament as calculated from the geometric area of their filament. Their conclusion that the low-temperature uptake of hydrogen corresponded to formation of β phase of the Pd/H₂ system must be viewed with reservation especially in view of the expected slow rate of diffusion at this temperature.

Starting from an oxygenated palladium black surface, Sermon⁹ has recently measured the surface area of palladium by extrapolating the amount of absorbed hydrogen to zero pressure. Values of the surface area were determined in this way at 0 and 30° and were in good agreement with the BET surface areas. It was the goal of this research to amplify Sermon's study to the region where adsorption is incomplete and it is hoped in this way to obtain information about the nature of the chemisorbed hydrogen which is in dynamic equilibrium with the absorbed hydrogen.

General Considerations of the Adsorption \leftrightarrow Absorption Equilibrium

The following elementary steps occur for absorption of hydrogen from the gas phase



where H* and [H] refer to adsorbed and absorbed states of hydrogen, respectively. $K_1 = (\text{H}^*)/p^{1/2}$ and $K_2 = [\text{H}]/(\text{H}^*)$ and therefore $K_1K_2 = K_s$ which is Sieverts' constant if [H] is expressed as n ($= \text{H}/\text{Pd}$). The known temperature dependence of K_s ^{7,8} leads to

$$\Delta\bar{H}_1^\circ + \Delta\bar{H}_2^\circ = -9.6 \text{ kcal}$$

where the standard designation refers to infinite dilution and $\Delta\bar{H}_2^\circ$ must be less than 24.3 kJ/g-atom of H because the energy of activation for diffusion of hydrogen in palladium is 24.3 kJ/g-atom of H.¹⁰ The value of $\Delta\bar{H}_2^\circ$ cannot be greater than the activation energy for diffusion because slow surface steps are not observed during studies of diffusion of hydrogen through palladium black-coated membranes.¹¹ The value of $-\Delta\bar{H}_1^\circ$ must therefore be ≤ 33.9 kJ/g-atom of H. (Consideration of a mobile layer of adsorbed hydrogen does not alter these conclusions.) This suggests that strongly chemisorbed hydrogen ($-\Delta\bar{H}_1^\circ = q > 67.8$ kJ/mol of H₂) cannot be in rapid equilibrium with absorbed hydrogen.

Experimental Section

An ultrahigh-vacuum apparatus was employed for the present studies which was, of course, grease- and mercury-free. Pressures were recorded with a series of diaphragm gauges (Barocel); the most sensitive one had a full-scale deflection of 10^{-4} mm. The gauge which had the intermediate range, overlapping the ranges of the other two gauges, was calibrated against a McLeod gauge. It

agreed, to within the error of reading the McLeod gauge, with the original calibration of the gauge. The vacuum system had an ion pump, oil diffusion pump, and all-metal valves.

The sample employed for the absorption studies (low surface area sample) was 6.9 g of palladium wire (purity 99.9%, 1 mm diameter). It had been previously used for studies of hydrogen absorption and was therefore active toward hydrogen absorption. It was heated to white heat before sealing into the vacuum system. After degassing to about 10^{-7} mm, doses of hydrogen were added to the sample from a known volume (182.7 cm³). The course of hydrogen uptake was recorded with a strip chart recorder operating from the diaphragm gauges. This allowed for the unambiguous determination of equilibrium. Data were also taken with a 3.35-g sample of palladium sheet (0.012 cm thickness) which had not been previously employed for absorption studies.

Palladium black (3.61 g) was obtained from the Engelhard Minerals and Mining Corp. It was inserted into the vacuum system and degassed to 10^{-6} mm pressure (40°). A trap was inserted into the line in order to remove water vapor resulting from the removal of oxygen from the surface of the black by hydrogen.

Results

Absorption. Data for the absorption of hydrogen (deuterium) by palladium can be described by

$$\frac{\Delta\bar{G}_H^{xs}}{RT} = \ln p^{1/2} \frac{(1-n)}{n} = \frac{\Delta\bar{H}_H^\circ}{RT} - \frac{\Delta\bar{S}_H^\circ}{R} + \frac{2W_{HH}n}{RT} + \frac{W_E(n)}{RT} \quad (3)$$

where W_{HH} is the attractive interaction energy per mole of H, $W_E(n)$ allows for the variable energy of electron donation as the collective bands of the palladium are filled by the hydrogen, and n is the H-to-Pd atomic ratio.¹² At low values of n the electron donation term is not a factor. Plots of $\Delta\bar{G}_H^{xs}/RT$ against n give $2W_{HH}/RT$ from their slopes and $\Delta\bar{H}_H^\circ/RT - \Delta\bar{S}_H^\circ/R$ from their intercepts.¹³ (In Wicke and Nernst's nomenclature,⁷ $E_H = 2W_{HH}$.)

Previous data have been determined over the same temperature range but not necessarily at the same temperatures by Wicke and Nernst for both Pd/H₂ and Pd/D₂,⁷ and by Simons and Flanagan for Pd/H₂.⁸ The former workers used hydrogen-transfer catalysts to obtain equilibrium and the latter workers used an electrochemical technique. More recently, Clewley, *et al.*,¹⁴ have determined equilibrium data for this system in the present apparatus but over a small range of n values where deviations from Sieverts' law were negligible. All of these absorption data were determined with low surface area samples where adsorption can be neglected. While the previous data are in reasonable agreement with each other, it was obvious that very precise absorption data were required here in order to obtain accurate adsorption data by differences between the amounts sorbed and absorbed. It was therefore necessary to redetermine some absorption data for both hydrogen and deuterium in the α -phase region.

Data are shown in Figure 1 plotted *via* eq 3 compared to some previous data obtained by Wicke and Nernst⁷ at the two common temperatures. Detailed data such as shown in Figure 1 were determined at 24, 37.5, 50, and 75° for hydrogen and deuterium. It proved unnecessary to obtain

TABLE I: Thermodynamic Data for Dissolved H(D) in Pd (25–75°)^a

$\Delta\bar{H}_H^\circ$	$\Delta\bar{H}_D^\circ$	$\Delta\bar{S}_H^\circ$	$\Delta\bar{S}_D^\circ$	W_{HH} (25°)	W_{DD} (25°)	Ref	Method
-10.2	-8.18	-55.2	-54.8	-23.45	-18.00	This work	UHV, bulk Pd
-10.0	-8.47	-54.0	-55.3	14	UHV, bulk Pd
-10.0	-8.70	-53.1	-56.0	14	From isochores
-10.0	...	-54.4	...	-23.08	...	8	Electrochemical
-9.67	-7.88	-53.5	-53.1	-23.63	-22.05	7	Transfer-catalyst

^a The units of $\Delta\bar{H}^\circ$ are kJ/g-atom of H; those of $\Delta\bar{S}^\circ$ are J/deg g-atom of H; and those of W are kJ/g-atom of H.

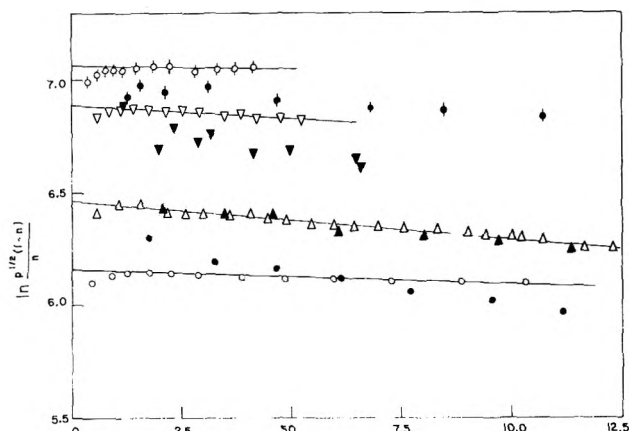


Figure 1. Representative plots of $\ln p^{1/2}[(1-n)/n]$ vs. n (= H-to-Pd, atomic ratio): ●, Pd/D₂(75°); ▽, Pd/D₂(50°); △, Pd/H₂(75°); ○, Pd/H₂(50°). Open symbols refer to present study and closed symbols refer to the data of ref. 7.

data at 0° because the previous data are in good agreement and because the extent of absorption is relatively small compared to adsorption at 0° so that small errors in the absorption data are not significant. Thermodynamic data derived from these plots are shown in Table I in comparison to the previous data from the literature.

Values of $W_{HH} = -14.13$ kJ/g-atom of H and -17.25 kJ/g-atom of H have been recently quoted by Burch¹⁵ as having been determined from the data of Wicke and Nernst⁷ by Burch and by Brodowsky,¹⁶ respectively. These values, which are larger than those in Table I, were calculated by Burch using the expression $W_{HH} = 6w$, where w is the interaction energy which appears in the quasichemical approximation, i.e., $W_{HH} = E_H/2 = 6RT[1 - (\exp -w/RT)]$. W_{HH} is however, not equal to $6w$ because it is not valid to expand the exponential term to only the first power since w and RT are of comparable magnitudes at 25°. The agreement of the various thermodynamic parameters is quite good generally. An exception is that the value of W_{DD} reported here is somewhat larger than that reported by Wicke and Nernst.⁷

The $\Delta\bar{G}_H^{xs}/RT$ vs. n plots exhibit a negative deviation from linearity as infinite dilution is approached. The data of Simons and Flanagan⁸ and Wicke and Nernst⁷ generally deviated in the opposite sense. This function is, of course, very sensitive to small errors in n and $p^{1/2}$ as $n \rightarrow 0$. Either a small amount of adsorption or segregation of interstitial hydrogen at line defects could cause the deviations noted.

Adsorption. Titration of an Oxygenated Palladium Surface with Hydrogen. The sample was evacuated for 24 hr in the UHV system before titration. (The term UHV system refers to the circumstances that a UHV apparatus was employed, i.e., grease- and mercury-free with the ability to reach ultrahigh vacuum if needed. In practice, there proved to be no necessity to attain ultrahigh vacuum for

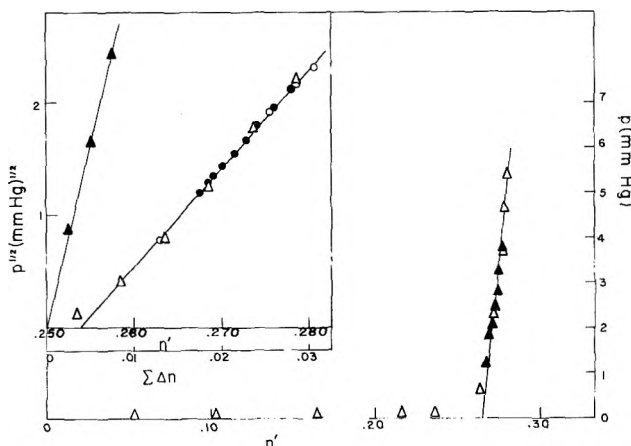
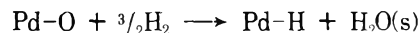


Figure 2. Plot of p vs. n' during titration of oxygenated surface with H₂(25°). n' has been calculated from the total hydrogen removal from the gas phase and is thus an apparent value during the titration: △, during addition of H₂; ▲, during desorption of H₂. Inset: plot of $p^{1/2}$ vs. n showing details of region where pressure buildup occurs following the titration of the oxygen: ○, addition of H₂; ●, desorption of H₂. Shown in comparison are data obtained following evacuation (12 hr) and subsequent addition of increments of H₂: △, sorption of H₂. Data for absorption behavior only is also shown, ▲ (25°).

the studies carried out here. The importance of having a grease- and mercury-free system should be emphasized however, because it has been previously noted that absorption equilibrium could not be obtained between hydrogen and bulk palladium below 120°. Until definite pressure increases were noted (Figure 2), the vacuum after each increment of hydrogen was added was of the order of 0.01 mm. The pressure started to increase at $n' = 0.248$ ($n = 0.0827$), where n' is the apparent H-to-palladium atomic ratio based on hydrogen removed from the gas phase, and n is determined from the reaction



and includes both adsorbed and absorbed hydrogen. The inset (Figure 2) shows the detailed behavior in the region where the pressure buildup occurs plotted as $p^{1/2}$ against n' . The behavior in this region was reversible.

Sermon⁹ has shown that the extrapolation of p against n' to the abscissa (zero pressure) yields a surface area for the palladium black which is in good agreement with BET determinations. This method of surface area measurement is based on one hydrogen atom chemisorbed per palladium and the average number of palladium atoms per square centimeter equal to 1.2×10^{15} .

Sermon⁹ states that adsorption of hydrogen is complete when absorption commences. This is not wholly true, however, as the inset in Figure 2 shows. The absorption datum determined here on the low surface area sample has a much greater slope than the sorption datum measured on the black following titration.

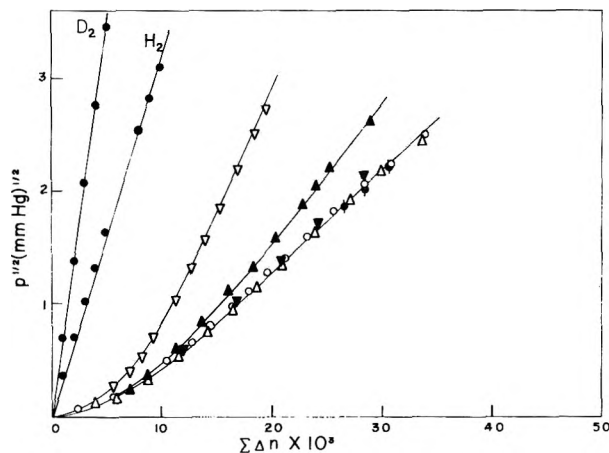


Figure 3. Plots of sorption of $H_2(D_2)$ following evacuation (12 hr) of titrated sample and then only evacuation between runs: \circ , initial run following titration and evacuation; Δ , ∇ , subsequent runs (25°). Absorption behavior determined here: \bullet , H_2 ; \circ , D_2 (25°). \blacktriangle , D_2 sorption following evacuation (12 hr) of sample previously titrated with H_2 ; ∇ , D_2 sorption following titration of sample with D_2 and subsequent evacuation (12 hr). A few desorption points are shown for H_2 sorption, \blacklozenge .

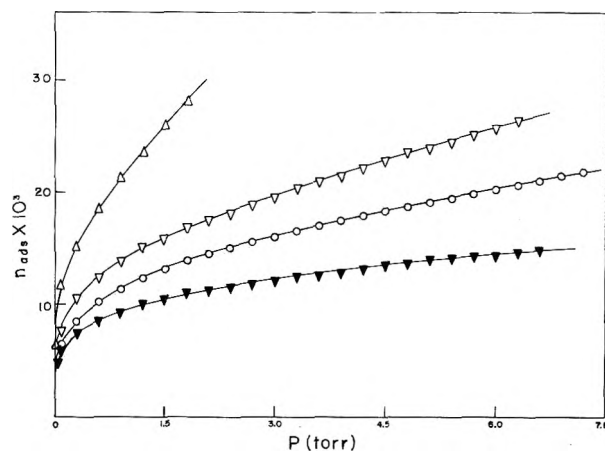


Figure 4. Representative isotherms for weak chemisorption plotted as $\Sigma \Delta n_{ads}$ vs. p : Δ , 0° ; ∇ , 25° ; \circ , 37.5° Pd/ H_2 and \blacktriangledown , 25° Pd/ D_2 .

Further evidence for adsorption occurring after the completion of the monolayer can be seen from Sermon's data, e.g., Figure 4 in his paper, where a comparison is made of p - n' relationships (0°) for a sample before and after heat treatment (HT). The slopes are quite different for the two runs. The sample before HT has a much smaller slope than after HT. If adsorption were completed, as suggested by Sermon, the sample after HT would have a greater fraction of bulk palladium relative to surface palladium, if continued adsorption were not a factor. In fact, the opposite occurs indicating the presence of adsorption after the completion of the oxygen removal.

Weak Chemisorption of Hydrogen on Palladium. Following titration of the oxygenated surface with hydrogen, it can be safely assumed that all of the oxygen has been removed and a monolayer of hydrogen has been formed. Support for this assumption is Sermon's finding that the area calculated from hydrogen chemisorption agrees with the BET area and also the reversible behavior observed following the titration suggests the complete removal of oxygen.

After titration the sample was evacuated for 12 hr (25°) while simultaneously removing the water which had been trapped during the titration. Doses of hydrogen were then added, and a sorption isotherm was determined (Figure 3) in which $\Sigma \Delta n$ is plotted against $p^{1/2}$ and $\Sigma \Delta n$ is the hydrogen sorbed by the sample after the titration. The hydrogen which is chemisorbed during titration is not removed during the prolonged evacuation since a measurable hydrogen pressure is observed when $\Sigma \Delta n$ is less than about 0.005. Equilibrium for sorption was rapid even at 0° (about 30 min) in marked contrast to earlier studies of hydrogen absorption by palladium black¹⁷ which were carried out in conventional vacuum systems where grease and mercury poisoning could play a role. Adsorption could not be separated from absorption on the basis of the kinetic behavior during hydrogen sorption. This supports the view that there is a rapid equilibrium between hydrogen in the weakly chemisorbed and absorbed states.

The data for this isotherm could be superimposed on that measured immediately following completion of the titration (Figure 2) if the oxygen were completely removed at $n = 0.0827$, rather than at the value obtained from Figure 1 resulting from the linear extrapolation of the p vs. n' plot. The corresponding surface areas are 39 and 41.5 $m^2 g^{-1}$, respectively. Sermon⁹ gives typical values as 30.8 (Kr, BET), 31.3 (N_2 , BET), and 32.7 $m^2 g^{-1}$ (extrapolation of p - n' plot) or for another sample, 7.1 (Kr, BET) and 7.4 $m^2 g^{-1}$ (extrapolation of the p - n plot). Therefore his areas from the p - n' extrapolation are about 5% larger than the BET values. This is about the same difference noted here if the areas are computed by the first appearance of hydrogen in the gas phase or by the linear extrapolation of the p - n' plot. The former method is more reasonable because hydrogen should appear in the gas phase only after the complete removal of the chemisorbed oxygen.

Several sorption runs were performed at 25° . A new run was done after the previous hydrogen was removed by evacuation at 25° for 12 hr. Prior to one run, the sample had been evacuated for 18 hr to a somewhat better vacuum than the others and this sorption isotherm agreed with the others (Figure 3). The reproducibility is quite good, indicating that there is a rather sharp division between the strongly held and weakly held hydrogen. The strongly chemisorbed hydrogen cannot be removed by evacuation at 25° . The sorption isotherms were reversible, i.e., desorption data coincided with sorption data. Sorption isotherms were also determined at 0 and 37.5° . After the sorption isotherm was measured at 37.5° , an isotherm was redetermined at 25° in order to demonstrate that sintering had not occurred. The β phase was not formed during any of these runs but a later isotherm (25°) was measured after some β phase had been formed, $n = 0.15$, and subsequently decomposed, and this agreed with the previous sorption isotherms.

Adsorption isotherms were determined by subtracting the absorption contribution at each pressure from the total sorption (Figure 3). Results are shown in Figure 4 and the isotherms show that adsorption continues after the monolayer is presumably complete. The isotherm at 0° shows no tendency to saturate and the magnitude of this weak chemisorption is great, e.g., at 0° , $\Sigma \Delta n_{ads} = 30 \times 10^{-3}$ ($p = 3$ mm). This represents an additional 0.43×10^{15} surface sites cm^{-2} in excess of the strongly held monolayer. It is suggested that the weakly chemisorbed hydrogen, which is in dynamic equilibrium with the absorbed hydro-

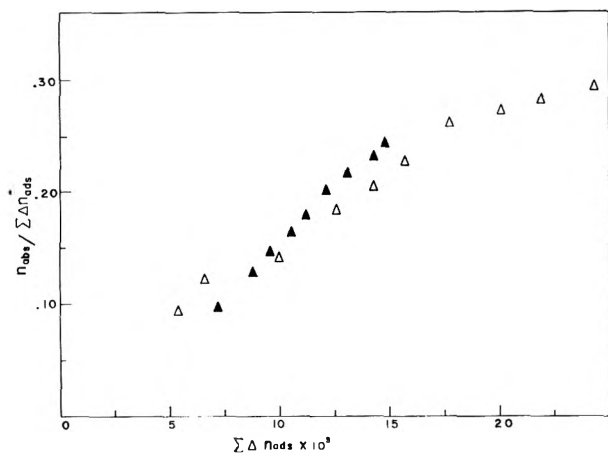


Figure 5. A plot of $n_{\text{abs}}/\Sigma\Delta n_{\text{ads}}$ plotted vs. $\Sigma\Delta n_{\text{ads}}(25^\circ)$: Δ , Pd/H₂; \blacktriangle , Pd/D₂.

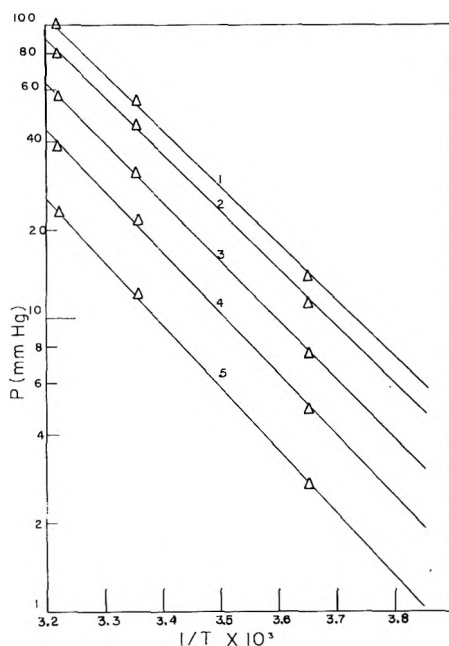


Figure 6. Representative Clausius-Clapeyron plots of $\log p$ vs. $1/T$ at constant surface coverage of weak chemisorption for Pd/H₂: 1, $\Sigma\Delta n_{\text{ads}} = 0.025$; 2, $\Sigma\Delta n_{\text{ads}} = 0.02$; 4, $\Sigma\Delta n_{\text{ads}} = 0.0175$; 5, $\Sigma\Delta n_{\text{ads}} = 0.015$.

gen, is held to a different type of surface site than the strongly chemisorbed hydrogen.

After an evacuation of 12 hr (25°) and consequent removal of weakly chemisorbed and adsorbed hydrogen, a sorption isotherm was determined for deuterium (Figure 3). It can be seen that its sorption behavior closely resembles that of hydrogen. It is possible that the strongly chemisorbed hydrogen may have exchanged with the deuterium so that the sample, in fact, contained mostly hydrogen. For this reason the sample was reexposed to oxygen and retitrated with deuterium. The sorption behavior following titration and the sorption behavior after subsequent evacuation of the sample agreed with each other, as was previously observed for hydrogen. Both of these sorption isotherms were quite different from the "deuterium" isotherm which had been determined when strongly chemisorbed hydrogen remained on the surface prior to the measurement of the isotherm (Figure 3). This clearly demonstrates that strongly chemisorbed hydrogen (or deuterium) resulting from the titration cannot be removed

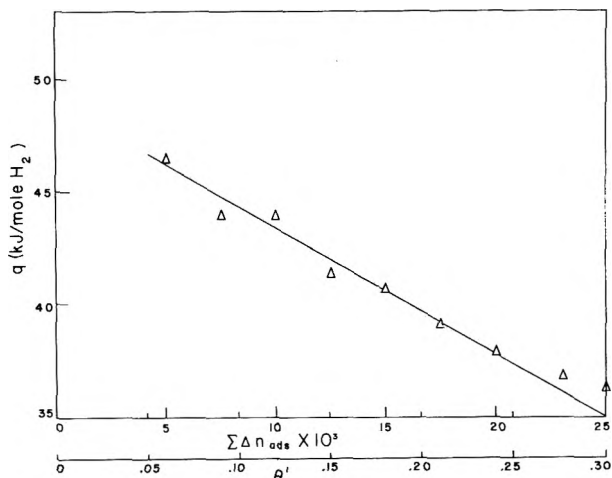


Figure 7. A plot of q_{iso} vs. $\Sigma\Delta n_{\text{ads}}$ (Pd/H₂).

from the surface by evacuation. This proves also that the strongly held hydrogen undergoes exchange with deuterium. The ratio of $n_{\text{abs}}^{\text{D}}$ to $\Sigma\Delta n_{\text{ads}}^{\text{D}}$ and the comparable ratio for hydrogen is shown in Figure 5 as a function of $\Sigma\Delta n_{\text{ads}}$. It can be seen that the two systems are quite comparable. The amount of absorption relative to weak chemisorption increases and then tends to level off at higher coverages. When the two-phase region of absorption is reached there must be a sudden jump in the value of the ratios.

The coverage corresponding to the weakly held hydrogen will be computed on the basis that the number of weak bonding sites to the surface is equal to the number of surface palladium atoms (see below). The coverage is therefore given by

$$\theta' = \Sigma\Delta n_{\text{ads}}/0.0827 \quad (4)$$

Isosteric heats have been calculated from the adsorption isotherms (Figure 4) at 0, 25, and 37.5°. Since these isotherms are reversible, the use of the Clausius-Clapeyron equation is justified for the determination of the heats of adsorption. Higher temperatures were not used because of the possibility of sintering the sample. Because of the limitation to three temperatures each isotherm was measured at least twice (Figure 4) and there was a good degree of reproducibility. The Clausius-Clapeyron plots are shown in Figure 6 and the heats of adsorption are shown as a function of coverage in Figure 7. They fall from approximately 46 kJ/mol of H₂ to 36.4 kJ/mol of H₂.

It is of interest that the heats of chemisorption determined here, 46 kJ/mol of H₂ to lower values, essentially commence at the value the Russian workers³ find when their chemisorption is complete; *i.e.*, at $\theta = 1$ they find $q = 52.5$ kJ/mol of H₂. This lends support to the hypothesis that there are strong and weak chemisorptions of hydrogen on palladium and that the properties of the weakly chemisorbed hydrogen are being examined here.

Corresponding entropies of adsorption have been determined from

$$\Delta\bar{S} = \frac{\Delta\bar{H} - RT \ln p}{T} \quad (5)$$

and are -69.3 J/deg mol of H₂ at $\theta' = 0.08$ and decrease to -83.6 J/deg mol of H₂ at $\theta' = 0.21$. This change corresponds about what would be expected from the configurational contribution for a mobile layer. However, at larger coverages the entropy change became about constant at the low value, ± 2 J/deg mol of H₂.

The Freundlich isotherm

$$\ln \theta' = (RT/q_m) \ln a_0 + (RT/q_m) \ln p$$

describes the adsorption data reasonably well from the lowest value of θ' to $\theta' = 0.26$ but thereafter deviations are noted; *i.e.*, $\ln \theta'$ increases too much with $\ln p$. The slopes of $\ln \theta'$ against $\ln p$ increase with temperature as expected and $q_m/2$, where $q/2 = -q_m/2 \ln \theta'$, is 8.6 kJ/mol of H_2 so that at, *e.g.*, $\theta' = 0.2$, $q = 28$ kJ/mol of H_2 compared to the corresponding isosteric heat of 39 kJ/mol of H_2 . It is concluded that the fit to the Freundlich isotherm is but a crude approximation to the actual state of the weakly chemisorbed hydrogen, *e.g.*, the heats appear to decline more linearly than logarithmically as required by the Freundlich isotherm. (The Temkin isotherm does not fit the data as well as the Freundlich isotherm despite the linear decline in the heats.)

Discussion

The fact that adsorption does not apparently saturate at the highest pressures studied here is characteristic of weak chemisorption—type C chemisorption.¹⁸ This is weak chemisorption, not physical adsorption. The observation that adsorption has not saturated is fully compatible with the experimental finding that absorption of hydrogen by palladium occurs rapidly even at very high pressures. For example, Baranowski and his coworkers¹⁹ have studied changes of electrical resistance due to hydrogen absorption in the range from 10,000 to 25,000 atm of H_2 . If the surface were completely saturated from reaction 2, further absorption at high pressure would be very difficult.

The nature of type C chemisorbed hydrogen on metals is in doubt; *i.e.*, some workers have suggested that it is molecular,^{20,21} and others that it is atomic.²² In order for this weakly chemisorbed hydrogen to be in rapid equilibrium with absorbed hydrogen, which is dissociated, it is reasonable to expect that type C chemisorbed hydrogen is atomic.

A chemisorbed hydrogen atom which is situated between the surface palladium atoms is a natural precursor to the absorbed state. This type of weakly chemisorbed hydrogen has been postulated to occur on platinum by Toya²³—the s state. This s-type chemisorbed hydrogen was suggested to be protonic and located in the interstices about 0.5 Å below the electronic surface of the platinum metal. Since absorbed hydrogen has been suggested to be protonic, *i.e.*, it donates an electron to the collective bands of palladium,^{24,25} and is then screened by the conduction electrons, this would also make the s-type state appropriate as a precursor to the absorbed state. Johnson²⁶ has recently examined the role of interstitially chemisorbed gases theoretically in some detail.

When hydrogen is absorbed into an interstitial site, it strains the palladium lattice. This has been discussed by Lewis,²⁷ von Stackelberg and Ludwig,²⁸ Brodowsky,²⁹ Wagner,³⁰ and Burch.¹⁵ The strain energy accompanying the insertion of one hydrogen atom into the lattice, $E_L/2$, is given by $E_L = -6w$ (w has been defined above). Alternatively, this can be estimated directly from the relationship

$$E_L = (4/3)GN_0\Delta V^2/V_1 \quad (6)$$

where G is the rigidity modulus, V_1 is the molar volume, and ΔV is the expansion per hydrogen atom of the interstitial site.¹⁵ Wagner³⁰ has pointed out that if deviations from ideality in the p - c - T relationships for metal-gas sys-

tems were measured at constant volume rather than at constant pressure the following relationship would hold

$$\left[\partial \ln p^{1/2} \frac{(1-n)}{n} / \partial n \right]_v = \left[\partial \ln p^{1/2} \frac{(1-n)}{n} / \partial n \right]_p + \frac{\bar{V}_H^2}{V_1 K_1 RT} \quad (7)$$

where \bar{V}_H is the molar volume of hydrogen in the metal and V_1 and K_1 are the molar volume and compressibility of the pure metal, respectively. If the interaction is negligible at constant volume, then

$$\left[\partial \ln p^{1/2} \frac{(1-n)}{n} / \partial n \right]_p = \frac{-\bar{V}_H^2}{V_1 K_1 RT} = \frac{-2E_L}{RT} \quad (8)$$

Wagner has shown for the Pd/ H_2 system³⁰ that eq 8 is approximately true. Substituting for the compressibility in terms of the rigidity modulus, eq 8 becomes

$$E_L = 1.83G\bar{V}_H^2/V_1 \quad (9)$$

and $\bar{V}_H^2/V_1 = N_0\Delta V/V_1$ so that eq 9 becomes

$$E_L = 1.83GN_0\Delta V^2/V_1 \quad (10)$$

and by comparison with eq 6 it can be seen that they differ only by a constant. Thus the assumption of no interaction at constant volume leads to the same dependence upon the properties of the metal/hydrogen system as the usual approach, *e.g.*, eq 6.

If it is naively assumed that the only difference between weak chemisorption and absorbed hydrogen is the strain energy contribution in the latter, then $q_{ads} = q_{abs} + E_L$. E_L can be calculated from eq 6 or 10 or can be obtained from the p - c - T data for the Pd/ H_2 system. The heat of absorption is 20 kJ/mol of H_2 at $n \rightarrow 0$ (Table I). This gives $q_{ads} = 36.4$ kJ/mol of H_2 if E_L is taken from the p - c - T data or 43.9 kJ/mol of H_2 if it is calculated using Wagner's relation for E_L (eq 8). In either case the agreement with the isosteric heats is satisfactory for such a crude model.

An interesting facet of these data is that thermodynamic data are now available for hydrogen at equilibrium in three different states: solid, surface, and gas. This constitutes a textbook type statistical mechanical situation. How is the chemical potential of the surface equal to that of the bulk hydrogen when the heat of chemisorption exceeds the heat of absorption (in the α phase)? This must obtain because of compensating values of the differential entropy of absorption and chemisorption. The entropy of chemisorption is more negative than the entropy of absorption presumably because of the different configurational contributions.

Acknowledgments. We wish to thank Dr. W. A. Oates and Dr. J. D. Clewley for helpful discussions of this work.

References and Notes

- (1) F. A. Lewis, "The Palladium/Hydrogen System," Academic Press, New York, N. Y., 1967.
- (2) O. Beeck, *Discuss. Faraday Soc.*, **8**, 118 (1950).
- (3) Z. L. Vert, I. A. Mosevitch, and I. P. Tverdovskii, *Dokl. Akad. Nauk SSSR*, **140**, 149 (1961).
- (4) V. Breger and E. Gileadi, *Electrochim. Acta*, **16**, 177 (1971).
- (5) B. Tardy and S. J. Teichner, *J. Chim. Phys.*, **67**, 1962 (1970).
- (6) A. W. Aldag and L. D. Schmidt, *J. Catal.*, **22**, 260 (1971).
- (7) E. Wicke and G. Nernst, *Ber. Bunsenges. Phys. Chem.*, **68**, 224 (1964).
- (8) J. W. Simons and T. B. Flanagan, *J. Phys. Chem.*, **69**, 3773 (1965).
- (9) P. A. Sermon, *J. Catal.*, **24**, 460, 467 (1972).
- (10) G. Holleck and E. Wicke, *Z. Phys. Chem. (Frankfurt am Main)*, **56**, 155 (1967).
- (11) G. Bohmholdt and E. Wicke, *Z. Phys. Chem. (Frankfurt am Main)*, **56**, 133 (1967).

- (12) J. W. Simons and T. B. Flanagan, *Can. J. Chem.*, **43**, 1665 (1965).
 (13) T. B. Flanagan and W. A. Oates, *Ber. Bunsenges. Phys. Chem.*, **76**, 706 (1972).
 (14) J. D. Clewley, T. Curran, T. B. Flanagan, and W. A. Oates, *J. Chem. Soc., Faraday Trans. 1*, **69**, 449 (1973).
 (15) R. Burch, *Trans. Faraday Soc.*, **66**, 749 (1970).
 (16) H. Brodowsky, *Z. Phys. Chem. (Frankfurt am Main)*, **44**, 129 (1965).
 (17) D. M. Nace and J. G. Aston, *J. Amer. Chem. Soc.*, **79**, 3619, 3623, 3627 (1957).
 (18) E.g., G. C. Bond, "Catalysis by Metals," Academic Press, London, 1962.
 (19) B. Baranowski, *Ber. Bunsenges. Phys. Chem.*, **76**, 714 (1972).
 (20) D. A. Dowden in "Chemisorption," W. E. Garner, Ed., Butterworths, London, 1958.
 (21) J. C. P. Mignolet, *Bull. Soc. Chim.*, **67**, 358 (1958).
 (22) P. M. Gundry and F. C. Tompkins, *Trans. Faraday Soc.*, **52**, 1609 (1956).
 (23) T. Toya, *Progr. Theoret. Phys. Suppl.*, **23**, 250 (1962).
 (24) N. F. Mott and H. Jones, "Theory of Metals and Alloys," Oxford University Press, Oxford, 1936.
 (25) C. A. Mackleit and A. I. Schindler, *Phys. Rev.*, **146**, A463 (1966).
 (26) O. Johnson, *J. Res. Inst. Catal. Hokkaido Univ.*, **20**, 95, 109, 125 (1972).
 (27) F. A. Lewis, *Naturwissenschaften*, **48**, 402 (1961).
 (28) M. von Stackelberg and P. Ludwig, *Z. Naturforsch.*, **19**, 93 (1964).
 (29) H. Brodowsky, *Ber. Bunsenges. phys. Chem.*, **76**, 740 (1972).
 (30) C. Wagner, *Acta Met.*, **19**, 843 (1971).

The Nature of Molecular Hydrogen Adsorbed on Zinc Oxide

C. C. Chang, L. T. Dixon, and R. J. Kokes*

Department of Chemistry, The Johns Hopkins University, Baltimore, Maryland 21218 (Received May 23, 1973)

Publication costs assisted by the Petroleum Research Fund

The reversibly adsorbed hydrogen and deuterium on zinc oxide at -195 and -183° (type III) has been examined by adsorption and ir techniques. The isotherms show a significant isotope effect and yield isosteric heats at low coverage of 2.2–2.5 kcal. Infrared studies and the temperature and pressure dependence show this hydrogen is present in molecular form and is limited to 5 to 10% of the surface. Poisoning studies with water suggest it occurs on the same sites as the dissociative type I hydrogen. Interpretation of the spectral results and the isotope effect suggest that there is a considerable barrier to rotation on the surface. The possible role of such a species in the ortho-para hydrogen conversion is discussed.

Introduction

Heterogeneous catalysts that are effective for hydrogenation reactions usually are also effective for hydrogen-deuterium exchange (and the related parahydrogen conversion).^{1–3} The nature of the "activated" hydrogen in these catalytic sequences has been the subject of much speculation.^{4,5} In one scheme, originally proposed by Bonhoeffer and Farkas,⁶ it is assumed that hydrogen (and deuterium) adsorb dissociatively and that a random recombination of atomic species effects the exchange. The corresponding mechanism for olefin hydrogenation assumes a two-step addition of adsorbed hydrogen atoms to olefins to form the product alkane. Although many features of the hydrogenation and exchange reactions are accounted for by the view that the "active" hydrogen involves only an atomic adsorbed species, there are some deficiencies in this view. In an attempt to overcome these deficiencies, Rideal⁷ (and later Eley⁵) assumed that exchange occurs *via* reaction of the adsorbed atomic species with *molecular* hydrogen (or deuterium). Twigg⁸ presented a parallel mechanism for hydrogenation wherein molecular hydrogen adds to the adsorbed olefin. Often, it is assumed that this reactive molecular hydrogen species is weakly adsorbed. Despite intensive efforts to obtain conclusive mechanistic evidence, a firm decision between these alternatives cannot yet be made. At present, it is not clear whether the "active" form of hydrogen is only atomic or includes a molecular species.

The nature of adsorbed hydrogen has also been examined by a number of nonmechanistic techniques. Infrared studies provide the strongest evidence that hydrogen adsorption on at least some metals^{9,10} and oxides¹¹ is atomic. For years the only nonmechanistic evidence for chemisorbed molecular hydrogen stemmed from heat¹² and adsorption measurements¹³ at low temperatures.¹⁴ Recently, analysis of chromatographic separation of hydrogen isotopes and allotropes strongly suggests there is a specific form of molecular hydrogen adsorption on oxides.^{15,16} This view is reinforced by recent observations in this laboratory of ir bands due to molecular species when hydrogen is adsorbed on zinc oxide at low temperature.¹⁷ In this preliminary communication¹⁷ we noted that this species seems specific to zinc oxide and does not resemble the physically adsorbed hydrogen reported by Sheppard and Yates.¹⁸ Thus, it may play the role of the molecular intermediate suggested in exchange reactions over this oxide.¹⁹ In this paper we further characterize this molecular hydrogen species.

Experimental Section

The zinc oxide used in this study was Kadox-25 obtained from the New Jersey Zinc Co. All gases were purified, if necessary, by standard techniques.

In the standard activation procedure the sample was degassed as the temperature was gradually raised from room temperature to 450° . Then oxygen was circulated

over the catalyst with a liquid nitrogen trap in the circulation loop for 2 hr at 450°. The sample was cooled to room temperature in dry oxygen and briefly degassed prior to the adsorption experiments. Previous experiments had shown that a sample thus treated had the same hydrogen adsorption characteristics as one activated in vacuum but the ir transmission properties were greatly improved.

Techniques used in ir experiments and the cell used has been described earlier. Temperatures in ir studies are those recorded by a thermocouple in contact with the zinc oxide disk about 3 mm from the edge. Heating by the ir beam may occur inside the disk; hence, the recorded temperature should be viewed as approximate.

Adsorption measurements were made on a 23.0-g sample of zinc oxide pressed into disks similar to those used in ir studies and broken into large chunks. After activation the BET V_m value for nitrogen was 1.61 cc/g corresponding to an area of 7.01 m²/g. Hydrogen and deuterium isotherms were run at liquid nitrogen (-195.8°) and liquid oxygen temperatures (-183°). Prior to these runs the catalyst was exposed to hydrogen at 135 mm at room temperature overnight, cooled to -183°, and evacuated for 1 hr. Check experiments revealed that essentially the same isotherms were obtained when the catalyst was cooled in hydrogen to -78°, evacuated for 1 hr, and then the isotherm was run at -183°. Isothermic heats of adsorption for hydrogen and deuterium were computed from the Clausius-Clapeyron equation.

Results

Adsorption Experiments. Two types of hydrogen chemisorption are evident on zinc oxide at room temperature:²⁰ type I is rapid and reversible; type II is slow (in part) and irreversible. Type II is unreactive in ethylene hydrogenation²⁰ and hydrogen-deuterium exchange.¹⁹ Type I is reactive and ir studies suggest that it forms ZnH and OH bonds by dissociation on a limited number of zinc oxide pair sites. At room temperature saturation of type I sites is evident above 50 mm. In line with this, if a sample at room temperature is exposed to hydrogen at 50 mm, there is little increase in the ZnH and OH band intensity when the sample is cooled to -195°. Some time ago, Taylor and Liang¹³ reported that when zinc oxide is exposed to hydrogen at 1 atm and room temperature and then cooled to -195°, there is an increase in hydrogen adsorption corresponding roughly V_m for a nitrogen monolayer. This adsorption that occurs on cooling (and seems too extensive to be simple physical adsorption) gives rise to the ir bands for molecular hydrogen. We term this molecular adsorption, type III.¹⁷ In order to study it we must first devise a way to separate it from the type I adsorption which also occurs readily at these low temperatures.²¹ We have made use of the fact that evacuation at -183° (or -78°) does not remove the ZnH and OH bands characteristic of type I hydrogen, but does remove the molecular bands characteristic of type III hydrogen.¹⁷ Accordingly, low-temperature adsorption isotherms were run as follows: first, after exposure to hydrogen for 16 hr at room temperature, the catalyst was cooled in hydrogen (at 135 mm) to -183° to saturate type I sites; then, the catalyst was evacuated to remove the reversible type III adsorption and the readsorption on top of the irreversibly adsorbed type I adsorption was measured. This readsorption, in principle, provides isotherms for the type III hydrogen and any physical adsorption that accompanies it.

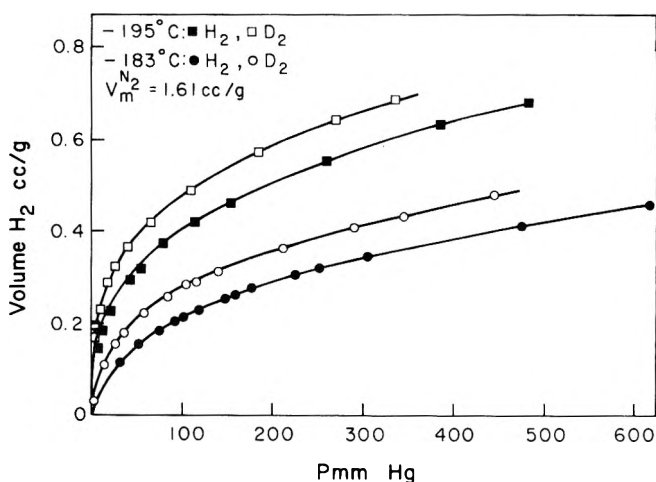


Figure 1. Isotherms for type III hydrogen and deuterium on zinc oxide.

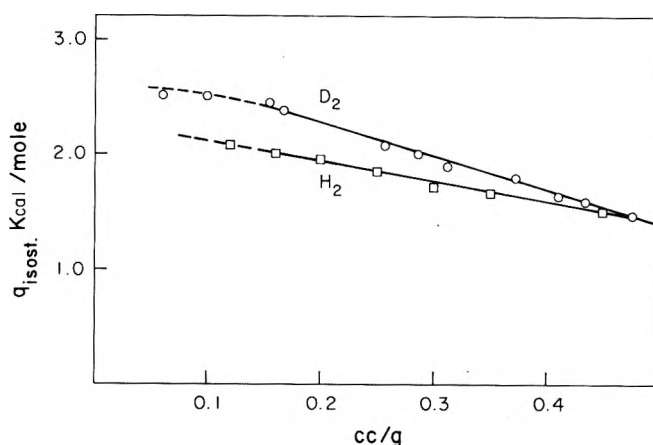


Figure 2. Isothermic heats for type III hydrogen and deuterium on zinc oxide.

Figure 1 shows isotherms for hydrogen and deuterium at -195 and -183° obtained by the above procedure. The amount of adsorption is extensive insofar as it approaches half the nitrogen V_m value at 1 atm and -195°. Furthermore, there appears to be a significant isotope effect for hydrogen compared to deuterium. The isotope effect is also reflected in isosteric heats shown in Figure 2. Values for both hydrogen and deuterium approach a common value at high coverage, but at low coverage, the value is about 2.2 kcal for hydrogen compared to 2.5 kcal for deuterium.

In a recent paper from this laboratory²¹ it was noted that the ratio of pressures for different isotopes at fixed θ should be represented by the formula

$$\left(\frac{P_{H_2}}{P_{D_2}}\right)_\theta = \frac{Q_{H_2} q_{D_2}}{Q_{D_2} q_{H_2}} \quad (1)$$

where Q is the partition function for the indicated gaseous species and q is the partition function for the indicated adsorbed species (including zero point energies) at zero coverage. Thus, a plot of P_{H_2} vs. P_{D_2} at fixed coverages should yield a straight line through the origin. Figure 3 shows that this prediction holds fairly well and that a single straight line can be drawn through the data points at both temperatures. The slope of this line is 1.57; implications of this value will be discussed in the Discussion section.

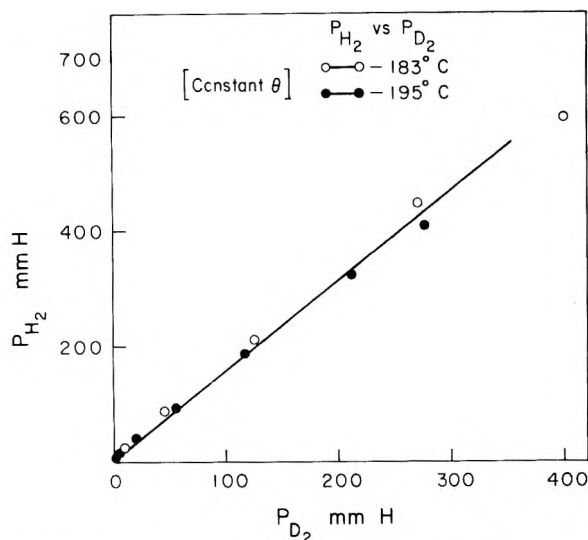


Figure 3. P_{H_2} vs. P_{D_2} at fixed θ : ●, -195° ; O, -183° .

Infrared Studies. When the infrared cell containing zinc oxide is exposed to hydrogen and cooled to -195° , bands are observed at 3502 and 1691 cm^{-1} , corresponding to the OH and ZnH bands previously assigned to type I hydrogen.^{9,21} In addition a somewhat weaker band is observed at 4019 cm^{-1} in a region near the upper limits of the spectrometer (Figure 4). This high-frequency band disappears after a brief evacuation whereas the bands ascribable to type I hydrogen are unaffected by evacuation at this temperature. If, after evacuation at -195° , the sample is exposed to deuterium, no bands due to OD and ZnD are observed, presumably, because the type I sites are saturated with hydrogen. A new band does appear, however, at 2887 cm^{-1} . This band, presumably due to adsorbed deuterium, is still evident when the temperature is raised to -183° (Figure 4). Even after exposure to deuterium for several hours at -195° , no OD or ZnD bands appear; hence, at -195° exchange between deuterium and type I hydrogen is a very slow process. Like the band at 4019 cm^{-1} (observed in hydrogen) the band at 2887 cm^{-1} (observed in deuterium) disappears on brief evacuation. These bands, together with the corresponding type I bands, are also observed when the catalyst is precooled to -195° in helium, then evacuated, and exposed to hydrogen (or deuterium).

When the catalyst is exposed to deuterium at room temperature, cooled to -195° , evacuated, and exposed to hydrogen, only OD (2591 cm^{-1}) and ZnD (1219 cm^{-1}) bands are observed along with a band at 4019 cm^{-1} . As with the reverse process, no OH or ZnH bands appear after several hours in hydrogen even when the temperature is increased to -183° . Thus, cooling in deuterium to -195° saturates the type I sites and no further adsorption on or exchange with the type I sites occurs. When the type I sites are thus deuterium saturated and the catalyst is evacuated and exposed to hydrogen deuteride, a band appears at 3507 cm^{-1} (Figure 4). This band is very close to the position for the type I OH band, but it is not due to type I hydrogen for the following reasons: (a) presaturation of type I sites with deuterium does not permit type I hydrogen adsorption; (b) no ZnH band is observed; (c) the 3507-cm^{-1} band, unlike type I bands, disappears on brief evacuation. Thus, we assume the 3507-cm^{-1} band observed at low temperature with hydrogen deuteride stems

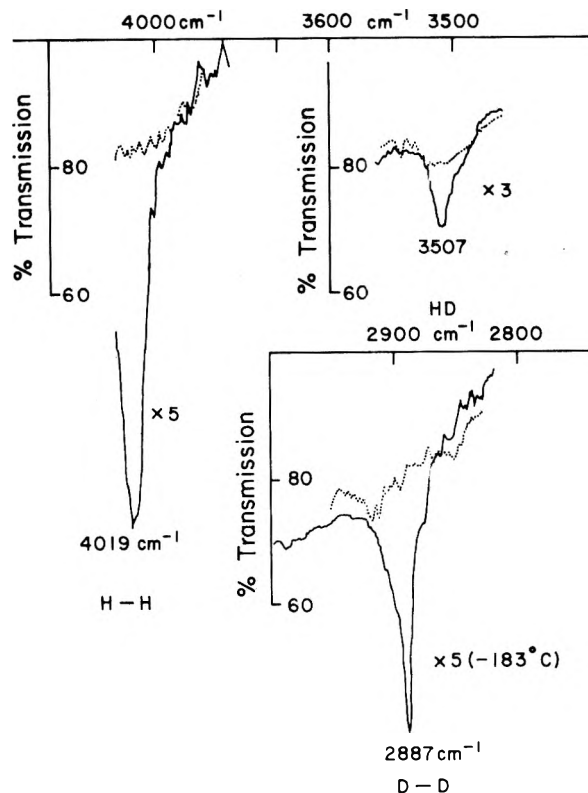


Figure 4. Spectrum of molecular H_2 , HD, and D_2 on zinc oxide. The dotted line is the spectrum in the absence of gaseous hydrogen or its isotopes.

TABLE I: Vibration Frequencies for Molecular Hydrogen

Species	$\omega(\text{gas}),^a$ cm^{-1}	$\omega(\text{ads}),$ cm^{-1}	$\Delta\omega, \text{cm}^{-1}$	$\frac{\Delta\omega}{\omega} \times 100$
H_2	4161	4019	142	3.41
HD	3627	3507	120	3.31
D_2	2990	2887	103	3.44
				Av 3.39 \pm 0.05

^a Reference 22.

from the same species as the 4019-cm^{-1} band for hydrogen and the 2887-cm^{-1} band for deuterium.

Table I compares the observed frequencies for weakly adsorbed hydrogen, hydrogen deuteride, and deuterium with the vibration frequencies tabulated by Herzberg²² for the gaseous species. It can be seen that the observed frequencies for the adsorbed species correspond to frequencies of gaseous molecular species with a downward shift much larger than that typically found for physically adsorbed molecules,^{18,23} i.e., about 20 cm^{-1} . Buckingham²⁴ has formulated a perturbation treatment of shifts in vibration frequencies for diatomic molecules induced by environment. According to this treatment the shift $\Delta\omega$ relative to the unshifted frequency should be independent of the isotopic species. The last column of Table I shows that the frequency shift for the adsorbed species is consistent with this prediction. Thus, these bands stem from pure vibrations of adsorbed molecular species.

The bands for molecular adsorption on zinc oxide are quite different from those assigned to "physical adsorption" on porous glass.^{18,25} For zinc oxide $\Delta\omega$ is five times that on porous glass. In simple interpretations of solvent effects,²⁶ the size of the shifts are proportional to interaction potential; hence, on this basis, the interaction poten-

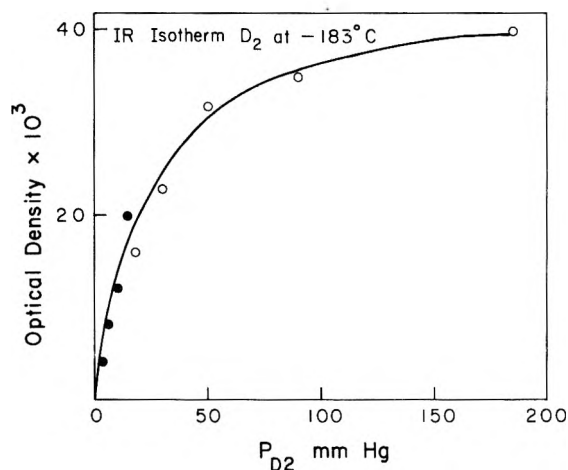


Figure 5. Ir isotherm for deuterium at -183° . Different symbols are for different runs.

tial of hydrogen with zinc oxide would be about five times that for hydrogen with porous glass provided the interaction distance is the same. Comparative intensity data for the two systems also suggest the interaction is greater on zinc oxide. If, like Sheppard and Yates,¹⁸ we assume the vibrational transition becomes allowed due to an effective electric surface field, we can estimate this surface field from intensity data. Our best estimate suggests the extinction coefficient for hydrogen on zinc oxide is greater than that on porous glass by a factor of 65. This leads to a computed field of 0.6 V/\AA on zinc oxide¹⁷ compared to the reported 0.07 V/\AA for porous glass.¹⁸ Thus, the nature of the molecular hydrogen (gauged by ir) appears to be highly specific to the adsorbent, zinc oxide, and, in that sense, it is chemisorption.²⁷

Isotherms based on the intensity of infrared bands as a function of pressure can be obtained for hydrogen and deuterium at both -195 and -183° . A typical ir isotherm is shown for deuterium at -183° in Figure 5. Such isotherms are not as precise as those obtained by volumetric measurements; the bands are weak and the reproducibility of the optical density is not much better than 10%. Furthermore, the nominal temperature may differ from the observed temperature by several degrees. Despite these uncertainties an estimate was made of the isosteric heat for deuterium based on such ir isotherms at -183 and -195° . The heat of adsorption thus computed at low coverage was about 2 kcal. In view of the uncertainties, we regard this value as quite close to that based on isotherm measurements (Figure 2); hence, it is tempting to assume that the initial hydrogen adsorption determined volumetrically is the species that gives rise to the ir bands for molecular hydrogen.

In order to specify the adsorption characteristics of the molecular species (termed type III) responsible for the ir spectra, we must devise a scheme for subtracting out the physical adsorption contributions to the volumetric isotherms in Figure 1. Contributions of physical adsorption should be most pronounced at higher pressures and should occur with heats of adsorption more comparable to the heat of liquefaction (0.216 kcal/mol ¹⁷) than the initial heats, characteristic of type III hydrogen. If we plot the amount of type III adsorption *vs.* the total adsorption, we would expect a linear plot through the origin at low coverage. At higher coverages, where additional adsorption is largely physical, III should become independent of total coverage. This limiting coverage defines the saturation

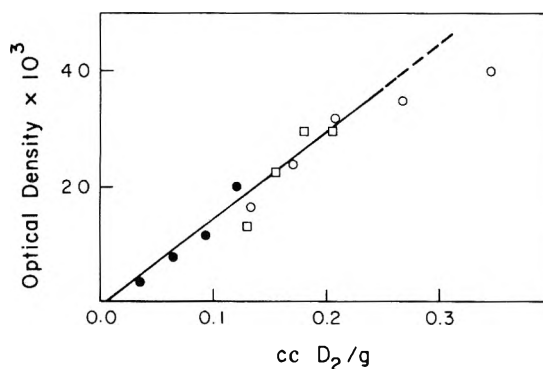


Figure 6. Optical density vs. adsorbed deuterium: O, \bullet , -183° ; \square , -195° .

amount of type III hydrogen. (We have assumed that type III adsorption occurs with significantly higher heat than physical adsorption, a supposition in line with the spectral characteristics of the ir bands.) We have constructed such a plot by using the optical densities in Figure 5 as a measure of III and the adsorption at corresponding pressures in Figure 1 as a measure of the total adsorption. The plot thus obtained (Figure 6) has the correct form and suggests the total amount of type III adsorption is roughly 0.2 cc/g . Since the errors inherent in this procedure are large, this value should be viewed as a tentative estimate.

The above experiments suggest that type III hydrogen adsorption occurs on a fraction of the surface comparable to that responsible for type I adsorption.²⁰ This would be expected if type I and type III adsorption occurred on the same sites. Effects of water adsorption on the hydrogen spectrum support this interpretation. Earlier²⁰ it was demonstrated that water adsorption selectively poisons the sites for type I adsorption. In our present study we have found that if sufficient water is adsorbed so that type I bands do not appear on exposure to hydrogen, type III bands are also absent. When the adsorbed water is removed in stages by evacuation at successively higher temperatures, the catalyst can be reactivated for both type I and type III hydrogen adsorption. Observation of the ir spectra in hydrogen during successive stages of the reactivation reveal that type I and type III bands both reappear and show a parallel growth in intensity at successive stages of the reactivation. There are, of course, other interpretations possible but the simplest, provisional interpretation of these results is that type I and type III hydrogen adsorption occurs on the same sites.

Discussion

Infrared bands for hydrogen are forbidden in the gas phase; they appear for the adsorbed species because the bond to the surface induces a dipole moment that depends on internuclear displacement, ξ .²⁸ Let us assume for simplicity that the induced dipole moment stems from an effective electric field, E_0 , in some special direction labeled the z direction. Then, there will be three components for the induced dipole

$$\mu_x = \alpha_{xz} E_0 \quad (2a)$$

$$\mu_y = \alpha_{yz} E_0 \quad (2b)$$

$$\mu_z = \alpha_{zz} E_0 \quad (2c)$$

In general α_{xz} , α_{yz} , and α_{zz} depend on the orientation of the diatomic molecule with respect to z . In terms of the polarization parallel and perpendicular to the molecular axis we find

$$\alpha_{zz} = \alpha_{\perp} + (\alpha_{\parallel} - \alpha_{\perp}) \cos^2 \theta \quad (3a)$$

$$\alpha_{xz} = (\alpha_{\parallel} - \alpha_{\perp}) \sin \theta \cos \theta \cos \phi \quad (3b)$$

$$\alpha_{yz} = (\alpha_{\parallel} - \alpha_{\perp}) \sin \theta \cos \theta \sin \phi \quad (3c)$$

where θ and ϕ have their usual meaning. As required for the homonuclear diatomic molecule the sign and magnitude of the induced dipole does not change when the molecule is rotated end for end ($\theta \rightarrow \pi - \theta$, $\phi \rightarrow \phi + \pi$). Expansion of α_{\perp} and α_{\parallel} in a power series in ξ and evaluation of the appropriate matrix elements leads to the conclusion that the appropriate selection rules are those usually applied to the Raman spectra. In other words, in this limit where the diatomic is freely rotating, we should see transitions corresponding to changes in vibrational quantum number, n , and $\Delta J = 0 \pm 2$. These are the selection rules that describe the induced spectra for gaseous hydrogen in a static electric field.²⁹ In adsorbed or condensed phases, however, the rotation is hindered rather than free. One might expect, therefore, the selection rules to be modified in condensed systems. In point of fact, however, both the induced ir³⁰ and Raman spectra³¹ of hydrogen in condensed phases follow selection rules appropriate for freely rotating molecules. Accordingly, in order to understand the effect of a barrier to rotation on the induced spectra, we must examine the characteristics of the wave functions and energy levels for a restricted rotor.

The principal limiting features of the restricted diatomic rotor were discussed by Pauling³¹ and Stern³² with the assumption that the potential barrier to rotation has the form $c \sin^2 \theta$. Recently, in connection with analysis of the chromatographic separation of hydrogen isotopes and allotropes, more detailed computations of energy levels *vs.* barrier height have been presented.^{33,34} We have extended these computations somewhat, also with the help of the tables of Stratton, *et al.*,³⁵ and the results are summarized in Figure 7 which shows the computed energy levels for a restricted deuterium rotor for rotational barriers of 0, 1, and 5 kcal. For the free rotor, components of the degenerate levels are shown as individual lines, broken and solid, for symmetric and antisymmetric levels, respectively. As the barrier height is increased the energy scale in the figure is compressed; the zero, however, is kept the same and the vertical arrow, corresponding to 1 kcal, provides a gauge for the energy scale. On the right we depict the energy levels in the limit where the barrier becomes very high and the molecule undergoes only angular vibrations. These energy levels are specified by the equation³²

$$\begin{aligned} E &= (N + |m| + 1)h\nu \\ N &= 0, 2, \dots \\ m &= 0, \pm 1, \pm 2, \dots \end{aligned} \quad (4)$$

Thus, as the barrier height increases m for the free rotor remains a "good" quantum number corresponding to vibrational angular momentum,³⁶ but l loses its original meaning. Equation 4 is the equation for a doubly degenerate vibration; the doubling of energy levels in Figure 7 stems from the same symmetry considerations that lead to inversion doubling.²⁷

It is easy to see what happens to the selection rules for induced transitions in the limit when the barrier is high. Transitions corresponding to $\Delta J = \pm 2$ (refer to Figure 7) become transitions involving a change in n and a change in the torsional energy level; such combination bands are forbidden in the harmonic oscillator approximation. Tran-

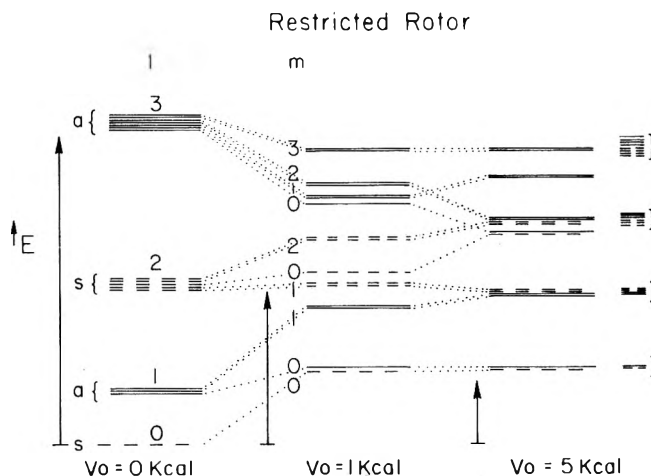


Figure 7. Correlation diagram for hindered rotor. See text for details.

sitions corresponding to $\Delta J = 0$ (with $\Delta m = 0$) become fundamentals and, thus, are allowed in the harmonic oscillator approximation. These conclusions can be verified by computation of the relevant matrix elements with wave functions appropriate for these limits, *i.e.*, those for the isotropic plane oscillator.³²

What is the height of the rotational barrier required for transitions corresponding to $\Delta J = \pm 2$ to become forbidden? Roughly, one might anticipate that libration is approximated only for barriers higher than the perturbed rotational levels. For hydrogen, with its low moment of inertia, and widely spaced rotational levels, the rotational barrier would have to be quite high compared to that required for a molecule like nitrogen with more closely spaced rotational levels. No doubt, this is why the Raman spectra of liquid hydrogen approximates that of a freely rotating molecule whereas that of nitrogen shows a single band.³⁸ This effect is also evident in Figure 7. When the barrier is 1 kcal only the lowest level approximates that for the degenerate oscillator. Even for a barrier of 5 kcal states stemming from $l = 2$ only approximate those for a degenerate oscillator.

Stratton, *et al.*,³⁵ show that the wave functions corresponding to the energy levels depicted in Figure 7 can be expanded in a power series in associated Legendre polynomials and they list coefficients. We have used this tabulation to explore how the matrix elements governing the transitions change with barrier height. These results for the P_z component show the $\Delta J = 2$ transition does not decrease by an order of magnitude until the barrier is several kcal. Computations with the P_x and P_y components suggest even higher barriers are required before the $\Delta J = 2$ transitions become very weak.

We have searched for a series of bands for adsorbed deuterium and have found only one. Since the shift for various isotopic species (Table I) suggests this band is a purely vibrational one, we conclude the band corresponds to $\Delta J = 0$. For "freely" rotating hydrogen at -195° the $\Delta J = 0$ and $\Delta J = 2$ bands are comparable in intensity.³⁰ Thus, our failure to observe $\Delta J = 2$ bands (which means their intensity is an order of magnitude less than the $\Delta J = 0$ bands) suggests the barrier to rotation is quite high. Accordingly, we would conclude that the first few energy levels, which are the only ones populated at this temperature, correspond to torsional vibrations rather than hindered rotations.

(A more realistic model should have a potential that depends on θ and ϕ . This dependence on ϕ can be introduced by a perturbation treatment. In the limit of high barriers this leads to a sequence energy levels corresponding to a harmonic oscillator with two different vibration frequencies. The corresponding levels, however, still occur in near degenerate pairs, consisting of wave functions symmetric and antisymmetric in inversion. Such changes in the correlation diagram do not change the selection rules in the limits and are unlikely to alter the qualitative conclusions based on the simpler ϕ -independent model.)

This detailed interpretation of the spectrum leads to the conclusion that the barrier to rotation is high but does not specify how high. In principle, measurements of the thermodynamic isotope effect coupled with heats and ir measurements should shed some light on this. We can rewrite eq 1 as a product of four terms

$$\left(\frac{P_{\text{H}_2}}{P_{\text{D}_2}}\right)_\theta = \left\{ \frac{Q_{\text{H}_2}^{\text{trans}}}{Q_{\text{D}_2}^{\text{trans}}} \frac{q_{\text{D}_2}^{xy}}{q_{\text{H}_2}^{xy}} \right\} \left\{ \frac{Q_{\text{H}_2}^{\text{st}}}{Q_{\text{D}_2}^{\text{st}}} \frac{q_{\text{D}_2}^{\text{st}}}{q_{\text{H}_2}^{\text{st}}} \right\} \times \left\{ \frac{Q_{\text{rot H}_2}}{Q_{\text{rot D}_2}} \frac{q_{\text{rot D}_2}}{q_{\text{rot H}_2}} \right\} \left\{ \frac{q_{\text{D}_2}^z}{q_{\text{H}_2}^z} \right\} \quad (5)$$

The first factor, I, contains partition functions for translation in the gas phase and in the plane of the surface (x, y). If, following King and Bensen (KB),³⁴ we assume two-dimensional mobility on the surface I becomes $1/\sqrt{2}$. The second factor, II, which includes vibrational partition functions for the stretching frequencies, can be computed from the measured ir frequencies and is 0.70. The third term, III, is a function of barrier height and can be computed on the basis of the restricted rotor model by the KB procedure. The fourth term, IV, can be estimated from the measured heats by an extension of the KB treatment which assumes that the potential energy as a function of distance from the surface has the form

$$U(z) = -\frac{A}{z^m} + \frac{B}{z^n} \quad (6)$$

where A and B are constants and the "best" values of m and n appear to be 5 and 9. In the harmonic oscillator approximation the vibration frequency (in cm^{-1}) perpendicular to the surface is given by

$$\sigma = \frac{(nm)^{1/2}}{z_0} \frac{U_c^{1/2}}{2\pi cM^{1/2}} \quad (7)$$

where U_c is the depth of the potential energy well, z_0 is the equilibrium distance, c is the speed of light, and M is the mass of the vibrating species if we assume the effective mass of the surface is infinite. The thermodynamic energy of desorption is given by the equation

$$\Delta E = \bar{E}_{\text{trans}} + \bar{E}_{\text{rot n}} + \bar{E}_{\text{st}} - \bar{\epsilon}_{xy} - \bar{\epsilon}_{\text{rot}} - \bar{\epsilon}_{\text{st}} + U_0 - \frac{1}{2}h\nu \quad (8)$$

wherein E and ϵ refer to the indicated energies in the gas and adsorbed phases, respectively. The value of ΔE is specified by the measured (initial) heat of adsorption. All terms in E and ϵ are specified by the model except for $\bar{\epsilon}_{\text{rot}}$. This term can be computed as a function of the barrier height and σ can be evaluated for each value of $\bar{\epsilon}_{\text{rot}}$ by combination of eq 7 and 8. Once σ is computed the fourth factor in eq 5 can be evaluated. Computed values of the isotope effect as a function of the barrier height for two values of z_0 are shown in Table II.

These computations involve two assumptions: those inherent in the restricted rotor treatment and the form of

TABLE II: Computed Isotope Effect Vs. Barrier Height

V_0 , kcal	I × II × III	IV ^a	$\frac{P_{\text{H}_2}}{P_{\text{D}_2}}^a$	IV ^b	$\frac{P_{\text{H}_2}}{P_{\text{D}_2}}^b$
0	0.50	2.32	1.14	1.92	0.96
0.5	0.57	2.44	1.40	2.01	1.14
1.0	0.78	2.57	2.00	21.0	1.64
2.0	1.06	2.94	3.12	2.32	2.46

^a The equilibrium distance z_0 is assumed to be 2.5 Å, i.e., approximately the value used in ref 34. ^b The equilibrium distance z_0 is assumed to be 2.9 Å, i.e., roughly the van der Waals diameter.

the potential function for hydrogen-surface interaction. Despite these assumptions the only experimental input needed is the stretching frequency of hydrogen and the heat of adsorption of hydrogen. To achieve agreement of the computations with the measured isotope effect (1.57) we must assume a sizeable barrier to rotation. Insofar as this result agrees with our conclusions based on the spectrum, the model appears to be realistic. Evaluation of the barrier height by these computations, however, is fruitless since the values n , m , and z_0 are uncertain and the computations are sensitive functions of these values. Thus, we regard our computations based on this model as useful primarily for qualitative conclusions.

Finally, let us note that we regard this type of adsorbed molecular hydrogen as a prime candidate for the intermediate in ortho-para conversion. The transition from an ortho to a para state is governed by terms of the kind

$$\langle \psi_o | H'_m | \psi_p \rangle^2 / (E_o - E_p)^2$$

where ψ and E are the wave functions and energies for ortho and para states. As pointed out by Van Cauwelaert and Hall,³⁹ $E_o - E_p$ is reduced by the imposition of a rotational barrier so that transition mechanisms trivial in the gas may become significant for the adsorbed phase. For example, transitions involving nuclear moments may play a more important role for adsorbed species even though their rate is trivial for gas-phase transitions.⁴⁰ Our spectral data suggest we are approaching the limit wherein low-lying levels become degenerate ortho-para levels and this conclusion is independent of the detailed form of the potential function defining the barrier. Thus, for this system the transition probability should become significant for a variety of mechanisms of only trivial importance in the gas phase. We are currently exploring this aspect of molecular hydrogen on zinc oxide in some detail.

Acknowledgment. This work was aided by funds from the National Science Foundation under Grant No. GP22830. Acknowledgment is made to the donors of the Petroleum Research Fund, administered by the American Chemical Society, for partial support of this research.

References and Notes

- G. C. Bond, "Catalysis by Metals," Academic Press, New York, N. Y., 1962.
- R. L. Burwell, Jr., G. L. Haller, K. C. Taylor, and J. F. Read, *Advan. Catal.*, **20**, 1 (1969).
- R. J. Kokes and A. L. Dent, *Advan. Catal.*, **22**, 1 (1972).
- B. M. W. Trapnell, "Catalysis," Vol. III, P. H. Emmett, Ed., Reinhold, New York, N. Y., 1955, Chapter I.
- D. O. Eley, ref 4, pp 60-63.
- K. F. Bonhoeffer and A. Farkas, *Z. Phys. Chem.*, **B12**, 231 (1931).
- E. K. Rideal, *Proc. Comb. Phil. Soc.*, **35**, 130 (1939).
- G. H. Twigg, *Discuss. Faraday Soc.*, **8**, 152 (1950).
- W. A. Pliskin and R. P. Eischens, *Z. Phys. Chem.*, **24**, 11 (1960).
- J. P. Contour and G. Pannetier, *J. Catal.*, **24**, 434 (1972).

- (11) R. P. Eischens, W. A. Pliskin, and M. J. D. Low, *J. Catal.*, **1**, 80 (1962).
- (12) R. A. Beebe and D. A. Dowden, *J. Amer. Chem. Soc.*, **60**, 2912 (1938).
- (13) H. S. Taylor and S. C. Liang, *J. Amer. Chem. Soc.*, **69**, 1036 (1947).
- (14) Such criteria are most definitive when the heat of chemisorption is high. In the above application the heat of chemisorption is low.
- (15) F. H. Van Cauwelaert and W. K. Hall, *J. Colloid Interface Sci.*, **38**, 1 (1972).
- (16) J. King and S. W. Benson, *J. Chem. Phys.*, **44**, 1007 (1966).
- (17) C. C. Chang and R. J. Kokes, *J. Amer. Chem. Soc.*, **93**, 7107 (1971).
- (18) N. Sheppard and D. J. C. Yates, *Proc. Roy. Soc., Ser. A*, **238**, 69 (1957).
- (19) S. Naito, H. Shimuzu, E. Hagiwara, T. Onishi, and K. Tamaru, *Trans. Faraday Soc.*, **67**, 1519 (1971).
- (20) A. L. Dent and R. J. Kokes, *J. Phys. Chem.*, **73**, 3772 (1969).
- (21) R. J. Kokes, C. C. Chang, L. T. Dixon, and A. L. Dent, *J. Amer. Chem. Soc.*, **94**, 4429 (1972).
- (22) G. Herzberg, "Molecular Spectra and Molecular Structure. I. Spectra of Diatomic Molecules," Van Nostrand, New York, N. Y., 1950, p 533.
- (23) L. H. Little, "Infrared Spectra of Adsorbed Species," Academic Press, New York, N. Y., 1966, pp 296-308.
- (24) A. D. Buckingham, *Proc. Roy. Soc., Ser. A*, **248**, 160 (1958).
- (25) Recently, M. Folman and Y. Kozirovski (*J. Colloid Interface Sci.*, **38**, 51 (1972)) reported spectra for hydrogen isotopes adsorbed at 20°K on NaCl and CsI. These are clearly molecular species. The heats of adsorption are roughly half and the band shifts are only one-third what is observed for zinc oxide; hence, we believe this type of adsorption is more like that on porous glass than on zinc oxide.
- (26) P. R. Monson, Jr., H. Chen, and G. E. Ewing, *J. Mol. Spectrosc.*, **25**, 501 (1968).
- (27) S. Brunauer, "The Adsorption of Gases and Vapors," Princeton University Press, Princeton, N. J., 1943, pp 27, 28.
- (28) The notation in this section is the same as that used by Herzberg.²²
- (29) The possibility of induced ir transitions by static electric fields and the applicability of Raman selection rules was first noted by E. U. Condon (*Phys. Rev.*, **41**, 759 (1932)) and experimentally verified by M. F. Crawford and I. R. Dagg (*ibid.*, **91**, 1569 (1953)).
- (30) G. E. Ewing and S. Trajmar, *J. Chem. Phys.*, **41**, 814 (1964); **42**, 4038 (1965).
- (31) L. Pauling, *Phys. Rev.*, **36**, 430 (1930).
- (32) T. E. Stern, *Proc. Roy. Soc., Ser. A*, **130**, 551 (1930).
- (33) D. White and E. N. Lassetre, *J. Chem. Phys.*, **32**, 72 (1960).
- (34) J. King and S. W. Benson, *J. Chem. Phys.*, **44**, 1007 (1966).
- (35) J. A. Stratton, P. M. Morse, L. J. Chu, J. D. C. Little, and F. J. Corbato, "Spheroidal Wave Functions," The Technology Press of Massachusetts Institute of Technology, Cambridge, Mass., 1956.
- (36) G. Herzberg, "Molecular Spectra and Molecular Structure. II. Infrared and Raman Spectra of Polyatomic Molecules," Van Nostrand, Princeton, N. J., 1945, p 80.
- (37) Reference 36, pp 220-227.
- (38) Reference 22, p 464.
- (39) F. H. Van Cauwelaert and W. K. Hall, *Trans. Faraday Soc.*, **66**, 454 (1970).
- (40) If, indeed, the occurrence of a barrier enhances the ortho-para rate, one would expect different enhancement for the ortho-para conversion of the different isotopes inasmuch as a given barrier brings the heavier isotope closer to the ortho-para degenerate limit. Some evidence that this occurs is found in the papers of E. W. Albers, P. Harteck, and R. R. Reeves (*J. Amer. Chem. Soc.*, **86**, 204 (1964); *Z. Naturforsch. A*, **18**, 197 (1963)). They report that the relative rates of ortho-para conversion of hydrogen, deuterium, and tritium occur with the expected rate ratio in the gas phase in the presence of NO. In the condensed phase, however, where a rotational barrier can occur, the conversion rate for tritium is much faster than one would predict based on rates for hydrogen.

The Nature of Molecular Nitrogen Adsorbed over Zinc Oxide

C. C. Chang and R. J. Kokes*

Department of Chemistry, The Johns Hopkins University, Baltimore, Maryland 21218 (Received May 23, 1973)

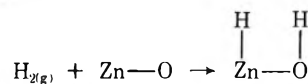
Publication costs assisted by the Petroleum Research Fund

A comparative study of oxygen and nitrogen adsorption on zinc oxide suggests oxygen adsorption is non-specific, but that the initial nitrogen adsorption occurs specifically on sites constituting about 15% of the surface. This nitrogen adsorption gives rise to a band in the ir close to that of the Raman vibrational frequency for gaseous nitrogen. It displaces the molecular hydrogen observable in the ir and couples vibrationally with the adsorbed dissociated hydrogen. Evidence is presented that this specific nitrogen adsorption occurs at the same sites that adsorb hydrogen molecularly and dissociatively. This nitrogen has a relatively low heat of adsorption (4.6 kcal). It is suggested that the specificity of the adsorption may be due to the interaction of a high field gradient at the sites with the quadrupole moment of nitrogen.

Introduction

There are at least three types of hydrogen chemisorption on zinc oxide:¹⁻⁵ type I is weakly chemisorbed and occurs rapidly and reversibly at room temperature; type II is tightly held and occurs irreversibly at room temperature; type III is very weakly held and detectable only at low temperature. Type II chemisorption has been found to be inert in many reactions and is nonobservable in the ir. Type I chemisorption is characterized in the ir by two bands at about 3500 and 1700 cm^{-1} which were first reported by Eischens, Pliskin, and Low⁴ who assigned them to an OH and ZnH species, respectively. Coupled ir and

adsorption studies lead to the conclusion that this mode of adsorption can be represented schematically as follows



wherein Zn-O represents a metal oxide pair site. Only 5 to 10% of the surface contains such sites and these appear to be isolated from one another and, at low temperature, are noninteracting. Further characterization⁵ of these sites suggests that adsorption is often accompanied by heterolytic cleavage of a chemical bond in the adsorbate; hence, one might assume that these sites represent a region of

very high effective electric fields or field gradients. Infrared studies suggest that type III hydrogen adsorption occurs at the same pair sites on which type I adsorption occurs.^{2,3} The ir spectrum consists of a single band for the normally forbidden transition corresponding to vibration of the homonuclear diatomic molecule. Such bands are allowed if the molecule is polarized by a strong electric field;^{6,7} hence, the appearance of these bands supports the view that the pair sites generate a rather high effective field.

If the above view is correct, the pair sites would constitute special sites for adsorption of a variety of molecular species with the heat of adsorption stemming from interaction of its permanent or induced dipole (or quadrupole) with the surface field. Creation of an induced dipole could result in the observation in the ir of normally forbidden bands stemming from the vibration of homonuclear diatomic molecules. If so, the details of resulting spectra should provide additional information on the nature of the pair sites. To this end we have studied the adsorption and ir spectrum of nitrogen and oxygen adsorption on zinc oxide and the interaction of these observed species with adsorbed hydrogen.

Experimental Section

Except for the adsorption measurements, all experimental details are similar to those described in earlier papers.^{3,8} Adsorption experiments were made in a conventional BET system equipped with a McLeod gauge. Corrections for thermal transpirations were not made for the runs at low temperatures, but estimated corrections suggested this had little effect on the values of q_{st} computed. (The diameter of the tubing at the high-temperature-low-temperature interface was 2 mm.) For these adsorption experiments we had a 22.0-g sample of Kadox 25 activated by the standard procedure. Temperatures of the runs were achieved by the following baths: -195° , liquid nitrogen; -183° , liquid oxygen; -160° , 2-methylbutane at its melting point; -119° , bromoethane at its melting point; -78° , a mixture of acetone and Dry Ice; -35° , 1,2-dichloroethane at its melting point. In all cases, the sample was precooled to the desired temperatures in about 50-mm of helium prior to adsorption measurements.

Results

Low-temperature isotherms for nitrogen and oxygen are shown in Figure 1. Since the pressures span four orders of magnitude, we have used a logarithmic pressure scale for clarity. Usually, the amount of physical adsorption at a given temperature correlates with the boiling point of the adsorbing gas with the higher boiling gas showing the more extensive adsorption. The boiling point of nitrogen (-195°) is less than that of oxygen (-183°); hence, on this basis alone, one would expect more extensive adsorption for oxygen than nitrogen at the same pressure. Figure 1 shows that this is not the case at low coverages. To achieve a coverage corresponding to one-fourth of a monolayer⁹ requires a higher pressure of oxygen than nitrogen by a factor of roughly 100 both at -195 and -183° . At higher coverages, *i.e.*, above half a monolayer, the curves cross and oxygen adsorption becomes greater than nitrogen adsorption at the same pressure.

Isosteric heats, q_{st} , computed from the isotherms are shown in Figure 2 as a function of coverage. For nitrogen the initial q_{st} was 4.6 kcal whereas that for oxygen was

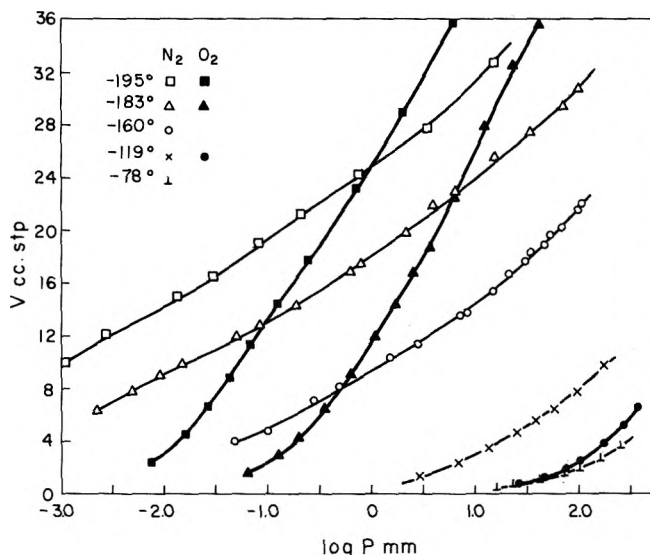


Figure 1. Isotherms for oxygen and nitrogen at low temperatures.

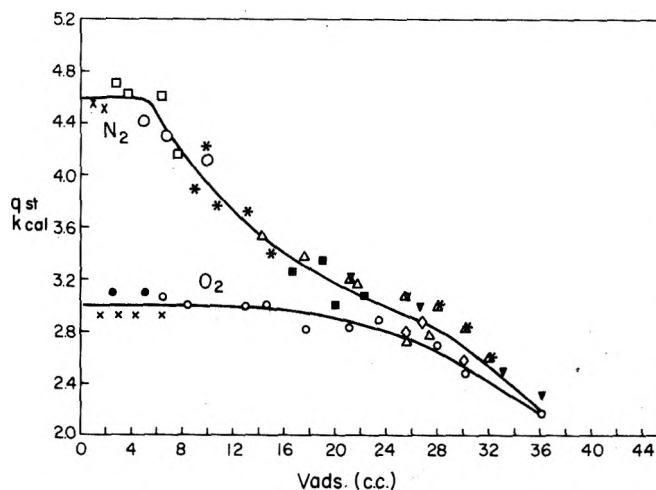


Figure 2. Isosteric heats for oxygen and nitrogen. Data indicated by squares are based on isotherms for three temperatures; other symbols are based on isotherms at two temperatures. Different symbols represent different sets of temperatures.

about 3.0 kcal. Thus, these measurements show that nitrogen is more strongly held than oxygen. These heats of adsorption, however, are sufficiently low in magnitude that one would say they fall in a range comparable to that often found for physical adsorption.¹⁰ Furthermore, at low temperatures the difference in q_{st} between nitrogen and oxygen is more than enough to account for the difference in the coverage at low pressures in the Langmuir limit.

The shapes of the q_{st} curves for oxygen and nitrogen differ markedly. For oxygen the heat of adsorption stays nearly constant at about 3 kcal for coverages up to half a monolayer; beyond this point, the q_{st} falls rapidly as the coverage increases. For nitrogen, however, the heat of adsorption decreases markedly as coverage increases even in the region well below a monolayer. A special effort was made to determine the initial shape of the curve for nitrogen by more extensive measurements of adsorption isotherms at higher temperatures. These data, shown in Figure 2, suggest that the initial heat of adsorption corresponding to the first tenth or so of a monolayer remains roughly constant; as the coverage increases beyond this

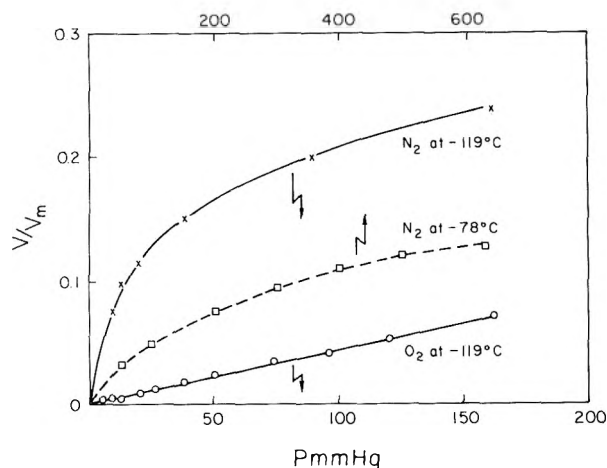


Figure 3. Isotherms for oxygen and nitrogen at high temperatures.

point, the q_{st} falls rapidly and above half a monolayer, it merges with the curve for oxygen. Although the experimental data are not sufficiently precise to define with certainty the extent (or even existence) of a plateau for the initial heats of adsorption, it seems clear that such behavior might be expected if a fraction of the surface, e.g., 10–20%, had sites at which the bonding energy was especially high.

Figure 3 compares the isotherms for oxygen and nitrogen at higher temperatures. At -119° and higher temperatures the isotherms for oxygen are linear. Even at -78° nitrogen isotherms are nonlinear. Such nonlinearity could stem from severe heterogeneity of the surface for nitrogen wherein only some small fraction of the surface adsorbs nitrogen with an especially high heat of adsorption. For these sites saturation effects will be evident at fairly low overall coverage and cause curvature in isotherms that would be linear, were the high energy sites not present. With such a picture, a crude assay of the number of such sites can be obtained by the difference in oxygen and nitrogen adsorption at -78 and -119° in the high-pressure region. At -119 and -78° this difference corresponds to $V/V_m = 0.15 \pm 0.02$. We view this as an upper limit because quadrupole effects with nitrogen^{11,12} might give the linear component of the isotherm a steeper slope for nitrogen. The above reasoning is a somewhat hazardous way of obtaining even a semiquantitative estimate of the number of special sites. Nevertheless, the estimate (0.2 to 0.3 cc/g) does agree with the extent of the plateau region of the heats of adsorption; hence, we regard the estimate as reasonable but not sharply defined. It is indeed suggestive that the number of sites for specially bound nitrogen is the same as the estimated number of sites for that specially bound molecular hydrogen that gives rise to an infrared band.³ These sites, in turn, were associated with the type I sites which effect dissociative adsorption of hydrogen even though the estimated number of type I sites is a bit lower than the number of sites that effect adsorption of infrared active molecular hydrogen.³

Figures 4 and 5 summarize the results of our infrared studies. If a fresh surface is exposed to hydrogen at room temperature or cooled to -195° and evacuated, dissociative adsorption (type I) leads to two strong bands at 3490 and 1710 cm^{-1} corresponding to OH and ZnH species. If gaseous hydrogen is present at a pressure of about 100 mm when the sample is cooled to -195° , a new band is evident

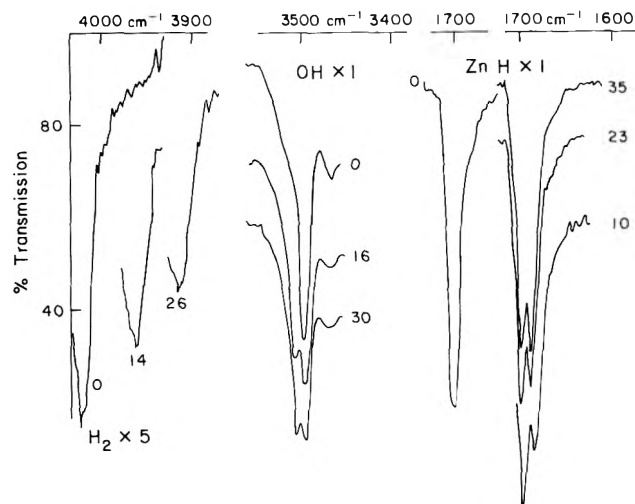


Figure 4. Spectra of dissociative and molecular hydrogen on zinc oxide. The numbers represent times in minutes after admission of a 0.1 cc dose of nitrogen.

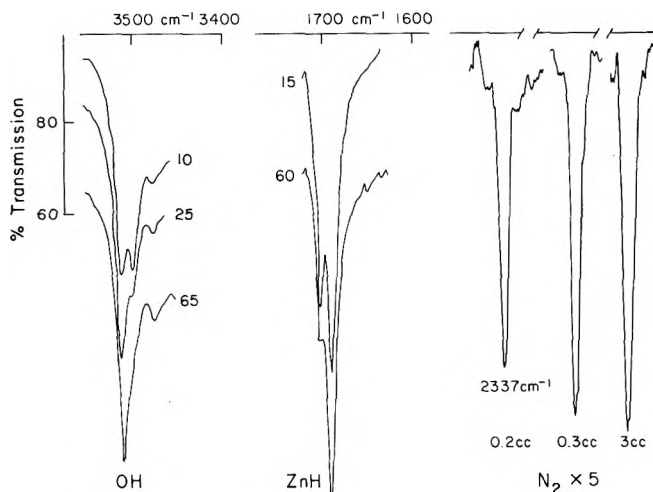


Figure 5. Spectra of dissociative hydrogen and molecular nitrogen on zinc oxide. The right side gives the stable nitrogen spectrum (in hydrogen gas) as a function of nitrogen dose size. Spectra for OH and ZnH represent changing spectrum after the second 0.1 cc dose of nitrogen and numbers represent times in minutes after admission of the second dose.

at 4019 cm^{-1} . This new band, shown on the left side of Figure 4 (labeled 0), is assigned to molecular hydrogen. When this new band is present, bands due to dissociative hydrogen shift to 3500 and 1700 cm^{-1} . After brief evacuation at -195° , the molecular band disappears, and the bands for dissociative hydrogen shift in position by about 10 cm^{-1} (OH down and ZnH up) but there is no large change in their intensities. When nitrogen is admitted to the sample in the presence or absence of hydrogen, a band appears at 2337 cm^{-1} which is assigned to molecular nitrogen. Such bands are shown on the right side of Figure 5 as a function of cumulative dose size. From our isotherms, the parameters of the system, and the monolayer capacity of the sample (~ 2 cc) we estimate that all of the first two doses are adsorbed and, after the third dose, the sample contains about 1 to 1.5 cc of adsorbed nitrogen. Since the band is very close to the maximum intensity after the initial dose, it appears that it is primarily the species formed in the initial dose that gives rise to the observed ir spectrum and the later doses simply saturate this limited

number of sites. Thus, the number of sites assayed by the ir spectrum corresponds to 10 to 15% of the surface in fair agreement with the estimates based on isotherms and heats of adsorption. We have also searched for bands accompanying oxygen adsorption, both in the presence and absence of hydrogen, but have failed to see such bands. Thus, there is no ir detectable species due to interaction of oxygen with special sites, as found with nitrogen; this is consistent with heat and isotherm data which suggest that there is no special interaction of oxygen with those sites that interact strongly with nitrogen.

Molecular nitrogen is more firmly bound than molecular hydrogen; the initial heat for nitrogen adsorption is over twice that for hydrogen (2.2 kcal). In line with this the band for molecular nitrogen persists after brief evacuation at -195° whereas that for hydrogen disappears. Since the amounts of ir active hydrogen and nitrogen are comparable, it seems reasonable to suppose that the special sites for hydrogen and nitrogen may be identical. If this is so, the more tightly held nitrogen might be expected to displace hydrogen from these binding sites, and we could effect a titration of the hydrogen band by the addition of nitrogen. Constraints imposed by the system require that hydrogen gas be present in order for the band to present; hence, we carried out the titration by admitting small doses of nitrogen to a cell containing hydrogen and observing the changes that occurred as the nitrogen diffuses to the sample. After admission of a nitrogen dose, about 45 min were required for a stable spectrum to be achieved. At this point we assumed that diffusion and adsorption of nitrogen was complete. The left-hand side of Figure 4 shows the hydrogen molecular band 0, 14, and 26 min after admission of a 0.1 cc dose of nitrogen. The hydrogen band obviously decreased with time and this decrease was accompanied by a parallel increase with time in the molecular nitrogen band. After addition of another 0.1 cc dose of nitrogen and achievement of a stable spectrum, no band due to molecular hydrogen was observed. Furthermore, at this point further doses of nitrogen did not substantially enhance the band intensity for molecular nitrogen. Thus, the titration, modified as required by the system, suggests that the more strongly bound nitrogen does, indeed, displace the weakly bound hydrogen from sites corresponding to about 10% of the V_m value for the surface. Back titration, that is, addition of nitrogen followed by addition of hydrogen and observation of the hydrogen band, suggested a higher titer; about 0.3 cc of nitrogen (15% of the V_m) was required to block the sites for ir active molecular hydrogen.

Isotherms and heat data suggest that oxygen adsorption is nonspecific. If we attempt to titrate the ir active hydrogen with 0.1 cc doses of oxygen, we find addition of the first few doses of oxygen has little effect on the hydrogen band. Only when the cumulative oxygen dose approaches the equivalent of a monolayer (corresponding to a coverage of about half a monolayer adsorbed with some residual pressure) is there an obvious decrease in the hydrogen band. Thus, oxygen does not adsorb preferentially on those sites preferred by nitrogen and hydrogen. The heat of oxygen adsorption is, however, greater than that found for hydrogen; hence, for large enough doses, even the nonspecific oxygen adsorption will block out the special sites for type III hydrogen adsorption.

It was shown earlier¹ that water adsorbs strongly and selectively (presumably on the pair sites) and eliminates

TABLE I: Positions cm^{-1} of Dissociatively Adsorbed Hydrogen Bands

Bands/ other species	None	Nitrogen	ΔN_2	Hydrogen	ΔH_2
ZnH	1710	1688	-22	1700	-10
OH	3490	3512	+22	3500	+10
ZnD	1232	1215	-17	1225	-7
OD	2580	2600	+20	2590	+10

type I adsorption. We have also made a qualitative study of the simultaneous effect of water chemisorption on the molecular nitrogen bands as well as both type I and type III hydrogen bands. Adsorption of water reduces the intensity of all three bands to very low, near zero, values, and stepwise desorption of water results in stepwise restoration of the bands to their initial intensities. These observations suggest that both molecular hydrogen and molecular nitrogen occur at the same sites as the dissociative type I chemisorption. It is of particular interest to note that whereas the molecular species compete with each other for these sites, the dissociative adsorption of hydrogen does not noticeably inhibit either form of molecular adsorption.

Further information on these sites is obtained by examination of the effect of doses of nitrogen on the OH and ZnH bands. Figure 4 shows the changes with time of these spectra after the admission of a 0.1 cc dose of nitrogen to the cell containing gaseous hydrogen. Initially, the OH and ZnH band positions (labeled 0) are at 3500 and 1700 cm^{-1} , respectively. After admission of nitrogen, both bands split. One component of each band stays at the original position; the new component occurs at higher and lower frequencies for OH and ZnH, respectively. As more of the nitrogen dose diffuses to and adsorbs on the sample, the component at the original position decreases in intensity and the new component increases in intensity. These changes occur in step; the new component for the OH band grows at a rate paralleling the growth rate for the new component of the ZnH band and the old components diminish at parallel rates. When a steady spectrum is achieved, the relative intensities of the new component and old component are comparable for both the ZnH and OH bands. Addition of a second 0.1 cc dose results in complete shifting of these bands (Figure 5). Since the ZnH and OH surface species appear to be adjacent, these results imply the following. Special sites for nitrogen are at or near those for the type I hydrogen. Adsorption of a small amount of nitrogen on these sites causes a shift in the bands for ZnH and OH species adjacent to the adsorbed nitrogen, but leaves the bands for the ZnH and OH species remote from these nitrogen sites unaffected. When the nitrogen is insufficient to saturate the sites, the ZnH and OH bands are split; addition of sufficient nitrogen to saturate the special sites results in formation of ZnH and OH bands at the shifted position.

Previous data suggest that molecular hydrogen also adsorbs on these same sites; hence, we would expect to find a shift in OH and ZnH bands due to molecular hydrogen adsorption. Such shifts are observed but they are smaller than those observed with molecular nitrogen. Accordingly, one does not see the sequence wherein a new shifted band appears at the expense of the initial unshifted band, instead an overall shift is observed with the OH band shift-

ed up and the ZnH band shifted down similar to the effect observed with molecular nitrogen. We have determined shifts not only for the ZnH and OH bands but also for the ZnD and OD bands. The shifts are summarized in Table I. Shifts are also observed when oxygen is adsorbed. These shifts, similar in magnitude to those with molecular hydrogen, are apparent only when the coverage approaches a monolayer; hence, on this basis also oxygen adsorption appears to be nonspecific.

Discussion

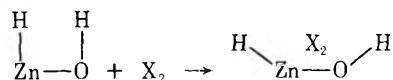
Interactions of oxygen and nitrogen with the pair sites on zinc oxide are dramatically different. We cannot ascribe these differences to polarization effects alone since the polarizability of oxygen and nitrogen are comparable.¹³ Drain,¹¹ however, has also noted that oxygen and nitrogen often show different adsorption characteristics on ionic solids. He attributes these differences to quadrupole effects. (The quadrupole moment of nitrogen is at least three times that of oxygen.¹³) In support of this viewpoint, his estimates indicate that quadrupole interactions of adsorbed nitrogen on the 001 surface of KCl add as much as 1 kcal to the heat of adsorption. For ions with greater charge, the field gradient and, hence, the quadrupole contribution could be even greater. Indeed, in a subsequent study, Drain and Morrison¹² found that, on titanium dioxide, the initial heat of nitrogen was 6.0 kcal compared to 4.0 kcal for oxygen. Such quadrupole effects may be the reason for the specific adsorption of nitrogen and the appearance of the infrared band. Since the energy involved in quadrupole interaction depends on the field gradient, this interpretation suggests that the specific sites for nitrogen adsorption have a rather high effective field gradient.

If, indeed, the special sites for nitrogen adsorption have a high electric field gradient, nitrogen on these sites would have an induced dipole moment. Such an induced dipole moment could lead to our observation of the vibrational transition normally forbidden in the gas-phase ir. This viewpoint, however, does not offer a ready explanation for the fact that the observed frequency (2337 cm⁻¹) is virtually identical with that for gaseous nitrogen¹⁴ (2335 cm⁻¹). In other cases where a specific interaction has led to the appearance of a molecular nitrogen band,^{15,16} one finds the frequency is also shifted down by about 100 cm⁻¹, suggesting that a strong bond to the surface requires some reduction in the force constant for the vibration. Let us consider, however, the stretching vibrations for the one-dimensional molecule, S-N-N, wherein S represents a surface atom of infinite mass and k' and k represent force constants for the SN and NN bond. Provided k' is much less than k , the observed frequencies are given by

$$\omega^2 = \frac{2k}{m} + \frac{k'}{2m} \quad \text{or} \quad = \frac{k'}{2m} - \frac{k^2}{8km}$$

where m is the mass of a nitrogen atom. The first term involves primarily the N-N vibration whereas the second term involves primarily the S-N vibration. From these expressions it is clear that if k were not reduced by adsorption, the high-frequency vibration would be higher than the frequency for the free molecule; hence, the appearance of the nitrogen band unshifted implies some reduction in k did, in fact, occur when the bond to the surface was made.

The effect of molecular hydrogen and nitrogen adsorption on the ZnH and OH bands can be rationalized on the basis of coupling effects. We can picture this adsorption schematically as follows



If X₂ interacts with both hydrogen atoms, this may introduce or increase coupling between these vibrations. Let us assume that the potential energy for OH and ZnH stretching in the absence of X₂ is represented by

$$V = \frac{1}{2}k_1\alpha_1^2 + \frac{1}{2}k_2\alpha_2^2$$

where k and α are stretching force constants and displacements from equilibrium and subscripts 1 and 2 designate OH and ZnH, respectively. When X₂ is present, we shall assume coupling adds the term $k\alpha_1\alpha_2$ to the potential where k depends on the nature of X₂. The new observed frequencies, for small k , are given by

$$\omega^2 = \omega_1^2 + (k/m)^2/(\omega_1^2 - \omega_2^2)$$

and

$$\omega^2 = \omega_2^2 - (k/m)^2/(\omega_1^2 - \omega_2^2)$$

where ω_1 and ω_2 are the unshifted OH and ZnH frequencies. In other words the effect of such coupling is to shift the OH frequency up and the ZnH frequency down. Qualitatively, this is observed; hence, coupling again offers a reasonable interpretation of the observed effects. Quantitatively, the relative magnitudes of the shifts for OH compared to ZnH and OD compared to ZnD do not conform to the above formulae, but this may be expecting too much of a grossly oversimplified model. In any case it seems clear that the molecular species are selectively bound at or very near the same sites that dissociatively adsorb hydrogen.

If the pair site does consist of a zinc oxygen pair with their normal spacing, the distance between the two ions is about 2.0 Å. Dissociative adsorption of hydrogen on these sites plus molecular adsorption must result in steric crowding. (This must be even more severe for adsorption of molecular nitrogen.) We shall not attempt to speculate on the configuration of such a molecular-dissociative hydrogen complex but we do wish to emphasize that the evidence for such a complex seems very good. This complex could very well provide a pathway for hydrogen-deuterium exchange via a Rideal-Eley¹⁷ mechanism wherein a weakly adsorbed molecular species reacts with the adsorbed dissociative species. Such a pathway has been suggested for zinc oxide.¹⁸ We currently have a study underway to see if the ir active molecular species can be the intermediate in the exchange reaction.

Acknowledgment. Acknowledgment is made to the donors of the Petroleum Research Fund, administered by the American Chemical Society, for support of part of this research. This research was also aided by funds from the National Science Foundation under Grant No. GP 34034X.

References and Notes

- (1) R. J. Kokes and A. L. Dent, *Advan. Catal.*, **22**, 1 (1972).
- (2) C. C. Chang and R. J. Kokes, *J. Amer. Chem. Soc.*, **93**, 7107 (1971).
- (3) C. C. Chang, L. T. Dixon, and R. J. Kokes, *J. Phys. Chem.*, **77**,

- 2634 (1973).
- (4) R. P. Eischens, W. A. Pliskin, and M. J. D. Low, *J. Catal.*, **1**, 180 (1962).
- (5) Unpublished results by C. C. Chang. A brief summary is given by R. J. Kokes, *Intra-Sci. Chem. Rep.*, **6**, 78 (1972).
- (6) E. U. Condon, *Phys. Rev.*, **41**, 759 (1931).
- (7) M. F. Crawford and J. R. Dagg, *Phys. Rev.*, **91**, 1569 (1953).
- (8) A. L. Dent and R. J. Kokes, *J. Amer. Chem. Soc.*, **92**, 1092, 6709, 6718 (1970).
- (9) The BET V_m values for this 22.0-g sample are 37 cc for nitrogen and 39 cc for oxygen. This sample, activated several times before determination of the reported isotherms, gave BET V_m values of 36 and 39 cc for nitrogen and oxygen, respectively.
- (10) S. Brunauer, "The Adsorption of Gases and Vapors," Princeton University Press, Princeton, N. J., 1943.
- (11) L. E. Drain, *Trans. Faraday Soc.*, **49**, 650 (1953).
- (12) L. E. Drain and J. A. Morrison, *Trans. Faraday Soc.*, **49**, 654 (1953).
- (13) J. O. Hirschfelder, C. F. Curtiss, and R. B. Bird, "Molecular Theory of Gases and Liquids," Wiley, New York, N. Y., 1954, p 950.
- (14) G. Herzberg, "Molecular Spectra and Molecular Structure. I. Spectra of Diatomic Molecules," Van Nostrand, New York, N. Y., 1950, p 62.
- (15) R. P. Eischens and J. Jacknow, *Proc. 3rd Int. Congr. Catal., Amsterdam, 1964*, 627 (1965).
- (16) R. Van Hardeveld and F. Hartog, *Advan. Catal.*, **22**, 75 (1972).
- (17) B. M. Trapnell, "Catalysis," Vol. III, P. H. Emmett, Ed., Reinhold, New York, N. Y., 1955, Chapter I; D. D. Eley, *op cit*, Chapter II.
- (18) S. Naito, H. Shimizu, E. Hagiwara, T. Onishi, and K. Tamaru, *Trans. Faraday Soc.*, **67**, 1519 (1971).

Electron Spin Resonance Spectra of Sulfanyl Radicals in Solution¹

J. R. Morton and K. F. Preston*

Division of Chemistry, National Research Council Canada, Ottawa, Canada (Received March 22, 1973)

Publication costs assisted by the National Research Council Canada

Radicals of the type $(R_fO)_3S$ and $(R_fO)_2SF$, where $R_f = CF_3, SF_5$, have been detected during the photolysis of hypofluorites and peroxides containing dissolved OCS, F_2SS , CS_2 , Cl_2CS , or F_2CS . The esr spectra of these radicals are interpreted in terms of a T-shaped structure (C_{2v} symmetry) and a 2A_1 ground state.

Introduction

In recent investigations² we were able to detect paramagnetic intermediates resulting from the addition of oxyl radicals (*e.g.*, SF_5O , CF_3O) and fluorine atoms to compounds of tetravalent sulfur (SF_4 , SOF_2 , and SO_2). Our success in observing radicals of the type SF_5 , F_3SO , and FSO_2 , arising from valence-shell expansion of sulfur, prompted us to search for SF_3 and related molecules, hitherto undetected spectroscopically, in the reactions of divalent sulfur compounds. We report here the results of a study of the reactions of oxyl radicals and F atoms with compounds containing the $=S$ function which has led to the detection of intermediates of the type $(R_fO)_3S$ and $(R_fO)_2SF$ (sulfanyl radicals).

Results

Esr spectra were recorded during the uv photolyses of liquid hypofluorites CF_3OF and SF_5OF containing small amounts of dissolved OCS, CS_2 , SSF_2 , Cl_2CS , or F_2CS . Attention was confined to the early stages of photolysis in order to minimize contributions from SF_5 derivatives² which complicated the spectra observed after long exposures. The OCS system was studied more extensively than the others, and it was found that certain of the species to be described could be generated by photolysis of OCS dissolved in the peroxide (CF_3OOCF_3 or SF_5OOSF_5) without the complication of the aforementioned SF_5 derivatives.

In the case of CF_3O attack on OCS two radicals (A and B) were observed in the $g = 2$ region of the spectrum (Figure 1). The ratio of their integrated intensities $[A]/[B]$

was independent of the light intensity, being approximately 3:1 at -120° and increasing to approximately 10:1 at -50° . The spectra of both radicals saturated at microwave power levels in excess of 2 mW, and both spectra revealed hyperfine interactions with several ^{19}F ($I = \frac{1}{2}$) nuclei. Radical B ($g = 2.0088$) had hyperfine interactions with six equivalent ^{19}F nuclei (1.09 G), whereas in the case of radical A ($g = 2.0060$) six ^{19}F nuclei had 1.38-G interactions, and another three had 0.27-G interactions. Synthesis of OCS enriched in ^{13}C ($I = \frac{1}{2}$) to 93% yielded no discernible ^{13}C hyperfine structure in the spectrum of radical A, but a 7.35-G ^{13}C interaction in radical B. In addition, both A and B were shown to contain a sulfur atom by the detection, using OCS enriched with ^{33}S ($I = \frac{3}{2}$), of ^{33}S hyperfine structure ($a_{33} = 59.9$ and 42.2 G in radicals A and B, respectively).

Photolysis of CF_3OF containing dissolved SSF_2 , Cl_2CS , or CS_2 yielded a spectrum identical with that of radical A within the accuracy of the measurements. Radical B, on the other hand, possessing a carbon atom originating with the OCS molecule, was demonstrably unique to the OCS system.

An exactly analogous situation arose when SF_5OF was used. With OCS, two species (A' and B') were detected, having g factors of 2.0059 (A') and 2.0090 (B'). Experiments with ^{13}C -enriched OCS proved B' to be the exact analog of B, both having ^{13}C hyperfine interactions of 7.35 G. Both A' and B' had resolvable hyperfine interactions with eight ^{19}F nuclei, the hyperfine constants being 1.49 (A') and 1.20 G (B'). Photolysis of SF_5OF con-

TABLE I: Summary of Data on Radicals Detected in Present Study

		CF ₃ OF	SF ₅ OF
OCS	A (CF ₃ O) ₃ S	$g = 2.0060^a$ $a_{19}(6) = 1.38^b$ $a_{19}(3) = 0.27$ $a_{33}(1) = 59.9$	A' (SF ₅ O) ₃ S $g = 2.0059$ $a_{19}(8) = 1.49$
	B (CF ₃ O) ₂ SC(O)OCF ₃ or (CF ₃ O) ₂ SC(O)F	$g = 2.0088$ $a_{19}(6) = 1.09$ $a_{13}(1) = 7.35$ $a_{33}(1) = 42.2$	B' (SF ₅ O) ₂ SC(O)OSF ₅ or (SF ₅ O) ₂ SC(O)F $g = 2.0090$ $a_{19}(8) = 1.20$ $a_{13}(1) = 7.35$
	SSF ₂ } SCS } Cl ₂ CS }	A (CF ₃ O) ₃ S $g = 2.0059$ $a_{19}(6) = 1.40$ $a_{19}(3) = 0.25$	A' (SF ₅ O) ₃ S $g = 2.0058$ $a_{19}(8) = 1.50$
F ₂ CS	C (CF ₃ O) ₂ SF $g = 2.0074$ $a_{19}(6) = 1.93$ $a_{19}(1) = 6.96$	C' (SF ₅ O) ₂ SF $g = 2.0076$ $a_{19}(8) = 2.28$ $a_{19}(1) = 6.16$	

^a g factors are accurate to ± 0.0001 . ^b Figures in parentheses indicate number of equivalent nuclei with given hyperfine interaction (quoted in Gauss, ± 0.05).

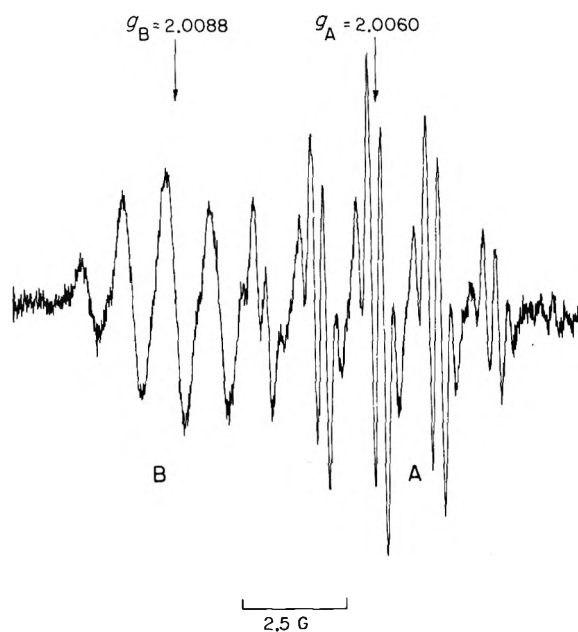


Figure 1. ESR spectra of (CF₃O)₃S (A) and (CF₃O)₂SC(O)X (B) in a solution of OCS in CF₃OOCF₃ photolyzed at -120° .

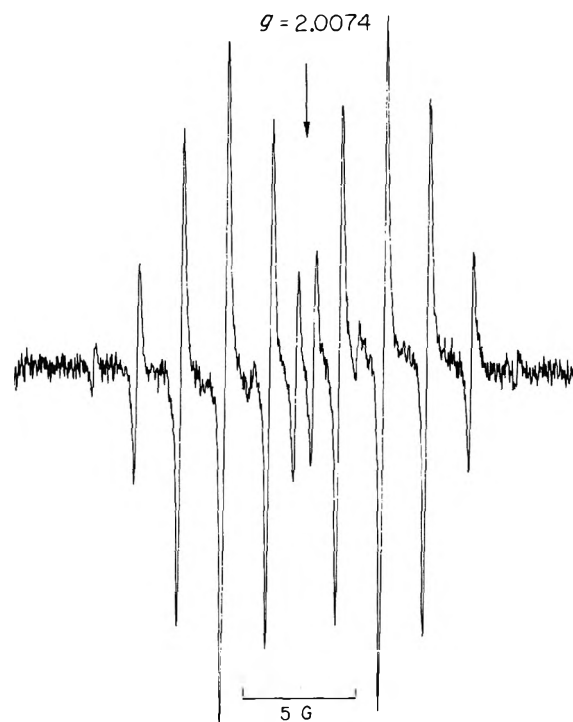


Figure 2. ESR spectrum of (CF₃O)₂SF (radical C) in a solution of F₂CS in CF₃OF photolyzed at -100° .

taining dissolved SSF₂, Cl₂CS, or CS₂ yielded a spectrum identical with that of A', within experimental error.

Photolysis of solutions of F₂CS in the two hypofluorites gave results in marked contrast to those described above for the other solutes. Instead of the expected radicals A and A' we observed two new species, C (Figure 2) and C', both showing hyperfine interactions with a single ¹⁹F nucleus (6.96 G in C, obtained with CF₃OF; 6.16 G in C', obtained with SF₅OF) and either six (C) or eight (C') equivalent ¹⁹F nuclei. This unexpected result suggested the occurrence of a "dark" (*i.e.*, before photolysis) reaction between F₂CS and the hypofluorites. To explore further this possibility F₂CS (20 μ l) was dissolved in CF₃OF (200 μ l) and allowed to stand for 0.5 hr at -96° , after which the CF₃OF was pumped off and replaced by either CF₃OOCF₃ or SF₅OOSF₅. Photolysis of the resulting solutions gave rise to the spectra of C or C', respectively. These radicals could not be detected, however, during the photolyses of the peroxides containing untreated F₂CS. We conclude that C and C' probably arise from the reac-

tion of oxyl radicals with a precursor of the type R_fSF generated by a thermal reaction between F₂CS and the hypofluorites, but we have not positively identified this intermediate.

Esr data on all the radicals mentioned above are collected in Table I.

Identification and Structure of Radicals

Radicals A and A'. The radicals A and A' are believed to be S(OR_f)₃, with R_f = CF₃ and SF₅, respectively. These species are formed in four of the five systems studied, and their parameters are virtually independent of the initial reactant, indicating that the latter contributes to the radical only its central sulfur atom. The value (59.9 G) of the ³³S hyperfine interaction in radical A, together with the absence of any detectable ¹³C hyperfine interaction, indicates that A and A' are sulfur-centered radicals.

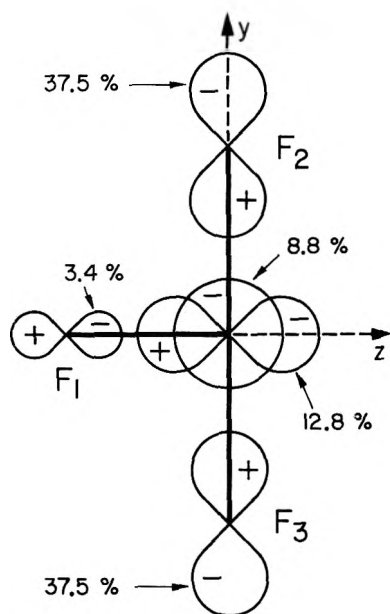


Figure 3. The $3a_1$ orbital of ClF_3 .

The presence of nine ^{19}F nuclei, six of one kind, three of another, leads us to identify A as $(\text{CF}_3\text{O})_3\text{S}$. By analogy with A, we identify A' as $(\text{SF}_5\text{O})_3\text{S}$ in which only two of the three SF_5O ligands give rise to resolvable hyperfine structure, in each case that of four equivalent ^{19}F nuclei. Our inability to determine the hyperfine interactions of the four equivalent ^{19}F nuclei of the unique ligand is probably because the two remaining ^{19}F nuclei on the equivalent ligands have small hyperfine interactions which vitiate adequate resolution of the spectrum.

The prototype radical SF_3 possesses one less electron than the molecule ClF_3 , and the nonequivalence of the three ligands in $(\text{CF}_3\text{O})_3\text{S}$ and $(\text{SF}_5\text{O})_3\text{S}$ led us to suspect that their structure was similar to that of ClF_3 , which is a slightly distorted T-shaped molecule.³ A molecular orbital description of ClF_3 has been given by Brown and Peel.⁴ Its ground state is $\dots 1b_1^2 3a_1^2$, 1A_1 (symmetry C_{2v}).⁵ The $3a_1$ orbital (Figure 3) should be a reasonable model on which to base a description of the orbital of the unpaired electron in SF_3 and radicals derived from it, although the proximity of the $1b_1$ orbital makes this assumption somewhat tentative. The dominant contributors to $3a_1$ are $2p_y$ atomic orbitals on F_2 and F_3 (37.5% each), followed by sulfur $3p_z$ (12.8%) and $3s$ (8.8%). The unique fluorine's $2p_z$ orbital contributes to the extent of only 3.4%. Several aspects of our data on radicals derived from SF_3 can be explained on the assumption that the unpaired electron in these radicals occupies an orbital similar to the $3a_1$ orbital of ClF_3 . For example, assuming free rotation about the S-O bonds, C_{2v} symmetry dictates that two of the CF_3O ligands in $(\text{CF}_3\text{O})_3\text{S}$ be equivalent and different from the third. Moreover, spin polarization in the bonds of the equivalent ligands would be expected to be greater than in those of the unique ligand, giving rise to a larger hyperfine interaction for the six equivalent ^{19}F nuclei than for the three ^{19}F nuclei on the unique ligand.

The ^{33}S hyperfine interaction in radical A was found to be 59.9 G. Comparison of this figure with that⁶ for $(8\pi/3)\gamma_e\gamma_{33}\psi^2_{3s}(0)$, 969 G, indicates a net 6.2% contribution by the $3s$ orbital of sulfur to the orbital of the unpaired electron. According to Brown and Peel's data,⁴ their $3a_1$ orbital requires an 8.8% sulfur $3s$ contribution, and our

estimate of 6.2% is therefore entirely reasonable, and rather larger than one would have anticipated for a 2B_1 ground state.

Quite recently Subramanian and Rogers⁷ presented data on the esr spectrum of AsF_3^- detected after γ -irradiation of glassy pellets of AsF_3 . Since AsF_3^- is a radical isoelectronic with SF_3 , except for the substitution of a third-row for a second-row central atom, it is of interest to compare our data and conclusions with those of Subramanian and Rogers. Two of the three ^{19}F nuclei in AsF_3^- have isotropic hyperfine interactions of 33 G, the third 12 G, thus establishing that this radical also possessed C_{2v} rather than C_{3v} or D_{3h} symmetry. The isotropic ^{75}As ($I = 3/2$) hyperfine interaction is 196 G, and according to data obtained from Froese's wave function,⁶ this represents a contribution of $196/3393$, or 5.8%, by the arsenic $4s$ orbital to the orbital occupied by the unpaired electron. It is gratifying to compare this figure with our estimated 6.2% sulfur $3s$ contribution in the case of $(\text{CF}_3\text{O})_3\text{S}$. However, their analysis of the anisotropic contributions to the ^{19}F and ^{75}As hyperfine structure and a somewhat contrived analogy with the PF_4 radical⁸ led Subramanian and Rogers to assign a 2B_1 ground state to AsF_3^- .

A positive deviation of the g factor from the free-spin value can also be explained with the aid of Brown and Peel's term scheme, according to which SF_3 and its derivatives would have the ground-state configuration $\dots 1b_1^2 3a_1^1$, 2A_1 . The separation between the ground state and a low-lying $\dots 1b_1^1 3a_1^2$, 2B_1 state⁵ is predicted to be $\Delta E \approx 12,000 \text{ cm}^{-1}$, and since this state is connected *via* spin-orbit interaction to the ground state by rotation about the y axis a positive value for $\Delta g_{y,y}$ would be anticipated. (Significant g shifts are not, however, expected for the other principal axes.) More precisely, since the $1b_1$ orbital is a pure central-atom $3p_x$ orbital, the expression for $\Delta g_{y,y}$ has the particularly simple form⁹

$$\Delta g_{y,y} = 2\rho\zeta_s/\Delta E$$

where ρ is the central-atom $3p_z$ contribution to the $3a_1$ molecular orbital (0.128), and ζ_s is the spin-orbit interaction constant for sulfur ($\sim 380 \text{ cm}^{-1}$).¹⁰ The isotropic g shift, one-third of $\Delta g_{y,y}$, can hence be estimated as 0.003, in reasonable agreement with the observed values (Table I).

Radicals B and B'. When OCS was dissolved in CF_3OF or CF_3OOCF_3 and photolyzed at -100° , a second radical (B) was observed; similarly, OCS photolyzed in SF_5OF or SF_5OOSF_5 revealed the presence of a second species (B'). By contrast with A and A', which were formed with four of the five reagents, radicals B and B' were peculiar to OCS. Experiments with enriched OCS confirmed this view. It was established that B and B' possessed not only a sulfur atom and (at least) two OR_f ligands, but also a carbon atom originating with the OCS molecule. Since the ^{13}C hyperfine interaction (in both cases 7.35 G) was too small to permit the possibility that they were derived from the prototype CF_3 ($a_{13} = 271.3 \text{ G}$),¹¹ we were forced to conclude that B and B' were sulfur-centered species, also related to SF_3 , and probably $(\text{R}_f\text{O})_2\text{SC}(\text{O})\text{X}$, where X is either F or OR_f . Another possibility, $(\text{R}_f\text{O})_3\text{S}=\text{CO}$, was discounted after comparison of the g factors and ^{33}S hyperfine interaction of B with those² of $\text{F}_3\text{S}=\text{O}$.

The Radicals C and C'. These radicals are formed when solutions of F_2CS in CF_3OF or SF_5OF , respectively, are photolyzed. It has been established that a dark reaction

occurs between F_2CS and the hypofluorite, with the probable formation of a sulfenyl fluoride R_fSF , and that C and C' are formed by subsequent oxyl radical attack on the intermediate. Elimination of reasonable alternatives has led us to identify C and C' as $(CF_3O)_2SF$ and $(SF_5O)_2SF$, respectively. The presence of a central sulfur atom, although not detected spectroscopically, can be inferred since the alternative is a central carbon atom. In this case the radicals would be derived from the prototype CF_3 , an untenable proposition when the hyperfine interaction of their unique ^{19}F nuclei is compared with those of CF_3 (145 G).¹¹

Origin of the Species

The production of sulfanyl radicals from photochemical reactions of $=S$ compounds with peroxides or hypofluorites is clearly a complex process comprising a number of consecutive free-radical reactions. We hesitate, in the absence of kinetic data, to propose a formal mechanism and will restrict discussion of the chemistry of radical formation at this time to a few comments based on our esr observations. An added complexity in the case of reaction with hypofluorites is the possibility of a "dark" reaction preceding photolysis, as observed in this work with F_2CS and by Bailey and Cady¹² with Cl_2CS and OCS . Thermal reaction between OCS and CF_3OF was only detectable¹² at elevated temperatures, however, so that under our experimental conditions the radicals B and B' undoubtedly arise through successive additions of photochemically generated oxyl radicals to OCS . $CF_3OSC(O)OCF_3$, tentatively identified¹² as a product of the thermal reaction, may well be an intermediate in the sequence of reactions leading to B. It would appear that the initial attack of an oxyl radical on OCS does not result in significant S-C bond rupture, since the complete absence of the radical $(CF_3O)_2SF$ (C) during $CF_3OF-OCS$ photolyses dictates against the participation of free CF_3OS radicals. (Unless, by chance, the latter are unreactive toward hypofluorite.) A, then, is probably a product of the same reaction sequence which leads to B and may even arise *via* the decarbonylation of B. The very low yield of radicals $(CF_3O)_nSF_{3-n}$, where $n = 0-2$, from the photolysis of $CF_3OF-OCS$ mixtures suggests that F atom attack on OCS results in SF formation and that SF and SF_2 are rapidly fluorinated by CF_3OF . Clearly, to obtain good yields of such sulfanyl radicals it is necessary to commence with compounds already containing the S-F bonds. In this connection it is interesting to note the great difference in behavior between F_2CS and Cl_2CS when they are mixed with CF_3OF and subjected to photolysis. Thermal reactions occur in both cases prior to photolysis leading to a sulfenyl fluoride (*vide supra*) with F_2CS , but to a thioperoxide compound $CF_3OSCFCl_2$ in the case of Cl_2CS .¹² In the ensuing photoyses alkoxy radical attack on these "dark" reaction products evidently determines the type of

radical observed, *viz.*, C, containing the original S-F bond of the sulfenyl fluoride, in the former case and A in the latter case.

Experimental Section

Trifluoromethyl hypofluorite was obtained from K & K Laboratories, Plainview, N. Y., and the peroxide CF_3OOCF_3 from PCR Inc., Gainesville, Fla. Pentafluorosulfur hypofluorite, SF_5OF , was prepared from thionyl fluoride and fluorine, using a CsF catalyst,¹³ and SF_5OOSF_5 was prepared by photolysis of the hypofluorite.¹⁴ Carbonyl sulfide was obtained from Matheson Inc., and carbonyl sulfide enriched with the isotopes ^{13}C or ^{33}S was prepared by heating 93% ^{13}CO (Merck Sharp and Dohme) with sulfur or by heating 50% ^{33}S (Oak Ridge National Laboratory) in CO . Disulfur difluoride SSF_2 was prepared¹⁵ by fluorination of S_2Cl_2 with KSO_2F , and SCF_2 was prepared by pyrolysis of the dimer.¹⁶ Thiophosgene Cl_2CS was obtained from PCR Inc., Gainesville, Fla.

The samples were photolyzed with a Schoeffel 1000-W Hg/Xe lamp, using two quartz lenses to condense the image of the arc onto the sample. The esr spectra were obtained with a Varian E-12 spectrometer equipped with an accessory for operation at low temperatures. The magnetic field was measured with a Varian F-8A fluxmeter, and the microwave frequency was obtained with the aid of a Hewlett-Packard 540B transfer oscillator.

Caution. Numerous explosions occurred during the course of this work, particularly with the hypofluorite SF_5OF above -80° . For this reason the quantity of (liquid) sulfide never exceeded 25 μl , and we allowed the solution (typically 200 μl total volume) to warm up from -196° to operating temperature (typically between -80 and -120°) in an armored box. In spite of these precautions, occasional detonations occurred in the microwave cavity, resulting in extensive damage to the equipment.

References and Notes

- (1) NRCC No. 13413.
- (2) J. R. Morton and K. F. Preston, *Chem. Phys. Lett.*, **18**, 98 (1973); *J. Chem. Phys.*, **58**, 2657 (1973).
- (3) D. F. Smith, *J. Chem. Phys.*, **21**, 609 (1953).
- (4) R. D. Brown and J. B. Peel, *Aust. J. Chem.*, **21**, 2605 (1968).
- (5) The designations b_1 and b_2 given to orbitals of ClF_3 in ref 4 have been interchanged in the present article. B_1 here is the representation of C_{2v} which is antisymmetric with respect to both reflection in the molecular plane and rotation about the C_2 axis. Our labeling of molecular axes (Figure 3) also differs from that of ref 4.
- (6) C. Froese, *J. Chem. Phys.*, **45**, 1417 (1966).
- (7) S. Subramanian and M. T. Rogers, *J. Chem. Phys.*, **57**, 4582 (1972).
- (8) J. Higuchi, *J. Chem. Phys.*, **50**, 1001 (1969).
- (9) D. W. Ovenall and D. H. Whiffen, *Mol. Phys.*, **4**, 135 (1961).
- (10) D. S. McClure, *J. Chem. Phys.*, **17**, 905 (1949).
- (11) R. W. Fessenden, *J. Magn. Resonance*, **1**, 277 (1969).
- (12) R. E. Bailey and G. H. Cady, *Inorg. Chem.*, **9**, 1930 (1970).
- (13) J. K. Ruff and M. Lustig, *Inorg. Chem.*, **3**, 1422 (1964).
- (14) C. I. Merrill and G. H. Cady, *J. Amer. Chem. Soc.*, **83**, 298 (1961).
- (15) F. Seel and H. D. Göltz, *Z. Anorg. Allg. Chem.*, **327**, 32 (1964).
- (16) W. J. Middleton, E. G. Howard, and W. H. Sharkey, *J. Org. Chem.*, **30**, 1383 (1965).

Equilibrium Studies by Electron Spin Resonance. V. The Role of the Cation in Hydrogen Bonding to the Nitrobenzene Anion Radical

Luis Echegoyen, Hector Hidalgo, and Gerald R. Stevenson*

Department of Chemistry, University of Puerto Rico, Rio Piedras, Puerto Rico 00931 (Received June 13, 1973)

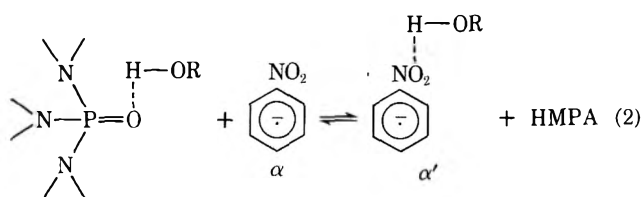
Publication costs assisted by the University of Puerto Rico

The alkali metal cation was found to have a pronounced effect upon the thermodynamics of the hydrogen bond exchange reaction between hydrogen bonded hexamethylphosphoramide (HMPA) and the nitrobenzene anion radical. This effect was found to be due to the participation of the hydrogen-bonded HMPA in the solvation sheath of the cation. When ammonia is used as a proton donor, a similar interaction was found to exist between the cation involved in ion pairing with the nitrobenzene anion radical and the hydrogen-bonded HMPA. This interaction leads to the formation of a hydrogen-bonded ion pair.

The nitrobenzene anion radical when formed by alkali metal reduction in hexamethylphosphoramide (HMPA) exists in two forms: the "free" ion (α) and the ion pair (β). Both of these species can be observed simultaneously by esr, and the enthalpies controlling the ion pair dissociation reaction are known (eq 1).^{1,2}



It has been previously reported that the addition of small amounts of water or alcohol to the system $\text{PhNO}_2\text{-HMPA-Li}$ affords increases in the nitrogen coupling constant for the formally "free" ion due to hydrogen bonding of the acidic proton of the alcohol with the nitro group of the PhNO_2 anion radical.³ However, no change in the nitrogen splitting for the ion pair (β) was observed. These results were explained by eq 2, in which a hydrogen bond is formed with α . This hydrogen bonding increases the charge and spin density on the NO_2 group, thus increasing the nitrogen isotropic coupling constant. The ion pair, however, is too tightly complexed with the cation to participate in hydrogen bonding.



Due to the fact that the nitrogen splitting of the hydrogen-bonded ion (α') increases smoothly with the addition of hydrogen-bonding donor, it was concluded that equilibrium 2 was fast on the esr time scale, and that the observed nitrogen coupling constant was the averaged coupling constant (\bar{A}_N) for the hydrogen bonded ion (α') and the "free" ion (α). This conclusion was supported by the fact that dramatic line width alternation was observed at lower temperatures (-10°), and by the fact that the concentration of the time-averaged species increased relative to that of β as the proton donor concentration was increased.³

Utilizing time averaging equations, expression 3 was developed for the thermodynamic equilibrium constant for reaction 3.

$$K_{\text{eq}} = (\bar{A}_N - 8.48)(\text{HMPA}) / (A_{N'} - \bar{A}_N)(\text{HMPA}') \quad (3)$$

$A_{N'}$ is the coupling constant for the completely hydrogen-bonded ion, and 8.48 is the coupling constant for α .

To better understand the role that the counterion plays in hydrogen bonding to anions and to obtain valuable information as to the structure of hydrogen bonded anions, we wish to report the effect of the cation upon the thermodynamic parameters controlling equilibrium 2 and the formation of the first hydrogen-bonded ion pair.

Experimental Section

The nitrobenzene (Eastman Organic Chemicals) was vacuum distilled before use. The HMPA was distilled under reduced pressure from calcium hydride and stored over molecular sieves 4A. The HMPA was distilled from the solvated electron under high vacuum directly into the reaction vessel. Quantitative additions of methanol were added to the HMPA solutions containing the PhNO_2 anion radical in the same manner as previously described.³ The ammonia was carefully degassed by the freeze-thaw method and distilled from the solvated electron into an evacuated bulb for storage.

Quantitative additions of NH_3 to the PhNO_2 anion radical solutions in HMPA were carried out with the use of a toeppler pump connected with a gas buret. Ammonia was allowed to enter the calibrated gas buret under high vacuum (10^{-5} Torr). The number of moles of ammonia was then calculated using the ideal gas equation. Initial pressures of NH_3 in the gas buret were between 10 and 400 Torr. This ammonia was then allowed to come in contact with the stirred HMPA solution of the PhNO_2 anion radical for a period of about 2 hr. The stopcock to the apparatus containing the HMPA solution was then closed and the remaining ammonia was toepled back into the gas buret. The difference between the initial and final number of moles of ammonia in the gas buret was taken as the number that had dissolved in the HMPA solution. The correction for the gaseous ammonia in the solution containing apparatus was found to be negligible.

The esr system and the method used to form the anion radicals were identical with those previously described.¹

Results and Discussion

Addition of small amounts of methanol or ammonia to the system $\text{PhNO}_2\text{-HMPA-Na}$ or $\text{PhNO}_2\text{-HMPA-Li}$ affords an increase in the nitrogen coupling constant for the

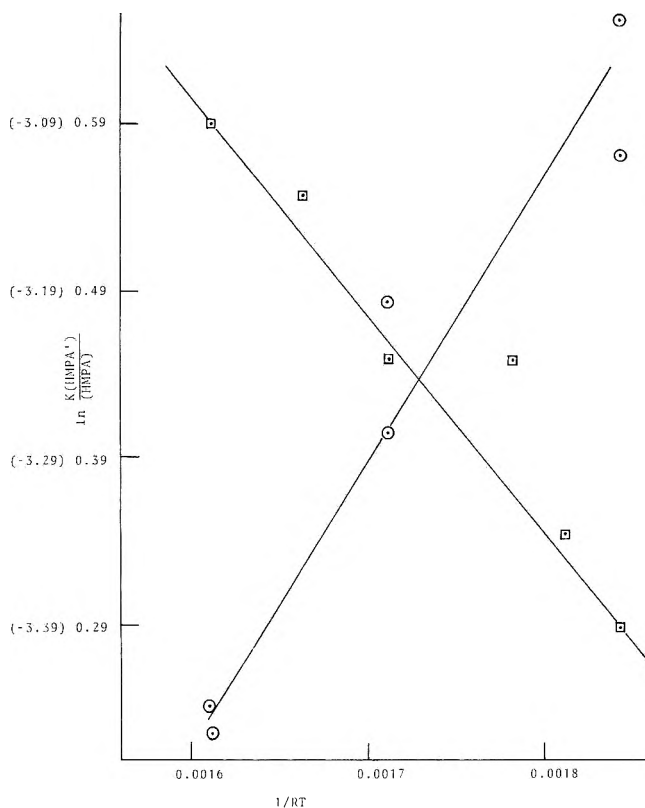


Figure 1. Modified van't Hoff plot for the systems $\text{PhNO}_2\text{-HMPA-M}^+$. For the Li system the numbers are given in parentheses and the plot is represented by \square . The line represented by \circ is for the Na system.

TABLE I: Thermodynamic Parameters Controlling Equilibrium 2 for the Systems

Systems	K_{eq} at 25°	ΔH° , kcal/mol	ΔS° , eu
$\text{PhNO}_2\text{-HMPA-Na-CH}_3\text{OH}$	2.0 ± 0.5	-1.9 ± 0.4^b	-5.1
$\text{PhNO}_2\text{-HMPA-Li-CH}_3\text{OH}$	3.5 ± 0.2	1.2 ± 0.2^b	1.6
$\text{PhNO}_2\text{-HMPA-Na-NH}_3$	<i>a</i>	0 ^c	
$\text{PhNO}_2\text{-HMPA-Li-NH}_3$		9.0 ± 2^c	

^a K_{eq} for the systems containing ammonia cannot be determined since it is unknown how many of the three possible protons are interacting with the PhNO_2 anion radical or with the HMPA. ^b The modified Van't Hoff plots for these systems are shown in Figure 1. ^c ΔH° for the systems with added ammonia are taken from a plot of $\ln \{(\bar{A}_N - 8.48) / (\bar{A}_N' - \bar{A}_N)\}$ vs. $1/RT$.

formally free ion due to hydrogen bonding of the acidic protons with the nitro group of the anion radical. However, for the methanol addition no change in the nitrogen splitting for the ion pair (β) is observed. These results are essentially the same as previously reported,³ however, upon quantitative analysis there remains a striking difference.

Utilizing the previously described technique and eq 3,³ the thermodynamic parameters controlling the hydrogen-bond exchange reaction (eq 2) were determined for the systems $\text{PhNO}_2\text{-HMPA-M}^+$ with added methanol and ammonia as proton donors. The results are shown in Table I.

From Figure 1 and Table I it is obvious that equilibrium 2 is very dependent upon the counterion. The same striking effect is observed for the systems containing

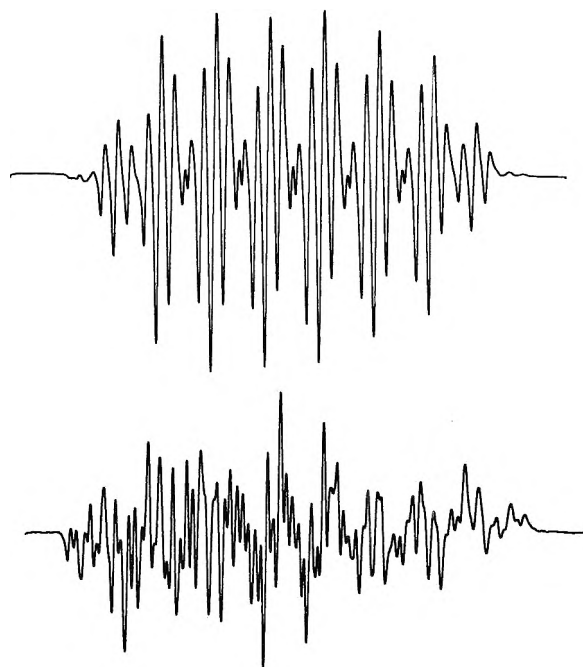
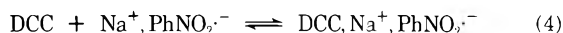


Figure 2. ESR spectra for the system $\text{PhNO}_2\text{-HMPA-Na}$. The lower spectrum is for the system containing 0.01 M NaClO_3 .

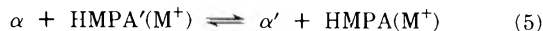
methanol and those containing ammonia. However, for the systems containing ammonia, the thermodynamics are complicated by other factors, which will be discussed later.

There are two possible simple explanations for this metal effect. Either α and/or α' are not completely free of interaction with the counterion, or the counterion is complexing with the HMPA and HMPA' that are involved in equilibrium 2. To check for the former possibility, sodium chlorate was added to the system $\text{PhNO}_2\text{-HMPA-Na}$. The addition of even 1 mg of NaClO_3 resulted in a dramatic increase in the ion pair to "free" ion ratio (Figure 2), but even relatively large concentrations of added Na^+ did not alter the nitrogen coupling constant for α (8.48 G). Further, the addition of dicyclohexyl-18-crown-6-ether (DCC) had no effect upon the coupling constants of either α , β , or the time-averaged species. Both of these experiments supported the original report that α is essentially free of interaction with the counterion.¹

The fact that the coupling constants for β , either A_N or A_{Na} , did not vary with the addition of DCC means that either the DCC cannot compete with the strongly cation solvating HMPA or that the ion pair of PhNO_2 remains intact even though the cation is complexed with the DCC. This latter explanation has been found to be the case for the tetracyanoethylene anion radical in dimethoxyethane,⁴ where the crown ether complexed the potassium cation in the ion pair, but the ion pair remained. For the case of PhNO_2 equilibrium 4 describes the process.



All of this indicates that the effect of the counterion upon the hydrogen bonding exchange equilibrium (eq 3) is due to the complexing of the counterion with the HMPA' and the HMPA that are involved in equilibrium 3. To account for this effect, eq 3 should be written to include this metal perturbation as shown in eq 5.



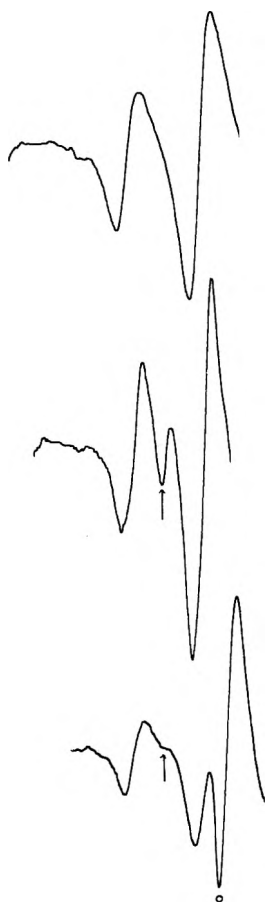


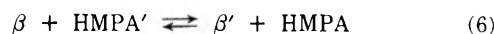
Figure 3. First two lines of the esr spectra due to the ion pair in the system $\text{PhNO}_2\text{-HMPA-Li}$. Top spectrum shows only the first two lines of the ion pair with Li. Middle shows spectrum after NaClO_3 has been added, and an extra line due to the ion pair with Na is observed. Bottom shows spectrum after methanol has been added (0.3 M) to the same solution, and the line due to the ion pair with Na has practically disappeared. The line marked O is the first line of the hydrogen bonded ion, which is shifted over due to the added methanol. The arrows indicate the lines due to the sodium ion pair.

To confirm the fact that there is a strong interaction between the cation and the hydrogen-bonded HMPA, sodium chlorate was added to the system $\text{PhNO}_2\text{-HMPA-Li}$ containing both α and β . The esr spectrum of this resulting solution indicated the presence of the "free" ion and two ion pairs. One of the ion pairs is due to the interaction with the sodium cation and one is due to the interaction with the lithium cation, Figure 3. Addition of methanol (0.3 M) to this solution containing both ion pairs resulted in the complete disappearance of the sodium ion paired species, Figure 3.

All of this leads us to conclude that α is free of interaction with the counterion and that the HMPA' and HMPA that are involved in equilibrium 5 are complexed with the alkali metal cation. Similar dependence upon the cation is observed for the systems $\text{PhNO}_2\text{-HMPA-M}^+$ with added ammonia. For these systems, however, the nitrogen coupling constant for the ion pair does not remain constant with addition of the ammonia. This indicates that the ammonia not only interacts with the "free" ion, but also forms a hydrogen bond with the ion pair resulting in the formation of a hydrogen bonded ion pair (β'). In fact the interaction of the ammonia with β is stronger than that with α as evidenced by the fact that the plot of the

hydrogen-bonded "free" ion over the hydrogen-bonded ion pair concentration *vs.* the NH_3 concentration has a negative slope for the systems $\text{PhNO}_2\text{-HMPA-Li}$ and -Na . This is in direct contrast with these same systems when methanol is acting as the hydrogen-bonding donor, where the slope is positive, and A_N for the ion pair is independent of the proton donor concentration.³ The only way a negative slope for this plot and the dependence of A_N for the ion pair upon the NH_3 concentration can be interpreted is to assume an exothermic interaction between the NH_3 and the ion pair to form the hydrogen-bonded ion pair (β').

Small additions of NH_3 to the $\text{PhNO}_2\text{-HMPA-M}^+$ systems results first in small increases in A_N due to the ion pair. At about 0.3 M NH_3 , A_N decreases and reaches a minimum at about 0.6 M NH_3 . It is interesting to note that A_N at this minimum is less than that for the ion pair in pure HMPA. As the concentration of the ammonia further increases A_N increases to approach its value in pure ammonia (10.9 G at room temperature). These results are nicely explained by the formation of the hydrogen-bonded ion pair and gradual increasing of the hydrogen bonding and simultaneous receding of the cation. At very low concentrations of NH_3 hydrogen bonding of the ion pair complements the cation in pulling charge and spin to the NO_2 group. With further increases in the NH_3 concentration, the cation becomes displaced by the ammonia and a decrease in A_N is noted. As the cation migrates further from the electronegative center, it is replaced by stronger interactions with the ammonia, and A_N again increases. Equation 6 accounts for the formation of the hydrogen bonded ion pair.



It has been previously reported that at lower temperatures and/or at higher concentrations of proton donor, the time-averaged spectra of α and α' exhibit line width alternation.⁵ If eq 7 is valid, line width alternation of the ion pair spectra is expected at higher concentrations of ammonia. This is exactly what is observed experimentally. At higher concentrations of ammonia and/or lower temperatures, pronounced line width alternation of the esr spectra due to the ion pair is observed. This is due to the rapid formation and breaking of the hydrogen bond to the ion pair.

Further additions of ammonia lead to further increases in the concentration of β' and the loss of a detectible concentration of α' . At very high concentrations of NH_3 (*ca.* 0.9 M), the line width alternation becomes less evident due to the displacement of equilibrium 6 far to the right. At the same time, the metal splitting for the sodium cation falls to zero. At 100% ammonia a single anion remains due to a strongly hydrogen-bonded PhNO_2 anion radical, which exhibits weak line width alternation as previously reported.^{1,5} It is interesting to note that this radical in 100% NH_3 results from the ion paired species in HMPA as ammonia is added.

The lack of formation of the hydrogen-bonded ion pairs from alcohol or water proton donors, despite the fact that β has a more highly negative nitro group than does α due to the presence of the cation, is due to the fact that the ion pair (β) is too highly complexed with the cation to allow the interference of the proton donor. The ammonia molecule hydrogen bonds to this NO_2 group and at the same time complexes with the metal cation to further stabilize the hydrogen-bonded ion pair as shown in I. This



conclusion is further supported by the earlier observation that there is close association between the hydrogen-bonded HMPA and the cation. A similar association is observed here with the ammonia HMPA complex and the cation involved in ion pairing.

Acknowledgment. The authors are grateful to the Research Corporation for the support of this work.

References and Notes

- (1) G. R. Stevenson, L. Echegoyen, and L. R. Lizardi, *J. Phys. Chem.*, **76**, 1439 (1972).
- (2) (a) G. R. Stevenson, L. Echegoyen, and L. R. Lizardi, *J. Phys. Chem.*, **76**, 2058; (b) G. R. Stevenson, and L. Echegoyen, *ibid.*, in press.
- (3) G. R. Stevenson and H. Hidalgo, *J. Phys. Chem.*, **77**, 1027 (1973).
- (4) M. T. Watts, M. L. Lu, and M. P. Eastman, *J. Phys. Chem.*, **77**, 625 (1973).
- (5) F. J. Smentowski and G. R. Stevenson, *J. Amer. Chem. Soc.*, **90**, 4661 (1968).

New Aromatic Anions. IX. Anion Radicals of the Monocyclic Oxocarbons¹

Elizabeth V. Patton and Robert West*

Department of Chemistry, University of Wisconsin, Madison, Wisconsin 53706 (Received June 27, 1973)

Publication costs assisted by the National Science Foundation

Electrolytic oxidation of bis(triphenylphosphine)iminium salts of squarate, croconate, and rhodizonate anions in dichloromethane gives electron spin resonance spectra attributed to $C_4O_4\cdot^-$, $C_5O_5\cdot^-$, and $C_6O_6\cdot^-$, respectively. Electrolytic reduction of the same species gave a radical only for rhodizonate, believed to be $C_6O_6\cdot^-$. A ^{13}C hyperfine splitting constant of 4.10 G was found for $C_5O_5\cdot^-$. The implications of this value, and of the g values for all the radicals, for electron distribution in these species is discussed.

The properties of the monocyclic aromatic anions, $C_nO_n^{m-}$, have been studied in some detail over the past 10 years.² Four members of the series are known. The dianions with $n = 4$ (squarate), $n = 5$ (croconate), and $n = 6$ (rhodizonate) are all extremely weak bases which form very stable, high-melting salts. The tetraanion $C_6O_6^{4-}$ has also been isolated as the tetrapotassium salt,³ but it is much more reactive, undergoing rapid oxidation in air.

The existence of intermediate one-electron oxidation and reduction products of the oxocarbon dianions has been predicted.² These radicals could be stabilized by electron delocalization in the same way as the parent dianions. Two groups have reported tentative evidence for the existence of oxocarbon anion radicals in the solid state. Air oxidation of the tetrapotassium salt of $C_6O_6^{4-}$, which leads ultimately to $C_6O_6^{2-}$, produces an intermediate paramagnetic solid surmised to be $C_6O_6\cdot^{3-}$.³ Also, Büchner and Lucken treated potassium metal with carbon monoxide at 250° and obtained a mixture of products containing a radical giving a single-line esr spectrum.⁴ This was attributed to the species $C_6O_6\cdot^{5-}$.

We wish to report the generation of oxocarbon anion radicals in solution by electrolytic oxidation or reduction of oxocarbon salts in dichloromethane at -85° . Repeated attempts to obtain esr signals of oxocarbon anion radicals upon electrolytic oxidation or reduction in aqueous solution were uniformly unsuccessful. We then wished to study oxocarbon anions in nonaqueous solvents, in which temperatures low enough to stabilize the radicals might be possible. Most oxocarbon salts are highly insoluble in solvents other than water, or water-alcohol mixtures, and it proved quite difficult to find oxocarbon salts with sufficient solubility in nonhydroxylic solvents. Ultimately, however, salts of the oxocarbon dianions with bis(triphenylphosphine)iminium cation⁵ were prepared and found to be soluble in organic solvents.

Upon electrolytic oxidation, the squarate, croconate, and rhodizonate salts all formed radicals giving single-line electron spin resonance spectra which we attribute to $C_4O_4\cdot^-$, $C_5O_5\cdot^-$, and $C_6O_6\cdot^-$, respectively. Confirmation of this assignment for $C_5O_5\cdot^-$ is given by the observation of ^{13}C sidebands with a hyperfine splitting of 4.10

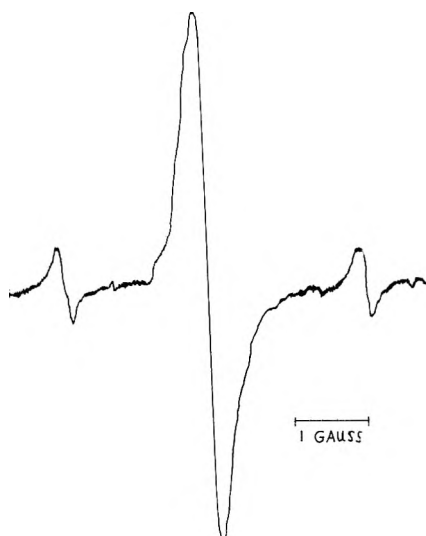
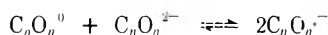


Figure 1. ESR spectrum of $C_5O_5^{\cdot-}$ radical obtained by oxidation of bis(triphenylphosphine)iminium croconate, showing sidebands attributed to hyperfine splitting by ^{13}C .

G (Figure 1). The area under each sideband was $2.5 \pm 0.5\%$ of the area under the central peak; for a species with electron delocalization over five equivalent carbon atoms, the sideband intensities are predicted to be 2.9%.

The species produced by oxidation of $C_4O_4^{2-}$ and $C_6O_6^{2-}$ gave only singlets. These oxidations were repeated many times under slightly different conditions but ^{13}C sidebands were never observed. It is curious that ^{13}C hyperfine splitting could be detected only for $C_5O_5^{\cdot-}$, and the reasons are not fully understood. It is possible that the anion radicals are in equilibrium with the two-electron oxidation product and the dianion



or electron exchange may take place between the anion radical and the unoxidized dianion present in the solution. Either exchange process, if rapid, would destroy the ^{13}C sidebands. Apparently whatever processes are averaging ^{13}C sidebands for $C_4O_4^{\cdot-}$ and $C_6O_6^{\cdot-}$ are slow for $C_5O_5^{\cdot-}$.

The ^{13}C coupling found from the sidebands of the $C_5O_5^{\cdot-}$ spectrum allows estimation of the spin density distribution in the radical. Using the σ - π polarization constants of Karplus and Fraenkel,⁶ the theoretical equation for the coupling constant may be written

$$a_C = 16.1\rho_{C'} - 13.9(\rho_{C'} + \rho_{C''}) + Q_{CO}^C\rho_{C'} + Q_{OC}^C\rho_O^{\cdot}$$

where C' and C'' are the carbons attached to the one in question. In this case, all of the carbons are equivalent, and $\rho_{C'} = \rho_{C''} = \rho_C$. Broze and Luz⁷ have measured values of Q_{CO}^C and Q_{OC}^C from a large number of carbonyl radicals and found the best values to be $Q_{CO}^C = 36.0$ G and $Q_{OC}^C = -24.3$ G. Substituting these in the above equation, an a_C of 4.10 G predicts $\Sigma\rho_C = 0.92$, $\Sigma\rho_O = 0.08$; an a_C of -4.10 G gives $\Sigma\rho_C = 0.08$, $\Sigma\rho_O = 0.92$.

Hückel molecular orbital calculations⁸ predict $\Sigma\rho_C = 0.24$ and $\Sigma\rho_O = 0.76$. Maclachlan calculations, which add a small perturbation to HMO's to take into account the effect of the spin of the unpaired electron on the energy of electrons of like spin, were also carried out.⁸ These predict a total spin density on oxygen of 0.90, quite consistent with the experimental result of $a_C = -4.10$. The ^{13}C peaks show no measurable difference in broadness so the sign of the coupling cannot be determined empirically.

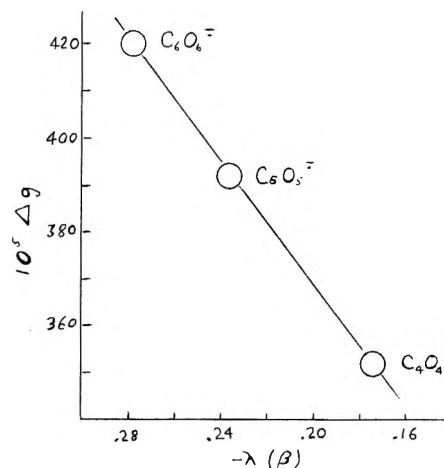


Figure 2. Differences in g value vs. λ (in units of β) for oxocarbon monoanion radicals.

TABLE I: g Values and HMO Unpaired Electron Energy Levels

Radical	g value	$\Sigma\rho_O$ (Mac-HMO) ^a	λ (Mac-HMO)
$C_4O_4^{\cdot-}$	2.00584	0.900	-0.174 β
$C_5O_5^{\cdot-}$	2.00624	0.898	-0.236 β
$C_6O_6^{\cdot-}$	2.00652	0.895	-0.278 β
$C_6O_6^{\cdot 3-}$	2.00457	0.671	-0.529 β

^a Reference 8.

Attempts were made to reduce all three oxocarbon anions electrolytically. An electron spin resonance signal was obtained only for $C_6O_6^{2-}$; it was again a simple singlet with no sidebands, probably due to $C_6O_6^{3-}$. No signals were observed from the reduction of $C_4O_4^{2-}$ or $C_5O_5^{2-}$. The energy levels which would contain the unpaired electrons for the trianion radicals $C_4O_4^{\cdot 3-}$ and $C_5O_5^{\cdot 3-}$ are predicted, in HMO calculations,^{8,9} to be much higher than that for $C_6O_6^{3-}$.

The g values measured for the four radicals are listed in Table I. The shift from the value for a free electron, 2.00232, is caused by coupling of the electron spin to the angular momenta of the nuclei in the molecule. This shift is expressed semiempirically by Stone's relationship¹⁰

$$\Delta g = \sum_n \rho_n (b_n + \lambda c_n)$$

in which n is the index for the nucleus in the radical, λ is the energy level, in β units, of the orbital containing the unpaired electron, and b and c are empirical constants related to the magnitude of spin-orbit coupling between the electron and n . For radicals which contain oxygen and carbon nuclei, Δg is found to be mainly a function of the spin density on oxygen, since the spin orbit coupling constant for oxygen is much larger than that for carbon.¹¹

Values of λ and $\Sigma\rho_O$ for each radical, predicted by the Maclachlan calculations, are given in Table I. The last two electrons of the ground-state dianions are slightly antibonding,^{8,9} thus λ values for the unpaired electrons in the oxidation products, as well as the reduction product, are negative. A plot of Δg vs. λ for the monoanions is presented in Figure 2. The plot is linear, with $b = 0.0026$ and $c = -0.0072$. Δg for the $C_6O_6^{\cdot 3-}$ radical does not lie on this line, probably because the unpaired electron is in a doubly degenerate energy level, subject to Jahn-Teller distortions from planarity.

Experimental Section

Synthesis of Bis(triphenylphosphine)iminium Salts. The bis(triphenylphosphine)iminium salts were prepared by combination of 5:1 molar ratios of the sodium or potassium oxocarbon salt and triphenylphosphineiminium chloride, respectively. These were dissolved separately in boiling water and combined. The product precipitated immediately upon mixing of the two solutions, and was recrystallized from CH_2Cl_2 and dried under vacuum. (It was necessary in the case of the rhodizonate anion to carry out the reaction and filtration quickly to prevent oxidative decarboxylation to croconate anion.)

$2[(\text{C}_6\text{H}_5)_3\text{P}]_2\text{N}^+ \text{C}_4\text{O}_4^{2-} \cdot 2\text{H}_2\text{O}$. Electronic spectrum (CH_2Cl_2): λ_{max} 275 nm (ϵ 2.8×10^4), 268 nm (2.9×10^4). *Anal.* Calcd for $[(\text{Ph}_3\text{P})_2\text{N}]_2\text{C}_4\text{O}_4 \cdot 2\text{H}_2\text{O}$: C, 74.50; H, 5.26; P, 10.11; N, 2.29; O, 7.38. Found: C, 74.37; H, 5.11; P, 10.30; N, 2.42; O, 7.58.

$2[(\text{C}_6\text{H}_5)_3\text{P}]_2\text{N}^+ \text{C}_5\text{O}_5^{2-}$. Electronic spectrum (CH_2Cl_2): λ_{max} 373 nm (ϵ 3.5×10^4), 275 nm (1.0×10^4), 268 nm (1.3×10^4), 262 nm (1.1×10^4). *Anal.* Calcd: C, 75.8; H, 5.0; P, 10.8; N, 2.3. Found: C, 75.8; H, 5.1; P, 10.3; N, 2.6.

$2[(\text{C}_6\text{H}_5)_3\text{P}]_2\text{N}^+ \text{C}_6\text{O}_6^{2-}$. Electronic spectrum (CH_2Cl_2): λ_{max} 487 (ϵ 4.0×10^4), 275 nm (1.0×10^4), 268 nm (1.3×10^4), 262 nm (1.1×10^4). *Anal.* Calcd: C, 75.2; H, 4.9; P, 9.9; N, 2.2. Found: C, 75.0; H, 5.0; P, 9.9; N, 2.4.

Electrolytic Oxidation and Reduction. Solutions in dichloromethane were made up to be approximately 0.001 M in sample and 0.01 M in tetra-*n*-butylammonium perchlorate, used as a supporting electrolyte. The electrolytic cells, sample preparation, and apparatus have been described elsewhere.¹²⁻¹³ Electrolysis was performed at the lowest potential necessary for passage of current through

the cell. On oxidation the $\text{C}_n\text{O}_n \cdot^-$ radicals appeared at a potential of about 5 V with a current of 0.3 μA . The signals were stable to -60° , but slowly decreased in intensity at higher temperatures. *g* values were measured with a dual cavity using peroxyamine disulfonate anion ($g = 2.00550 \pm 0.0001$) as a reference.¹⁴

Acknowledgment. This work was partially supported by a grant from the National Science Foundation. We are indebted to Professor John Ruff for suggesting the preparation of bis(triphenylphosphine)iminium salts of the oxocarbon anions.

References and Notes

- (1) Previous paper in this series: E. Patton and R. West, *J. Phys. Chem.*, **74**, 2512 (1970).
- (2) For reviews, see R. West and J. Niu in "Non-Benzenoid Aromatic Compounds," Vol. 1, J. Snyder, Ed., Academic Press, New York, N. Y., 1969, p 312; R. West and J. Niu in "The Chemistry of the Carbonyl Group," Vol. 11, J. Zabicky, Ed., Interscience, New York, N. Y., 1970, pp 241-275.
- (3) R. West and H. Y. Niu, *J. Amer. Chem. Soc.*, **84**, 1324 (1962).
- (4) W. Buchner and E. A. C. Lucken, *Helv. Chim. Acta*, **47**, 2113 (1964).
- (5) R. Appel and A. Huass, *Z. Anorg. Allg. Chem.*, **311**, 290 (1961); J. K. Ruff, *Inorg. Chem.*, **6**, 2080 (1967).
- (6) M. Karplus and G. K. Fraenkel, *J. Chem. Phys.*, **35**, 1312 (1961).
- (7) M. Broze and Z. Luz, *J. Chem. Phys.*, **51**, 749 (1969).
- (8) E. V. Patton, Ph.D. Thesis, University of Wisconsin, 1971. These calculations used $h_0 = 0.3$, $k_{\text{CO}} = 1.4$. Maclachlan calculations were carried out with the same h_0 and k_{CO} parameters, and an adjustable parameter, λ , of 1.0. For earlier Hückel MO studies see N. C. Baenziger and J. J. Heigenbarth, *J. Amer. Chem. Soc.*, **86**, 3250 (1964); R. West and D. L. Powell, *ibid.*, **85**, 2577 (1963).
- (9) K. Sakamoto and Y. I. l'Haya, *Bull. Chem. Soc. Jap.*, **44**, 1201 (1971).
- (10) A. J. Stone, *Mol. Phys.*, **6**, 509 (1963).
- (11) B. G. Segal, M. Kaplan, and G. K. Fraenkel, *J. Chem. Phys.*, **43**, 4171 (1965).
- (12) E. Carberry, R. West, and G. E. Glass, *J. Amer. Chem. Soc.*, **91**, 5446 (1969).
- (13) G. E. Glass and R. West, *Inorg. Chem.*, **11**, 2847 (1972).
- (14) M. K. Carter and G. Vincow, *J. Chem. Phys.*, **47**, 292 (1967).

Raman Spectra of Thorium(IV) Fluoride Complex Ions in Fluoride Melts¹

L. M. Toth* and G. E. Boyd

Oak Ridge National Laboratory, Oak Ridge, Tennessee 37830 (Received July 11, 1973)

Publication costs assisted by the Oak Ridge National Laboratory

Raman spectra of LiF-NaF-ThF₄ mixtures at 650° have been examined to establish the coordination behavior of Th(IV) in molten fluorides. Eight coordinated Th(IV) has been identified in melts with excess fluoride ion by comparing their spectra with that of crystalline K₅ThF₉. Seven coordinated Th(IV), present in fluoride ion deficient melts, was identified by shifts in the frequency of ν_1 with melt composition changes. These results are compared with previous coordination studies of U(IV) and Zr(IV).

Introduction

The presence of either alkaline earth or transition metal complex ions in molten salts frequently has been inferred from Raman spectral measurements. However, there has been little attempt to compare the spectra of various cat-

ions which are expected to have similar coordination geometries in the liquid state. The ions, Th(IV), U(IV), and Zr(IV), have been regarded as structurally similar in molten salts because they form many analogous crystalline compounds. A consequence of considering these ions as similar in molten salt solutions is that their thermody-

dynamic activity coefficients are also presumed to be the same, principally because there are no data by which to distinguish these ions. Therefore an indication of structural differences in the complex ions which these three cations form would exemplify the limitations in the above thermodynamic approximations.

We have recently reported² that the coordination behavior of Zr(IV) in molten alkali-metal fluorides varies from eight to less than six. In contrast, we have shown by absorption spectroscopy³ that U(IV) exists as either seven- or eight-coordinated complexes in molten LiF–BeF₂ solutions depending on the free fluoride ion concentration of the system. These two different sets of measurements suggest that the coordination behavior of U(IV) and Zr(IV) are not similar as had been anticipated or that the two experimental methods were not corroborative. The absorption spectral measurements were most ideally suited for U(IV) solutions which absorb in the visible while the transparent solutions of Zr(IV) were more suited to Raman spectral measurements. Th(IV) in molten fluoride was studied in this research in an attempt to resolve the apparent difference in the coordination chemistry of U(IV) and Zr(IV). Raman spectroscopy was employed because the solutions of Th(IV) in fluoride melts are transparent.

The coordination numbers of the Th(IV) species present in the molten state were identified by comparison with crystalline spectra when it was possible to legitimately do so. However, when this method failed, it was necessary to turn to identification based on frequency shifts in the spectra with changes in solvent composition. The results of these measurements are compared with the previous data for U(IV) and Zr(IV).

Experimental Section

The experimental procedure used here has been described previously in detail.^{2,4} In brief, the molten fluorides were contained in a nickel windowless cell sealed in a quartz capsule, and their spectra were measured with a Jarrell-Ash 25-300 Raman spectrometer using the 4880-Å line of a Coherent Radiation Model 52B argon-ion laser operating at 1.0 W output power for excitation.

The fluoride salts were prepared from laboratory reagents which were purified by sparging the molten mixtures with HF + H₂ gas to remove oxide impurities. Subsequent handling of the purified salts was performed in a helium-filled glove box of less than 1 ppm O₂ and H₂O content. Ternary mixtures of LiF–NaF–ThF₄ were employed because they melted at lower temperatures throughout the range of ThF₄ concentrations studied than did simple binary mixtures of alkali-metal fluoride and ThF₄.⁵

Raman spectra of LiF–NaF–ThF₄ melts were measured at constant temperature as a function of the ThF₄ concentration. The ThF₄ composition was varied from 14 to 40 mol % while the LiF/NaF mole ratio was held fixed at 0.87. This method of varying the melt composition may be visualized by considering a ternary phase diagram illustrated as an equilateral triangle with each corner occupied by a pure component. The composition change is then described as moving along a line drawn from the ThF₄ corner of the triangle to a point on the opposite edge corresponding to the LiF/NaF ratio chosen.⁵ A constant LiF/NaF ratio was maintained to minimize the complications in interpreting the melt spectra which arise from changes in the alkali-metal ion.

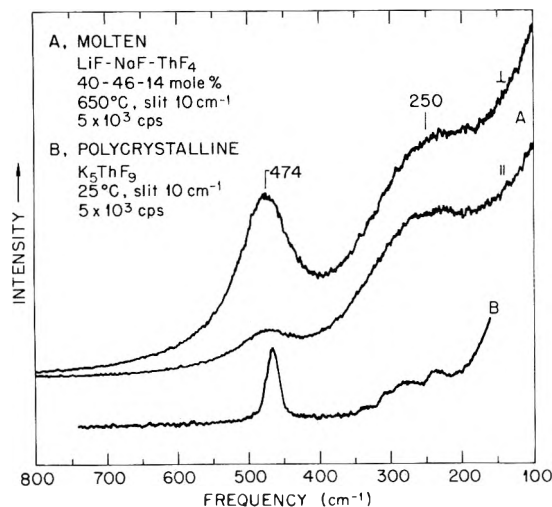


Figure 1. Raman spectra of (A) molten LiF–NaF–ThF₄ (40–46–14 mol %) at 650° under perpendicular and parallel polarizations of incident beam and (B) polycrystalline K₅ThF₉ at 25°.

Results and Discussion

The Raman spectrum of 14 mol % ThF₄ in LiF–NaF (40–46 mol %) at 650° is shown in Figure 1, curve A, where the polarization of the incident beam is indicated as perpendicular or parallel to the plane defined by the incident beam and the direction of the scattered light. Two broad bands are evident, a strong polarized band at 474 cm⁻¹ assigned to the symmetric stretch of ThF_x^{4-x} and a depolarized band centered at 250 cm⁻¹. Under parallel polarization and resulting decrease in the Raleigh wing, two components at ca. 270 and 225 cm⁻¹ are indicated within the broad depolarized band profile. Furthermore, if the spectrum in Figure 1 is compared with that of 14 mol % ZrF₄ in LiF–NaF (40–46 mol %) shown in Figure 2 of ref 2, a remarkable similarity in the two spectra can be noted. By analogy with the ZrF₄ melt spectrum, an additional band would be suggested in the ThF₄ spectrum on the high-frequency side of the 250-cm⁻¹ band. The band was observed in the ZrF₄ melt because it disappeared when the melt composition was changed. However, in the case of the ThF₄ melts, increasing the ThF₄ content did not have as pronounced an effect. As shown in Figure 2, the depolarized band for various concentrations of Th(IV) in LiF–NaF mixtures only decreased in intensity and shifted from 250 (curve A) to 280 cm⁻¹ (curve D).

Increases in the ThF₄ concentration produced limited shifts in the frequency of the polarized band at 474 cm⁻¹ (which is also in contrast to that seen for the ZrF₄ system²). The position of the band remained fixed for composition changes from 14 to 20 mol %, increased to 478 cm⁻¹ in going from 20 to 25 mol %, and then showed no change for subsequent additions of ThF₄ (see Figure 3). These experimental observations are compared in Table I with those for similar ZrF₄ melts in both the polarized and the depolarized regions of the ThF₄ and ZrF₄ spectra. The comparison is intended to suggest that up to a point, namely, 25 mol % ThF₄ and ZrF₄, the behavior of the two is the same. The changes in the ThF₄ and ZrF₄ melt spectra for this composition range are interpreted as due to a transition from an eight- to a seven-coordinated complex in solution. The melt composition at which the polarized band frequency begins to increase (*viz.*, 20 mol %) supports the identification that the higher coordinated species is eight. Furthermore, the spectrum of polycrystal-

TABLE I: Comparison between ThF_4 and ZrF_4 in LiF-NaF Melts at 650° where LiF-NaF Mole Ratio is Constant at $0.87/1.0^a$

Frequency position of	Polarized region	Depolarized region	Interpretation (suggested presence of)
ThF ₄ melt	(1a) At 474 cm^{-1} for 14 mol % ThF ₄ (1b) Does not shift for 14–20 mol % ThF ₄	(1) Broad band seen at 250 cm^{-1} for 14–20 mol % ThF ₄ . By comparison with spectrum of ZrF ₄ , a shoulder at ca. 300 cm^{-1} is suggested	ThF ₈ ⁴⁻
	(2) Shifts to 478 cm^{-1} for 25 mol % ThF ₄	(2) Increasing ThF ₄ content from 20 to 40 mol % only produces a gradual decrease in intensity	ThF ₇ ³⁻
	(3) Does not change for 25–40 mol % ThF ₄		Fluoride bridging
ZrF ₄ melt	(1a) At 555 cm^{-1} for 14 mol % ZrF ₄ (1b) Does not shift for 14–20 mol % ZrF ₄	(1) Broad band seen at 250 cm^{-1} for 14–20 mol % ZrF ₄ . By comparison with 33 mol % ZrF ₄ spectrum, a shoulder at 322 cm^{-1} is also present	ZrF ₈ ⁴⁻
	(2) Shifts to 568 cm^{-1} for 25 mol % ZrF ₄		ZrF ₇ ³⁻
	(3a) Shifts to 577 cm^{-1} for 33 mol % ZrF ₄	(2) Band at 322 cm^{-1} disappears. Spectrum matches that of Li_2ZrF_6	ZrF ₆ ²⁻
	(3b) Shifts continuously to higher values for 25–40 mol % ZrF ₄	(3) Further increases up to 40 mol % cause appearance of band at 165 cm^{-1}	ZrF ₅ ⁻ or ZrF ₄

^a ZrF₄ melt data taken from ref 2.

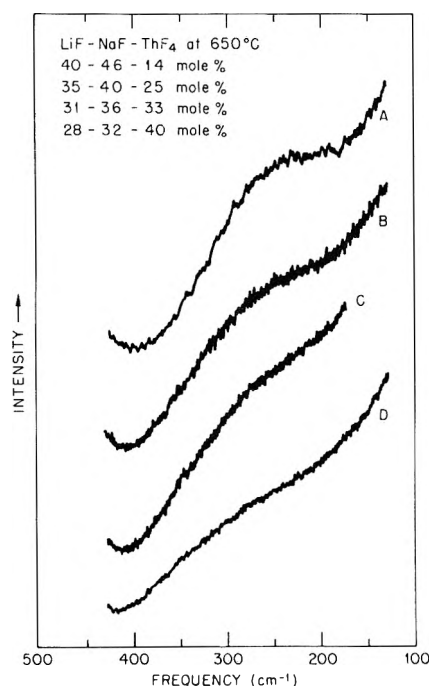


Figure 2. Raman spectra of $100\text{--}400\text{-cm}^{-1}$ region at 650° of LiF-NaF-ThF_4 melts with the above indicated compositions (slit = 10 cm^{-1} , 5×10^3 counts per second, cps).

line K_5ThF_9 (cf., curve B, Figure 1), which contains discrete ThF_8^{4-} groups (the ninth fluorine atom displaced 4.53 \AA from the nearest thorium atom⁶), also supports the identification of the ThF_8^{4-} complex in the melts with 14–20 mol % ThF_4 . The bands at approximately 270 and 225 cm^{-1} in the melt can be identified with corresponding bands in K_5ThF_9 at 280 and 235 cm^{-1} , and the shoulder in the melt spectrum at ca. 300 cm^{-1} is identified with the additional weaker bands in the spectrum of K_5ThF_9 at 310 and 338 cm^{-1} . The displacement of the strong band at 474 cm^{-1} in the melt relative to that in K_5ThF_9 at 467 cm^{-1} is attributed to the difference in the alkali-metal cations which alter the strengths of the repulsive

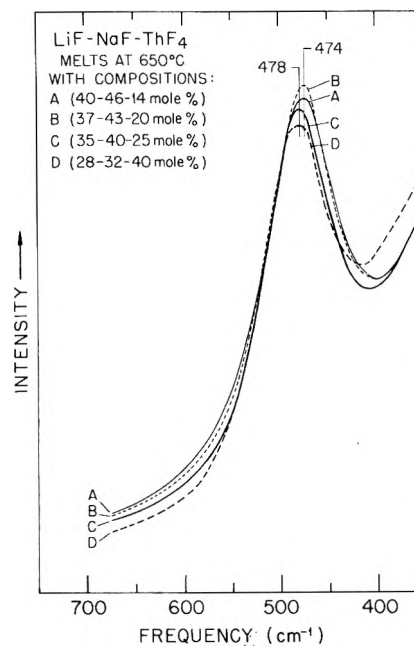


Figure 3. Raman spectra band profiles in the region $400\text{--}700\text{ cm}^{-1}$ of LiF-NaF-ThF_4 melts at 650° with the compositions as indicated (slit = 10 cm^{-1} , 5×10^3 cps).

forces between nonbonded fluoride ions (i.e., fluoride ions on neighboring ThF_x^{4-x} groups). This arises because the smaller alkali-metal ion, Li^+ , allows closer approach of the neighboring ThF_x^{4-x} groups. Despite these expected differences, the close similarity in the spectra of the polycrystalline K_5ThF_9 and the 14 mol % ThF_4 melt supports the identification of ThF_8^{4-} ion as the highest coordinated species in the molten state.

When the ThF_4 content in the melt is increased, the position of the symmetric stretching frequency increases the same as in the ZrF_4 melts; but for ThF_4 melts, the upward shift stops at 478 cm^{-1} for 25 mol % and shifts no more for further increases in the ThF_4 content. The spectrum at 33 mol % ThF_4 is not appreciably different from that at 25 mol %. It is not similar to the 33 mol % ZrF_4

melt spectrum which was identified as arising from a ZrF_6^{2-} species. Therefore, the lowest coordination number in the ThF_4 melts is established as seven because the shift in the polarized band stops at 25 mol % ThF_4 and the entire spectrum never does correspond to one which can be identified with ThF_6^{2-} (by analogy to the ZrF_6^{2-} melt spectrum).

If the minimum coordination number in ThF_4 melts is seven, then melts of ThF_4 composition greater than 25 mol % must share fluoride ions (*i.e.*, form bridging links between neighboring thorium ions) to maintain that coordination number. However no spectral evidence for fluoride bridging is observed. Bridging is expected to cause a progressive decrease in the symmetric stretching frequency position arising from the decreases in the bond order and the consequent decrease in the force field associated with a particular bond. Still, the degree of bridging must be greatly limited even at 40 mol % ThF_4 (*e.g.*, from the melt stoichiometry, an average of three bonds are bridged if the minimum coordination number is seven) and perhaps for this reason is not observed. The same is found in the ZrF_4 melt case; there is no spectral evidence for the bridging which must occur in melts of high ZrF_4 composition if the proposed coordination complexes are present.

As a result of these measurements, it is now possible to explain the previous experiments and the dissimilarities of the three ions of Th(IV), Zr(IV), and U(IV), in molten fluoride solutions. The Raman experiments with ThF_4 melts have proved to be consistent with those of the visible-uv spectral results for U(IV), *i.e.*, there is an equilibrium between seven- and eight-coordinated species which is dependent upon the melt composition. Six coordination, or lower, does not occur for either Th(IV) or U(IV) in fluo-

ride melts. These results show that it was not the different experimental approaches which were responsible for the difference in the results for the three cations, but rather, the nature of the ions themselves.

Zirconium behaves much like Th(IV) and U(IV) in melts with excess fluoride ion concentration because it, too, manifests a seven-eight coordination equilibrium in the same melt composition limits. However, Zr(IV) is unique in that coordination numbers lower than seven also occur, especially the octahedral six coordination for which there is strong evidence. Lower coordination numbers are possible for Zr(IV) melts undoubtedly because Zr(IV) has a much smaller ionic radius and therefore can accommodate fewer fluoride ions with little decrease in the stability of the complex ion. An analogous behavior occurs in crystals; no six-coordinated Th(IV) or U(IV) inorganic crystalline fluoride salts are known, whereas six-coordinated Zr(IV) fluorides are readily obtainable.⁷

References and Notes

- (1) Research sponsored by the Oak Ridge National Laboratory operated by the Union Carbide Corporation.
- (2) L. M. Toth, A. S. Quist, and G. E. Boyd, *J. Phys. Chem.*, **77**, 1384 (1973).
- (3) L. M. Toth, *J. Phys. Chem.*, **75**, 631 (1971).
- (4) A. S. Quist, J. B. Bates, and G. E. Boyd, *J. Chem. Phys.*, **54**, 4896 (1971).
- (5) The phase diagram for the LiF-NaF-ThF system has never been reported. However the analogous LiF-NaF-UF₄ system was used from R. E. Thoma, H. Insley, B. S. Landau, H. A. Friedman, and W. R. Grimes, *J. Amer. Ceram. Soc.*, **42**, 22 (1959).
- (6) R. R. Ryan and R. A. Penneman, *Acta Crystallogr., Sect. B*, **27**, 829 (1971).
- (7) R. A. Penneman and R. R. Ryan, "Structural Systematics in Actinide Fluoride Complexes," in "Structure and Bonding," Vol. 13, Springer-Verlag, New York, N. Y., 1973.

Vibrational Transitions in Anharmonic Oscillators^{1a}

Hyung Kyu Shin

Department of Chemistry,^{1b} University of Nevada, Reno, Nevada 89507 (Received July 5, 1973)

Publication costs assisted by the U. S. Air Force Office of Scientific Research

The $0 \rightarrow 1$ vibrational transition probability of an anharmonic oscillator, P_{01} , has been formulated using the potential function which is a sum of quadratic and cubic terms in the vibrational coordinate. The potential fits the Morse function closely in the region of interatomic distance where the first two energy levels of the anharmonic oscillator lie. For small energy transfer ($\epsilon \ll 1$), P_{01} is larger than the harmonic oscillator probability, P_{01}^* , by a constant factor. For large energy transfer, the difference between P_{01} and P_{01}^* varies with ϵ . It is shown that P_{01} is always larger than P_{01}^* . In HF, $P_{01}/P_{01}^* = 1.094$ for $\epsilon < 0.1$. Above this amount of energy transfer, P_{01}/P_{01}^* varies with ϵ but the ratio is not greatly different from 1.10.

I. Introduction

One of the simplest and most often encountered dynamical problems is that of a particle in an elastic field of force, corresponding to the one-dimensional harmonic oscillator potential function. The mathematics involved in

the problem is simple, and it is often possible to obtain rigorous solutions. Consequently, the model of harmonic oscillation has been widely applied to the calculation of vibrational energy transfer probabilities in molecular collisions.² The use of the model may be justified for vibrational transitions among low-lying levels of homonuclear

diatomic molecules in which the anharmonicity is not severe.^{2,3a} However, in heteronuclear diatomic molecules, the anharmonicity may become important even for the $0 \rightarrow 1$ transition.^{3b}

The direct use of anharmonic potential energies such as the Morse function in the calculation of vibrational transition probabilities eliminates the problem of anharmonicity,⁴ but the difficulty is that the pertinent equations are now much too complicated to be soluble. Such equations are becoming soluble numerically because of the development of electronic computers, but the numerical result can be obtained only after an extensive use of computers. To determine the effects of anharmonicity on transition probabilities, on the other hand, we can choose an approximate anharmonic potential which is simple enough to allow the analytical solution of the problem, and yet complicated enough to be realistic. Such an analytical solution, even if it is approximate, will yield detailed information on the importance of anharmonicity without the use of sophisticated computing devices.

In the present paper we report the investigation of vibrational transitions in anharmonic oscillators in terms of the oscillator potential energy constructed as a sum of quadratic and cubic terms in the oscillator coordinate. The $0 \rightarrow 1$ vibrational transition probability of the anharmonic oscillator will be obtained in an explicit form showing rigorously how the anharmonicity affects the efficiency of energy transfer. For this purpose, we shall compare the result with that of the $0 \rightarrow 1$ probability of the harmonic oscillator. Application is made to HF; this molecule is chosen because the vibrational energy transfer in the collision systems involving HF is particularly important in the development of chemical lasers.⁵

II. Interaction Energies

Imagine an oscillator (BC) and an incident particle (A, a molecule or an atom) in interaction in a one-dimensional system. Let q be the displacement of the oscillator from its equilibrium position ξ_e (i.e., $q = \xi - \xi_e$) and let x be the distance between the centers of mass of BC and A. We shall express the interaction potential energy for the collinear collision in the form $U(z) = D \exp(-z/a)$, where z is the distance between the nearest atom of BC, say C, and A; D and a are potential constants. This distance is $z = x - \rho(\xi_e + q) \equiv z(x, q)$, where $\rho = m_B/(m_B + m_C)$. Then, we can approximate $U(z)$ as

$$U(x, q) = D' \exp(-x/a) \left(1 + \frac{\rho}{a} q \right) \equiv U(x) - F(x)q \quad (1)$$

where $D' = D \exp(\rho\xi_e/a)$. The second relation defines the perturbing force $F(x) = -(\rho/a)D' \exp(-x/a)$. Since the solution of the classical equation of motion gives $x(t)$, $F(x)$ can be readily transformed into the time-dependent perturbing force $F(t)$. Note that the potential $U(x)$ is a typical intermolecular interaction energy, determining the relative translational motion of the two colliding particles. The collision model is a simplified one, but we shall not attempt to test its accuracy here; studies on such a test can be found elsewhere.^{2,6}

We shall express the intramolecular potential energy of the oscillator BC by

$$U_{BC}(\xi) = \frac{1}{2} M \omega^2 (\xi - \xi_e)^2 + \alpha (\xi - \xi_e)^3 \quad (2)$$

where M and ω are the reduced mass and the angular fre-

quency of the oscillator, and α is the constant which determines the contribution of the cubic term. During the interaction with the incident particle, the anharmonic oscillator is perturbed by the force $F(t)$, so it becomes necessary to know the wave function of the anharmonic oscillator under the influence of $F(t)$. The vibrational transition probability can then be derived from this perturbed wave function.

III. Perturbed Wave Function

To derive vibrational transition probabilities for an anharmonic oscillator for which the intramolecular potential function is given by eq 2 we need to know the vibrational matrix elements of q^3 that are not zero. They are

$$\int_{-\infty}^{\infty} \phi_n(q) q^3 \phi_{n-3}(q) dq = \left(\frac{\hbar}{M\omega} \right)^{3/2} \left[\frac{1}{8} n(n-1)(n-2) \right]^{1/2} \quad (3)$$

$$\int_{-\infty}^{\infty} \phi_n(q) q^3 \phi_{n-1}(q) dq = \left(\frac{\hbar}{M\omega} \right)^{3/2} \left[\frac{9}{8} n^3 \right]^{1/2}$$

where $\phi_n(q)$ is the orthonormal harmonic oscillator wave function. By use of these results, it can be shown that the vibrational wave function for the anharmonic oscillator is^{7,8}

$$\begin{aligned} \psi_n(q) = & \phi_n(q) + \frac{K}{6(2)^{1/2}} \{ [(n+1)(n+2)(n+3)]^{1/2} \phi_{n+3}(q) + q(n+1)^{3/2} \phi_{n+1}(q) - \\ & 9n^{3/2} \phi_{n-1}(q) - [n(n-1)(n-2)]^{1/2} \phi_{n-3}(q) \} \quad (4) \end{aligned}$$

and that the approximate expression for the energy levels is⁹

$$E_n = \hbar\omega \left(n + \frac{1}{2} \right) - \frac{15}{4} \hbar\omega K^2 \left(n^2 + n + \frac{11}{30} \right) \quad (5)$$

where $K = (\alpha/\hbar\omega)(\hbar/M\omega)^{3/2}$. Equation 4 is an unperturbed function, but the interaction with the incident particle A leads to a perturbed system. The wave function describing such a system can be obtained as a sum of the unperturbed wave functions, in which the coefficients are determined from the nature of the perturbation.^{3a} Once this function is at hand, the vibrational transition probability ($k \rightarrow n$) can be readily calculated from

$$P_{kn} = \lim_{t \rightarrow \infty} \left| \int_{-\infty}^{\infty} \psi_n(q) \psi(t, q) dq \right|^2 \quad (6)$$

in which the oscillator is initially in the k th state. The information on the initial state of the oscillator is contained in $\psi(t, q)$. Therefore, the important problem is to find the perturbed wave function $\psi(t, q)$ of the anharmonic oscillator in terms of the harmonic oscillator functions as the basis set; the following material is devoted to this solution.

The Hamiltonian of the harmonic oscillator system perturbed by $-F(t)q$ is

$$\begin{aligned} H = & \frac{P^2}{2M} + \frac{1}{2} M \omega^2 q^2 - F(t)q \quad (7) \\ = & \hbar\omega \left(N + \frac{1}{2} \right) - F(t) \left(\frac{\hbar}{2M\omega} \right)^{1/2} (a + a^*) \end{aligned}$$

In the second relation, we used the phonon creation operator a^* , the destruction operator a , and the eigenvalue operator $N = a^*a$.¹⁰ In the present model the perturbed wave function can be given in the form^{3a,11}

$$\psi(t, q) = e^{-1/2C^2} e^{iCa^*} e^{Ca} \psi_k(q) \quad (8)$$

where

$$C = (2M\hbar\omega)^{-1/2} \left| \int_{-\infty}^t F(t') \exp(i\omega t') dt' \right|^2$$

Therefore, the operators e^{iCa^*} and e^{iCa} transform the unperturbed anharmonic oscillator wave function $\psi_k(q)$ given by eq 4 into the time-dependent perturbed function $\psi(t, q)$. Since $\psi_k(q)$ is a linear combination of $\phi_{k-3}(q)$, $\phi_{k-1}(q)$, $\phi_k(q)$, $\phi_{k+1}(q)$, and ϕ_{k+3} , the product of these perturbation operators acts to make the following transformation

$$[\phi_{k-3}(q), \phi_{k-1}(q), \phi_k(q), \phi_{k+1}(q), \phi_{k+3}(q)] \rightarrow [\phi_0(q), \phi_1(q), \dots, \phi_k(q), \dots]$$

If $\psi_k(q)$ in eq 8 were replaced by the harmonic oscillator wave function $\phi(q)$, the time-dependent function would simply describe the harmonic oscillator perturbed by $-F(t)q$. For the anharmonic oscillator initially in the ground state, the perturbed function is given by

$$\psi(t, q) = e^{-1/2C^2} e^{iCa} e^{iCa^*} \psi_0(q) = e^{-1/2C^2} e^{iCa^*} e^{iCa} \left[\phi_0(q) - \frac{3K}{2(2)^{1/2}} \phi_1(q) - \frac{K}{2(3)^{1/2}} \phi_3(q) \right] \quad (9)$$

in which the ϕ_1 and ϕ_3 states are due to the anharmonicity. By use of the recursion relations

$$\begin{aligned} a^* \phi_m &= (m+1)^{1/2} \phi_{m+1} \\ a \phi_m &= m^{1/2} \phi_{m-1} \quad (m \neq 0) \\ a \phi_0 &= 0 \quad N \phi_m = m \phi_m \end{aligned} \quad (10)$$

we can successively perform the exponential operations e^{iCa} and e^{iCa^*} on ϕ 's in eq 9 to find

$$\begin{aligned} \psi(t, q) &= \left[1 - \frac{3K}{2(2)^{1/2}} iC - \frac{K}{6(2)^{1/2}} (iC)^3 \right] \sum_{m=0}^{\infty} \frac{(iC)^m}{(m!)^{1/2}} \times \\ &\phi_m(q) - \left[\frac{3}{2(2)^{1/2}} + \frac{1}{2(2)^{1/2}} (iC)^2 \right] K \sum_{m=3}^{\infty} \frac{(iC)^m}{m!} \times \\ &[(m+1)!]^{1/2} \phi_{m+1}(q) - \frac{K}{2} (iC) \sum_{m=0}^{\infty} \frac{(iC)^m}{m!} \left[\frac{(m+2)!}{2} \right]^{1/2} \times \\ &\phi_{m+2}(q) - \frac{K}{2(3)^{1/2}} \sum_{m=0}^{\infty} \frac{(iC)^m}{m!} \left[\frac{(m+3)!}{3!} \right]^{1/2} \phi_{m+3}(q) \quad (11) \end{aligned}$$

For the discussion presented below, we shall write this expression symbolically as

$$\psi(t, q) = ([0 + [1 + [3]\Sigma_1 + ([1 + [3]\Sigma_2 + ([3]\Sigma_3 + ([3]\Sigma_4 \quad (11a)$$

For example, [1 in the first part represents $[-3/(8)^{1/2}]KiC$ which resulted from the $\phi_1(q)$ term of eq 9. Three coefficients of the first sum of eq 11 or 11a come from the three functions of $\psi_0(q)$; the origin of the coefficients of other sums is obvious. The perturbed wave function contains two contributions, the anharmonicity K and the time-dependent perturbation C .

If $\psi_0(q)$ in eq 9 were replaced by $\phi_0(q)$, the perturbed wave function would take the simple form

$$\psi(t, q) = \sum_{m=0}^{\infty} \frac{(iC)^m}{(m!)^{1/2}} \phi_m(q) \quad (12)$$

IV. Transition Probability

From eq 4 and 6, the $0 \rightarrow 1$ transition probability can be obtained in the form

$$P_{01} = \lim_{t \rightarrow \infty} \left| \int_{-\infty}^{\infty} \left[\frac{3K}{2(2)^{1/2}} \phi_0(q) + \phi_1(q) - 3K\phi_2(q) - \frac{K}{(3)^{1/2}} \phi_4(q) \right] \psi(t, q) dq \right|^2 \quad (13)$$

where

$$\psi_1(q) = \frac{3K}{2(2)^{1/2}} \phi_0(q) + \phi_1(q) - 3K\phi_2(q) - \frac{K}{(3)^{1/2}} \phi_4(q)$$

and $\psi(t, q)$ is given by eq 9. To calculate the integral in eq 13, we need to use the orthogonal relation $\int_{-\infty}^{\infty} \phi_i(q)\phi_j(q) dq = \delta_{ij}$. When eq 11a is substituted in eq 13, we find that the integral $\int_{-\infty}^{\infty} \psi_1(q)\Sigma_1 dq$ yields four nonvanishing terms; we shall write these four terms and others from Σ_2, Σ_3 , and Σ_4 as

$$\begin{aligned} \int_{-\infty}^{\infty} \psi_1(q)\Sigma_1 dq &= [0 + [1 + [2] + 4] \\ \int_{-\infty}^{\infty} \psi_1(q)\Sigma_2 dq &= [1 + [2] + 4] \\ \int_{-\infty}^{\infty} \psi_1(q)\Sigma_3 dq &= [2] + 4] \\ \int_{-\infty}^{\infty} \psi_1(q)\Sigma_4 dq &= 4] \end{aligned} \quad (14)$$

From eq 11a and 14, we can write the integral in eq 13 in the form

$$\begin{aligned} \int_{-\infty}^{\infty} \psi_1(q)\psi(t, q) dq &= ([0 + [1 + [3][0] + [1] + \\ &2] + 4]) + ([1 + [3][1] + [2] + 4]) + \\ &([3][2] + 4]) + [34] \equiv \sum_{i,j=0}^{i=3, j=4} [ij] \quad (15) \end{aligned}$$

Here i 's represent the coefficients of $\psi(t, q)$ and j 's the contribution of the final anharmonic oscillator function as shown by eq 14. It should be noted that $[ij]$ has no relation to $\int_{-\infty}^{\infty} \phi_i(q)\phi_j(q) dq$; this integral has been previously used in the form of the orthogonality relation to derive eq 14. Although many terms are involved, the calculation of the explicit form of the i, j sums is trivial. The final result is

$$P_{01} = \left\{ \left[1 + \frac{K^2}{24} \left(125 - 111\epsilon + 13\epsilon^2 - \frac{1}{3}\epsilon^3 \right) \right]^2 + \frac{K^2}{2} \left(5 - \frac{1}{3}\epsilon \right)^2 \epsilon \right\} \exp(-\epsilon) \quad (16)$$

where

$$\epsilon = \frac{1}{2M\hbar\omega} \left| \int_{-\infty}^{\infty} F(t) \exp(i\omega t) dt \right|^2 \quad K = \frac{\alpha}{\hbar\omega} \left(\frac{\hbar}{M\omega} \right)^{3/2}$$

We note that ϵ is the amount of vibrational energy transferred to the harmonic oscillator expressed in units of $\hbar\omega$. The amount of energy transferred to an anharmonic oscillator cannot be calculated in the present approach; the appearance of ϵ in eq 16 is due to the harmonic oscillator functions in $\psi_n(q)$. All K -dependent terms in eq 16 are

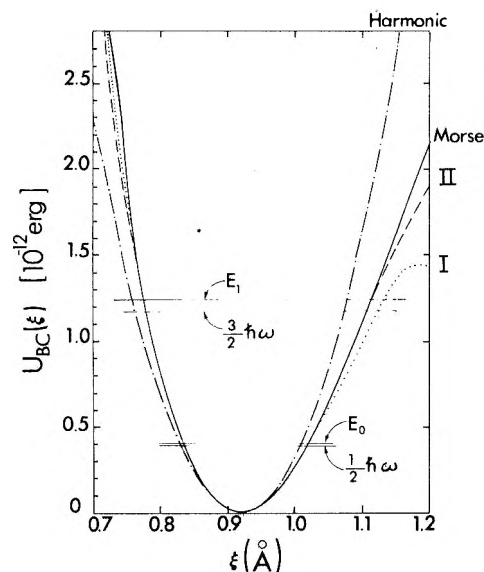


Figure 1. Intramolecular potentials in the neighborhood of ξ_e : The Morse, harmonic, and cubic potentials are shown. The cubic potentials are obtained with (curve II) and without (curve I) introducing $c = 1/1.25$ in K . The eigenvalues E_0 and E_1 for the cubic potential with $c = 1/1.25$ and the harmonic potential are also shown.

from the anharmonicity. For $K = 0$, eq 16 reduces to the well-known expression¹² $P_{01}^* = \epsilon \exp(-\epsilon)$ for the harmonic oscillator perturbed by $-F(t)q$. The ratio P_{01}/P_{01}^* is then a measure of the effect of anharmonicity in the present model; we shall denote this ratio by f in what follows and refer to it as the anharmonicity factor.

For small energy transfer, $\epsilon \ll 1$, eq 16 reduces to

$$P_{01} = \left[1 + \frac{125}{24} K^2 \right]^2 \epsilon \exp(-\epsilon) \quad (17)$$

The anharmonicity factor is then simply $f = [1 + (125/24)K^2]^2$ and is independent of the type of the incident particle. It is solely determined by the molecular constants of the oscillator being excited or deexcited. For example, eq 17 applies to all HF-containing systems (*i.e.*, HF + He, HF + Ar, HF + HF, HF + CO₂, etc.) in which HF is vibrationally excited or deexcited. However, as the velocity increases, all ϵ -dependent terms in eq 16 have to be included. These terms are determined not only by the properties of the oscillator BC but also by the type of the incident particle and the collision velocity.

For the collinear collision system with the interaction potential described by eq 1, the amount of vibrational energy transfer can be determined from¹³

$$\epsilon = \frac{2\omega}{M\hbar} (\pi\rho\mu\alpha)^2 \operatorname{csch}^2 \left(\frac{\pi\omega\alpha}{v} \right) \quad (18)$$

where v is the collision velocity and μ is the reduced mass of the collision system. Note that in the HF + Ar system, $\rho = 0.95$ when Ar is approaching the H side of the oscillator and is 0.05 when Ar approaches the F side.

Numerical Results and Discussion

To investigate the importance of the anharmonicity in the $0 \rightarrow 1$ transition, we first fit eq 2 to the Morse potential $U_{BC}(\xi) = D_e[1 - \exp\{b(\xi - \xi_e)\}]^2$, where D_e is the dissociation energy and b is a potential parameter to be determined. By expanding this potential in the neighborhood of the equilibrium bond distance, we obtain $U_{BC}(\xi)$

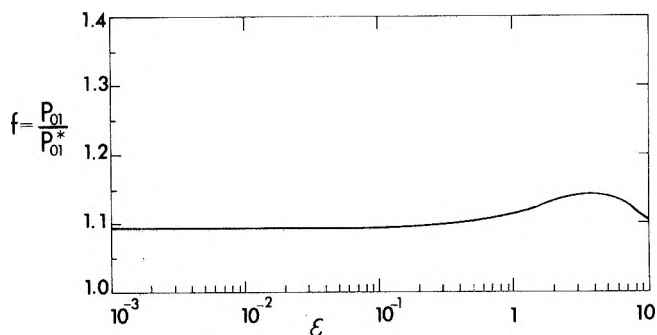


Figure 2. Dependence of the anharmonicity factor $f = P_{01}/P_{01}^*$ on the amount of vibrational energy transfer ϵ for HF.

$= D_e b^2 [(\xi - \xi_e)^2 - b(\xi - \xi_e)^3 + (1/4)b^2(\xi - \xi_e)^4 + \dots]$, so α introduced in eq 2 can be taken as $-D_e b^3$, while the coefficient of $(\xi - \xi_e)^2$ shows that $(1/2)M\omega^2 = D_e b^2$. For HF, the values of D_e and b are known¹⁴ as 141 kcal/mol and 2.232 \AA^{-1} , from which we calculate $-D_e b = -1.089 \times 10^{14} \text{ erg cm}^{-3}$. Other molecular constants are¹⁵ $\omega_e = 4138.52 \text{ cm}^{-1}$ and $\omega_e \chi_e = 90.069 \text{ cm}^{-1}$. Therefore, the value of K is -0.1174 .

In Figure 1, we compare eq 2 with the Morse curve in the neighborhood of the equilibrium value ξ_e ; for comparison we also plot the harmonic oscillator potential. Equation 2, which gives curve I, does not represent the whole of the Morse potential curve, but does give a better approximation than the harmonic oscillator function for values of $q = \xi - \xi_e$ not too large. For $\xi < \xi_e$, it is very close to the Morse curve, but for $\xi > \xi_e$ the deviation is serious. Obviously, if the fourth- and higher-order terms in $(\xi - \xi_e)$ are included, we would obtain closer agreement. Without including such terms, however, we can adjust the parameter α such that eq 2 can closely approximate the Morse potential over a wider range. By use of $K = c(\alpha/\hbar\omega)(\hbar/M\omega)^{3/2}$ with $c = 1/1.25$, we obtain curve II, which is in close agreement with the Morse potential curve for $0.75 < \xi < 1.2 \text{ \AA}$. The energy levels E_0 and E_1 given by eq 5 with the introduction of $c = 1/1.25$ are also shown in the figure; these levels lie in the range of interatomic separations for which curve II closely approximates the Morse curve. Equation 16 derived above applies to the transition between these two levels. For comparison, the corresponding energy levels for the harmonic oscillator are also shown. In the following calculation of the effect of anharmonicity, we shall introduce $c = 1/1.25$ in K ; the corresponding potential is represented by curve II.

In the thermal range, ϵ is very small compared with unity. Then, for HF-containing systems, the anharmonicity factor is $f = P_{01}/P_{01}^* = 1.094$ from eq 17. For example, for HF + Ar in which Ar is approaching the H side of the oscillator, from eq 18 we find $\epsilon = 2.90 \times 10^{-16}$, 1.73×10^{-9} , 4.58×10^{-4} , and 0.515 at $v = 2 \times 10^5$, 3×10^5 , 5×10^5 , and $8 \times 10^5 \text{ cm/sec}$, respectively. Note that for Ar approaching the F side, the values of ϵ given above have to be reduced by the factor $(0.05/0.95)^2$. The average speed for this system takes the values of 1.26×10^5 , 1.78×10^5 , and $2.18 \times 10^5 \text{ cm/sec}$ at 1000, 2000, and 3000°K, respectively. Therefore, these calculations indicate that at thermal collision energies (or velocities) $\epsilon \ll 1$ and $f = 1.094$ for the vibrational excitation of HF, so the probability is larger than that for the harmonic oscillator by 9.4%.

In Figure 2 we plot the values of f as a function of ϵ for HF-containing collision systems; this plot is independent

of the type of the incident particle or the nature of the interaction. Up to the value of ϵ about 0.1, the anharmonicity factor is essentially 1.094. We can calculate ϵ as a function of v by use of eq 18 to determine the dependence of f on v . As ϵ increases (*i.e.*, v increases), the effect of higher-order terms in ϵ becomes important and the first (squared) term of eq 16 slowly decreases from 1.094, while the second term increases somewhat rapidly. Consequently, the anharmonicity becomes larger; it increases to about 1.14 at $\epsilon = 4$. Thereafter, f falls with increasing v because the change of the second term is only slight. For $\epsilon > 10$, f tends to rise with v , but such a large energy transfer can only take place at extremely high collision velocities and the result is not shown in Figure 2. The variation of f at higher ϵ (or higher v) is large due to the increased importance of the $[ij]$ terms with large values of i or j , or both. These $[ij]$ terms are from $\phi_{n+3}(q)$ and $\phi_{n+1}(q)$.

In eq 16, the leading term in the first (squared) quantity is due to [01] as to be expected. The ϵ -independent term $(125/24)K^2$, also shown in eq 17, resulted from [10], [12], and [32]. Note that [10] is not the same as [01] because their coefficients are different. While [01] is originated from the harmonic term $\phi_n(q)$ in eq 4, [10] is the result of the integration of the product of $\phi_1(q)$ of $\psi(t, q)$ and $\phi_{n+1}(q)$ of eq 4. The ϵ -dependent terms in the squared quantity are from [30], [32], [34], and [14]. The second quantity of eq 16 is a sum of [02], [11], [31], [04], and [31].

VI. Concluding Remarks

The present study on the importance of anharmonicity in vibrational transitions in molecular collisions is based on a simple anharmonic potential. The importance is determined by comparing the vibrational transition probability for this potential with that for the harmonic oscillator potential. The anharmonic potential, which contains quadratic and cubic terms in the oscillator coordinate, closely fits to the Morse potential in the region of interatomic distance where the energy levels for the $0 \rightarrow 1$ transition lie. An analytic expression of the transition proba-

bility showing the contribution of anharmonicity is obtained from the perturbed oscillator wave function, which is a linear combination of several harmonic oscillator functions. To calculate the $0 \rightarrow 1$ transition probability it is therefore necessary to include the ϕ_0 , ϕ_1 , ϕ_2 , ϕ_3 , and ϕ_4 harmonic oscillator functions.

Application to HF shows that for the amount ϵ of energy transferred to the oscillator measured in units of $\hbar\omega$ less than 0.1 the transition probability P_{01} is greater than that for the harmonic oscillator, P_{01}^* , by a constant factor of 1.094. As the amount of vibrational energy transfer increases, P_{01}/P_{01}^* rises to a maximum value. At still larger amounts of energy transfer, the ratio now decreases but it is not significantly different from 1.10. The probability P_{01} is always greater than P_{01}^* indicating that the anharmonicity determined from the cubic term of the intramolecular potential always increases the result of the harmonic oscillator and that the factor of about 1.10 has to be introduced in the latter result.

References and Notes

- (1) (a) This work was supported by the Air Force Office of Scientific Research, Grant No. AFOSR-72-2231. (b) Theoretical Chemistry Group Contribution No. 1047.
- (2) For example, see a review article by D. Rapp and T. Kassal, *Chem. Rev.*, **69**, 61 (1969).
- (3) (a) H. K. Shin, *J. Phys. Chem.*, **75**, 4001 (1971); (b) F. H. Mies, *J. Chem. Phys.*, **40**, 523 (1964).
- (4) For example, see (a) D. J. Locker and P. F. Endres, *J. Chem. Phys.*, **51**, 5482 (1969); (b) G. C. Berend and R. L. Thommarson, *ibid.*, **58**, 3454 (1973).
- (5) J. F. Bott and N. Cohen, *J. Chem. Phys.*, **58**, 934 (1973), and references therein.
- (6) H. K. Shin, *J. Chem. Phys.*, **47**, 3302 (1967).
- (7) R. C. Herman and K. E. Shuler, *J. Chem. Phys.*, **22**, 481 (1954).
- (8) R. D. Sharma and C. W. Kern, *J. Chem. Phys.*, **55**, 1171 (1971).
- (9) L. D. Landau and E. M. Lifshitz, "Quantum Mechanics," Addison-Wesley, Reading, Mass., 1958, p 136.
- (10) A Messiah, "Quantum Mechanics," Vol. I, North-Holland Publishing Co., Amsterdam, 1968, Chapter 12.
- (11) D. ter Haar, "Selected Problems in Quantum Mechanics," Academic Press, New York, N. Y., 1964, pp 152-154.
- (12) C. E. Treanor, *J. Chem. Phys.*, **43**, 532 (1965); **44**, 2220 (1966).
- (13) D. Rapp, *J. Chem. Phys.*, **32**, 735 (1960).
- (14) R. F. Barrow and J. W. C. Johns, *Proc. Roy. Soc., Ser. A*, **251**, 504 (1959). Also see R. L. Wilkins, *J. Chem. Phys.*, **58**, 2326 (1973).
- (15) G. Herzberg, "Spectra of Diatomic Molecules," Van Nostrand, Princeton, N. J., 1950, Table 39.

Reactions of Hydroxyl Radicals with Unsaturated Aliphatic Alcohols in Aqueous Solution. A Spectroscopic and Electron Spin Resonance Radiolysis Study

M. Simic,^{1a} P. Neta,^{1b} and E. Hayon*^{1c}

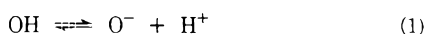
Pioneering Research Laboratory, U. S. Army Natick Laboratories, Natick, Massachusetts 01760, Radiation Biology Laboratory, Zoology Department, University of Texas, Austin, Texas 78712, and Radiation Research Laboratories, Mellon Institute of Science, Carnegie-Mellon University, Pittsburgh, Pennsylvania 15213 (Received May 29, 1973)

Publication costs assisted by Natick Laboratories

The reactions of OH and O⁻ radicals with allyl alcohol, 1,4-pentadien-3-ol, and 2,4-hexadien-1-ol in aqueous solutions were studied using the spectrophotometric pulse radiolysis and the *in situ* steady-state radiolysis-esr techniques. The reaction rate constants of the OH radicals with these compounds ranged from 6.0 to 10.0 × 10⁹ M⁻¹ sec⁻¹ and of O⁻ radicals from 2.4 to 4.3 × 10⁹ M⁻¹ sec⁻¹. The transient absorption, extinction coefficients, and decay kinetics of the intermediates produced from the reactions of OH, O⁻, and H atoms with these alcohols were determined. The OH radicals were found to add predominately to the carbon-carbon double bonds, but a measurable proportion (10–20%) were found to abstract hydrogen from allylic positions (α -hydroxy positions). With conjugated double bonds, *e.g.*, 1,4-pentadien-3-ol, the extent of abstraction by OH radicals increased by a factor of 2. The O⁻ radicals were found to react predominately by hydrogen atom abstraction. The presence of double bonds conjugated to the α -hydroxy radical site was found to considerably increase the acidity of these radicals. Thus, the pK_a of the CH₂=CHCHOH and CH₂=CHC(OH)CH=CH₂ radicals are 9.6 ± 0.1 and 8.9 ± 0.1, respectively. The esr experiments confirm the abstraction reactions of O⁻ radicals with these compounds. The importance of the abstraction reactions of OH radicals from substituents in an α position to double bonds are discussed. These reactions may be of importance in the fields of radiation polymerization and biological radiation damage.

Introduction

Differences in the reaction rate constants and the site of reaction of hydroxyl radicals, OH, and their conjugate base O⁻ with compounds containing carbon-carbon double bonds have recently been demonstrated.² The equilibrium constant



is well established, pK_a = 11.9³ and 11.8.⁴ Due to the relatively high dissociation constant of the OH radical and the lower reactivity of O⁻ radicals,^{5,6} the reactions of O⁻ have to be studied at pH 14 or higher.

In this work, the reactions of OH and O⁻ radicals with aliphatic alcohols containing a single double bond, and conjugated and nonconjugated double bonds have been examined and compared. Conjugated double bonds are found in many biological compounds, *e.g.*, carotenoids, porphyrins, etc., and the systems studied here can serve as simple model compounds.

The technique of pulse radiolysis and kinetic absorption spectrophotometry was used to study to reactions of hydroxyl radicals with allyl alcohol, 1,4-pentadien-3-ol, and 2,4-hexadien-1-ol in aqueous solutions. The radicals produced in steady-state irradiated solutions have also been identified by esr.

Experimental Section

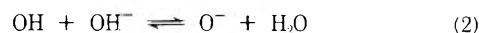
The pulse radiolysis experiments were performed using single pulses of 2.3 MeV electrons and ~30 nsec duration (Febetron 705 machine), and the technique and conditions employed have been described.^{7,8} The esr experiments were performed using the steady-state *in situ* radiolysis set-up previously described.⁹

Allyl alcohol (Eastman Organic) and both dienes (Chemical Samples Co.) were used without further purification. The pH of the solutions were adjusted using perchloric acid, potassium hydroxide, and ~1 mM phosphate and tetraborate buffers. Dosimetry was carried out using 0.05 M KCNS solutions (1 atm N₂O) and the extinction coefficients calculated on the basis $G(\text{OH}) = G(e_{\text{aq}}^-) = 2.8$.

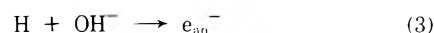
The solutions were prepared immediately before use and protected from exposure to light from the monitoring lamp using a synchronized shutter.

Results

The radiolysis of water generates e_{aq}⁻, OH radical, and H atoms with *G* values 2.8, 2.8, and 0.6, respectively. In the presence of N₂O (1 atm) e_{aq}⁻ is virtually completely converted to O⁻, which is in rapid equilibrium with OH



with $k_2 = 1.2 \times 10^{10}$ M⁻¹ sec⁻¹ and $k_{-2} = 9.2 \times 10^7$ sec⁻¹ (ref 6). Also in N₂O solutions, the H atoms contribute ~12% of the total radicals formed and this can be accounted for. In alkaline solutions, H atoms react with OH⁻ ions



with $k_3 = 2.0 \times 10^7$ M⁻¹ sec⁻¹ (ref 10), and the e_{aq}⁻ produced are in turn converted to O⁻ on reaction with N₂O. In acidic solutions, e_{aq}⁻ reacts with H₃O⁺ to give H atoms with a $k_4 = 2.3 \times 10^{10}$ M⁻¹ sec⁻¹.



The reactions of H atoms were therefore studied at pH ≤ 1.0 to ensure complete conversion of e_{aq}⁻ to H atoms,

TABLE I: Reaction Rate Constants of OH and O⁻ Radicals with Unsaturated Aliphatic Alcohols in Aqueous Solution^a

Solute, S	Formula	$k(\text{OH} + \text{S}), M^{-1} \text{sec}^{-1}$ at pH 7.0	$k(\text{O}^- + \text{S}), M^{-1} \text{sec}^{-1}$ at pH 14.0
Allyl alcohol	$\text{CH}_2=\text{CHCH}_2\text{OH}$	$6.0 \pm 1.5 \times 10^9$	$2.9 \pm 0.5 \times 10^9$
1,4-Pentadien-3-ol	$\text{CH}_2=\text{CHCH}(\text{OH})\text{CH}=\text{CH}_2$	$1.0 \pm 0.2 \times 10^{10}$	$2.4 \pm 0.5 \times 10^9$
2,4-Hexadien-1-ol	$\text{CH}_3\text{CH}=\text{CHCH}=\text{CHCH}_2\text{OH}$	$9.8 \pm 1.0 \times 10^9$	$4.3 \pm 0.8 \times 10^9$

^a Determined by following the formation kinetics of the transients produced from the reaction of OH and O⁻ radicals with the alcohols at the appropriate wavelengths.

and in the presence of *tert*-butyl alcohol (usually $\sim 1.0 M$) to scavenge the OH radicals. The radical produced⁷ from *t*-BuOH absorb below 280 nm with $\lambda_{255} \sim 900 M^{-1} \text{cm}^{-1}$, and are relatively unreactive. The concentration of the solutes was high enough to ensure complete scavenging of OH or O⁻ radicals and at the same time avoid their reaction with e_{aq}^- .

The reaction rate constants of OH and O⁻ radicals were obtained by following the formation kinetics of the resulting transient species produced at the appropriate wavelength. The conditions were adjusted for the reaction to take place after the equilibrium between OH and O⁻ was reached. Under these conditions, the observed rate constant is a composite

$$k_{\text{obsd}} = k_{\text{OH}+\text{S}} \frac{[\text{H}^+]}{[\text{H}^+] + K_{\text{OH}}} + k_{\text{O}^-+\text{S}} \frac{1 - [\text{H}^+]}{[\text{H}^+] + K_{\text{OH}}}$$

where $K_{\text{OH}} = 1.26 \times 10^{-12}$. At pH <10, the $k_{\text{O}^-+\text{S}}$ term is negligible since usually $k_{\text{OH}+\text{S}} > k_{\text{O}^-+\text{S}}$. At pH 14 for the solutes studied the $k_{\text{OH}+\text{S}}$ contribution was relatively low (a few per cent). The results obtained and the corrected rate constants are presented in Table I.

Spectra of Intermediates

The absorption spectra of the transients were measured at $\sim 1 \mu\text{sec}$ or at a few μsec after the pulse, depending on the acid-base equilibration time of the transients produced, and before any noticeable decay of the transient occurred. The observed changes in the absorption spectra of the intermediates are taken as an indication of either the acid-base properties of the radicals produced or to a change in the site(s) of attack on the solutes by O⁻, compared to OH radicals. Hence, at pH <11.0 the changes in OD vs. pH were associated with the acid-base properties of the radicals and pK_a values were derived. At pH >11.0, positive assignment of the dissociation constants is not always possible. Fortunately, in our systems the pK_a values of the radicals produced were below the pK_a of the OH radical ($pK_a = 11.9$).

The transient absorption spectra resulting from the reaction of OH and O⁻ radicals and of H atoms with allyl alcohol, 1,4-pentadien-3-ol, and 2,4-hexadien-1-ol are given in Figures 1-3, respectively. The dependence of the transient spectra on the pH and the experimental conditions used are also given. The data concerning the spectral characteristics, decay kinetics, changes in the site(s) of attack, and pK_a values of the radicals produced are given in Table II. The rates of radical-radical reactions may be incorrect in cases where two or more radicals are produced in the system. Hence, the extinction coefficients and decay rates given are the overall experimentally observed values. In spite of this difficulty, the results do

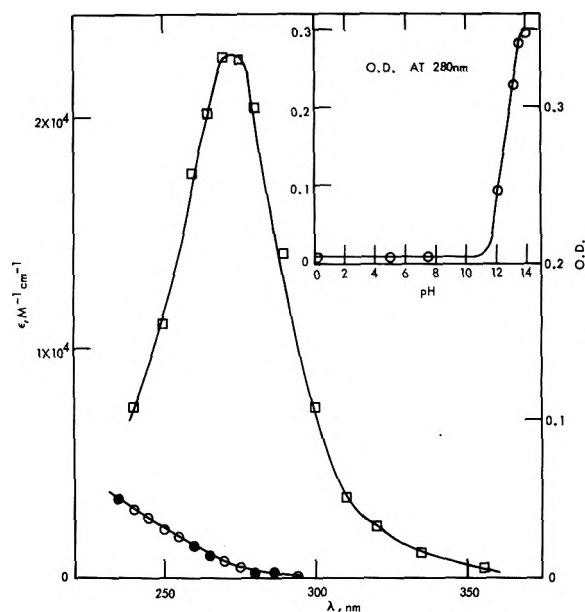
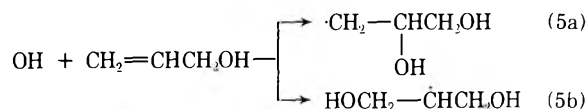


Figure 1. Transient absorption spectra of intermediates produced in aqueous solutions of 3 mM allyl alcohol from the reaction with H atoms (●, pH 0.7, in the presence or absence of 1.0 M *t*-BuOH), OH radicals (○, pH 5.0, 1 atm of N₂O), and O⁻ radicals (□, pH 14.0, 1 atm of N₂O). Insert shows change in absorbance at 280 nm with pH due to the change in the site of attack by O⁻ radicals (total dose = 1.3 krad/pulse).

clearly indicate the changes occurring and the assignment of the various absorption bands produced.

Discussion

Hydroxyl radicals readily abstract a hydrogen atom from C-H bonds and other bonds, as well as add to unsaturated compounds (double bonds, aromatic and heterocyclic rings, etc.). The rate constants¹¹ for addition of OH radicals to unsaturated compounds are a few times higher, $k > 6.0 \times 10^9 M^{-1} \text{sec}^{-1}$, than those for abstraction from saturated compounds, $k \leq 2.0 \times 10^9 M^{-1} \text{sec}^{-1}$. Hence, in the case of solutes with unsaturated groups one would expect predominantly an addition reaction



Both radicals are saturated β -hydroxy aliphatic radicals and are expected to absorb below $\sim 250 \text{ nm}$.⁷ The tail absorption of these radicals can be seen in Figure 1. It is interesting to point out that the reaction of H atoms with allyl alcohol produces a similar transient absorption (Figure 1) and similar radicals, indicating that H atoms also add predominantly to double bonds.

TABLE II: Absorption Maxima, Extinction Coefficients, Decay Kinetics, and Ionization Constants of the Radicals Produced from the Reaction of OH and O⁻ Radicals with Unsaturated Aliphatic Alcohol in Aqueous Solutions

Solute	Reacting radical	pH	pK _a		Suggested radicals	Spectral data			Decay kinetics			
			Obsd	Actual		λ _{max} , nm	Obsd	Calcd	pH	λ, nm	2k/ε	
Allyl alcohol	H	0.7			CH ₃ CHCH ₂ OH and ·CH ₂ CH ₂ CH ₂ OH	<235	>3,500	>3,500				
	OH	3.0-8.0			CH ₂ (OH)CHCH ₂ OH ^b CH ₂ =CHCHOH	<235	>3,500	>3,500				
	O ⁻	14.0	≥12.6	9.6 ^a	CH ₂ =CHCHO ⁻ CH ₂ =CCH ₂ OH H atom adducts ^c OH radical adducts and CH ₂ =CHC(OH)CH=CH ₂ CH ₂ =CHC(O ⁻)CH=CH ₂ and OH radical adducts	272	23,000	10,000 ^d >10,000	14	295	2.0 × 10 ⁵	
1,4-Pentadien-3-ol	H	0.7			H atom adducts ^c	<235	>3,500	>3,500				
	OH	3.0-7.0			OH radical adducts and CH ₂ =CHC(OH)CH=CH ₂ CH ₂ =CHC(O ⁻)CH=CH ₂ and OH radical adducts	<235 270 295	4,300 2,800	~10,000 ^d ~10,000 ^d	3.5	270	4.8 × 10 ⁵	
2,4-Hexadien-1-ol	H	0.7			CH ₂ =CHC(O ⁻)CH=CH ₂ and CH ₂ =CC(OH)CH=CH ₂ H atom adducts ^c	295	20,000	>10,000 >3,500	4.0	300	1.7 × 10 ⁴	
	OH	3.0-8.0			OH radical adducts and -CH(OH) -CH=C-	<235 <235	>3,500	>3,500 >3,500				
	OH	11.2	9.6	9.6	OH radical adducts -CH(O ⁻) and -CH=C- -CH(O ⁻) and -CH=C-	270	17,500	35,000 ^d				
						310	5,000	~30,000 ^d				
						270	11,000	>11,000				
O ⁻	14.0	≥12.7	9.6		-CH(O ⁻) and -CH=C-	310	13,500		14.0	310	6.0 × 10 ⁴	
						270	31,000	~50,000 ^e	14.0	270	1.0 × 10 ⁵	

^a From ref 12. ^b Also some ·CH₂CH(OH)CH₂OH radicals formed. ^c Abstraction of H atoms from C₁ position also possible. ^d Calculated from per cent value given in Table III. ^e Calculated based on ε₃₁₀ = 30,000 M⁻¹ cm⁻¹ for the -CH(O⁻) radical, and a 3X increase in absorption by O⁻ radicals at pH 14.0, assuming that O⁻ radicals do not add.

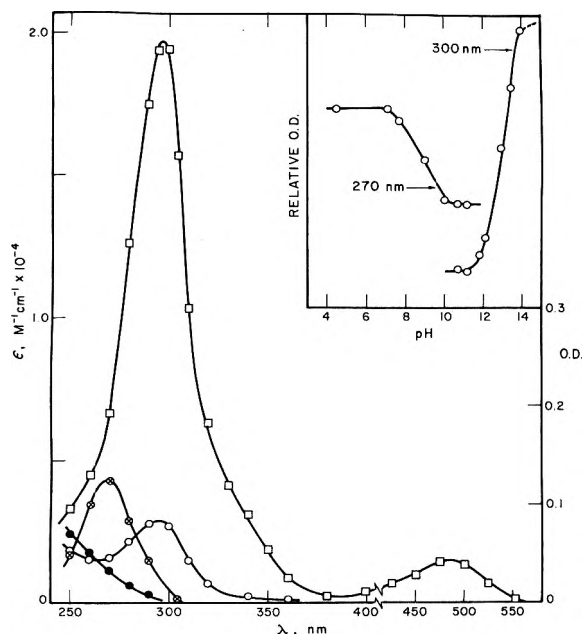
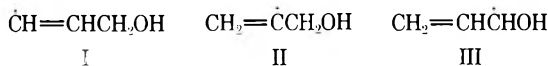


Figure 2. Transient absorption spectra of intermediates produced in aqueous solutions of 1 mM 1,4-pentadien-3-ol from the reaction with H atoms (●, pH 0.7, 1.0 M *t*-BuOH, corrected for absorption due to *t*-BuOH radical), OH radicals (⊗, pH 3.2, 1 atm N₂O and ○, pH 10.7, 1 atm N₂O), and O⁻ radicals (□, pH 14.0, 1 atm N₂O). Insert shows change in absorbance at 270 and 300 nm with pH (total dose = 2.5 krads/pulse).

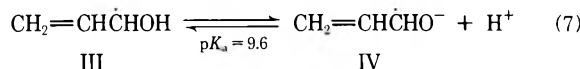
At higher pH values (pH > 12), the O⁻ radicals become the reacting species, reaction 1, and a new very strong transient absorption appears with λ_{max} 272 nm (see Figure 1 and Table II). This absorption is suggested to be due to a radical produced from the abstraction of an H atom from allyl alcohol by O⁻ radicals. Three isomeric forms are possible (I–III) but abstraction from the allylic posi-



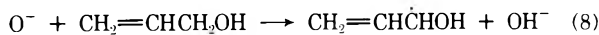
tion to produce III is expected to predominate. Radical III has previously been produced from the reaction of e_{aq}⁻ with acrolein



and the equilibrium constant determined¹²



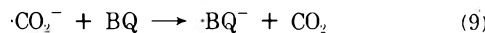
Since the transient absorption obtained at pH 14.0, Figure 1, is quite similar to that reported¹² for radical IV, it is concluded that O⁻ radicals abstract from the α-carbon position in allyl alcohol, reaction 8 followed by 7



The change from reaction 5 to reaction 8 is in agreement with the previous observation.²

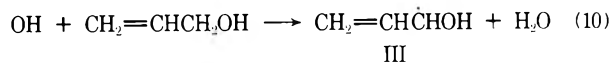
The formation of radical III from the reaction of OH radicals with allyl alcohol in neutral solutions was also demonstrated using the electron transfer to *p*-benzoquinone method described elsewhere.^{13,14} Briefly, α-hydroxyalkyl radicals readily transfer an electron to a quinone while the β- and γ-hydroxy radicals do not. *p*-Benzoquinone (BQ) was used as the electron acceptor and the formation of the semiquinone radical anion ·BQ⁻ was monitored at 430 nm.¹⁴ The efficiencies (expressed as percent-

age) of the electron transfer reactions were derived relative to the reaction

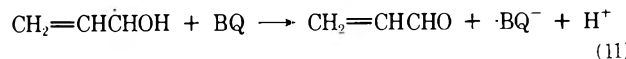


taken as 100% efficient. The results obtained are given in Table III.

From the benzoquinone titration method it follows that ~12% of the OH radicals produce radical III

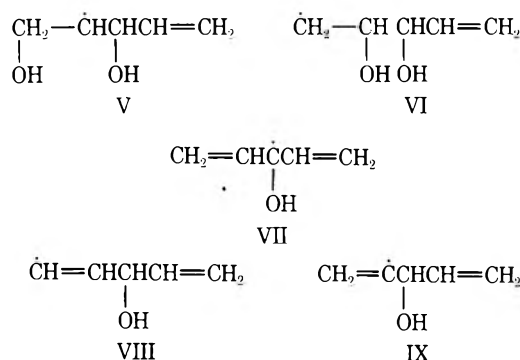


based on the reaction

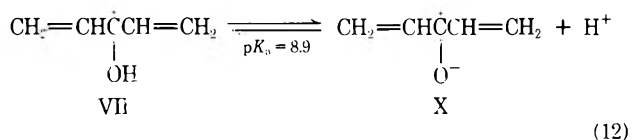


It is difficult, from spectroscopic observations, to assess the extent of forms I and II produced by attack of O⁻ on allyl alcohol. It appears that forms I and II could have higher ε values than radical IV and somewhat similar absorption maxima. The probability of formation of forms I and II is, however, rather small.

Pentadienol. Five different species (V–IX) could be pro-



duced from the reaction of OH radicals with 1,4-pentadien-3-ol. Forms V and VI are expected to have a rather weak absorption, similar to that of the H atom adduct, Figure 2. Form VII is the only one to have acid-base properties due to the α-hydroxyl group



It is interesting to note that this pK_a is considerably lower than that of the CH₃Ċ(OH)CH₃ radical, due to the strong conjugation of the odd electron with the double bonds. The spectra for this radical (Figure 2) show the presence of some contribution from forms V and VI. Furthermore, the BQ titration method indicates that ~25% of the OH radicals produced form VII (see Table III). This relatively high percentage indicates that the C₃-H bond is rather labile due to the conjugation with the double bonds on both sides.

Forms VIII and IX probably have a strong absorption and its apparent absence would seem to indicate a small probability for their formation on reaction of OH radicals with 1,4-pentadien-3-ol. Hence, one can assume that OH predominantly adds to this diene to give radical V and also some radical VI.

The O⁻ radicals are expected, as with allyl alcohol, to abstract an H atom (with very little, if any, addition) leading to the transient spectrum with λ_{max} 295 nm

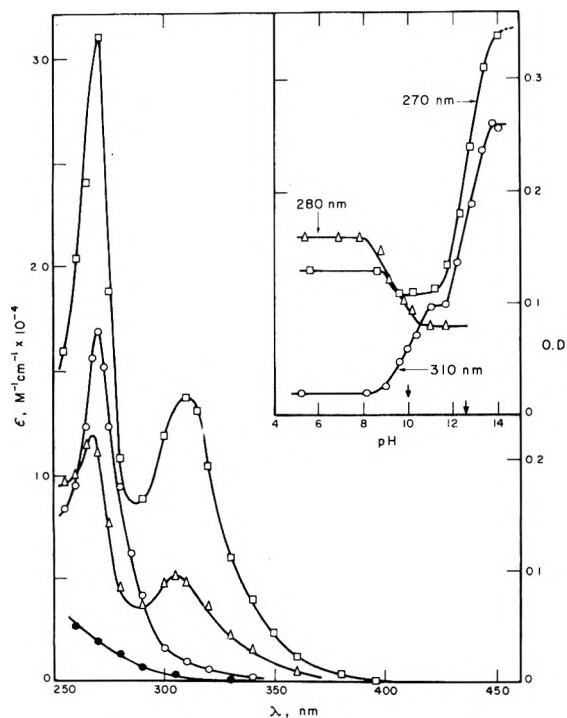
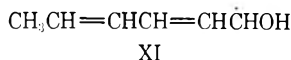


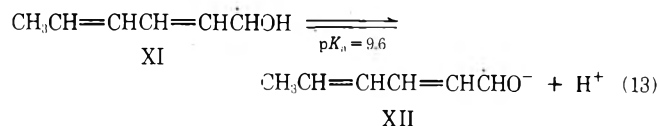
Figure 3. Transient absorption spectra of intermediates produced in aqueous solutions of 1 mM 2,4-hexadien-1-ol from the reaction with H atoms (●, pH 0.7, 1.0 M *t*-BuOH, corrected for absorption due to *t*-BuOH radicals), OH radicals (○, pH 5.0, 1 atm of N₂O and △, pH 11.2, 1 atm N₂O), and O⁻ radicals (□, pH 14.0, 1 atm of N₂O). Insert shows change in absorbance at 270, 280, and 310 nm with pH (total dose = 1 krad/pulse).

shown in Figure 2. This spectrum is suggested to be due to radical X, as well as to VIII and IX. From the observed overall absorption at 295 nm and the percentage formation (25%) from the OH radical, one can calculate an $\epsilon_{295} \sim 1 \times 10^4 M^{-1} \text{ cm}^{-1}$ for radical X. Comparison of this value with the overall observed $\epsilon = 2 \times 10^4 M^{-1} \text{ cm}^{-1}$ suggests that forms VIII and IX must have extinction coefficients $\leq 2 \times 10^4 M^{-1} \text{ cm}^{-1}$. Only form VII is expected to have a delocalized unpaired electron.

Hexadienol. While in 1,4-pentadien-3-ol the double bonds are symmetrically positioned on either side of the α -hydroxy radical (form VII above), in 2,4-hexadien-1-ol both double bonds are on side of the α -hydroxy radical



Here also the unpaired electron is, to a certain extent, delocalized. From the BQ titration method (see Table III), ~13% of the OH radicals produce radical XI. Only this radical is expected to show acid-base properties



The maximum at 310 nm in Figure 3 is considered to be due to radical XII while radical XI absorbs at ~275 nm. Due to the asymmetry of 2,4-hexadien-1-ol, a greater variety of transient species can be produced from the attack of OH radicals. The addition reaction of OH to the double bonds can result in the formation of four radicals, all of which are expected to absorb weakly and have spectra similar to that of the H atom adduct (Figure 3, ●). The

TABLE III: Fraction (Expressed as Per Cent) of α -Hydroxyl Alkyl Radicals, $>\dot{\text{C}}\text{-OH}$, Produced from the Reaction of OH Radicals with Unsaturated Aliphatic Alcohols in Aqueous Solution^a

Solute	Nature of radical donor ^c	% of $>\dot{\text{C}}\text{OH}$ radicals produced ^b
Allyl alcohol	$\text{CH}_2=\text{CH}\dot{\text{C}}\text{HOH}$	12.0
1,4-Pentadien-3-ol	$\text{CH}_2=\text{CH}\dot{\text{C}}\text{CH}=\text{CH}_2$	25.0
2,4-Hexadien-1-ol	$\text{CH}_3\text{CH}=\text{CHCH}=\text{CH}\dot{\text{C}}\text{HOH}$	13.0

^a Determined based on the transfer of an electron from $>\dot{\text{C}}\text{OH}$ radicals to *p*-benzoquinone (BQ), see text. Formation of $\cdot\text{BQ}^-$ monitored at 430 nm during the pulse radiolysis of 2 mM aqueous solutions of alcohols at pH 7.0 in presence of 20 μM BQ and N₂O (1 atm). Total dose ~1.0 krad/pulse. ^b 100% was determined from the reaction of e_{aq}^- or $\cdot\text{CO}_2^-$ radicals with BQ, under otherwise identical experimental conditions (values good to $\pm 15\%$). ^c The structures showing the conjugation of the odd electron with the double bonds are not shown for convenience.

abstraction of an H atom by OH radicals can, in addition to XI, yield another five radicals of the type $>\text{C}=\dot{\text{C}}-$. These species are expected to have high ϵ and apparently have maxima in the 270-nm region (Figure 3, △). This conclusion follows from the observed absorption remaining (at 270 nm) at pH 11.2 when conversion of radical XI to XII has occurred.

The O⁻ radicals predominantly abstract an H atom. From the increase in absorption at 270 and 310 nm a threefold increase is observed at pH 14.0 compared to pH 11.2. Based on 13% formation of radical XII from reaction with OH radicals (Table III), ~40% of O⁻ radicals produce radical XI. The majority of the remaining O⁻ radicals presumably give $>\text{C}=\dot{\text{C}}-$ type of radicals and these must have high extinction coefficients ($\sim 50,000 M^{-1} \text{ cm}^{-1}$), see Table II.

Esr Observations

In order to verify the assignments given to the radicals produced by the reactions of O⁻ esr experiments have been carried out. Solutions containing 0.01 M of the alcohol and saturated with N₂O at pH 13.7 have been irradiated continuously by 2.8-MeV electrons while flowing through a silica cell within the esr cavity and the spectra recorded under steady-state conditions as described previously.⁹ The hyperfine constants and *g* factors calculated from the spectra are summarized in Table IV together with the suggested structures of the radicals.

With solutions of allyl alcohol the spectrum consisted of lines resulting from two different radicals with relative concentration of about 1:1.5. The parameters calculated from the more intense lines are shown first in Table IV. Both radicals contain three inequivalent protons with hyperfine constants between 11 and 13 G and one proton with ~2-G splitting. These values are characteristic of allyl-type radicals as previously observed for the allyl radical itself¹⁵ and for the hydroxyallyl radical.¹⁶ In the latter case, as in the present study, two geometrical isomers of the radical have been observed. In both cases it is not possible to assign the parameters to a specific isomer and the distinction made in Table IV is only tentative, although it is supported from the results for the third radical in that table. Comparing the esr parameters determined in the present study with those obtained previously for the pro-

TABLE IV: ESR Parameters and Suggested Structures of Radicals Produced by Reaction of O⁻ with Allyl Alcohol and 1,4-Pentadien-3-ol^a

Solute	Radical	<i>g</i> factor ^b	Proton hyperfine constants ^c
Allyl alcohol		2.00317	12.85
			12.38
			11.99
			1.87
1,4-Pentadien-3-ol		2.00335	13.27
			12.41
			11.08
			2.49
1,4-Pentadien-3-ol		2.00300	8.76(2)
			8.40(2)
			1.99(2)

^a Experiments carried out with aqueous solutions containing 10⁻² M of the alcohol, 0.5 M KOH, and saturated with N₂O under continuous irradiation with 2.8-MeV electrons directly in the esr cavity. ^b Determined by comparison to the peak from the silica cell and accurate to ±0.00005. ^c Given in gauss and accurate to ±0.03 G. The number of protons displaying the splitting is given in parentheses if different than one.

tonated form of the radical,¹⁶ it is seen that dissociation of the OH group causes increase in the *g* factors and decrease in the hyperfine splittings as observed for simple α-hydroxyalkyl radicals.⁹ These changes indicate that the shift of spin density to the O⁻ is larger than that to the OH.

The reaction of O⁻ with 1,4-pentadien-3-ol is expected similarly to result in abstraction of the central hydrogen atom and to produce a five carbon conjugated system. Again, because of lack of free rotation around all the C-C bonds, several isomers can be produced of which two are symmetrical and one is asymmetrical. The spectrum recorded with this compound consisted of lines of one radical only. Because three sets of two equivalent protons have been observed, the structure of this radical must be symmetrical. The structure shown in Table IV seems more likely than the other possible orientation, where the end carbons will be very close to each other.

Experiments with 2,4-hexadien-1-ol were not successful because the complexity of the esr spectrum resulted in very low signal-to-noise ratio.

Summary

The OH radicals have been shown to predominantly add to carbon-carbon double bonds, and a small propor-

tion (~10–20%) can abstract from allylic positions or more generally from CH groups. The extent of the abstraction reactions are enhanced by about a factor of 2 from C-H bonds conjugated with double bonds, as in the case of 1,4-pentadien-3-ol. Similarly, it is anticipated that a small fraction of the OH radicals will abstract an H atom from aromatic substituents (*e.g.*, benzyl alcohol, toluene, etc., and other higher homologs) and from heterocyclic substituents (*e.g.*, thymine, 6-methyluracil, methylpyridines, etc.).

The O⁻ radicals, on the other hand, predominantly abstract H atoms since their rate constants for addition to double bonds and aromatic rings are lower.

The acidity of the hydroxyl group in α-hydroxy radicals is further increased by the presence of adjacent double bonds, *e.g.*, the p*K*_a of CH₂=CHC(OH)CH=CH₂ is 3.3 units lower than that of the CH₃C(OH)CH₃ radical (p*K*_a = 12.2).¹⁷ Similarly, the CH₃CH=CHCH=CHCHOH radical has a p*K*_a of ~2 units lower than that of the CH₃CHOH radical (p*K*_a = 11.6).¹⁷

It is suggested that the reactions demonstrated here may be of importance in the fields of radiation polymerization and biological radiation damage.

Acknowledgments. This work has been partly supported by NIH Grant No. GM-13557, AEC Contract No. AT-(40-1)-3408, granted to Radiation Biology Laboratory, Austin, Texas, and AEC Contract No. AT (11-1)-3238 with the Radiation Research Laboratory of Carnegie Mellon University.

References and Notes

- (1) (a) Austin, Texas; (b) Pittsburgh, Pennsylvania; (c) Natick, Massachusetts.
- (2) P. Neta, M. Z. Hoffman, and M. Simic, *J. Phys. Chem.*, **76**, 847 (1972).
- (3) J. Rabani and M. S. Matheson, *J. Phys. Chem.*, **70**, 761 (1966).
- (4) J. L. Weeks and J. Rabani, *J. Phys. Chem.*, **70**, 2100 (1966).
- (5) B. L. Gall and L. M. Dorfman, *J. Amer. Chem. Soc.*, **91**, 2199 (1969).
- (6) G. V. Buxton, *Trans. Faraday Soc.*, **65**, 2150 (1969); **66**, 1656 (1970).
- (7) M. Simic, P. Neta, and E. Hayon, *J. Phys. Chem.*, **73**, 3794 (1969).
- (8) J. P. Keene, E. D. Black, and E. Hayon, *Rev. Sci. Instrum.*, **40**, 1199 (1969).
- (9) K. Eiben and R. W. Fessenden, *J. Phys. Chem.*, **75**, 1186 (1971).
- (10) J. Jortner and J. Rabani, *J. Phys. Chem.*, **66**, 2078, 2081 (1962); J. Rabani, *Advan. Chem. Ser.*, **No. 50**, 242 (1965).
- (11) M. Anbar and P. Neta, *Int. J. Appl. Radiat. Isotop.*, **18**, 493 (1967).
- (12) J. Lilie and A. Henglein, *Ber. Bunsenges. Phys. Chem.*, **73**, 170 (1969).
- (13) M. Simic and E. Hayon, *Int. J. Radiat. Biol.*, **22**, 507 (1972).
- (14) M. Simic and E. Hayon, *Biochem. Biophys. Res. Commun.*, **50**, 364 (1973).
- (15) R. W. Fessenden and R. H. Schuler, *J. Chem. Phys.*, **39**, 2147 (1963).
- (16) R. Livingston and H. Zeldes, *J. Chem. Phys.*, **44**, 1245 (1966).
- (17) K. D. Asmus, A. Henglein, A. Wigger, and G. Beck, *Ber. Bunsenges. Phys. Chem.*, **70**, 756 (1966).

Combining Rules for Intermolecular Potential Parameters.

III. Application to the Exp 6 Potential

Chang Lyoul Kong* and Manoj R. Chakrabarty

Department of Chemistry, Marshall University, Huntington, West Virginia 25701 (Received May 25, 1973)

A set of combining rules for intermolecular pair potentials recently formulated and shown to be satisfactory for both the Lennard-Jones (12-6) potential and the Morse potential is applied to the exp 6 potential. Examination of the transport properties of the noble gas systems indicates that the same combining rules are also satisfactory for the exp 6 potential and, in fact, superior to the other combining rules previously suggested for the exp 6 potential model.

Introduction

In part II of this series,¹ a new set of combining rules for intermolecular pair potentials has been formulated based on Smith's model² of atomic distortion for the repulsive potentials and Zener's model³ of atomic interactions for the attractive potentials. Examination of virial data and transport properties indicated that the new rules are satisfactory in correlating the effective pair interactions of noble gas atoms when the pair interactions are represented by simple analytical potential functions such as the Lennard-Jones (12-6) potential and the Morse potential. This paper presents the application of the same combining rules to the exp 6 potential as a part of the continuous test of the proposed rules. Evidence from the transport properties of noble gas systems again indicates the new rules to be very satisfactory in correlating the pair interactions of noble gas atoms given by the exp 6 potential. Several other combining rules previously suggested for the exp 6 potential are also examined in comparison with the new rules.

The Combining Rules

The exp 6 potential is of the form

$$U(R) = \frac{\epsilon}{1 - (6/\alpha)} \left[\frac{6}{\alpha} e^{\alpha[1 - (R/r)]} - \left(\frac{r}{R}\right)^6 \right] \quad (1)$$

When the new combining rules, eq 1, 2, and 4 of ref 1 are applied to this potential, the following relationships are obtained

$$\left[\frac{\epsilon_{12}\alpha_{12}e^{\alpha_{12}}}{(\alpha_{12} - 6)r_{12}} \right]^{2r_{12}/\alpha_{12}} = \left[\frac{\epsilon_{11}\alpha_{11}e^{\alpha_{11}}}{(\alpha_{11} - 6)r_{11}} \right]^{r_{11}/\alpha_{11}} \left[\frac{\epsilon_{22}\alpha_{22}e^{\alpha_{22}}}{(\alpha_{22} - 6)r_{22}} \right]^{r_{22}/\alpha_{22}} \quad (2)$$

$$\frac{r_{12}}{\alpha_{12}} = \frac{1}{2} \left(\frac{r_{11}}{\alpha_{11}} + \frac{r_{22}}{\alpha_{22}} \right) \quad (3)$$

and

$$\frac{\epsilon_{12}\alpha_{12}r_{12}^6}{(\alpha_{12} - 6)} = \left[\frac{\epsilon_{11}\alpha_{11}r_{11}^6}{(\alpha_{11} - 6)} \frac{\epsilon_{22}\alpha_{22}r_{22}^6}{(\alpha_{22} - 6)} \right]^{1/2} \quad (4)$$

For a given pair of unlike molecules, the parameters ϵ_{12} , r_{12} , and α_{12} can be predicted from a knowledge of those for the corresponding like pairs by numerical solution of eq 2-4.

Test of the Combining Rules

To test the adequacy of the combining rules, the binary diffusion coefficients, D_{12} , of noble gas systems were computed from the unlike-pair parameters predicted by eq 2-4, and the results are compared with experimental data. The like-pair parameters of Ne, Ar, Kr, and Xe determined by Hogervorst⁴ from recent viscosity measurements between 100 and 1600°K were used in the calculation. The predicted parameters for the unlike-pair interactions are given in Table I together with the Hogervorst's experimentally deduced values from his extensive D_{12} data.⁵ The parameters of He-Ne, He-Ar, and He-Xe were obtained using the like-pair parameters of helium presently estimated from the parameters of Kr-Kr⁴ and He-Kr⁵ with the combining rules. The diffusion coefficients were calculated to the first-order approximation⁶ employing the Z^* integrals tabulated by Mason and Rice.^{7,8} In all necessary interpolations of Z^* values, at least four significant figures were retained. This computational accuracy is expected to be sufficient for the present purpose. In each mixture examined by Hogervorst, the heavier component is a small admixture⁹ and for a mixture with this kind of composition the second-order correction factor to D_{12} is very close to unity.⁶ Thus the neglect of the higher order correction in the present calculation would not result in any significant computational error. When the calculated D_{12} was compared with the smoothed experimental values given by Hogervorst, the agreement was excellent in every mixture over the entire temperature range of 300-1400°K with the highest per cent deviation of only 0.5% occurring in the mixture of He-Xe. The overall accuracy of the experimental measurements is reported as $\pm 2\%$.

Various combining rules have been suggested for the exp 6 potential in previous studies.^{4,10-12} Table II shows four sets of those rules reported to be quite effective for certain molecular systems. To have a comparative test on these rules, the calculated D_{12} of the noble gas mixtures from the unlike-pair parameters predicted by each set of the combining rules were again compared with the experimental data. For all systems not containing helium, the rules of Hogervorst work very well giving practically the same successful results obtained with the new combining rules. The successes of the other three sets of rules are very much mixed depending on the system considered. Figure 1 shows an example of the comparisons for the system of Ne-Xe, and Table III gives the potential param-

TABLE I: Unlike-Pair Parameters of the Exp 6 Potential

System	$\epsilon_{12}/k, ^\circ\text{K}$		$r_{12}, \text{\AA}$		α_{12}	
	pred	expt ^b	pred	expt ^b	pred	expt ^b
Ne-Ar	68.89	64.5 ± 4	3.447	3.46 ± 0.03	15.52	15.5
Ne-Kr	77.25	71.5 ± 4	3.594	3.60 ± 0.03	15.74	15.5
Ne-Xe	79.32	73 ± 4	3.841	3.87 ± 0.04	15.78	15.5
Ar-Kr	163.1	150 ± 7	3.893	3.94 ± 0.03	14.91	15
Ar-Xe	181.0	174 ± 6	4.106	4.13 ± 0.04	14.88	15
He-Ne ^a	28.13	20 ± 4	2.857	2.91 ± 0.03	16.00	16
He-Ar ^a	39.85	40 ± 3	3.322	3.31 ± 0.03	15.73	16
He-Xe ^a	43.13	49 ± 4	3.743	3.72 ± 0.04	16.12	16

^a Predictions are made using the estimated He-He parameters of $\epsilon_{11}/k = 19.67^\circ\text{K}$, $r_{11} = 2.662 \text{\AA}$, and $\alpha_{11} = 15.88$. See the text. ^b Reference 5.

TABLE II: Combining Rules for the Exp 6 Potential Parameters

Combining rules		Ref
Mason-Rice	$\frac{\alpha_{12}}{r_{12}} = \frac{1}{2} \left(\frac{\alpha_{12}}{r_{12}} + \frac{\alpha_{12}}{r_{12}} \right)$	(i) 10
	$\frac{\epsilon_{12}e^{\alpha_{12}}}{\alpha_{12} - 6} = \left(\frac{\epsilon_{12}e^{\alpha_{12}} \cdot \epsilon_{12}e^{\alpha_{12}}}{\alpha_{12} - 6} \right)^{1/2}$	(ii)
Srivastava	Equation 4 $\epsilon_{12} = (\epsilon_{11}\epsilon_{22})^{1/2}$	(iii) 11
	Equation i Equation 4	
Hogervorst	$\epsilon_{12} = \frac{2\epsilon_{11}\epsilon_{22}}{\epsilon_{11} + \epsilon_{22}}$	(iv) 4
	$\alpha_{12} = \frac{1}{2}(\alpha_{11} + \alpha_{22})$	(v)
	Equation 4	
Calvin-Reed	$r_{12} = (r_{11}r_{22})^{1/2}$	(vi) 12, 14
	$\alpha_{12} = (\alpha_{11}\alpha_{22})^{1/2}$	(vii)
	Equation iii	
New rules	Equations 2, 3, and 4	

ters predicted by the different set of combining rules for this system. The success of Hogervorst's rules, however, seems to be a limited one. When his rules are applied to He-Xe mixture, the calculated diffusion coefficients show deviations from the observed values in excess of the estimated error limit of the experimental measurements at the entire temperature range. This result is rather significant because the same rules work very well for mixtures such as He-Ne and Ne-Xe indicating it is unlikely that the poor prediction of D_{12} for He-Xe mixture is simply due to improper parameters adopted for He-He or Xe-Xe interactions. The D_{12} of He-Xe mixture calculated with Hogervorst's rules are also plotted in Figure 1.

Discussion

It has been shown that within the framework of the exp 6 potential, the new combining rules give very satisfactory correlation of the pair interactions for the noble gas atoms. Although the present test of the various combining rules is by no means an exhaustive one, the new rules show a clear advantage over the other rules. Mason and Rice's rules are based on the commonly assumed geometric-mean relationship of the repulsive potentials, $U_{12}^{\text{rep}}(R) = [U_{11}^{\text{rep}}(R)U_{22}^{\text{rep}}(R)]^{1/2}$. Since the Mason-Rice rules and the new combining rules both adopt the same formula of eq 4 for the attractive interactions, the

TABLE III: Unlike-Pair Parameters of the Exp 6 Potential Predicted by Various Combining Rules

System	Combining rules	$\epsilon_{12}/k, ^\circ\text{K}$	$r_{12}, \text{\AA}$	α_{12}
Ne-Xe ^a	Mason-Rice	134.8	3.501	15.13
	Srivastava	105.7	3.663	15.83
	Hogervorst	73.80	3.878	15.40
	Calvin-Reed	105.7	3.651	15.39
	New rules	79.32	3.841	15.78
He-Xe	Hogervorst	44.71 ^b	3.716 ^b	15.90 ^b
	New rules	43.13	3.743	16.12

^a Predictions are made using the like-pair parameters of ref 4. ^b Predictions are made using the He-He parameters ($\epsilon_{11}/k = 24.46^\circ\text{K}$, $r_{11} = 2.584 \text{\AA}$, and $\alpha_{12} = 17.0$) obtained from the Kr-Kr and He-Kr parameters with Hogervorst's rules.

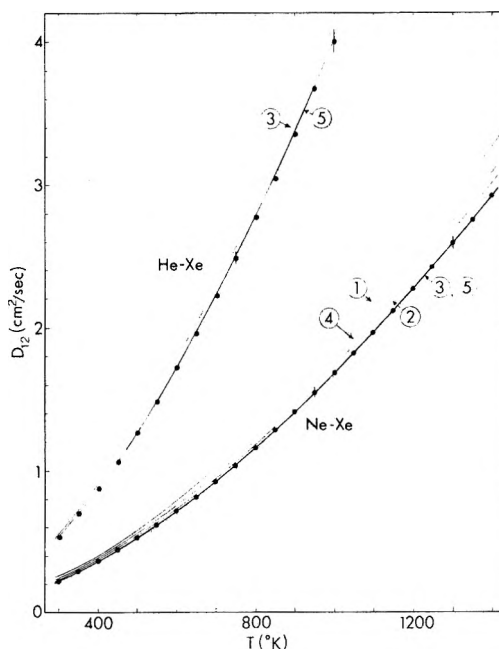


Figure 1. Comparison of calculated and experimental diffusion coefficients: dots, smoothed experimental results; curve 1, Mason-Rice rules; curve 2, Srivastava-Srivastava rules; curve 3, Hogervorst rules; curve 4, Calvin-Reed rules; curve 5, the new rules.

present test provides another evidence indicating the superior nature of Smith's rule² over the geometric-mean rule for the repulsive interactions. The rules used by Hogervorst⁴ include the purely empirical relationship of eq iv in Table II. This formula has been extensively tested by Lin and Robinson¹³ in conjunction with the Dymond-Alder potential, and has been concluded as a more successful formula for the noble gas systems except for the systems containing He as a component. The present result is in accordance with Lin and Robinson's conclusion. Calvin and Reed's rules¹⁴ were first proposed for the Mie ($n-6$) potential and recently applied¹² to the exp 6 potential with some apparent success in correlating the second virial coefficients of polyatomic gases.

The result of the present test on the new combining rules together with the results obtained in part II of this series¹ seems to indicate that the new rules contain elements of truly wide range of applicability. Extended applications of the present rules to the more realistic multi-parameter potential models are presently under investigation.

References and Notes

- (1) C. L. Kong, *J. Chem. Phys.*, in press.
- (2) F. T. Smith, *Phys. Rev. A*, **5**, 1708 (1972).
- (3) C. Zener, *Phys. Rev.*, **37**, 556 (1931).
- (4) W. Hogervorst, *Physica*, **51**, 77 (1971).
- (5) W. Hogervorst, *Physica*, **51**, 59 (1971).
- (6) J. O. Hirschfelder, C. F. Curtiss, and R. B. Bird, "Molecular Theory of Gases and Liquids," Wiley, New York, N. Y., 1964.
- (7) E. A. Mason, *J. Chem. Phys.*, **22**, 169 (1954).
- (8) E. A. Mason and W. E. Rice, *J. Chem. Phys.*, **22**, 843 (1954).
- (9) See ref 5.
- (10) E. A. Mason and W. E. Rice, *J. Chem. Phys.*, **22**, 522 (1954); E. A. Mason, *ibid.*, **23**, 49 (1955).
- (11) B. N. Srivastava and K. P. Srivastava, *J. Chem. Phys.*, **24**, 1275 (1956).
- (12) D. W. Calvin and T. M. Reed, III, *J. Chem. Phys.*, **56**, 2484 (1972).
- (13) H. M. Lin and R. L. Robinson, Jr., *J. Chem. Phys.*, **54**, 52 (1971).
- (14) D. W. Calvin and T. M. Reed, III, *J. Chem. Phys.*, **54**, 3733 (1971).

The Effective Molecular Quadrupole Moment of Water

P. T. Eubank

Department of Chemical Engineering, Texas A & M University, College Station, Texas 77843 (Received November 27, 1972; Revised Manuscript Received June 29, 1973)

Publication costs assisted by the National Science Foundation

The theoretical equations for the dipole-quadrupole contribution to the second virial coefficient, $\Delta B_{\mu Q}$, are reviewed for molecules with either weak or strong electrical moments and which possess either axial symmetry or not. A method for calculation of the effective quadrupole moment for molecules lacking axial symmetry is shown to be exact for weak electrical moments. The use of Q_{zz} as the effective moment is proven incorrect together with the recent conclusion of Kubin that $\Delta B_{\mu Q}$ is unimportant for water at 100°.

Introduction

In a recent issue of this journal, Kubin¹ used an effective quadrupole moment for water of $Q = Q_{zz} = -0.266 \times 10^{-26}$ esu cm², where

$$Q_{\alpha\beta} = \sum_i (3e_i r_{i\alpha} r_{i\beta} - q_{i\gamma} \delta_{\alpha\beta}) \quad (1)$$

and

$$q_{\alpha\beta} = \sum_i e_i r_{i\alpha} r_{i\beta} \quad (2)$$

This definition of $Q_{\alpha\beta}$ provides values twice that of Buckingham,² Stogryn and Stogryn,³ and others. The present paper contends that the use of $Q = Q_{zz}$ for molecules with less than threefold symmetry (such as water) is faulty as a first-order approximation and, thus, the resultant conclusion of Kubin that the dipole-quadrupole contribution to the second virial coefficient, $\Delta B_{\mu Q}$, is negligible at 100° is erroneous.

General Theory

For molecules with axial symmetry

$$Q = Q_{zz} = -(1/2)Q_{xx} = -(1/2)Q_{yy} \quad (3)$$

and the electrical pair potential contribution due to the interactions of the permanent dipole and quadrupole moments is given by Buckingham and Pople⁴

$$U_{e1} = \mu^2 r^{-3} \cdot g_1 - (3/4)\mu Q r^{-4} g_2 + (3/16)Q^2 r^{-5} \cdot g_3 \quad (4)$$

where μ is the dipole moment, r is distance between centers of mass, and g_1 , g_2 , and g_3 are each trigonometric functions of the angles of orientation of the two molecules. Addition of the familiar Lennard-Jones central pair poten-

tial to eq 4 followed by exact integration over the angles of orientation and r yields⁵

$$B^*(y) = F(y, \tau) + G_1(y, \tau, \gamma) + G_2(y, \tau, \gamma) \quad (5)$$

where $B^* = [3B(T)/2\tilde{N}\pi\sigma^3]$ is the reduced second virial coefficient, $B(T)$ is the second virial coefficient, \tilde{N} is Avogadro's number, σ is the collision diameter, $y = 2(\epsilon/\kappa T)^{1/2}$ is the reduced temperature, ϵ is the minimum energy, κ is the Boltzmann constant, $\tau = (\mu^2/\epsilon\sigma^3)$ is the reduced dipole moment, $\gamma = (Q^2/4\epsilon\sigma^5)$ is the reduced quadrupole moment, $F(y, \tau)$ is the dipole-dipole contribution (a power series in τ), $G_1(y, \tau, \gamma)$ is the dipole-quadrupole contribution (a matrix in τ and γ), and $G_2(y, \tau, \gamma)$ is the quadrupole-quadrupole contribution. The leading term of the G_1 matrix is $-(64)^{-1}\gamma\tau \cdot H_8(y)$, where H_8 is one of the temperature-dependent functions introduced by Buckingham and Pople. For molecules with small dipole and quadrupole moments, the above element of G_1 matrix is sufficient. With molecules that are axial symmetric and possess strong dipoles and quadrupoles (*i.e.*, ammonia), a number of leading elements of the G_1 matrix must be added to obtain an accurate value of the second virial coefficient. These methods were developed about 20 years ago by Buckingham and Pople; digital computers now make possible the accurate calculation of $\Delta B_{\mu Q}$ regardless of the temperature or the strength of the dipole moment or quadrupole moment. Truncation of the G_1 matrix to the single term given above is inexcusable for axial symmetric molecules with strong dipoles and quadrupoles.

Calculation of $\Delta B_{\mu Q}$ for molecules *not axially symmetric* (such as water) involves further complications as there are two independent elements from Q_{zz} , Q_{xx} , and Q_{yy} of the

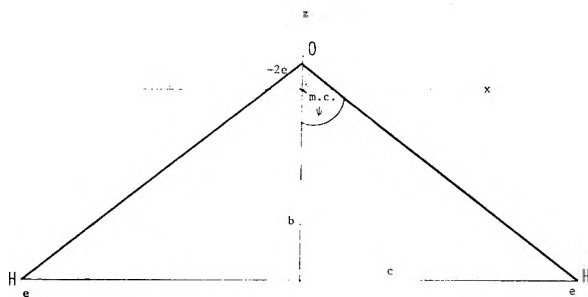


Figure 1. Atomic charge distribution for the water molecule.

traceless, diagonal matrix of the quadrupole moment tensor, \mathbf{Q} . For molecules with weak dipole and quadrupole moments, Kielich⁶ has shown that

$$\Delta B_{\mu Q} = - \left[\frac{\tilde{N}}{12(\kappa T)^2} \right] \langle r^{-8} \rangle [\mu^2(\mathbf{Q} : \mathbf{Q})] \quad (6)$$

where $\langle r^{-8} \rangle$ for a Lennard-Jones central pair potential is $[\pi H_8(y)/3y^4\sigma^5]$. In general, $\mathbf{Q} : \mathbf{Q} = Q_{xx}^2 + Q_{yy}^2 + Q_{zz}^2$. Equation 6 yields $-(64)^{-1}\gamma\tau H_8(y)$ for an axially symmetric molecule [$Q_{zz} = -(1/2)Q_{xx} = -(1/2)Q_{yy}$] in agreement with the discussion above. The effective quadrupole moment Q is defined⁷ as

$$Q^2 = (2/3) \mathbf{Q} : \mathbf{Q} \text{ or } Q^2 = \frac{2}{3} [9 \text{ trace}(q_{\gamma\gamma}^2) - 3(\text{trace } \mathbf{q})^2] \quad (7)$$

so that for molecules with weak dipoles and quadrupoles eq 5 and 6 are consistent. It can also be shown that $Q^2 = -4I_2/3$, where

$$I_2 = Q_{xx}Q_{yy} + Q_{xx}Q_{zz} + Q_{yy}Q_{zz} \quad (8)$$

is the second invariant of \mathbf{Q} . Equation 7 is temperature independent under the assumption of weak electrical moments.

The theory is thus complete except for molecules such as water which are neither axially symmetric nor possess weak electrical moments. Preliminary investigations⁸ into the extension of Kielich's methods to include molecules of stronger moments indicate considerable complexity leading to prohibitive calculation time and costs even with a modern digital computer. As with Kubin,¹ an effective quadrupole moment for water must be assumed. However, Kubin's use of $Q = Q_{zz}$ does not agree with eq 6 (the correct first-order approximation to $\Delta B_{\mu Q}$ for a molecule of less than threefold symmetry).

Calculations for Water

Measured values of Q_{zz} for water are always small, $|Q_{zz}| < 0.3 \times 10^{-26}$ esu cm²,^{3,9-13} where the principal axes and quadrupole moment definition of Kubin are used. Values of Q_{yy} and Q_{xx} are much larger ($2-6 \times 10^{-26}$) with $Q_{yy} \approx -Q_{xx}$ in the traceless, diagonal tensor. This can be understood from the triangular, atomic model shown by the diagram. From eq 1 and 2, $q_{zz} = 2e(b^2 - l^2)$, $q_{xx} = 2ec^2$, $q_{yy} = 0$, $q_{\alpha\beta} = 0$ ($\alpha \neq \beta$), $Q_{zz} = 2e[2(b^2 - l^2) - c^2]$, $Q_{xx} = 2e[2c^2 - b^2 + l^2]$, and $Q_{yy} = 2e[l^2 - b^2 - c^2]$. As $l \ll b$ and $l \ll c$, $\tan \psi \approx c/b$, and $Q_{zz} \approx 2e[2b^2 - c^2]$ is zero if $\tan \psi = \sqrt{2}$ or $\psi = 54.2^\circ$ whereas actually $\psi = (\angle \text{HOH})/2 \approx 52.3^\circ$. Likewise, $Q_{xx} \approx 3ec^2$ and $Q_{yy} \approx -3ec^2$. From eq 7, $Q \approx 2\sqrt{3}ec^2$.

Rowlinson¹⁴ used a similar triangular, atomic model to

calculate the charge e from the molecular dipole moment, $\mu = eb$. A single quadrupole moment corresponding to $q_{xx} = 2ec^2 = 1.81$, was then found and used as the effective moment in the dipole-quadrupole term of the pair potential. Since the pair potential used by Rowlinson is consistent with the definition of $Q_{\alpha\beta}$ that yields values one-half that of eq 1, $Q = 2q_{xx} = 3.62$. Kubin first misinterprets Rowlinson's model by failing to double the moment to correspond to the definition of eq 1. Second, Kubin assumes that Rowlinson's q_{xx} is Q_{zz} . The present atomic model, which is more detailed than that of Rowlinson, yields $Q \approx 2\sqrt{3}ec^2$ compared to Rowlinson's $Q = 4ec^2$ or a difference of $\sim 15\%$.

A modification of Rowlinson's procedure based on bond dipole moments for charge assignments⁷ does yield values of the diagonal elements: $Q_{zz} = -0.12$, $Q_{xx} = +2.80$, $Q_{yy} = -2.68$, $Q(\text{eq 7}) = 3.16$.

With the measured moments used by Kubin of ref 10, $Q = 5.92$ from eq 7. The measured moments of ref 9, 11, 12, and 13 yield $Q = 4.24$, 4.72, 4.50, and 2.60, respectively. These values may be compared to the effective moment selected by O'Connell and Prausnitz¹⁵ of -2.0 and Buckingham² of 4.0.

With $Q = 2.60$, we⁵ recently calculated dipole-quadrupole contributions to $B(T)$ from 150 to 450° using the data of Kell, *et al.*¹⁶ ($\Delta B_{\mu Q}/B$) is 15% at 150° decreasing to 11% at 450° or ($\Delta B_{\mu Q}/\Delta B_{\mu\mu}$) = 21% over the temperature range compared to Rowlinson's value of 24%.

Note. The values of the quadrupole moments given above depend on the molecular location of the coordinate origin. As equations such as 4 for the pair potential are based on the center of mass (ref 2), that coordinate origin (see Figure 1) was used above in regard to both estimated and measured quadrupole moments. For water the nucleus of the oxygen atom is sometimes used as the coordinate origin as in the quantum-mechanical calculations of ref 13 for the quadrupole and octupole moments. Use of this origin results in an increase of 8.96% in each quadrupole moment quoted above. Since $\Delta B_{\mu Q} \approx Q^2$, ($\Delta B_{\mu Q}/B$) would be about 18% at 150° decreasing to 14% at 450° or ($\Delta B_{\mu Q}/\Delta B_{\mu\mu}$) = 25% over the entire temperature range where the Q values are again based on ref 13. Interestingly, the simple model of Rowlinson yields a quadrupole moment independent of the position of the coordinate origin on the z axis of Figure 1.

References and Notes

- (1) R. F. Kubin, *J. Phys. Chem.*, **76**, 2901 (1972).
- (2) A. D. Buckingham, *Quart. Rev. Chem. Soc.*, **13**, 183 (1959).
- (3) D. E. Stogryn and A. P. Stogryn, *Mol. Phys.*, **11**, 371 (1966).
- (4) A. D. Buckingham and J. A. Pople, *Trans. Faraday Soc.*, **51**, 1173 (1955).
- (5) J. R. Johnson and P. T. Eubank, *Ind. Eng. Chem., Fundam.*, **12**, 156 (1973).
- (6) S. Kielich, *Physica*, **31**, 444 (1965).
- (7) P. T. Eubank, *AIChE J.*, **18**, 454 (1972).
- (8) J. R. Johnson, Ph.D. Thesis, Texas A & M University, College Station, Tex., 1970.
- (9) S. G. Kukolich and W. H. Flygare, *Mol. Phys.*, **17**, 127 (1969).
- (10) J. Verhoeven and A. Dymanus, *J. Chem. Phys.*, **52**, 3222 (1970).
- (11) D. Neumann and J. W. Moskowitz, *J. Chem. Phys.*, **49**, 2056 (1968).
- (12) S. Aung, R. M. Pitzer, and S. I. Chan, *J. Chem. Phys.*, **49**, 2071 (1968).
- (13) R. M. Gjaesner and C. A. Coulson, *Trans. Faraday Soc.*, **49**, 217 (1953).
- (14) J. S. Rowlinson, *Trans. Faraday Soc.*, **47**, 120 (1951).
- (15) J. P. O'Connell and J. M. Prausnitz, *Ind. Eng. Chem., Fundam.*, **8**, 453 (1969).
- (16) G. S. Kell, G. E. McLaurin, and E. Whalley, *J. Chem. Phys.*, **48**, 3805 (1968).

Application of the Quasilattice Model to Association in Dilute Reciprocal Molten Salt Mixtures. The System Silver Sulfate–Potassium Nitrate¹

C. E. Vallet*² and J. Braunstein

Reactor Chemistry Division, Oak Ridge National Laboratory, Oak Ridge, Tennessee (Received May 10, 1973)

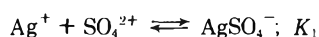
Publication costs assisted by Oak Ridge National Laboratory

New emf measurements of the molten salt concentration cell $\text{Ag}|\text{KNO}_3, \text{AgNO}_3(\text{ref})|\text{KNO}_3, \text{AgNO}_3, \text{K}_2\text{SO}_4|\text{Ag}$ were carried out over a wide range of silver nitrate concentrations (2×10^{-4} to 10^{-2} mole ratio) and with a new temperature cycling procedure. Experimental results are compared with previous data and analyzed in terms of conventional association constants and the generalized quasilattice model. The pair association energy corresponding to the equilibrium constant K_1 of $(\text{AgSO}_4)^-$, ΔA_1 , is found temperature dependent with $-(\partial \Delta A_1 / \partial T) \sim 2.5 \times 10^{-3}$ kcal/K. The dinuclear association constant K_{12} and association energy, ΔA_{12} for $\text{Ag}-\text{SO}_4-\text{Ag}$, are found to be significant in this molten reciprocal system.

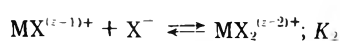
Introduction

Measurements of association equilibria in dilute reciprocal molten salt mixtures (*i.e.*, dilute solutions of at least one foreign cation and one foreign anion in a molten salt solvent) provide valuable tests of physical models such as the quasilattice model of molten salts.^{3,4} The system silver sulfate–potassium nitrate is of particular interest for a number of reasons, as indicated by previous investigations by means of emf measurements^{5,6} and phase diagrams.⁷

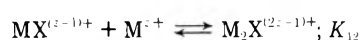
First, it is one of few systems in which a temperature dependence of the association energy has been reported,⁵ but this temperature dependence has been questioned in a more recent study.⁶ Second, systems of mixed charge type offer a number of problems connected with the Temkin activities of various charged and neutral species and the counting of sites on the quasilattice.^{3,4,8} Third, the phase diagram investigation⁷ provided a confirmation of the applicability of conformal ionic solution theory⁹ to the concentrated solution region of Ag_2SO_4 in molten KNO_3 . Data in the dilute solution region, where a quasilattice correction term becomes important,¹⁰ appeared to be more consistent with a temperature-dependent association energy⁵ rather than with a more recent report of a constant association energy.⁶ It therefore seemed worthwhile to carry out a careful reinvestigation of the possible temperature dependence. Finally, the previous investigations were carried out over only a limited range of silver concentrations, making it impossible to analyze the data for higher order associations than the pairwise association



In most dilute reciprocal molten salt systems in which further association has been observed, it has been found that the association

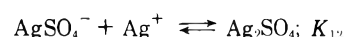


is considerably stronger than dinuclear association

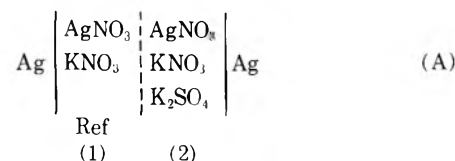


where M is Ag or Cd. In the case of Cd, K_{12} is found to be negligible, probably by virtue of the high charge of the cation. It therefore seemed reasonable to design new ex-

periments to permit evaluation of K_{12} for the silver–sulfate association



Accordingly, in this paper we report association equilibria and energies obtained from new emf measurements of the concentration cell



The silver concentrations were varied over a wide range (mole ratio 2×10^{-4} to 10^{-2}) in order to make possible the determination of K_{12} and consequent evaluation of the second association energy. Measurements were carried out at a series of silver concentrations at two temperatures (622 and 663 K). However, in order to establish definitely whether or not the association energy ΔA_1 is temperature dependent, in some of the experiments a cell with a given silver concentration was cycled in temperature before and after several sulfate additions, the difference of values of the emf's providing a more direct measure of the temperature dependence of ΔA_1 . This new technique was essential because of the very small emf change observed in this system and the very small magnitude of ΔA_1 .

Experimental Section

Chemicals. Potassium nitrate used was ACS reagent from Baker. Before use it was vacuum dried at 200°, dried under an argon flow as the temperature was increased to 300°, then melted and vacuum filtered at 370°. The potassium sulfate used was ACS reagent from Mallinckrodt, recrystallized before use.¹¹ Analysis indicates concentrations less than 10 and 5 ppm, respectively, of Cl^- and OH^- . The silver nitrate used was Spectropure crystals from the American Platinum Works.

Furnace and Temperature Control. The furnace was a $3.5 \times 3.5 \times 4$ -in. Cooley resistance furnace (700 W). The cell was set in an aluminum block in the furnace core to minimize the temperature gradient in the melt. The tem-

TABLE I: Reproducibility of Emf Data Obtained in a Temperature Cycle

Time, hr	$R_2(\text{Ag})$	$R_2(\text{SO}_4)$	Emf at 622 K, mV	Emf at 663 K, mV
0			...	-32.14
2.5	2.6×10^{-3}		-33.05	...
4.5			...	-37.34
5.5			-38.53	...
6.75	2.6×10^{-3}	5.6×10^{-3}	...	-37.17
7.75			-38.52	...
8.5			-42.01	...
10.0			...	-40.58
22.0	2.6×10^{-3}	10×10^{-3}	...	-40.95
23.5			-42.14	...

perature was controlled by means of a chromel-alumel thermocouple in the aluminum block, its hot junction being at the same level as the middle of the liquid in the cell, connected to a Leeds and Northrup D.A.T. controller and Speedomax H recorder.

The temperature of the melt, measured with a second chromel-alumel thermocouple dipping in the cell, was found constant to $\pm 0.2^\circ$ over the runs. The temperature of the melt was recorded continuously with a Honeywell potentiometric recorder.

Cell and Electrodes. The reference compartments were of Pyrex tubing (8 mm o.d.) with an asbestos fiber sealed into the bottom as described previously.¹² They contained molten (K-Ag)NO₃ solutions (mole ratio $R_1(\text{AgNO}_3) \sim 4 \times 10^{-3}$) with a silver wire electrode dipped in the melt.

The measuring compartment was a 250-ml Pyrex beaker into which was dipped a bare silver wire electrode. The melt (KNO₃-AgNO₃-K₂SO₄)($R_2(\text{Ag})$, $R_2(\text{SO}_4)$) in the beaker was vigorously stirred and sparged with oxygen-free argon in each experiment.

The emf's obtained were mostly in the range -50 to +50 mV. The quantities of KNO₃ employed in the beaker as solvent were approximately 1 mol. Emf measurements were made with a Keithley dc differential voltmeter.

Electrode Behavior. (a) *Potassium Nitrate-Silver Nitrate Melt.* Previously,¹³ similar cells have been used extensively and it was shown they follow well Nernst's law

$$E = \frac{RT}{F} \ln \frac{x_2(\text{AgNO}_3)}{x_1(\text{AgNO}_3)} \quad (1)$$

where 1 refers to the reference compartment, $x_i(\text{AgNO}_3)$ being the mole fraction of AgNO₃ in compartment i .

First, we checked our electrodes for comparison with Nernst's law by isothermal runs; we found very good agreement, better than 0.1 mV. Furthermore, runs carried out at two temperatures provided a test of Nernst behavior of the electrodes by means of the difference $[(T'/T)E(T) - E(T')]$. The average deviation was found less than 0.1 mV for ten runs and three electrodes. Although we observed after two working weeks a shift of the Nernst line, the E vs. $\ln R_2(\text{AgNO}_3)$ relation was still a linear one during a run.

(b) *Potassium Nitrate-Silver Nitrate-Potassium Sulfate Melt.* An estimation of the errors was provided by simultaneous emf measurements with two reference electrodes in many of the cells. In such cases we found an average

discrepancy through a run of 5×10^{-2} mV. The emf's were unchanged if measured relative to different silver electrodes in the beaker. In this way, random errors arising from variations of bulk melt composition or temperature variation are separated from errors associated with the reference electrodes.

When we operated at 663 and 622 K in a run, we checked the reproducibility of the emf measurements on returning to the initial temperature. An emf measurement was taken first at temperature T , and then the temperature was fixed at T' and another emf measurement made; the temperature was then returned to T and a new measurement was made, followed by another at T' . Table I gives results of one such cycle (this one being the worst case in terms of Nernst behavior before adding sulfate). The relative variation in measured emf changes is less than 1% at the lower temperature and less than 5% at the higher temperature.

The Evaluation of Association Constants and Quasilattice Parameters from Emf Measurements

Calculation of Conventional Constants K_1 , K_{12} . The emf change upon K₂SO₄ addition to compartment 2 of cell A is given by

$$\Delta E = \frac{RT}{F} \ln \frac{x(\text{Ag})x(\text{NO}_3)}{\bar{x}(\text{Ag})\bar{x}(\text{NO}_3)} \gamma(\text{AgNO}_3) \quad (2)$$

where $\bar{x}(\text{Ag})$ and $\bar{x}(\text{NO}_3)$ are ionic fractions before the K₂SO₄ addition and $\gamma(\text{AgNO}_3)$ is the activity coefficient of silver nitrate.

In terms of ionic and mole ratios R , the activity coefficient may be expanded in power series for dilute solutions in AgNO₃ and K₂SO₄.¹⁴

$$\ln \frac{1}{\gamma(\text{AgNO}_3)} = K_1 R(\text{K}_2\text{SO}_4) + \left(K_1 K_2 - \frac{1}{2} K_1^2 \right) R(\text{K}_2\text{SO}_4)^2 + (2K_1 K_{12} - K_1^2) R(\text{AgNO}_3) R(\text{K}_2\text{SO}_4) + \dots \quad (3)$$

where K_i 's are the conventional association constants

$$K_1 = \frac{R(\text{AgSO}_4)}{R(\text{Ag})R(\text{SO}_4)}; \quad K_2 = \frac{R(\text{Ag}(\text{SO}_4)_2)}{R(\text{AgSO}_4)R(\text{SO}_4)}; \\ K_{12} = \frac{R(\text{Ag}_2\text{SO}_4)}{R(\text{AgSO}_4)R(\text{Ag})} \quad (4)$$

Equation 2 can be rewritten in terms of the mole ratios R , since the experiments are most conveniently carried out at constant mole ratios of silver nitrate rather than at constant mole fractions of silver nitrate. The resulting expression for the emf change is

$$\Delta E = \frac{RT}{F} \times \left[\ln \frac{(1+R(\text{AgNO}_3))^2}{(1+R(\text{AgNO}_3)+R(\text{K}_2\text{SO}_4))(1+R(\text{AgNO}_3)+2R(\text{K}_2\text{SO}_4))} - \ln \frac{1}{\gamma(\text{AgNO}_3)} \right] \quad (5)$$

For experiments carried out in dilute solutions, i.e., $R(\text{K}_2\text{SO}_4)$ and $R(\text{AgNO}_3) \ll 1$, and at constant mole ratios of silver nitrate, the slope of ΔE vs. the mole ratio of

potassium sulfate can be written as the infinite series in the stoichiometric mole ratios

$$\left[\frac{\partial \Delta E}{\partial R(\text{K}_2\text{SO}_4)} \right]_{R(\text{AgNO}_3)} = -\frac{RT}{F} [(3 + K_1) - R(\text{AgNO}_3)(3 + K_1^2 - 2K_1K_{12}) - R(\text{K}_2\text{SO}_4)(5 + K_1^2 - 2K_1K_2) + \dots] \quad (6)$$

after substituting eq 3 for the activity coefficient of AgNO_3 into eq 5 and expanding the logarithmic expression in the mole ratios. K_1 and K_{12} are evaluated by first determining the limiting slope (s) of eq 6 at vanishing $R(\text{K}_2\text{SO}_4)$ from a plot of ΔE vs. $R(\text{K}_2\text{SO}_4)$ at each silver nitrate concentration.

$$(s) = \lim_{R(\text{K}_2\text{SO}_4) \rightarrow 0} \left[\frac{\partial \Delta E}{\partial R(\text{K}_2\text{SO}_4)} \right]_{R(\text{AgNO}_3)} = \frac{RT}{F} [(3 + K_1) - R(\text{AgNO}_3)(3 + K_1^2 - 2K_1K_{12}) + \dots] \quad (7a)$$

These limiting slopes (s) are then plotted as a function of the silver nitrate mole ratio. The extrapolated limit of this second plot

$$i = \lim_{R(\text{AgNO}_3) \rightarrow 0} (s)$$

leads to K_1

$$K_1 = - \left[3 + \frac{F}{RT} i \right] \quad (7b)$$

The slope of this second plot at vanishing mole ratio of silver nitrate leads to K_{12}

$$K_{12} = \frac{1}{2K_1} \left[3 + K_1^2 - \frac{F}{RT} \lim_{R(\text{AgNO}_3) \rightarrow 0} \left(\frac{d(s)}{dR(\text{AgNO}_3)} \right) \right] \quad (7c)$$

The numerical values of the mole ratios (R_i) and the ion fractions (x_i) differ little. However, the definition of the activity coefficient in terms of Temkin ion fractions, and the fact that the ion fraction of silver is changed by the addition of potassium sulfate in the experiment, gives rise to the additive numerical factors 3 and 5 in eq 6. With strong associations (e.g., $K > 100$), these numerical factors are negligible. The silver-sulfate association constants, however, have values about 13 and hence the numerical factor 3 in eq 7b cannot be ignored. The factor 3 in eq 7b is not an approximation but results from the evaluation of the limit. Because the measurements in this study were carried out over a wide range of silver contents and extrapolated to zero silver concentration, eq 7b gives an evaluation of K_1 that is independent of the quasilattice model. In previous investigations of this system only a very limited range of silver concentration was investigated, and it had therefore been necessary to employ the quasilattice model in the evaluation of the association constants. Our wide range of silver concentration also made possible the evaluation of K_{12} from eq 7c, which was not possible with earlier investigations.

Quasilattice Model Calculations. With the quasilattice model,¹⁵ the association constants obtained from the above relations are related to energy parameters for non-random mixing on the quasilattice. In the present case, ions of differing charge type are present in the melt; hence the asymmetric approximation¹⁶ for a single kind of lig-

and and the same bond energy, ΔA_1 , for successive associations (AgSO_4^- , (Ag_2SO_4) , $(\text{Ag}_2\text{SO}_4)^{(2-2)+}$) was first applied. In this approximation K_1 and K_{12} are given in terms of the bond energy ΔA_1 as

$$K_1 = Z(e^{-\Delta A_1/RT} - 1) \quad (8a)$$

$$K_{12} = \frac{Z-1}{2}(e^{-\Delta A_1/RT} - 1) \quad (8b)$$

where Z is coordination number of the lattice.

The generalized quasilattice model proposed by Blander¹⁵ considers the possibility of different bond energies for successive associations with a single kind of ligand. This model is therefore more appropriate for the evaluation of the successive association energies, ΔA_1 , ΔA_{12} , etc. Since associations such as $(\text{AgSO}_4)^-$, $(\text{Ag}-\text{SO}_4-\text{Ag})$ are more probable than $(\text{SO}_4-\text{Ag}-\text{SO}_4)^{3-}$ because of the relative ion sizes and charges, the solute anion, sulfate, rather than the solute cation, silver, is taken as the central ion in the asymmetric approximation. In the generalized model, the relation between K_1 and ΔA_1 is the same as in the asymmetric (or symmetric) approximation with a single bond energy, i.e., eq 8a. However, the relation between K_{12} and the bond energy ΔA_{12} for formation of $\text{Ag}-\text{SO}_4-\text{Ag}$ becomes¹⁵

$$K_{12} = \frac{Z-1}{2!} \left[\frac{e^{-\Delta A_1/RT}(e^{-\Delta A_{12}/RT} - 1)}{e^{-\Delta A_1/RT} - 1} - 1 \right] \quad (9)$$

Equation 9 reduces to eq 8b in the special case $\Delta A_{12} = \Delta A_1$.

The assumption made in this calculation is that the second Ag^+ ion can attach itself to a SO_4^{2-} ion in $(Z-1)$ equivalent positions. If only a single orientation, such as linear, is possible for the second silver ion, a slightly different relation for K_{12} results.^{15,17}

$$K_{12}^l = \frac{Z-1}{2!} \left[\frac{e^{-\Delta A_1/RT} \left(\frac{e^{-\Delta A_{12}^l/RT}}{Z-1} - 1 \right)}{e^{-\Delta A_1/RT} - 1} - 1 \right] \quad (10)$$

Results

Emf Measurements. Since previous investigators^{5,6} reported very small emf changes in cell A on potassium sulfate additions and a discrepancy in the temperature dependence of the association energy, we carried out a rather large number of experiments¹⁸ in order to resolve the discrepancy conclusively. We made measurements mainly at 349 and 390°, the higher temperature being below 400° to avoid salt decomposition, mentioned as a possibility in the discussion of results in ref 6. A few measurements were made also at 430°.

Calculations. Determination of Association Constants from the Emf Measurements. In the K_2SO_4 concentration range studied, $0 < R_2(\text{K}_2\text{SO}_4) < 10^{-2}$ we found a linear dependence of the emf changes on the potassium sulfate mole ratio. From the experimental data, $[\partial \Delta E / \partial R_2(\text{K}_2\text{SO}_4)]_{R_2(\text{AgNO}_3)}$ was derived with a least-squares eq 7b and 7c, values of $(s) = [\partial \Delta E / \partial R_2(\text{K}_2\text{SO}_4)]_{R_2(\text{AgNO}_3)}$ are plotted against the mole ratio of silver nitrate ions were employed to reduce the subjectivity of the results.) The data scattering being very small, the least-squares lines are very close to each experimental result; at $R_2(\text{K}_2\text{SO}_4) = 0$, for example, the zero shift, $|\Delta E|$, is always found to be less than 0.1 mV. The least-squares fits to the data are shown in Table II.

TABLE II: Least-Squares Limiting Slopes (s) = $[\partial\Delta E/\partial R_2(K_2SO_4)]_{R_2(AgNO_3)}$ at $R_2(K_2SO_4) = 0$ Fitted to the Emf Measurements

T = 622 K			T = 663 K					
$R_2(AgNO_3)$ $\times 10^{-3}$	(s), V	Zero shift, $V \times 10^{-5}$	$R_2(AgNO_3)$ $\times 10^{-3}$	(s), V	Zero shift, $V \times 10^{-5}$	$R_2(AgNO_3)$ $\times 10^{-3}$	(s), V	Zero shift, $V \times 10^{-5}$
0.207	-0.850 ₈	-3.9	0.17	-0.888 ₀	-4.5	3.87	-0.910 ₀	-5.8
0.486 ^a	-0.853 ₇	-5.6	0.38	-0.904 ₇	-2.4	4.4	-0.909 ₀	-1.5
0.96	-0.857 ₂	3.2	0.486 ^a	-0.908 ₀	-19	4.77	-0.922 ₅	-1.4
1.43	-0.872 ₀	3.4	0.759	-0.963 ₀	-6	4.77	-0.934 ₀	-0.74
1.43	-0.873 ₇	3.9	0.89	-0.949 ₉	-1.5	6.96 ^d	-0.979 ₄	2
2.6 ^b	-0.881 ₇	-2.5	2.2	-0.935 ₈	-0.8	7.38	-0.947	0.17
2.66 ^c	-0.866 ₀	5.3	2.6 ^b	-0.912 ₀	-11	7.77	-0.901	-1.3
6.96 ^d	-0.842 ₆	-5.8	2.66 ^e	-0.883 ₅	-4.3	8.7 ^e	-0.906 ₄	-0.4
8.3	-0.858 ₄	-1.4						
8.7 ^e	-0.795 ₂	-14						

^{a-e} Values obtained in temperature cycles.

In order to obtain the association constants as given by eq 7b and 7c, values of (s) = $[\partial\Delta E/\partial R_2(K_2SO_4)]_{R_2(AgNO_3)}$ are plotted against the mole ratio of silver nitrate $R_2(AgNO_3)$ at both temperatures, 622 and 663 K, as shown in Figure 1. The least-squares equations of these lines are: for 10 silver concentrations at 622 K

$$(s) = \lim_{R_2(K_2SO_4)=0} \left[\frac{\partial\Delta E}{\partial R_2(K_2SO_4)} \right]_{R_2(AgNO_3)} = -0.8700(\pm 0.0172) + 4.3985(\pm 3.7367)R_2(AgNO_3)$$

and for 16 silver concentrations at 663 K

$$(s) = \lim_{R_2(K_2SO_4)=0} \left[\frac{\partial\Delta E}{\partial R_2(K_2SO_4)} \right]_{R_2(AgNO_3)} = -0.9170(\pm 0.0200) - 1.3915(\pm 4.3463)R_2(AgNO_3)$$

The corresponding value of the association constant for the equilibrium



calculated by means of eq 7b is

$$\text{at 622 K: } K_1 = 13.232 \pm 0.321$$

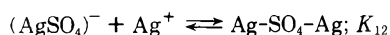
$$\text{at 663 K: } K_1 = 13.051 \pm 0.350$$

Since the evaluation of K_{12} involves both the intercept and the less accurate slope of the least-squares line, the accuracy of K_{12} will depend on the relative magnitudes of the second and third terms on the right-hand side of eq 7c. Since

$$\frac{1}{K_1} \frac{F}{RT} \lim_{R_2(AgNO_3) \rightarrow 0} \left(\frac{ds}{dR_2(AgNO_3)} \right) \approx 5$$

compared to about 13 for K_1 , the uncertainty of K_{12} will be greater than that of K_1 .

From the larger set of data (16 points) at 663 K we find for the equilibrium



$$K_{12} = 7.6 \pm 3.0; T = 663K^{19}$$

Comparison with the Quasilattice Model. $(AgSO_4)^-$ Association Energy. In either the asymmetric, symmetric, or generalized approximations, the association energy (ΔA_1) of the $(AgSO_4)^-$ grouping is given by eq 8a. Watt and Blander⁵ found an unexpected temperature dependence for ΔA_1 ; more recently, Sacchetto, *et al.*,⁶ concluded that ΔA_1 was temperature independent. As shown in

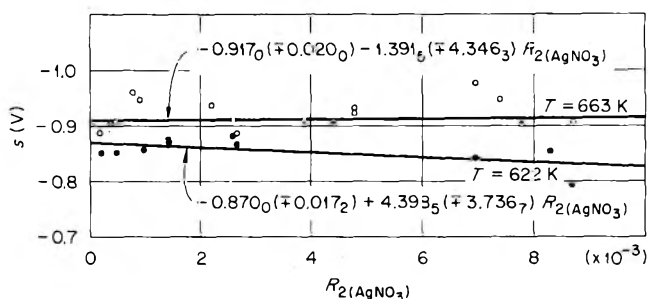


Figure 1. Least-squares extrapolation of limiting slopes (s) to zero silver nitrate mole ratio.

$$(s) = \lim_{R_2(K_2SO_4)=0} \left[\frac{\partial\Delta E}{\partial R_2(K_2SO_4)} \right]_{R_2(AgNO_3)}$$

vs. mole ratio of silver nitrate at 622 (●) and 663 K (○).

Table III, the disagreement between these authors is greatest at the highest temperature (440°).

Our measurements at 430° were in excellent agreement with Watt and Blander's result at this temperature as seen in Figure 2. In further calculations we omitted the discordant result arising probably from a systematic error. Assuming a linear variation of pair formation energy with temperature, and taking $Z = 5$, we found the following results for least-squares fits. By taking all the data

$$\Delta A_1/\text{kcal} = 0.3345(\pm 3.3 \times 10^{-2}) - 3.01 \times 10^{-3} (\pm 2.5 \times 10^{-5})T/\text{K} \quad (\text{Fit I})$$

and by taking only our data

$$\Delta A_1/\text{kcal} = -0.2873(\pm 1.9 \times 10^{-2}) - 2.11 \times 10^{-3} (\pm 9.05 \times 10^{-6})T/\text{K} \quad (\text{Fit II})$$

These lines are drawn in Figure 2 along with the experimental results. The data from ref 5 are given without error estimation, but from the scattering of the emf measurements we believe this error may be in the range of 100 cal.

In order to compare the results of this investigation with a previous estimate of the $(AgSO_4)^-$ association energy from the K, Ag/NO₃, SO₄ phase diagram,⁷ we calculated ΔA_1 at 607 K, the melting point of KNO₃

$$\text{Fit I: } \Delta A_1/\text{kcal} = -1.493 \pm 0.029$$

$$\text{Fit II: } \Delta A_1/\text{kcal} = -1.568 \pm 0.018$$

The range of values of ΔA_1 estimated from the liquidus

TABLE III: Temperature Dependence of (AgSO₄)⁻ Pair Formation Energy (ΔA₁) Assuming Z = 5

T/K	-ΔA ₁ /kcal	Ref
622	1.55 ± 0.05	6
622	1.599 ± 0.023	Our work
636	1.53	5
646	1.61 ± 0.05	6
663	1.691 ± 0.026	Our work
680	1.63 ± 0.05	6
681	1.69	5
703	1.77 ± 0.05	Our work
706	1.80	5
715	1.52 ± 0.05 ^a	6
722	1.90	5

^a Value omitted from least squares calculation.

TABLE IV: (AgSO₄)⁻ and (Ag-SO₄-Ag) Association Energies Calculated Assuming Z = 5

T/K	ΔA ₁ /kcal	ΔA ₁₂ /kcal ^a	ΔA ₁₂ /kcal ^b
622	-1.599 ± 0.022		
663	-1.691 ± 0.026	-1.97 ± 0.29	-3.8 ± 0.29

^a From eq 9, random orientation for second Ag⁺ and with experimental results taken at 663 K. ^b From eq 10, fixed (e.g., linear) orientation for second Ag⁺ and with experimental results taken at 663 K.

measurements,⁷ -1.5 to -1.2 kcal, overlaps the values obtained from the emf investigations. It may be concluded that all the experimental results, including those of Sacchetto, *et al.*,⁶ if one omits their highest temperature result, are in accord with a temperature dependence of the (AgSO₄)⁻ pair formation energy, the small temperature coefficient being in the range of -2 to -3 × 10⁻³ kcal/K between 622 and 722 K.

Temperature Coefficient of ΔA₁ from Temperature Cycles. From the results of cycles such as that illustrated in Table I, the limiting slopes

$$\lim_{R \rightarrow K_2SO_4} \left[\frac{\partial \Delta E}{\partial R_2(K_2SO_4)} \right]$$

at differing silver nitrate concentrations always exhibited a more negative value for the higher temperature, the average difference being $s_{622} - s_{663} = 0.070 (\pm 0.052)$ V.

This difference between the slopes at 622 and 663 K corresponds to a difference of the association energy $\Delta A_1(622) - \Delta A_1(663) = 0.127 (\pm 0.061)$ kcal. The small variation of the limiting slope with $R(\text{AgNO}_3)$ is neglected in this estimate, whose purpose was to verify the sign and magnitude of the difference of ΔA₁ at the two temperatures. The above differences of slope and of ΔA₁ obtained from the series of temperature cycles in a single cell may be compared with the corresponding differences obtained from the series of isothermal measurements in different cells reported in the previous section: $s_{622} - s_{663} = 0.047 (\pm 0.038)$ V and $\Delta A_1(622) - \Delta A_1(663) = 0.092 (\pm 0.049)$ kcal.

Ag-SO₄-Ag Association Energy. Our results were sufficiently accurate to allow a determination of K₁₂ at 663 K with eq 7b and 7c. The association energy ΔA₁₂ was calculated from eq 9 and 10 of the generalized quasilattice model and assuming either random or fixed orientation of the Ag-SO₄-Ag groupings. The results are given in Table

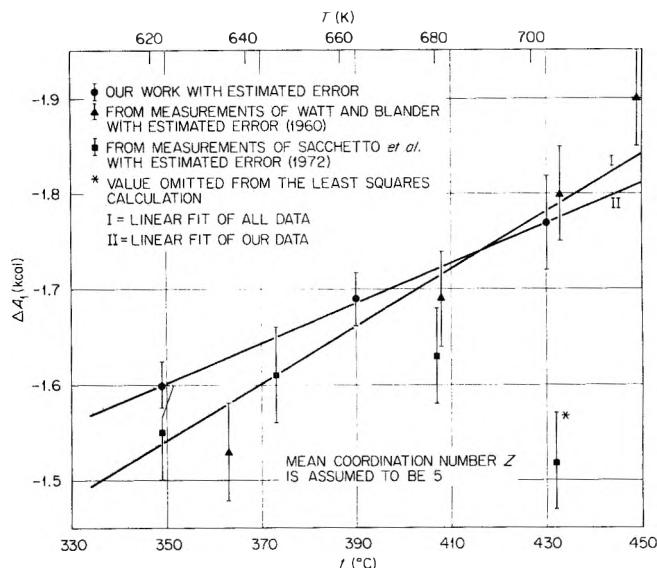


Figure 2. Temperature dependence of (Ag-SO₄)⁻ pair association energy: ▲, data from ref 5; ■, data from ref 6; ●, omitted value in least squares calculations; ○, our work. Fit I is obtained from all these data. Fit II is obtained from our results.

IV. Although the uncertainty of ΔA₁₂ does not permit a determination of whether it too, like ΔA₁, is temperature dependent, it is clear that this second association is significant and may have a higher stability than the first association.²⁰

A more negative association energy for the second (dinuclear) association than for the pair-wise association has been reported²¹ for the association of Ag⁺ and I⁻ ions in molten KNO₃. The association energy corresponding to a fixed (e.g., linear) grouping would indicate an unusually high degree of stabilization for addition of the second Ag⁺ which seems highly unlikely.

Conclusions

We have reported new emf measurements for the dilute charge unsymmetric reciprocal molten salt system K,Ag/NO₃,SO₄ (dilute in Ag⁺ and SO₄²⁻).

Investigations over a wide range of silver nitrate concentrations permitted an evaluation for the first time of the (Ag-SO₄-Ag) triplet association energy. The (Ag-SO₄-Ag) groupings probably do not have fixed orientation (e.g., linear) since such an assumption would lead to unusually high stabilization for addition of the second Ag⁺. Even with unrestricted orientation of the (Ag-SO₄-Ag) groupings, the dinuclear association energy is comparable to and may be more negative than for the (AgSO₄)⁻ pair.

Our study confirms the increased stability of (AgSO₄)⁻ pairs with increasing temperature.⁵ This dependence is in the same direction as observed for AgCN pairs²² and for the charge unsymmetric CdX⁺ (X = Br⁻ or I⁻) pairs.²³ In the quasilattice calculations only configurational entropy is taken into account; the variation of ΔA₁ with the temperature, $[-\partial \Delta A_1 / \partial T] \sim 2.5 \times 10^{-3}$ kcal/K, may be understood as the "specific entropy of association" characterizing a change in the internal degrees of freedom of the SO₄²⁻ ion.

Acknowledgment. C. E. V. is pleased to acknowledge a grant from the Ministère des Affaires Etrangères Français during the academic year 1972-1973.

Supplementary Material Available. Detailed tables of data will appear following these pages in the microfilm edition of this volume of the journal. Photocopies of the supplementary material from this paper only or microfiche (105 × 148 mm, 20× reduction, negatives) containing all of the supplementary material for the papers in this issue may be obtained from the Journals Department, American Chemical Society, 1155 16th St., N.W., Washington, D. C. 20036. Remit check or money order for \$3.00 for photocopy or \$2.00 for microfiche, referring to code number JPC-73-2672.

References and Notes

- (1) Research sponsored by the U. S. Atomic Energy Commission under contract with the Union Carbide Corporation.
- (2) On leave from the Laboratoire de Thermodynamique, associe au C.N.R.S., Universite de Provence, Marseille, France, under a research grant from the Ministere des Affaires Etrangeres Francais (1972-1973).
- (3) M. Blander in "Molten Salt Chemistry," M. Blander, Ed., Interscience, New York, N. Y., 1964, p 221.
- (4) J. Braunstein in "Ionic Interactions," Vol. I, S. Petrucci, Ed., Academic Press, New York, N. Y., 1971, p 179.
- (5) W. J. Watt and M. Blander, *J. Phys. Chem.*, **64**, 729 (1960).
- (6) G. A. Sacchetto, C. Macca, and G. G. Bombi, *J. Electroanal. Chem.*, **36**, 319 (1972).
- (7) M. L. Saboungi, C. E. Vallet, and Y. Doucet, *J. Phys. Chem.*, **77**, 1699 (1973).
- (8) J. Braunstein, H. Braunstein, R. E. Hagman, and A. S. Minano, *Inorg. Chem.*, **12**, 1407 (1973).
- (9) M. Blander and S. Yosim, *J. Chem. Phys.*, **39**, 2610 (1963).
- (10) M. Blander and L. E. Topol, *Electrochim. Acta*, **10**, 1161 (1965).
- (11) D. E. LaValle, Analytical Chemistry Division, ORNL.
- (12) J. Braunstein, *J. Chem. Educ.*, **44**, 223 (1967).
- (13) M. Blander, F. F. Blankenship, and R. F. Newton, *J. Phys. Chem.*, **63**, 1259 (1959).
- (14) Reference 4, p 228.
- (15) M. Blander, *J. Chem. Phys.*, **34**, 432 (1961); M. Blander and J. Braunstein, *Ann. N. Y. Acad. Sci.*, **79**, 838 (1960).
- (16) M. Blander, *J. Phys. Chem.*, **63**, 1262 (1959).
- (17) Reference 4, p 233.
- (18) See paragraph at end of paper regarding supplementary material.
- (19) The value calculated from the smaller set of data (10 points) at the lower temperature, $K_{12} = 3.6 \pm 2.9$ is considered less reliable and, unlike the results at 663 K, the slope was more sensitive to the omission or retention of any one of the data points.
- (20) The results at 622 K indicate a less negative, but still significant second association energy -1.4 ± 0.45 kcal/mol, if all the low-temperature data are retained. However, if the point at the highest silver concentration is discarded the low temperature result is more consistent with the high-temperature result, -1.64 ± 0.26 kcal/mol.
- (21) A. Alvarez-Funes, J. Braunstein, and M. Blander, *J. Amer. Chem. Soc.*, **84**, 1538 (1962).
- (22) D. L. Manning and M. Blander, *Inorg. Chem.*, **1**, 594 (1962).
- (23) J. Braunstein and R. M. Lindgren, *J. Amer. Chem. Soc.*, **84**, 1531 (1962).

Photoconductive Properties of Arylethynylcopper Polymers. Effects of Structure and Oxygen

Yoshiyuki Okamoto*¹ and Samar K. Kundu

Research Division, Department of Chemical Engineering, New York University, University Heights, New York, New York 10453
(Received August 3, 1973)

Eleven selected arylethynylcopper compounds were synthesized from their corresponding acetylenic compounds with cuprous salt. The dark resistivities of the compounds were in the range of 10^7 - 10^{11} Ω cm. Under illumination by a tungsten light (100 W), the resistivities dropped to 10^5 - 10^9 Ω cm. The dark conductivities were increased when electron-donating groups were introduced on the aromatic ring. The conductivities were also enhanced if the size of aryl groups were increased. More conductive compounds were generally smaller in their photoconductive responses. The photocurrents of the copper compounds on surface cells tended to be considerably lower when measured under vacuum, compared with those under dry air. This phenomenon was attributed to the fact that oxygen in air reduced the recombination rate of the carrier, *i.e.*, oxygen traps the electron and increases the hole conductivity. However, these results contradicted Myl'nikov's observation that the photocurrent of phenylethynylcopper was increased when measured under vacuum. The photocurrent-intensity dependence and the Seebeck effect of these compounds were measured under vacuum and dry air. These results confirmed our observations.

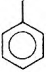

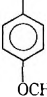
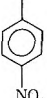
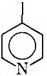

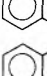
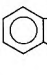
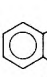
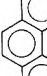
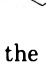
Introduction

Arylethynylcopper compounds ($R-C\equiv C-Cu$) are coordination polymers having substantial back coordination from filled metal d orbitals to antibonding orbitals of acetylene groups toward the metal as shown in Figure 1.^{2a} The coordination bondings were not affected by adding various electron-donating substances such as pyridine, bipyridyl, and triethylamine. However, we have found recently that the electrical conductivities of arylethynylcopper compounds were greatly increased by adding a small

amount of nitrocellulose.^{2b} This was attributed to formation of a charge-transfer complex between the copper compounds and nitrocellulose.

Recently, Myl'nikov and Terenin have reported interesting electrical properties for phenylethynylcopper.³ The dark and photoconductivities of the copper compound were found to be depressed by oxygen and water vapor.⁴ These phenomena accounted for the fact that the oxygen forms new effective recombination centers, thus diminishing the whole carrier lifetime. However, we have found

TABLE I: Physical Constants and Electrical Properties of Copper Arylethynylides

Compounds	Infrared absorption triple bond, cm^{-1}		Melting point (dec), $^{\circ}\text{C}$	Resistivity at 25° , $\Omega \text{ cm}$	Dark current, I_d , A	Light current, I_p , A
	$\nu \text{C}\equiv\text{C}-\text{H}$	$\nu \text{C}\equiv\text{C}-\text{Cu}$				
	2115	1933	229	2.3×10^{11}	3.0×10^{-8}	1.4×10^{-7}
	2114	1935	236	1.6×10^{11}	2.5×10^{-6}	3.0×10^{-6}
	2103	1890	260	2.3×10^{10}	1.6×10^{-8}	4.0×10^{-7}
	2108	1940	301	6.2×10^{14}	1.0×10^{-10}	2.0×10^{-10}
	2127	1938	221	5.2×10^9	3.6×10^{-8}	5.2×10^{-8}
	2130	1950	233	6.7×10^{11}	2.1×10^{-9}	2.4×10^{-9}
	2100	1928	250	2.1×10^{11}	8.0×10^{-10}	3.0×10^{-8}
	2100	1930	201	6.0×10^{10}	6.0×10^{-9}	1.2×10^{-7}
	2145	1985	272	6.7×10^7	8.0×10^{-6}	1.2×10^{-5}
	2100	1918	322	5.0×10^9	2.2×10^{-6}	5.9×10^{-6}
	2100	1915	301	5.2×10^9	1.8×10^{-7}	1.1×10^{-6}

that the oxygen in phenylethynylcopper increases both the dark and photoconductivities. Therefore, in order to investigate the discrepancy, various arylethynylcopper compounds were synthesized and effects of oxygen and their chemical structures on the electrical properties of the compounds were investigated.

Experimental Section

Eleven selected arylethynylcopper compounds such as phenyl-, *p*-methylphenyl-, *p*-methoxyphenyl-, *p*-nitrophenyl-, α -pyridyl-, β -pyridyl-, α -naphthyl-, β -naphthyl-, 9-anthracenyl-, *N*-carbazolyl-, and 2-pyrenylethynylcopper compounds were synthesized from the corresponding acetylenic compounds⁵ with cuprous salt. Since the resulting copper compounds were insoluble in organic solvents, the products were washed thoroughly with water, ethanol, and benzene, and were dried under vacuum. The copper derivatives were generally stable in dry air up to around 200° . The decomposition points were determined by using Du Pont 90C thermal analyzer.

Electrical measurements were performed on both sandwich and surface cells. The latter was of comb design with

14 pairs of legs. Each leg was a 100 mm length of gold or nichrome deposited on a quartz plate (15×20 mm) with a gap of 0.25 mm. Powdered samples were placed uniformly on the plate.

The electrical characteristics of the surface cells were measured in a chamber described in the literature.^{6,7} The monochromatic light source for surface cells was a Bausch and Lomb grating monochromator No. 33-86-45 with a Hanovia 800-W xenon light pressure arc lamp. Entrance and exit slits were 5 and 2 mm, respectively. An Eppley bismuth-silver thermopile provided a calibration of light intensity. The final data were normalized to equal intensity throughout the 300-600- $\text{m}\mu$ range after the light intensity at 470 $\text{m}\mu$ (highest intensity of xenon lamp) was standardized at 15 mW/cm^2 .

The sandwich cells consisted of compressed pellets of sample to a thickness of 0.02-0.04 cm and transparent quartz plates coated with tin oxide. The contact between the electrodes and sample was attained by applying pressure. For both types of cells, we regulated dc voltage by means of a Keithley high-voltage supply Model 241 and recorded the photocurrents measured by a Keithley elec-

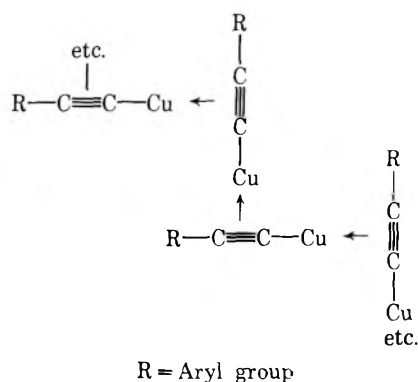


Figure 1. Structure of arylethynylcopper polymers.

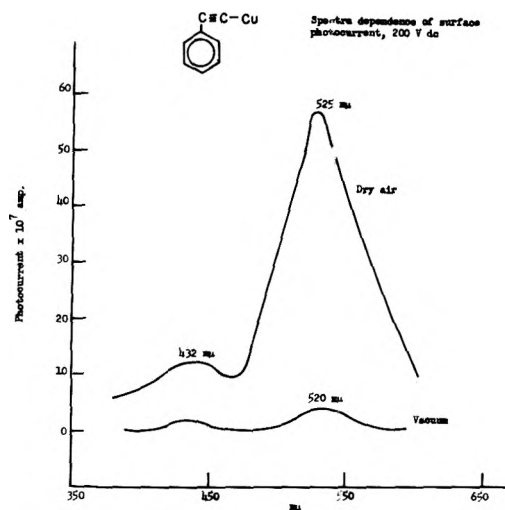


Figure 2. Spectral distribution of the photocurrent of phenylethynylcopper (surface cell).

trometer Model 610B on the Electronic Associates X-Y variplotter Model 1100. Sandwich cells were irradiated by tungsten light (100 W) from a distance of 10 cm.

The apparatus for measuring the variation of the current with light intensity consisted of a 200-V dc battery power supply with a set of Kodak neutral density filter. The measurements were taken on surface cell under air and vacuum with monochromatic radiation at the range of 525–565 μ .

Results and Discussion

The electrical properties of the arylethynyl compounds are summarized in Table I. The dark as well as the photocurrents showed linear (ohmic) behavior up to applied 200 V.

The dark resistivities of the arylethynylcopper compounds studied were in the range of 10^7 – 10^{11} Ω cm. In the presence of illumination by a tungsten light (100 W), the resistivities dropped to 10^5 – 10^9 Ω cm.

From Table I, it can be seen that the conductivity of the copper compound was increased when electron-donating groups were introduced on the ring. The conductivity was also enhanced if the size of aryl groups were increased, e.g., from phenyl to anthracenyl. Similar trends were also reported in triphenyl dyestuffs⁸ and pyrazine compounds.⁹

As a qualitative generalization, the electric conductivities appear to correlate with the number as well as the de-

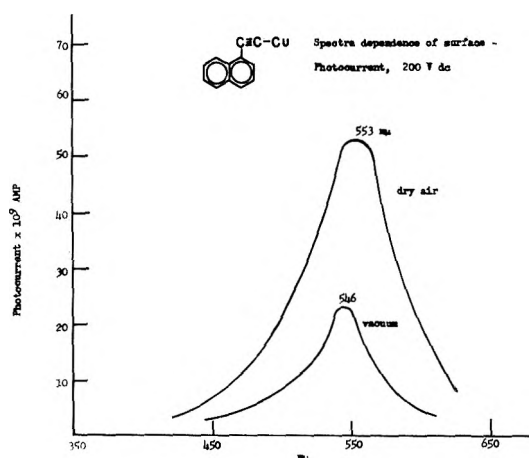


Figure 3. Spectral distribution of the photocurrent of α -naphthylethynylcopper (surface cell).

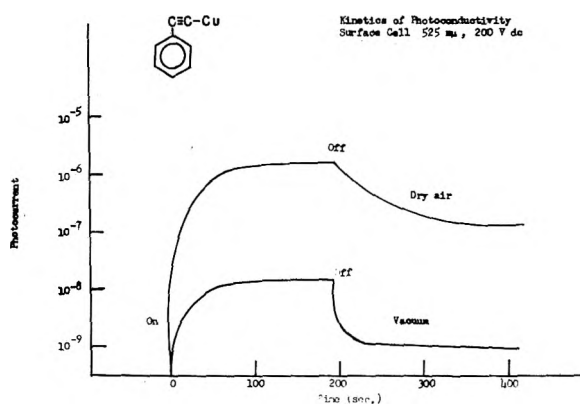


Figure 4. Kinetics of photoconductivity of phenylethynylcopper.

gree of delocalization of the π electrons. Hence an increase in the number of aromatic rings or methyl or methoxy substitution enhances conductivity while substitution of electron-withdrawing groups diminishes it. Thus, the nitro group on the ring resulted in the decrease of conductivity and the photoconductive response was quenched. It is also found that the more conductive compounds were generally smaller in the photoconductive response, e.g., *p*-methylphenylethynylcopper (1.6×10^{11} Ω cm), $I_p/I_d = 100$ vs. 9-anthracenylethynylcopper (5.0×10^9 Ω cm), $I_p/I_d = 3$.

Figures 2 and 3 show the typical spectral distributions of the photocurrent of the copper compounds. For phenylethynylcopper, the spectral curve of photocurrent has two clearly pronounced maxima at 432 and 525 μ (vs. 430 and 500 μ , reported by Myl'nikov). However, the spectral curve for α -naphthylethynylcopper has only one maxima at 553 μ in the 350–600- μ range. The photocurrents of all copper compounds measured in the present study using surface cells tend to be considerably lower when measured under vacuum, compared with those under dry air. In apparent contradiction to the present results, Myl'nikov observed that the photocurrent of phenylethynylcopper is increased when measured under vacuum. The source of this discrepancy is not clear. However, the conductivity of organic compounds were often found to be increased when measured in dry air. This phenomenon is generally attributed to the fact that the oxygen in air reduced the recombination rate of the carrier, i.e., oxygen traps the electron and increases the hole conductivity.¹⁰

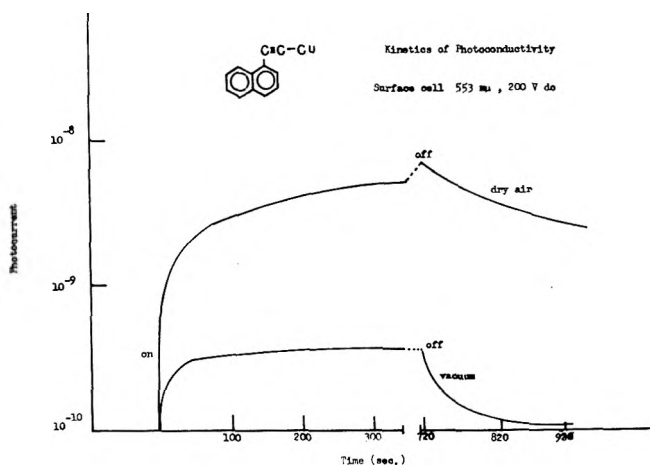


Figure 5. Kinetics of photoconductivity of α -naphthylethynylcopper.

Figures 4 and 5 show the typical path of the increase and drop of the photocurrent on the layer of the copper compounds in air and under vacuum at the same intensity of monochromatic illumination. As are seen from these figures, both the photocurrent response and the decay in dark were very slow. This indicates that the photocarriers were deeply trapped in the polymers. It was also found that evacuation of air from the vessel leads to reduction in the conductivity and a faster response to light.

The photocurrent-intensity dependence was studied in order to further clarify the effect of the oxygen. The intensity dependency of the photocurrent measured under dc conditions is shown plotted in Figure 6 on a log-log scale for phenyl-, *p*-methylphenyl, and α - and β -naphthylethynylcopper compounds. The figure shows that a good linear plot is obtained for all intensities, *i.e.*, the photocurrent varies as a power(s) of the light intensity. The slopes, S , were calculated using an equation $I_0 = KL^S$, where I_0 = photocurrent, K = constant, and L = light intensity and the values were the range from 0.5 to 1.2. The measurements under vacuum have slopes close to 0.5 while same samples measured in dry air have slopes equal to unity. These results further supported that when the samples were explored in air, the oxygen in air traps the electron and the conductivity is due mainly to hole carriers.¹¹ The Seebeck effects were measured on these copper compounds under vacuum and the results indicated that the conductivities are p type. These observations also support the above results.

Acknowledgment. We gratefully acknowledge support of this research by the Space Physics Laboratory, Air Force Cambridge Research Laboratories (Contract No. F19628-

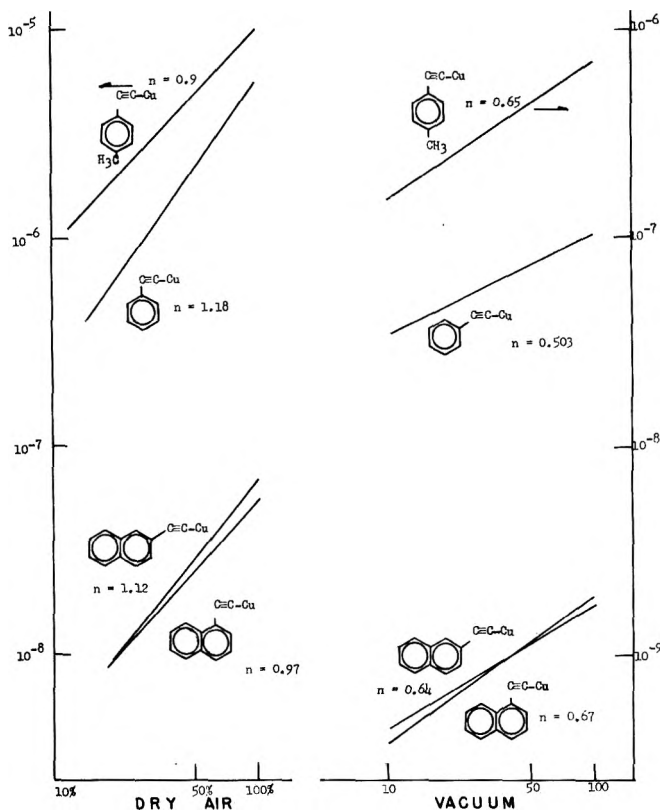


Figure 6. Photocurrent vs. light intensity of aryethynylcopper compounds.

69-C-0154). We also are indebted to Dr. Aleksandar Golubovic for the measurements of photoconductive properties and many helpful discussions.

References and Notes

- (1) Address correspondence to the Department of Chemistry, Polytechnic Institute of New York, Brooklyn, N. Y. 11201.
- (2) (a) G. E. Coates, M. L. H. Green, and K. Wade, "Organometallic Compounds," Methuen, London, 1968, p 271; (b) Y. Okamoto, M. Mincer, A. Golubovic, and N. Dimond, *Nature (London)*, **229**, 157 (1971).
- (3) V. S. Myl'nikov and A. N. Terenin, *Dokl. Akad. Nauk. SSSR*, **153**, 1361 (1963).
- (4) V. S. Myl'nikov, *Dokl. Akad. Nauk. SSSR*, **164**, 622 (1965).
- (5) The preparation and physical and spectroscopic properties of these acetylenic compounds were reported previously: Y. Okamoto, K. L. Chellappa, and S. K. Kundu, *J. Org. Chem.*, **37**, 3185 (1972).
- (6) H. Meier, *Z. Wiss. Phot., Photophys. Photochem.*, **53**, 1 (1958).
- (7) J. Kaufhold and K. Hauffe, *Z. Elektrochem.*, **69**, 168 (1965).
- (8) N. Noddack, H. Meier, and A. Haus, *Z. Phys. Chem.*, **212**, 55 (1959).
- (9) A. Golubovic, *J. Phys. Chem.*, **73**, 1352 (1969).
- (10) F. Gutmann and L. E. Lyons, "Organic Semiconductors," Wiley, New York, N. Y., 1967, p 209.
- (11) N. Almeleh and S. E. Harrison, *J. Phys. Chem. Solids*, **26**, 1571 (1965).

Acidity Scales in Mixed Water-Acetonitrile Buffer Solutions¹

Frank Jordan²

The James Bryant Conant Laboratory of the Department of Chemistry, Harvard University, Cambridge, Massachusetts 02138
(Received May 24, 1973)

Spectrophotometric H_0 and potentiometric pH_{app} (with a glass electrode) measurements were performed in H₂O-CH₃CN mixtures containing acetate buffers and mineral acid (HCl). The results indicate that, to a good degree of approximation, the effective pH of the solutions can be calculated from the concentration of the acid in the aqueous portion of the solvent, neglecting the cosolvent altogether. The results with mineral acid indicate that the notion of the chemical hydration of the proton also extends to mixed solvent systems.

In a recent nmr study on the mechanism of the hydrolysis of the enamine ethyl β -cyanomethylaminocrotonate it became necessary to establish an approximate pH scale in aqueous buffer-acetonitrile (AN) mixtures.³ A brief survey of the literature indicated that there had not been any previous attempts to define an H_0 scale in such mixtures of AN with pH 4 and 5 buffers. This note is concerned with such a study involving a comparison of hydronium ion activity measured by a glass electrode and *via* the H_0 indicator method.⁴

The major conclusion of this work is that the effective pH of solutions of acids in aqueous acetonitrile can be calculated, to a good degree of approximation, from the concentration of the acid in the aqueous portion of the solvent, neglecting the cosolvent altogether.

Experimental Section

pH and H_0 Determinations. The pH of all solutions was measured with a Radiometer pHM 4b pH meter employing a combination glass electrode. The H₂O-CH₃CN mixtures studied exhibited no drift and quick response to the electrode employed.

The spectrum of the indicator *p*-chloroaniline in the various solutions was recorded on a Cary 15. *p*-Chloroaniline exhibits the following spectral properties:⁵

Solvent	nm	ϵ	nm	ϵ
2 N HCl	215.5	9200	239	11,700
0.1 N NaOH	263	360	290	1,500

Under acidic conditions (0.1 or 1.0 N HCl) no absorption was detected at 290 nm. This wavelength was chosen for all the subsequent H_0 work.

First the pK_a of *p*-chloroanilinium ion was determined spectrophotometrically at 290 nm at 30° and 0.1 ionic strength using various aqueous buffers. Since the protonated form has no absorbance at this wavelength any absorption will be due entirely to the basic form of the indicator. Measurement of the absorption at seven different pH's between 2.2 and 6.0 gave an average value of 4.05 ± 0.05 for the pK_a in satisfactory agreement with the literature value of 4.15 at 25°. ⁶

Next the extinction coefficient of *p*-chloroaniline in aqueous alkali-CH₃CN and dilute mineral acid-CH₃CN mixtures was measured at 290 nm to provide the values for totally protonated and totally deprotonated forms in the mixtures. Finally, the absorption at 290 nm was measured in the aqueous buffer-CH₃CN mixtures of interest.

According to the definition of H_0 ⁴ (assuming one for the activity coefficient ratio)

$$H_0 = pK_a + \log ([I]/[IH^+]) \quad (1)$$

where [I] and [IH⁺] represent fractions of deprotonated and protonated forms of the indicator, respectively. Since the protonated form does not absorb at 290 nm, H_0 for any CH₃CN-H₂O mixture can be obtained from the formula

$$H_0 = pK_a + \log \frac{\epsilon_{CH_3CN-buffer}}{\epsilon_{CH_3CN-base} - \epsilon_{CH_3CN-buffer}} \quad (2)$$

where $\epsilon_{(CH_3CN-buffer)}$ is the molar extinction coefficient for any mixture with the desired buffer and $\epsilon_{(CH_3CN-base)}$ is the extinction coefficient for the totally deprotonated form in the same volume per cent mixture.

The pH of each solution was also measured with a conventional glass electrode and such apparent pH values are quoted along with the H_0 values in Table I and Figure 1.

Distilled, deionized water was used in the preparation of aqueous buffers. Commercial, reagent grade chemicals were employed without further purification.

Fischer spectrograde CH₃CN (stored over molecular sieves) was used in the H_0 determinations, along with Eastman highest purity *p*-chloroaniline.

Results and Discussion

The H_0 measurements indicate that addition of acetonitrile decreases the acidity of acetic acid-acetate type buffer systems (Table I). Qualitatively, this agrees with the effect on proton activity of AN addition (AN is a cosolvent of lower basicity and dielectric constant than H₂O). The results also parallel those of Bates and Schwarzenbach⁷ in water-ethanol mixtures.

The pK_a of anilinium type indicators has been shown to be essentially independent of AN concentration to perhaps 60-70% (v/v) AN added,⁸ which finding would justify the choice of the indicator in the present study.

Vedel studied the behavior of two different functions: a ferrocene-ferrocinium couple and a colorimetric indicator in H₂O-CH₃CN mixtures with varying amount of HClO₄ added.⁹ In the mole fraction AN region here employed both functions indicated much lowered acidities with increased AN concentration as is observed in the present study.

It was of some interest to compare the H_0 values with

TABLE I: H_0 and pH Scales in H_2O - CH_3CN -Acetate Buffers^a

v/v % mol % ϵ basic (0.1 N NaOH)	% CH_3CN in Mixture						
	0	10	20	30	40	50	60
	0.0	3.83	7.93	12.87	18.68	25.63	34.07
	0.730	0.727	0.730	0.730	0.724	0.718	0.718
			pH 3.95 Buffer ^b				
ϵ buffer		0.454	0.595	0.665	0.706	0.716	0.716
pH_{obsd}	3.94	4.12	4.34	4.58	4.80	5.06	5.31
$pa_H^*{}^c$		4.18	4.42	4.71	4.99	5.34	5.74
H_0^e		4.30	4.69	5.07	5.62	5.94	
			pH 2.92 Buffer ^d				
ϵ buffer		0.096	0.210	0.371	0.555	0.650	0.700
pH_{obsd}	2.92	3.05	3.25	3.54	3.79	4.03	4.28
$pa_H^*{}^c$		3.11	3.33	3.67	3.98	4.31	4.71
H_0^e		3.24	3.67	4.06	4.53	4.93	5.33

^a Ionic strength in aqueous layer maintained at 0.1; pH_{obsd} measured with a glass electrode, H_0 as defined in text based on indicator ratio. ^b Acetic acid-acetate buffers. ^c pH_{obsd} corrected with δ values as given in ref 11. ^d Chloroacetic acid-chloroacetate buffers. ^e Calculated with a pK_a of 4.05 for the ρ -chloroanilinium ion.

TABLE II. Acidity Scales in H_2O - CH_3CN -HCl Mixtures^a

v/v % mol % δ^b	% CH_3CN in Mixture						
	0	10	20	30	40	50	60
	0.0	3.83	7.93	12.87	18.68	25.63	34.07
	-0.00	-0.06	-0.08	-0.13	-0.19	-0.28	-0.43
			0.002 M HCl				
pH_{obsd}	2.715	2.650	2.600	2.544	2.500	2.400	2.270
pa_H^*	2.715	2.71	2.68	2.68	2.69	2.68	2.70
pH_{calcd}	2.700	2.65	2.60	2.544	2.477	2.400	2.300
Δ^c	0.00	-0.05	-0.10	-0.15	-0.20	-0.30	-0.43
			0.02 M HCl				
pH_{obsd}	1.725	1.680	1.650	1.605	1.500	1.485	1.380
pa_H^*	1.725	1.74	1.73	1.73	1.69	1.76	1.81
pH_{calcd}	1.710	1.660	1.610	1.560	1.490	1.420	1.320
Δ^c	-0.01	-0.03	-0.06	-0.11	-0.21	-0.23	-0.33

^a pH_{obsd} measured with glass electrode; pa_H^* operational pH as defined in text; pH_{calcd} molar concentration of HCl per volume of H_2O added. ^b From ref 11. ^c Δ values equal to $pH_{obsd} - (-\log(H^+))$.

pH meter readings. In mixtures of H_2O with cosolvent one needs to define a reference point for apparent hydrogen ion activity. Bates approached this problem by defining an "operational pH" quantity¹⁰ pa_H^* where a_H^* "is the hydrogen ion activity referred to the standard state in the mixed solvent" (Bates); with

$$pa_H^* = pH_{obsd} - \bar{E}_S + \log \gamma_H = pH_{obsd} - \delta \quad (3)$$

where pH_{obsd} is measured with a glass electrode employing standard aqueous buffers for calibration, \bar{E}_S is the liquid junction potential, and γ_H is the activity coefficient of the proton. δ then is the difference between the liquid junction potential effect and the medium effect on hydrogen ions. Values of δ have been tabulated by Douheret¹¹ for aqueous mixtures of AN and some other solvents.

Table I and II and Figures 1 and 2 provide pH (measured with glass electrode), pa_H^* (corrected with the δ values extracted from ref 11), along with the δ values for aqueous acetate buffer-AN mixtures.

A study with strong acid (HCl) added to H_2O -AN mixtures is included. In this case pH_{obsd} decreases with added AN, again as suggested by Bates and Schwarzen-

bach;⁷ the pa_H^* , on the other hand, remains essentially constant as expected, irrespective of AN concentration.

The pH_{obsd} in H_2O -AN solutions of HCl is, within experimental error limits, identical with the pH_{calcd} a quantity equal (in each mixture) to molar concentration of H^+ per liters of H_2O (only) present.

One can also define a quantity, Δ , the difference between pH_{obsd} and $-\log(H^+ \text{ molar concentration})$. Such Δ values in HCl solutions are essentially identical with Douheret's δ values¹¹ (the latter arrived at by a much more rigorous process) and thus their application to any buffer solution leads immediately to pa_H^* values for any H_2O -AN mixture, i.e., an "operational pH scale."

As Table I indicates such acidities (pa_H^*) are uniformly below H_0 values for acetate type buffers.

It should be emphasized that the phenomenon concerning the behavior of the pH_{obsd} in H_2O - CH_3CN solutions of HCl is preceded. Bascombe and Bell¹² and Wyatt¹³ advanced the notion of the chemical hydration of proton¹⁴ based on the fact that very similar H_0 values are obtained for similar acid molalities of strong acid solutions independent of the anion present. H_0 depends only

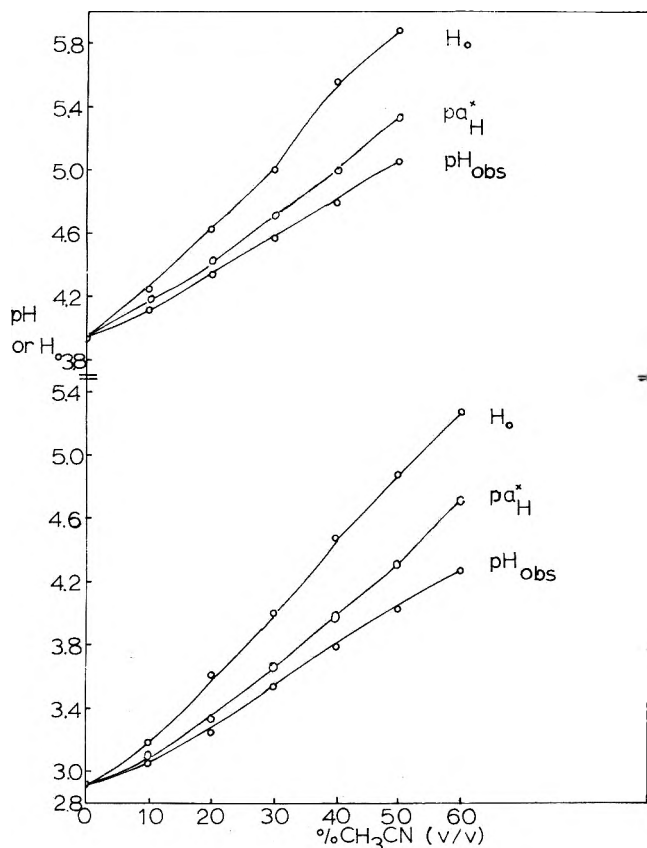


Figure 1. Behavior of the glass electrode and the indicator. (H_0) in H₂O-CH₃CN mixtures.

on the ratio of the number of hydrogen ions to the number of water molecules. The present finding extends the proton hydration theory to mixed solvent systems. The fact that the pH_{obsd} for any mixture with HCl corresponds to the pH_{calcd} values can be explained with the above theory since the increased acidity is accompanied by a decreased water activity.

Acknowledgment. Helpful advice and encouragement provided by Professor F. H. Westheimer during the course of this study is much appreciated. Financial support of the author in the form of an NIH postdoctoral fellowship is acknowledged with pleasure.

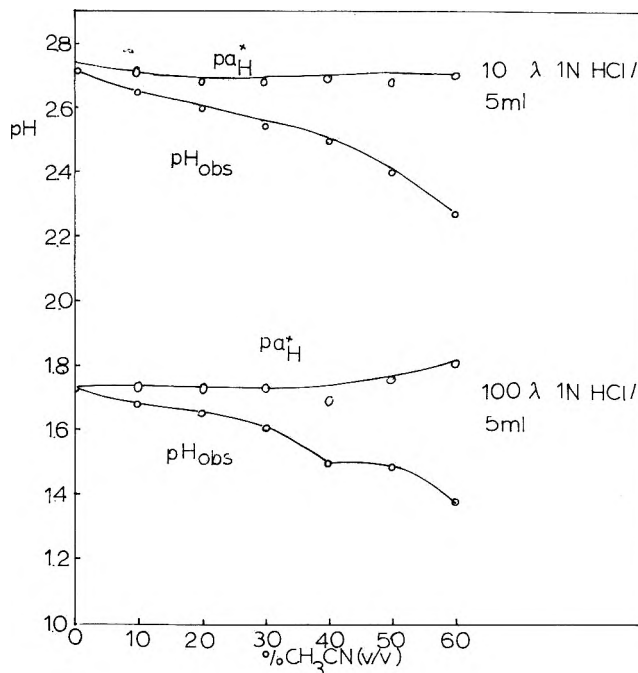


Figure 2. Response of the glass electrode to mineral acid in H₂O-CH₃CN.

References and Notes

- (1) Supported by GM 04712 from the Institute of General Medical Sciences of the National Institute of Health.
- (2) NIH Postdoctoral Fellow; Present address, Department of Chemistry, Newark College of Arts and Sciences, Rutgers University, Newark, N. J. 07102.
- (3) F. Jordan, submitted for publication.
- (4) M. A. Paul and F. A. Long, *Chem. Rev.*, **57**, 1 (1957).
- (5) L. Doub and J. M. Vandenberg, *J. Amer. Chem. Soc.*, **69**, 2715 (1947).
- (6) "Handbook of Chemistry and Physics," The Chemical Rubber Publishing Co., 50th ed, Cleveland, Ohio, 1969, p D-115.
- (7) As discussed in R. G. Bates, "Determination of pH, Theory and Practice," Wiley, New York, N. Y., 1964, p 211.
- (8) J. Desbarres, *Bull. Soc. Chim. Fr.*, 3240 (1966).
- (9) J. Vedel, *Ann. Chim. (Paris)*, **2**, 335 (1967).
- (10) Reference 7, p 223.
- (11) G. Douheret, *Bull. Soc. Chim. Fr.*, 3122 (1968).
- (12) K. N. Bascombe and R. P. Bell, *Discuss. Faraday Soc.*, **24**, 158 (1957).
- (13) P. A. H. Wyatt, *Discuss. Faraday Soc.*, **24**, 163 (1957).
- (14) The author wishes to express his appreciation to a referee for calling his attention to M. Liler's, "Reaction Mechanisms in Sulphuric Acid," Academic Press, New York, N. Y., 1971, p 52-56, which presents a concise summary of this theory.

Self-Diffusion Coefficients of Sodium Ion in Aqueous Sodium Polyacrylate Solutions Containing Sodium Chloride

Daniel S. Dixler and Paul Ander*

Department of Chemistry, Seton Hall University, South Orange, New Jersey 07079 (Received May 7, 1973)

Publication costs assisted by Seton Hall University

Self-diffusion coefficients of sodium ion in aqueous sodium polyacrylate solutions containing sodium chloride have been measured using a capillary method. The experimental values were found to be in good agreement with the values predicted by the line charge model for the polyion of Manning. The counterion self-diffusion constant was observed to be inversely dependent on the polyelectrolyte concentration at constant simple salt concentration. An additivity rule for the self-diffusion coefficients of the counterion in a polyelectrolyte-simple salt solution was found.

The model which has been considered the most realistic representation for a polyelectrolyte in solution is an infinitely long rod with a continuous charge distribution along its surface. This model was first used approximately 20 years ago^{1,2} and since then it has received much attention.³⁻⁹ Unfortunately, for a polyelectrolyte solution containing simple salt, the adjustable parameters which have been used to bring the theoretical predictions into agreement with the experimental results were inconsistent for different polyelectrolytes. Recently, Manning developed limiting laws for polyelectrolyte solutions which obviate these short comings.¹⁰ There are no adjustable parameters in the theory. He considered the polyelectrolyte to be an infinitely long line charge which interacts with the small ions about it *via* Debye-Hückel interactions. Central to the theory is a nonadjustable linear charge density parameter which is determined from a knowledge of the charge spacing of the polyelectrolyte. Comparison of experimental activities in salt and salt-free solutions with the values predicted from the theory are good, especially in very dilute solutions where the assumptions of the theory are more reasonable.

There are few theoretical studies reported dealing with the transport properties of polyelectrolyte solutions, especially for diffusion. Lifson, Jackson, and Coriell¹¹⁻¹³ were the first to develop theoretical expressions for the self-diffusion of ions in polyelectrolyte solutions. Manning¹⁴ was able to extend their procedure to consider polyelectrolyte solution behavior in an electric field. More recently, Manning's limiting laws have been developed for transport properties as well as for equilibrium properties.¹⁵ The only additional assumption is that the condensed counterions have negligible mobility along the chain as compared to the uncondensed counterions. Comparison of conductance and self-diffusion results in salt-free solutions indicated a good correlation with theory.

Since Manning's theory is most simple in concept, being an extension of simple electrolyte theory, and simple to use, it should be subjected to extensive experimental verification. In this light, we have initiated a systematic study of self-diffusion experiments for ions in salt and salt-free aqueous polyelectrolyte solutions. Here we report the results of the determination of the self-diffusion coefficients of Na⁺ in aqueous solutions of sodium polyac-

rylate (NaPA) containing sodium chloride at 25°. Sodium polyacrylate was the polyelectrolyte chosen because the Na⁺ diffusion coefficients determined in salt solutions could be compared with the classical transport results of Wall, *et al.*,¹⁶ for salt-free NaPA solutions.

To minimize the quantity of radioactive sodium ions used, a capillary method was used rather than the porous cell procedure. A uniform capillary of known length and closed at one end is filled with an isotopically tagged solution of known radioisotope concentration and immersed in a vessel containing a relatively larger amount of an inactive solution of the same material at the same concentration. While the inactive solutions should be stirred gently, Fernandez-Prini and coworkers^{17,18} showed that the use of an unstirred inactive solution gave accurate, reproducible results for aqueous solutions of polystyrenesulfonate. They used an approximate solution to the Fick equation developed by McKay¹⁹

$$D = \frac{\pi}{4} \left(1 - \frac{C_{av}}{C_0}\right)^2 \frac{l^2}{t} \quad (1)$$

where D is the diffusion constant, C_{av} is the average concentration of radioisotope in the capillary at time t , C_0 is the concentration of radioisotope at $t = 0$, and l is the length of the capillary. McKay's solution given by eq 1 is valid for the experimental conditions employed in this work.

Experimental Section

Preparation of Solutions. Sodium polyacrylate was obtained from Pfaltz and Bauer. It was purified by repeated dissolution in water followed by precipitation using a methanol-acetone mixture. The purified product was dried in an oven, ground, redried, and handled with minimum exposure to air. It has a molecular weight of 16,300, as determined by its viscosity in aqueous 0.10 *N* NaCl solution.²⁰

To prepare 0.0300 *N* polyelectrolyte solutions, accurately weighed quantities of polymer were transferred to volumetric flasks and were dissolved in some of the required water. The required quantity of NaCl was then added, allowed to dissolve, and water was added to the mark.

To prepare 0.100 *N* polyelectrolyte solutions, the same

procedure was followed as for the 0.0300 *N* solutions. However, in some cases, aliquots of the 0.0300 *N* solutions were transferred to another volumetric flask, the required quantity of sodium chloride was calculated and added, and the solution made up to the mark.

Solutions of partially neutralized polyacrylic acid (PAA) were prepared from the purified sodium salt. The stoichiometric quantity of salt was transferred to a volumetric flask and some water was added to dissolve it. Then standardized HCl solution was added from a buret equivalent to one-fourth the salt to make the $\frac{3}{4}$ neutralized acid, or one-half the salt to make the one-half neutralized salt. Additional NaCl was added to bring the total NaCl content to the desired value, making allowance for the NaCl formed *in situ* when the HCl was added to the salt. It should be noted that when the half-neutralized 0.0300 *N* solution was prepared, there was formed *in situ*, a 0.0150 *N* NaCl solution. This solution was used as prepared, and the solution containing only 0.0100 *N* NaCl was not run in this series since it could not be prepared by this procedure.

Radioactive sodium ^{22}Na , a γ -ray emitter (half-life of 2.6 years), was obtained from Amersham-Searle Corp. A nominal 0.1 μCi of ^{22}Na in the form of NaCl was obtained in 0.1 ml of HCl solution. The long half-life of this radioisotope made it unnecessary to correct for its loss of activity during the course of an experimental run.

The contents of the ampoule were transferred to a small beaker, and the excess HCl was neutralized with dilute, standardized NaOH solution, using a pH meter. The neutralized solution was transferred to a 250-ml volumetric flask and made up to volume. This stock solution was used to prepare all the tagged solutions.

It was found that if 1 or 2 ml of this solution of $^{22}\text{NaCl}$ were diluted to 10 ml, and the resultant dilute solution was used to fill a capillary as described previously, the quantity of radiosodium in the capillary was suitable for convenient counting. Under these conditions a count in the range of 10,000 to 20,000 disintegrations was obtained in approximately 10 min.

To prepare a solution containing $^{22}\text{NaCl}$ for introduction into a capillary, the inactive solution was first prepared as described above. The bulk of the solution was used as the inactive solution, and a few milliliters (approximately 10 ml) were used to prepare the tagged material.

Approximately 1 or 2 ml of the stock $^{22}\text{NaCl}$ solution was placed in a clean beaker. The beaker was placed in an oven at 70° and the water was evaporated until the residue (no residue was visible!) was dry. After cooling, approximately 3 ml of the polyelectrolyte was added to the beaker and the contents were stirred continually for at least 5 min to dissolve the small quantity of $^{22}\text{NaCl}$ and disperse it uniformly through the polyelectrolyte solution. The solution was covered to prevent evaporation, allowed to stand for 0.5 hr, then restirred for 5 min. The tagged solution was transferred to a storage vessel. The beaker was rinsed twice with fresh portions of the polyelectrolyte solution and the rinsings were added to the storage vessel. After stirring the contents of the storage vessel to assure homogeneity, this tagged solution was stored until used.

Validation of the Capillary Technique. To compute the diffusion coefficients from eq 1, it is necessary to measure the ratio of the amounts of radioisotope in the capillary before diffusion starts and after diffusion has occurred for a measured time. In order to assure that this ratio could

be measured reproducibly, samples containing different concentrations of $^{22}\text{NaCl}$ were prepared and counted at two counting stations. The counting ratios for each of three pairs of samples gave reproducibilities of better than 1% at the two counting stations. The counting ratios for one pair of samples were found to be constant when counted on eight consecutive days. Counting ratios for pairs of samples were found to be independent of the counting rates between 2000 and 25,000 counts per 10 min. It was shown that the transfer of radioactive material from the capillary to the culture tube used for counting was very reproducible. Also, it was demonstrated that the counting and transfer procedure accurately reflected a difference in radioisotope concentration by counting a tagged solution and counting an aliquot of this solution which was accurately diluted in half. The ratio was found to be 0.501.

The Fernandez-Prini capillary method¹⁸ for measuring diffusion coefficients was used because it required a smaller amount of untagged outer solution and the time required for a run was significantly less than for other methods. Also, because stirring of the outer solution is not required, larger capillaries could be used. The error in the Fernandez-Prini procedure was found to be 2–3%. Employing this method, self-diffusion coefficients for Na^+ in 0.0100 and 0.100 *N* aqueous NaCl solutions at 25° were found to be $1.32 \pm 0.01 \times 10^{-5}$ and $1.32 \pm 0.01 \times 10^{-5}$ cm^2/sec , respectively, which is in good agreement with the literature value of 1.31×10^{-5} cm^2/sec for these concentrations.²¹ An additional check of this method was made by determining the self-diffusion coefficient for Na^+ in salt-free aqueous NaPA at 25°. The results in 0.0100 and 0.0300 *N* NaPA were found to be $0.485 \pm 0.006 \times 10^{-5}$ and $0.468 \pm 0.005 \times 10^{-5}$ cm^2/sec , respectively, which is also in good agreement with the respective literature values of 0.484×10^{-5} and 0.472×10^{-5} cm^2/sec .¹⁶ All diffusion experiments were carried out in a bath thermostated at $25.00 \pm 0.02^\circ$.

Results and Discussion

Self-diffusion coefficients for Na^+ were determined in dilute aqueous solutions of NaPA, at three different degrees of neutralization, containing NaCl at 25°. To be consistent with the NaPA concentrations reported for the self-diffusion coefficients for Na^+ in salt-free aqueous solutions, concentrations of NaPA in the range of 0.00500–0.0300 *N* were used. The NaCl concentrations ranged from 0.0100 to 0.100 *N*. Thus the values of the quantity *X* defined by

$$X = n_e/n_s \quad (2)$$

where n_e and n_s are the equivalent concentrations of the polyelectrolyte and sodium chloride, respectively, ranged from $0.0500 \leq X \leq 1.00$ for 0.0100 *monomolar* NaPA to $0.150 \leq X \leq 3.00$ for 0.0300 *monomolar* NaPA.

The classic work of Huizenga, Grieger, and Wall¹⁶ showed that the self-diffusion coefficient D_1 for Na^+ in a salt-free NaPA solutions showed a strong inverse dependence upon the degree of neutralization α at constant polyelectrolyte concentration and a very weak inverse dependence on the polyelectrolyte concentration at constant degree of neutralization. From Table I it can be seen that for the NaPA–NaCl– H_2O system, at constant α and n_e , the values for D_1 increase as n_s increases, no doubt due to increased screening. Also, at constant α and n_s , the values

TABLE I: Self-Diffusion Coefficients for Na⁺ in NaPA–NaCl–H₂O Solutions at 25°

α	n_e	n_s	$D_1 \times 10^5$, cm ² /sec	$D_1 \times 10^5$, cm ² /sec (theor)
0.50	0.00500	0.0100	1.13 ± 0.03	1.12
	0.00500	0.0500	1.25 ± 0.03	1.25
	0.00500	0.100	1.29 ± 0.01	1.27
	0.0150	0.0150	0.99 ± 0.02	1.04
	0.0150	0.0500	1.12 ± 0.01	1.17
0.75	0.0150	0.100	1.22 ± 0.03	1.22
	0.00750	0.0100	0.94 ± 0.02	0.96
	0.00750	0.0500	1.20 ± 0.01	1.20
	0.00750	0.100	1.22 ± 0.02	1.24
	0.0225	0.0100	0.76 ± 0.01	0.75
1.00	0.0225	0.0500	1.01 ± 0.03	1.05
	0.0225	0.100	1.09 ± 0.02	1.15
	0.0100	0.0100	0.84 ± 0.01	0.84
	0.0100	0.0500	1.11 ± 0.03	1.15
	0.0100	0.100	1.21 ± 0.01	1.21
	0.0300	0.0100	0.66 ± 0.01	0.61
	0.0300	0.0500	0.99 ± 0.02	0.95
	0.0300	0.100	1.11 ± 0.03	1.08

TABLE II: Values for $A(1; \xi^{-1}X)$

$\xi^{-1}X$	$A(1; \xi^{-1}X)$	$\xi^{-1}X$	$A(1; \xi^{-1}X)$
0.0351	0.017	0.211	0.084
0.0702	0.030	0.351	0.125
0.105	0.045	1.05	0.235

for D_1 decrease as n_e increases; at constant n_e and n_s , the values for D_1 decrease as α increases.

The data in Table I could be used as a test of the infinite line charge model of Manning. Since the theory gives rise to limiting laws, the results are strictly valid at infinite dilution of all ions. However, the assumptions of the model are realistic for low equivalent concentrations of polyelectrolyte. Central to Manning's model is the experimentally determined linear charge density parameter ξ

$$\xi = Z_p e^2 / \epsilon k T b \quad (3)$$

where Z_p is the valence of a charged group on the polyion, e is the unit of electrical charge, ϵ is the dielectric constant of the pure bulk solvent, k is the Boltzmann constant, T is the absolute temperature, and b the distance between charges on the polyion. For a fully charged vinylic polyelectrolyte $b = 2.5$ Å. If α is the degree of neutralization of polyacrylic acid, i.e., the fraction of vinyl group charged on the polyion, $b = 2.5\alpha^{-1}$ Å. Three values for ξ were used in the present work, 1.43, 2.14, and 2.85 for half neutralized, three-fourths neutralized, and full neutralized polyacrylic acid, respectively.

From Manning's model, a condition of instability arises for $\xi > 1$, thereby causing counterions to condense onto the polyion to achieve an effective ξ value of unity. Thus, the concentration of condensed counterions is $(1 - \xi^{-1})n_e$ and the concentration of uncondensed counterions is $(\xi^{-1}n_e + n_s)$. Assuming that the mobility of the condensed counterions is much less than for the uncondensed counterions, the resulting equation for the self-diffusion coefficient D_1 for uncondensed counterions is

$$D_1 / D_1^0 = (\xi^{-1}X + 1)(X + 1)^{-1} [1 - (1/3)A(1; \xi^{-1}X)] \quad (4)$$

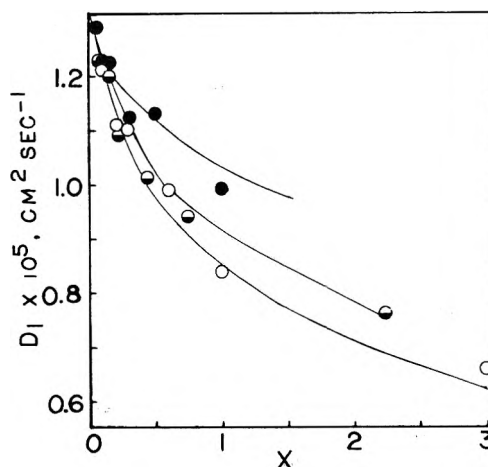


Figure 1. Dependence of D_1 on X for sodium polyacrylate in aqueous NaCl solutions at degrees of neutralization: $\alpha = 0.50$, \bullet ; $\alpha = 0.75$, \circ ; $\alpha = 1.00$, \circ . The points are experimental and the lines are theoretical.

where D_1^0 is the self-diffusion coefficient of counterion in pure solvent and $A(1; \xi^{-1}X)$ is a rapidly converging series given by eq 32 of ref 15. Values for $A(1; \xi^{-1}X)$ pertinent to the present investigation are given in Table II. The values of D_1/D_1^0 were calculated from eq 4. From this ratio, the values for D_1 were calculated using the value of $D_1^0 = 1.31 \times 10^{-5}$ cm²/sec²¹ for all concentrations, since the literature reveals no significant change in D_1^0 values over the concentration range of interest here. Also, the values obtained for D_1 are plotted against X in Figure 1. From Table I and Figure 1 it is noted that the observed and theoretical values for D_1 are in good agreement throughout the range of measurement, thereby giving further support to Manning's model. The relative deviation of the theoretical values of D_1 from the experimental values vary from 0 to 5%, except for the highest X values which is 8%. In light of this verification, other self-diffusion experiments are in progress to examine the model more critically. The theory predicts that the ratio of D_1/D_1^0 is much smaller than the analogous ratio for the coion; thus the self-diffusion coefficients of the coion are being determined for the system described here. Also, since all polyelectrolytes with the same charge spacing should give the same theoretical value for the ratio D_1/D_1^0 this ratio is being determined for Na⁺ for different vinylic polyelectrolytes containing NaCl.

Empirical additivity rules for the counterion polyelectrolyte-simple salt solutions have been explored experimentally²²⁻²⁵ and theoretically.^{10,26} Applying this concept to self-diffusion coefficients

$$D_1 = \frac{D_1^* n_p + D_1^0 n_s}{n_p + n_s} \quad (5)$$

where D_1^* is the self-diffusion coefficient for Na⁺ in salt-free sodium polyacrylate at concentration n_p . Using the literature values for D_1^0 ²¹ and D_1^* ,¹⁶ the additivity values of D_1 were calculated from eq 5. A comparison of these calculated values with the observed values, together with their per cent deviation $\Delta\%$, is made in Table III.²⁷ Within the range of salt concentration studied, it is evident that the per cent deviation for almost all concentrations is better than 5%. The additivity rule for the counterion activity coefficients^{24,25} was found to show larger deviations

from the experimental values than those reported here for counterion diffusion coefficients. Also, it should be pointed out Manning's theory predicts that the additivity rule for the counterion does not hold. Moreover, the additivity rules should be viewed as empirical rules only, since their theoretical basis is unsound.²⁸

Supplementary Material Available. Table III will appear following these pages in the microfilm edition of this volume of the journal. Photocopies of the supplementary material from this paper only or microfiche (105 × 148 mm, 20× reduction, negatives) containing all of the supplementary material for the papers in this issue may be obtained from the Journals Department, American Chemical Society, 1155 16th St., N.W., Washington, D. C. 20036. Remit check or money order for \$3.00 for photocopy or \$2.00 for microfiche, referring to code number JPC-73-2684.

References and Notes

- (1) T. Alfrey, P. W. Berg, and H. Morawitz, *J. Polym. Sci.*, **7**, 543 (1951).
- (2) R. M. Fuoss, A. Katchalsky, and S. Lifson, *Proc. Natl. Acad. Sci. U. S.*, **37**, 579 (1951).
- (3) U. P. Strauss and P. Ander, *J. Amer. Chem. Soc.*, **80**, 6494 (1958).
- (4) T. E. Hill, *Arch. Biochem. Biophys.*, **57**, 229 (1955).
- (5) L. Kotin and M. Nagasawa, *J. Chem. Phys.*, **36**, 873 (1962).
- (6) Z. Alexandrowicz, *J. Polym. Sci.*, **56**, 97, 115 (1962).
- (7) A. Katchalsky, Z. Alexandrowicz, and O. Kedem, in "Chemical Physics of Ionic Solutions," B. E. Conway and R. G. Barradas, Ed., Wiley, New York, N. Y., 1966, p 335.
- (8) L. Gross and U. P. Strauss, ref 7, p 361.
- (9) F. Oosawa, "Polyelectrolytes," Marcel Dekker, New York, N. Y., 1971.
- (10) G. S. Manning, *J. Chem. Phys.*, **51**, 924 (1969).
- (11) S. Lifson and J. L. Jackson, *J. Chem. Phys.*, **36**, 2410 (1962).
- (12) J. L. Jackson and S. R. Coriell, *J. Chem. Phys.*, **38**, 959 (1963).
- (13) S. R. Coriell and J. L. Jackson, *J. Chem. Phys.*, **39**, 2418 (1963).
- (14) G. S. Manning, *J. Chem. Phys.*, **47**, 2010 (1967).
- (15) G. S. Manning, *J. Chem. Phys.*, **51**, 934 (1969).
- (16) J. R. Huizenga, P. F. Grieger, and F. T. Wall, *J. Amer. Chem. Soc.*, **72**, 2636, 4228 (1950).
- (17) E. Baumgartner, S. Liberman, and A. E. Lagos, *Z. Phys. Chem. (Frankfurt am Main)*, **61**, 211 (1968).
- (18) R. Fernandez-Prini, E. Baumgartner, S. Liberman, and A. E. Lagos, *J. Phys. Chem.*, **73**, 1420 (1969).
- (19) R. McKay, *Proc. Phys. Soc.*, **42**, 547 (1930).
- (20) H. Fujita, K. Mitsuhashi, and T. Homma, *J. Colloid Sci.*, **9**, 466 (1954).
- (21) A. M. Friedman, Ph.D. Thesis, Washington University, St. Louis, Mo., 1960.
- (22) M. Nagasawa, M. Izumi, and I. Kagawa, *J. Polym. Sci.*, **37**, 375 (1959); **38**, 213 (1959).
- (23) Z. Alexandrowicz, *J. Polym. Sci.*, **43**, 337 (1960); **56**, 115 (1962).
- (24) J. W. Lyons and L. Kotin, *J. Amer. Chem. Soc.*, **87**, 1670 (1965).
- (25) T. J. Podlas and P. Ander, *Macromolecules*, **2**, 432 (1969).
- (26) Z. Alexandrowicz, *J. Polym. Sci., Part A*, **1**, 2093 (1963).
- (27) See paragraph at end of paper regarding supplementary material.
- (28) G. S. Manning, *Ann. Rev. Phys. Chem.*, **23**, 117 (1972).

Pressure Dependence of Weak Acid Ionization in Aqueous Buffers

Robert C. Neuman, Jr.,^{1*} Walter Kauzmann, and Adam Zipp

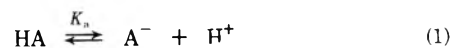
Frick Chemical Laboratory, Princeton University, Princeton, New Jersey 08540 (Received December 18, 1972; Revised Manuscript Received June 22, 1973)

Publication costs assisted by the National Science Foundation

Changes in the pH of buffer solutions under pressure have been monitored using the optical indicators 2,5-dinitrophenol and *p*-nitrophenol. Data were obtained to 6500 kg/cm² for acetate, cacodylate, phosphate, and Tris buffers. The results give the pressure dependences of the ionization constants for the weak acid components of these buffers. These can be described by the equation $RT \ln (K_p/K_0) = -\Delta V_a^\circ P + 0.5\Delta\kappa^\circ P^2$ where ΔV_a° is the limiting volume change on ionization at atmospheric pressure and $\Delta\kappa^\circ$ reflects the pressure dependence of ΔV_a° . Respective values of ΔV_a° (cc/mol) and $\Delta\kappa^\circ$ (cc/mol/(10³kg/cm²)) determined using acetic acid (-11.2, -1.44) as a reference are 2,5-dinitrophenol, -11.3, -1.28; *p*-nitrophenol, -11.3, -1.41; cacodylic acid, -13.2, -1.94; H₂PO₄⁻, -24, -3; TrisH⁺, +1, ~0.

Ionization constants of weak acids increase with increasing applied pressure.² The changes are substantial and range from factors of about 2 (carboxylic acids) to 8 (carbonic acid) over a pressure change of 2000 kg/cm². One important consequence of this is that the pH of aqueous buffer solutions varies with pressure.³ Since biochemical systems are best studied under buffered conditions, quantitative interpretation of results arising from pressure experiments on them requires detailed knowledge of pressure-induced changes in buffer pH. The data obtained in this study have been extensively used in an investigation of pressure effects on myoglobin spectral changes which will be reported in a separate communication.³

The pressure dependence of K_a , the molal equilibrium constant, (eq 1) gives the apparent volume change for ion-



ization ($\Delta\bar{V}_a$) of the acid (eq 2). This volume change can

$$\Delta\bar{V}_a = -RT \partial \ln K_a / \partial P \quad (2)$$

be measured at 1 atm by density measurements. However, the pressure dependence of $\ln K_a$ is not linear and values of $\Delta\bar{V}_a$ change with pressure. Thus, direct pressure experiments are necessary to obtain accurate measures of pH changes with pressure.

Using the optical pH indicators 2,5-dinitrophenol and *p*-nitrophenol, the effects of pressure on the acid dissociation of acetic acid, cacodylic acid ($\text{Me}_2\text{AsO}_2\text{H}$), dihydrogen phosphate (H_2PO_4^-), and TrisHCl (tris(hydroxymethyl)aminomethane hydrochloride) have been examined to 6500 kg/cm^2 . These are the acidic components of the commonly employed acetate, cacodylate, phosphate, and Tris buffer solutions.

Extensive pressure studies of acetic acid utilizing conductance measurements have been reported and these serve as reference data for the optical experiments reported here.⁴ No data have been available for cacodylic acid. However, values of $\Delta\bar{V}_a$ at atmospheric pressure for ionization of H_2PO_4^- and Tris have recently been reported from limited pressure studies utilizing a glass electrode,⁵ and for H_2PO_4^- using density experiments at 1 atm.²

Procedure

The pH of buffer solutions depends on the $\text{p}K_a$ of the buffer weak acid and the concentration ratio of the acid (HA) and its conjugate base (A) (eq 3). When buffer con-

$$\text{pH} = \text{p}K_a + \log \left(\frac{[\text{A}]}{[\text{HA}]} \right) \quad (3)$$

centration is sufficiently high as in these studies (0.05–0.10 *M*), pressure-induced changes in pH do not significantly alter the concentration ratio term and can be attributed directly to changes in $\text{p}K_a$ (eq 4).

$$\partial(\text{pH})/\partial P \simeq (\text{p}K_a)/\partial P \quad (4)$$

The pH of solutions can be determined using optical indicators and eq 5 applies if the concentration of the conju-

$$\text{pH} = \text{p}K_1 - \log \left[\frac{[\text{OD}_1 - \text{OD}]}{[\text{OD}]} \right] \quad (5)$$

gate base of the indicator is followed spectrophotometrically; $\text{p}K_1$ is the dissociation constant of the acid form of the indicator, OD_1 is the optical density at λ_{max} corresponding to complete conversion of the indicator to its conjugate base, and OD is the observed optical density at the same wavelength due to the conjugate base of the indicator. Changes in pH with pressure can be determined from the pressure dependence of OD (eq 6) if the pressure

$$\partial(\text{pH})/\partial P = \partial(\text{p}K_1)/\partial P - \partial \log \left[\frac{[\text{OD}_1 - \text{OD}]}{[\text{OD}]} \right] / \partial P \quad (6)$$

dependence of $\text{p}K_1$ is known. The effect of pressure on $\text{p}K_a$ can thus be determined using eq 7 which arises from combination of eq 4 and 6.

$$\partial(\text{p}K_a)/\partial P = \partial(\text{p}K_1)/\partial P - \partial \log (\Delta\text{OD}/\text{OD})/\partial P \quad (7)$$

The observable quantity $\partial \log (\Delta\text{OD}/\text{OD})/\partial P$ reflects the difference in the pressure dependences of $\text{p}K_1$ and $\text{p}K_a$. The pressure dependence of $\text{p}K_1$ for 2,5-dinitrophenol ($\text{p}K_1 = 5.10$) was calculated from data available for acetic acid.⁴ The indicator 2,5-dinitrophenol was then used to monitor the pressure dependences of $\text{p}K_a$ for cacodylic acid and H_2PO_4^- . The pressure dependences of the $\text{p}K_a$ values for H_2PO_4^- and TrisHCl were calculated from experimental results using the indicator *p*-nitrophenol ($\text{p}K_1 = 7.05$). The pressure dependence of its acid dissociation was obtained from experiments with cacodylate buffer,

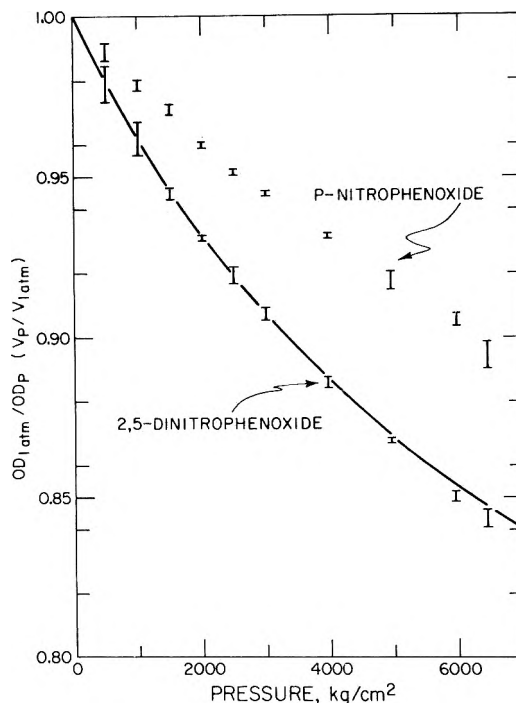


Figure 1. Pressure dependence of OD at λ_{max} (400 $\text{m}\mu$) for *p*-nitrophenoxide ion in aqueous basic cacodylate, phosphate, and Tris solutions, and at λ_{max} (440 $\text{m}\mu$) for 2,5-dinitrophenoxide ion in aqueous basic cacodylate, acetate, and phosphate solutions. Each error bar represents spread of data for the three salt solutions. The solid line shows the pressure dependence of the molar volume of pure water (20°).

and $\partial(\text{p}K_a)/\partial P$ for cacodylic acid determined using 2,5-dinitrophenol.

Measured values of OD were corrected for compression of the solutions under pressure. Correction factors were obtained by monitoring the change in OD values for aqueous solutions of 2,5-dinitrophenoxide ion and of *p*-nitrophenoxide ion under conditions approximating the buffer studies. The correction factors also include any pressure-induced changes in molar absorptivity of the absorption bands in question.⁶

Results and Discussion

The OD values for solutions containing *p*-nitrophenoxide ion and 2,5-dinitrophenoxide ion increase with increasing pressure (Figure 1). This is expected because solution volumes decrease with pressure leading to increased concentrations of solutes. The pressure decrease in the volume of a sample of pure water (20°) is shown by the solid line (Figure 1).⁷ The difference in the behavior of the two phenoxide ions reflects a difference in the pressure dependence of their respective molar absorptivities. The fact that the data for 2,5-dinitrophenoxide ion fall on the pure water curve suggests that the molar absorptivity of this ion is relatively pressure insensitive. On the other hand, the OD values for *p*-nitrophenoxide ion increase less than expected with pressure. The absorption band itself does not, however, show any change in shape with pressure, and there is no detectable shift in the position of the maximum. Evidently this behavior of the OD reflects a decrease in the integrated molar absorptivity of the *p*-nitrophenoxide ion by about 4% when the pressure is increased from 1 atm to 6500 kg/cm^2 . The pressure dependences of OD for the phenoxide ions are independent of

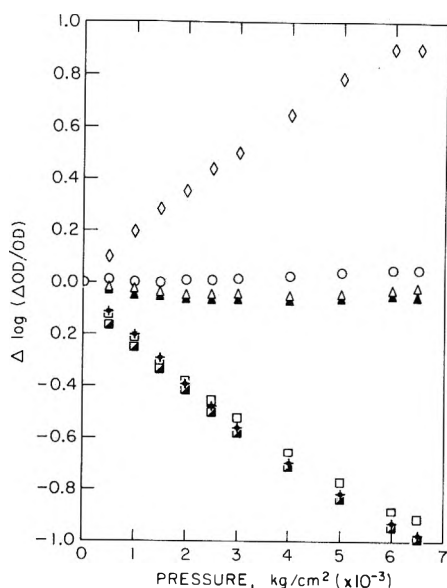


Figure 2. Pressure dependence of $\log (\Delta OD/OD)$ for the optical indicator 2,5-dinitrophenol in acetate (O), cacodylate (Δ), and phosphate ($\square, \blacksquare, +$) buffers, and for *p*-nitrophenol in cacodylate (\blacktriangle), phosphate ($+$), and Tris (\diamond) buffers.

the specific added buffer salt within experimental error; the bars in Figure 1 in each case represent the spread of data for three buffer salts (see caption, Figure 1).

After correction of the values of OD using the data presented in Figure 1, values of $\log (\Delta OD/OD)$ were calculated for each buffer-indicator system and a summary of these data is presented in Figure 2.⁸ The values of $\Delta \log (\Delta OD/OD)$ are equal to $\Delta pK_1 - \Delta pK_a$ where the Δ symbol indicates the difference between the quantity at 1 atm and at some pressure *P*.

The values of $\Delta \log (\Delta OD/OD)$ for 2,5-dinitrophenol in acetate buffer in conjunction with previously available data for the pressure dependence of pK_a for acetic acid permitted the determination of the pressure dependence of pK_1 for 2,5-dinitrophenol. These values together with the data for 2,5-dinitrophenol in cacodylate and phosphate buffers allowed calculation of ΔpK_a values for cacodylic acid and $H_2PO_4^-$. The results for cacodylic acid taken with those for *p*-nitrophenol in cacodylate buffer (Figure 2) gave values of ΔpK_1 for this indicator. These ΔpK_1 values in conjunction with the data for *p*-nitrophenol in phosphate and Tris buffers gave an alternate determination of ΔpK_a values for $H_2PO_4^-$ and a new set of values for TrisHCl ionization. The results are given in Figure 3.⁸ These data have not been extrapolated to infinite dilution. They correspond to the behavior of the weak acids in solutions whose overall solute concentrations are roughly 0.05–0.10 *M* and of variable ionic strength. They are adequate, however, for the purposes intended since errors in kinetic or equilibrium studies of biological systems will generally be substantially greater than those in these results.³

With the exception of TrisHCl, dissociation of the acids is favored by pressure. The increases in ΔpK_a values for acetic acid, cacodylic acid, and the two phenols are very similar. The changes in pK_a for $H_2PO_4^-$ are much greater. While the pH of an acetate or cacodylate buffer would decrease by less than one pH unit over a pressure range of 6500 kg/cm², pH of phosphate buffers would change by

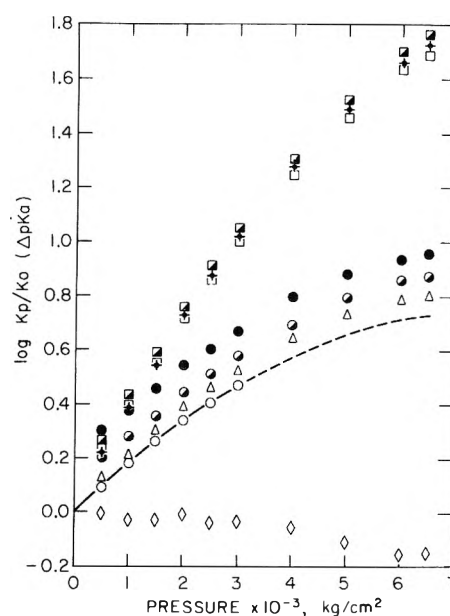
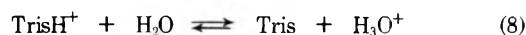


Figure 3. Pressure dependence of calculated values of $\log K_p/K_0$ for acetic acid (O), 2,5-dinitrophenol (\bullet), *p*-nitrophenol (\bullet), cacodylic acid (Δ), $H_2PO_4^-$ ($\square, \blacksquare, +$) and TrisHCl (\diamond) in aqueous buffer solutions. The points for 2,5-dinitrophenol and *p*-nitrophenol are displaced upward 0.1 and 0.2 units on the vertical axis.

almost two units. In striking contrast to these results is the fact that the pH of a Tris buffer solution is almost pressure insensitive; over the 6500 kg/cm² range, pK_a appears to *decrease* by less than 0.2 units. This is understandable in terms of the ionization equilibrium. While the other acids ionize increasing the number of formal charges (*e.g.*, eq 1), acid dissociation of TrisHCl occurs without a change in the number of charged species (eq 8). When charges are created, substantial volume contraction occurs due to solvation effects and processes characterized by volume decreases are favored by increasing pressure (see eq 2). Little volume change would be expected for reaction 8 and hence a small pressure dependence is predicted.



Experimental values of $\log K_p/K_0$ for acetic acid were available only to a pressure of 3059 kg/cm² (Table I).⁴ Values to 6500 kg/cm² were calculated from eq 9 with

$$2.303RT \log (K_p/K_0) = -\overline{\Delta V}_a^\circ P + C.5\overline{\Delta \kappa}^\circ P^2 \quad (9)$$

$\overline{\Delta V}_a^\circ$ and $\overline{\Delta \kappa}^\circ$ equal to -11.2 cc/mol and -1.44×10^{-3} cc/mol/(kg/cm²), respectively.⁴ Such a quadratic equation has been found to be useful in fitting observed pressure dependences of both equilibrium and rate constants. In this particular case, $\overline{\Delta V}_a^\circ$ is the limiting volume change for ionization of the weak acid at atmospheric pressure and $\overline{\Delta \kappa}^\circ$ is a compressibility term which accounts for the pressure dependence of $\overline{\Delta V}_a^\circ$. These two quantities were obtained from the slope and intercept of a plot of $[\log (K_p/K_0)]/P$ vs. *P* (eq 10) using the experimental data

$$[\log (K_p/K_0)]/P = -\overline{\Delta V}_a^\circ/2.303RT + (\overline{\Delta \kappa}^\circ/4.606RT)P \quad (10)$$

to 3059 kg/cm² (Table III). Lown, *et al.*, obtained a slightly different value of $\overline{\Delta \kappa}^\circ$ from the same data, but it

TABLE I: Experimental and Calculated Values of $\log K_p/K_0$ for Acetic Acid Ionization in Water (25°)

<i>P</i> , bars ^a	<i>P</i> , kg/cm ²	$\log K_p/K_0$	
		Exptl	Calcd ^b
400	40E	0.0759	0.0764
1000	1020	0.1824	0.1833
1400	142E	0.2453	0.2494
2000	2039	0.3347	0.3408
2400	2447	0.3925	0.3966
3000	3059	0.4748	0.4726
4000	4079		0.5786
5000	5099		0.6589
6000	6118		0.7134
7000	7138		0.7422

^a Pressures reported in bars for experimental data, see ref 4; calculations carried out using this pressure unit for convenience. ^b Calculated using eq 9, as described in text.

did not give calculated values which fit the experimental data (Table I) as well as those obtained using our value. The extrapolated pressure dependence of $\log K_p/K_0$ for acetic acid above 3059 kg/cm² is shown as the dashed portion of the curve in Figure 2.

Since the data for acetic acid above 3059 kg/cm² are derived from an extrapolation, all of the absolute values of $\log K_p/K_0$ for the various weak acids are subject to greater error above this pressure. However, the values of Δ \log ($\Delta OD/OD$) for the various buffer-indicator systems do not depend on this extrapolation and when experimental values of $\log K_p/K_0$ become available for the full pressure range for acetic acid or any of the other weak acids, appropriate corrections can be made.

Values of $\overline{\Delta V}_a^\circ$ and $\overline{\Delta \kappa}^\circ$ were calculated, using eq 10, from the experimental values of $\log K_p/K_0$ (Figure 2) for 2,5-dinitrophenol, *p*-nitrophenol, cacodylic acid, and H₂PO₄⁻. These are given in Table II along with an approximate value of $\overline{\Delta V}_a^\circ$ for TrisHCl obtained from a plot of $\log K_p/K_0$ vs. *P* (see eq 2). The small change in K_a for this acid together with scatter in the data precluded the use of eq 10.

The similarity in the values of $\overline{\Delta V}_a^\circ$ for the two phenols is gratifying and supports the validity of the procedures used. They are also close to a previously reported value of -10.3 cc/mol for *p*-nitrophenol determined from data at only two pressures,² and a value of -11.8 cc/mol determined for 2,5-dinitrophenol at three pressures.^{9a} The results for cacodylic acid are comparable to a $\overline{\Delta V}_a^\circ$ of ca. -12 determined from dilatometric measurements at atmospheric pressure.^{9b} The values of $\overline{\Delta V}_a^\circ$ for H₂PO₄⁻ ionization are slightly smaller than a value of -28 cc/mol reported from a density experiment at 1 atm,² and similar to a value of -24.0 cc/mol calculated from data obtained using a glass electrode to 1000 kg/cm².⁵ The small value of $\overline{\Delta V}_a^\circ$ for TrisHCl ionization is close to that obtained recently (+2.5 cc/mol) by Distech.⁵

Experimental Section

Materials. *p*-Nitrophenol. A sample of *p*-nitrophenol (Eastman) was dissolved in absolute ethanol and treated with charcoal. Recrystallization twice from ethanol-water gave long needles which were filtered and dried *in vacuo* over phosphorous pentoxide; mp 112-114° (lit.¹⁰ mp 114.5-115°). 2,5-Dinitrophenol. A sample of 2,5-dinitro-

TABLE II: Values of $\overline{\Delta V}_a^\circ$ and $\overline{\Delta \kappa}^\circ$ for Weak Acids^a

Weak acid	$\overline{\Delta V}_a^\circ$, cc/mol	$\overline{\Delta \kappa}^\circ \times 10^3$, cc/mol/(kg/cm ²)
2,5-Dinitrophenol	-11.3	-1.28
<i>p</i> -Nitrophenol	-11.3	-1.41
Cacodylic acid	-13.2	-1.94
H ₂ PO ₄ ⁻	-25.3 ^b	-3.05 ^b
	-24.5 ^c	-2.98 ^c
	-23.8 ^d	-2.62 ^d
TrisH ⁺	+1	
(Acetic acid)	-11.2	-1.44

^a Calculated using the data in Figure 2 and eq 9. ^b 2,5-DNP indicator, pH 6.31. ^c 2,5-DNP indicator, pH 6.11. ^d *p*-NP indicator, pH 7.97.

TABLE III: Determination of pK_a for 2,5-Dinitrophenol

Buffer	pH	(OD ₁ - OD)/OD	Calcd pK_a
0.1 M acetate	5.63	0.3001	5.10
	5.63	0.2940	5.11
	5.52	0.4270	5.15
	5.22	0.7812	5.11
0.05 M cacodylate	6.00	0.1365	5.14
	5.77	0.2075	5.09
	5.64	0.2801	5.09
	5.53	0.3657	5.09
	5.37	0.5158	5.08

phenol (Aldrich) mp 106-107° was used as received. *Buffers.* Buffers were prepared according to published formulations.¹¹ Sodium cacodylate (MCB) was used as received. Tris buffer was prepared from Trizma Base (Sigma) and Trizma HCl (Sigma) which had been dried *in vacuo* over phosphorous pentoxide prior to use. Other components were reagent grade chemicals.

Sample Preparation. 2,5-Dinitrophenol Solutions. Stock solutions of 2,5-dinitrophenol in water (0.036 M) were prepared by bringing 0.165 g of indicator to a volume of 25 ml using water containing an equivalent amount of sodium hydroxide. Solutions of this indicator in the various buffers were prepared just prior to use by diluting 0.5 ml of the stock solution to 50 ml with the appropriate buffer. Samples of this concentration (3.6×10^{-4} M) were suitable for use in 1-cm uv cells. Samples for pressure studies were prepared by bringing either 5- or 10-ml aliquots of the latter solution to a volume of 25 ml with the same buffer (7.2×10^{-5} and 1.44×10^{-4} M, respectively). *p*-Nitrophenol Solutions. A stock solution of *p*-nitrophenol in water (0.01 M) was prepared by bringing 0.069 g of indicator to 50 ml with distilled water. Solutions of this indicator in the various buffers were prepared just prior to use in the same way as described above. High-pressure samples were 2×10^{-5} or 4×10^{-5} M. "Basic" Solutions. "Basic" solutions used to obtain the data in Figure 1 were prepared just prior to use from the indicator stock solutions using the same dilutions as above. In place of buffer solutions, aqueous solutions of the appropriate buffer conjugate base (same concentration as buffer) were used. Additionally, one pellet of sodium hydroxide (0.1 g) was added during the dilution to 50 ml except in the case of 2,5-dinitrophenol in aqueous Na₂HPO₄ solution.

Uv Spectra at High Pressures. Samples of indicators in

buffers were placed in 3.4-cm quartz cells which were then enclosed in a high-pressure optical bomb. A spectrum from 650 to 350 $m\mu$ was recorded at atmospheric pressure and then at a series of higher pressures to 6500 kg/cm^2 . After release of pressure, another spectrum was recorded. The adjusted optical density at λ_{max} typically differed by no more than 1% between the initial and final 1-atm spectra. Some baseline shift was observed with increasing pressure and this was taken into account in calculating the optical density at λ_{max} . Shifts of less than 3 $m\mu$ were observed in the positions of the absorption bands over the 6500- kg/cm^2 pressure range.

pH Measurements. For the purpose of checking the pH values at 1 atm, measurements were made on the various buffers and other solutions using a Radiometer pH meter and Radiometer electrodes.

pK_1 Measurements for Indicators at 1 atm. Measurements¹⁰ in buffer of pK_1 for *p*-nitrophenol give a value of 7.05 and our data are in agreement with this number. Several pK_1 values in the range 5.1–5.2 have been reported for 2,5-dinitrophenol.¹² Using acetate and cacodylate buffers the data shown in Table III were obtained at atmospheric pressure. Reliable data could not be obtained at pH values less than 5.1 to 5.2 because of the development of an interfering absorption band at 360 $m\mu$ from the neutral phenol. Absorption bands of *p*-nitrophenoxide ion and 2,5-dinitrophenoxide ion used in these studies were at 400 and 440 $m\mu$, respectively.

Acknowledgments. Financial support for this work was provided by NSF grants to W. K. and R. C. N., and an NIH fellowship to R. C. N. The pressure apparatus used in this work was obtained through an NIH grant to W. K.

Supplementary Material Available. Tables containing the data shown in Figures 1 and 2 will appear following these pages in the microfilm edition of this volume of the journal. Photocopies of the supplementary material from this paper only or microfiche (105 × 148 mm, 20× reduction, negatives) containing all of the supplementary material for the papers in this issue may be obtained from the Journals Department, American Chemical Society, 1155 16th St., N.W., Washington, D. C. 20036. Remit check or money order for \$3.00 for photocopy or \$2.00 for microfiche, referring to code number JPC-73-2687.

References and Notes

- (1) (a) National Institutes of Health Special Research Fellow, 1971–1972. (b) Permanent address and address for correspondence: Department of Chemistry, University of California, Riverside, Calif. 92502. (c) Presented at the 165th National Meeting of the American Chemical Society, Dallas, Tex., April 8–13, 1973, INDE 038.
- (2) For a general review see S. D. Hamann, "High Pressure Physics and Chemistry," Vol. 2. R. S. Bradley, Ed., Academic Press, New York, N. Y., Chapter 7ii.
- (3) (a) A preliminary report has been published: A. Zipp, G. Ogunmola, R. C. Neuman, Jr., and W. Kauzmann, *J. Amer. Chem. Soc.*, **94**, 2541 (1972); (b) A. Zipp and W. Kauzmann, *Biochemistry*, **12**, 4217 (1973).
- (4) (a) The values of $\log K_p/K_0$ for acetic acid^{4b} are molal quantities obtained in dilute solution at 25°. (b) D. A. Lown, H. R. Thirsk, and Lord Wynne-Jones, *Trans. Faraday Soc.*, **64**, 2073 (1968).
- (5) A. Distèche, *Symp. Soc. Exp. Biol.*, **26**, 27 (1972).
- (6) (a) The use of optical indicators to measure effects of pressure on pH has been previously attempted, however, no quantitative results were reported.^{6b} (b) R. E. Gibson and O. H. Loeffler, *Trans. Amer. Geophys. Un.*, 503 (1941).
- (7) P. W. Bridgman, *Proc. Amer. Acad. Arts Sci.*, **48**, 309 (1912).
- (8) See paragraph at end of paper regarding supplementary material.
- (9) (a) S. D. Hamann, Division of Applied Chemistry, Technical Paper No. 3, CSIRO, Australia, 1972. (b) Unpublished experiments by Dr. Frank Gasparro in this laboratory.
- (10) F. J. Kezdy and M. L. Bender, *Biochemistry*, **1**, 1097 (1962).
- (11) G. Gomori, "Methods of Enzymology," Vol. 1, Academic Press, New York, N. Y., 1955, pp 138–146.
- (12) C. M. Judson and M. Kilpatrick, *J. Amer. Chem. Soc.*, **71**, 3110, 3113 (1949).

Prehydration Scavenging of e_{aq}^- and the Yields of Primary Reducing Products in Water γ -Radiolysis

Z. D. Draganic[†] and I. G. Draganic*

Boris Kidric Institute of Nuclear Sciences, Beograd, Yugoslavia (Received May 14, 1973)

The formation of primary reducing yields of water radiolysis was examined in neutral aqueous solutions of alanine and glycine. Increase in concentration of the amino acids was found to lead to decrease in $G(e_{aq}^-)$, $G(H)$, and $G(H_2)$. Low reactivities toward e_{aq}^- in the solutions studied suggest that the prehydration scavenging of e_{aq}^- is the cause of decrease in $G(e_{aq}^-)$ and therefore in $G(H)$ and $G(H_2)$. The consequences of prehydration scavenging for the water decomposition yield are considered.

Introduction

Experimental testing of the free-radical model of water radiolysis has confirmed the importance of e_{aq}^- reactions for the formation of primary yields of H and H_2 .^{1,2} It might be expected, therefore, that a possible prehydration scavenging of e_{aq}^- should influence not only $G(e_{aq}^-)$ but

also $G(H)$ and $G(H_2)$. It should also affect the values of $G(-H_2O)$ calculated from the data on the yields of primary reducing species by the equation of material balance. The accumulating evidence on the importance of e_{aq}^- precursor reactions^{3–6} and some inconsistency concerning $G(-H_2O)$ dependence on the reactivities toward

e_{aq}^- and OH^{\cdot} pointed out that the prehydration scavenging could be important for the formation of all primary yields in irradiated water. The present work provides some clear evidence for the reducing products. The solutes used were alanine and glycine, both known as fairly inefficient in scavenging e_{aq}^- , H, and OH, but assumed to react effectively with the precursor of the hydrated electron.^{5,7} The irradiated solutions (natural pH) consisted of the amino acids studied at various concentrations and of appropriate amounts of nitrite, or formate and nitrate, to react with the primary free radicals in the bulk only. The amount of chemical change and the steady-state kinetics were used in the calculations of the primary yields.

Experimental Section

The chemicals used were BDH or Merck of the highest purity available. Irradiations were carried out in a radioactive cobalt source giving $2.1 \times 10^{19} \text{ eV g}^{-1} \text{ hr}^{-1}$; the absorbed doses ranged from 2×10^{17} to $7 \times 10^{17} \text{ eV g}^{-1}$. Molecular hydrogen was determined by gas chromatography and the nitrite concentration by spectrophotometry. Sample preparation, irradiations, and chemical analyses were described in full detail in the preceding paper.⁷

Results and Discussion

Table I summarizes the yields of stable products determined in irradiated solutions and used in the calculations of primary yields.

$G(H_2)$. Primary yield of molecular hydrogen was directly measured in aqueous solutions of amino acids (AA) containing the nitrite ion (0.01 or 0.05 M). Nitrite is effective in scavenging OH, H, and e_{aq}^- without producing H_2 . Its concentration was sufficient to prevent some additional formation of hydrogen by reaction $H + AA \rightarrow H_2 + P$, and

$$G(H_2) = G(H_2)_{\text{meas}} \quad (1)$$

The measured yields are lower than 0.45 because of interference with the H_2 formation in the spurs, caused by somewhat higher reactivities of nitrite toward e_{aq}^- .

$G(H)$. In aqueous solutions of amino acids we had nitrate ion to scavenge e_{aq}^- and $HCOO^-$ to remove OH and H species from the bulk. Because of the reaction $H + HCOO^- \rightarrow H_2 + COO^-$, we had

$$G(H_2)_{\text{meas}} = G(H_2) + G(H) \quad (2)$$

The nitrate ion present (5×10^{-3} or $2.5 \times 10^{-2} \text{ M}$) removes the hydrated electron from the bulk. However, at higher concentrations of amino acid one has also to take into consideration the reaction $e_{aq}^- + NH_3^+CH(R)COO^- \rightarrow H + NH_2CH(R)COO^-$ and the values of $G(H)$ have to be calculated from the following relation

$$G(H_2)_{\text{meas}} = G(H_2) + G(H) + fG(e_{aq}^-) \times \left\{ 1 + \frac{k_{e_{aq}^- + NO_3^-} [NO_3^-]}{k_{e_{aq}^- + AA} [AA]} \right\}^{-1} \quad (3)$$

The value of f amounts to 0.09 and 0.37 for alanine and glycine, respectively. It takes into account the fraction of e_{aq}^- yield leading to the formation of H atoms in a solution of the given amino acid; we have derived it from the following values of H_2 yields reported for neutral aqueous solutions of 1 M alanine and 1 M glycine: 1.25⁸ and 2.02,⁹ respectively. As $G(H_2)$ in eq 2 and 3 we have used the experimental values of H_2 measured at corresponding amino

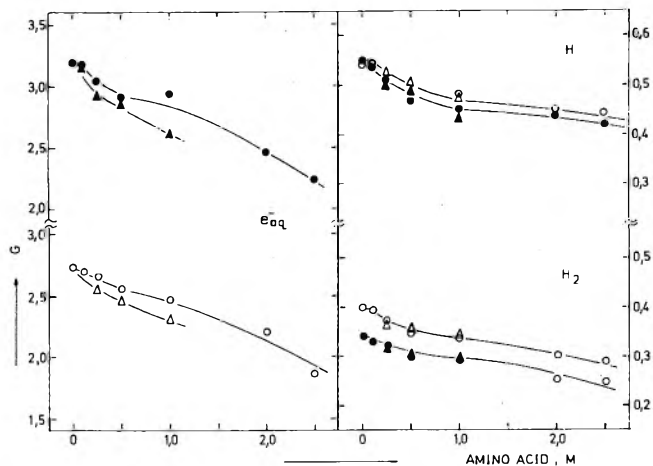


Figure 1. Dependence of experimentally derived primary yields of e_{aq}^- , H, and H_2 on the concentration of amino acid: Δ , alanine; \circ , glycine. The open symbols refer to a solution containing $5 \times 10^{-3} \text{ M NaNO}_3$ and 0.1 M HCOONa . The solid symbols refer to a solution containing $2.5 \times 10^{-2} \text{ M NaNO}_3$ and 0.1 M HCOONa .

acid concentration (Table I). The reactivities of nitrite ion in these solutions corresponded to the reactivities of nitrate (5.25×10^7 and $2.6 \times 10^8 \text{ sec}^{-1}$) toward the hydrated electron.

$G(e_{aq}^-)$. The yield of the hydrated electron was measured in aqueous solutions of amino acid containing a small amount of nitrate, to remove e_{aq}^- from the bulk, and the formate ion to react with the H and OH radicals and to convert the intermediate of nitrate-hydrated electron reaction to the nitrite ion. Under these conditions the yield of nitrite was used as a measure of e_{aq}^- yield. Since some hydrated electrons are lost in the reaction with amino acid we had to use for $G(e_{aq}^-)$ calculation the following relation

$$G(e_{aq}^-) = G(NO_2^-) \left\{ 1 + \frac{k_{e_{aq}^- + AA} [AA]}{k_{e_{aq}^- + NO_3^-} [NO_3^-]} \right\} \quad (4)$$

Since the pH of solutions was about 5.4, the values of $k(e_{aq}^- + AA)$ used in eq 4 refer only to the reactions of the hydrated electron with the dipolar ions of amino acids.¹⁰ The eventual contribution of undissociated molecules, formed within the spurs due to the H_3O^+ from the water radiolysis, could not be taken into account because of the complex pH situation within the places of localized energy deposit in the systems studied. As can be seen in Table I, the presence of sodium hydroxide in irradiated samples does not affect the nitrite ion yields, which suggests that this contribution can be neglected.

Dependence of the Primary Yields on Amino Acid Concentration. Relations 1-4 and the data given in Table I were used to calculate the primary yield vs. amino acid concentration curves shown in Figure 1. As was to be expected, the increasing concentrations of amino acids lead to depression of all the primary reducing yields. Solid and open symbols are used to distinguish between the solutions with various reactivities toward the hydrated electron. At increased reactivities, represented by solid symbols, the absolute values are different because of some scavenging from the spurs but the trends are practically the same. Alanine is somewhat more effective in reducing the yield of e_{aq}^- than glycine; the difference is not significant. In solutions containing simultaneously up to 1 M of alanine and of glycine, the decrease in the yield is very

TABLE I: Yields of Stable Radiolytic Products Measured in Deaerated, Neutral, Aqueous Solutions of Alanine and Glycine

[Amino acid], M	Alanine			Glycine		
	$G(H_2)_{meas}$	$G(H_2)_{meas}^a$	$G(NO_2^-)^a$	$G(H_2)_{meas}$	$G(H_2)_{meas}^a$	$G(NO_2^-)^a$
	$5 \times 10^{-3} M NaNO_3$					
	0.40 ^b	0.94	2.73	0.40 ^b	0.94	2.73
0.1				0.40 ^b	0.94	2.66
0.25	0.37 ^b	0.90	2.50	0.37 ^b		2.54
0.5	0.36 ^b	0.85	2.35	0.35 ^b		2.37
1.0	0.34 ^b	0.83	2.12	0.34 ^b	0.96	2.15
2.0				0.30 ^b	1.00	1.68
2.5				0.29 ^b	1.11	1.33
	$2.5 \times 10^{-2} M NaNO_3$					
	0.34 ^c	0.88	3.19	0.34 ^c	0.88	3.19
0.1			3.15	0.33 ^c	0.88	3.17
0.25	0.32 ^c	0.82	2.92	0.32 ^c	0.83	3.04
0.5	0.31 ^c	0.83	2.75	0.30 ^c	0.80	2.85
0.5			2.82; ^d 2.65 ^e			
1.0	0.30 ^c	0.75	2.57	0.29 ^c	0.78	2.87
2.0				0.25 ^c	0.78	2.35
2.0						2.34; ^f 2.29; ^g 2.33 ^h
2.5				0.25 ^c	0.74	2.06

^a Solution contains 0.1 M HCOO⁻. ^b Solution contains 0.01 M NaNO₂; NaNO₃ absent. ^c Solution contains 0.05 M NaNO₂; NaNO₃ absent. ^d $2 \times 10^{-2} M$ NaOH added (pH 8.6). ^e 0.1 M NaOH added (pH 9.4). ^f $1 \times 10^{-2} M$ NaOH added (pH 7.6). ^g $5 \times 10^{-2} M$ NaOH added (pH 8.4). ^h 0.1 M NaOH added (pH 8.7).

TABLE II: Yields of e_{aq}^- in Aqueous Solutions of Alanine and Glycine Mixtures^a

[Amino acid], M		$G(NO_2^-)$	$G(e_{aq}^-)$	
Alanine	Glycine		b	c
0.5	0.5	2.70	2.77	2.52
1.0	1.0	2.35	2.45	2.30
0.5	2.0	2.40	2.58	1.97
1.0	2.0	2.14	2.30	1.73

^a $2.5 \times 10^{-2} M NaNO_3$ and 0.1 M HCOONa present in irradiated samples. ^b Calculated from nitrite yield. ^c Derived from Figure 1.

nearly equal to the sum of their combined effects (Table II).

The prehydration scavenging of e_{aq}^- should also influence the formation of $G(OH)$ and $G(H_2O_2)$. According to the free-radical model, an efficient removal of the hydrated electron leads to an increase in OH yield because of depression of water re-formation in reaction $e_{aq}^- + OH$. This increase was experimentally proved with various systems⁷ and points out that, at the amino acid concentrations used in this work, it should be about 10% because of prehydration scavenging.

The Yield of Water Decomposition and the Prehydration Scavenging. In calculating the radiation chemical yield of water decomposition, use is widely made of the assumption of material balance, $G(-H_2O) = G(e_{aq}^-) + G(H) + 2G(H_2)$. When the data from Figure 1 are used, the calculated $G(-H_2O)$ values decrease considerably with increasing amino acid concentration. At 2.5 M glycine, for example, this decrease is about 1.3G units. It shows that the water decomposition yield cannot be derived only from the measurements in the bulk of the solutions and that one has to take into account the water molecules decomposed due to the prehydration scavenging. This contribution is for the present not well defined. One can only estimate the yield of the precursor scavenged from the difference between $G(-H_2O)$, calculated from

the primary reducing yields, obtained in the absence and in the presence of amino acid.

It is worth noticing that previously reported correlation of primary yields with reactivities turned out to be less successful in the case of the reducing products of water radiolysis than for the oxidizing ones.^{1,2,7} Also, significant deviations from the yield-reactivity curves have still remained after the dependence of the e_{aq}^- rate constant on ionic strength has been taken into account.^{7,11} The present work suggests that a better understanding of the reactions between the e_{aq}^- precursor and the solutes used in the examination might be helpful for a satisfactory explanation of these inconsistencies.

The experimental results obtained in this work do not allow any conclusion about the nature of the precursor species or the scavenging mechanism. The prehydration scavenging takes place already at low amino acid concentrations and the results do not contradict the assumption that we are dealing with a highly mobile electron which can traverse rather long distances before it has fully developed its ionic atmosphere.

References and Notes

- (1) Z. D. Draganić and I. G. Draganić, *J. Phys. Chem.*, **76**, 2733 (1972).
- (2) Z. D. Draganić and I. G. Draganić, *J. Phys. Chem.*, **75**, 3950 (1971).
- (3) W. H. Hamill, *J. Phys. Chem.*, **73**, 1341 (1969).
- (4) R. K. Wolff, M. J. Bronskill, and J. W. Hunt, *J. Chem. Phys.*, **53**, 4211 (1971).
- (5) J. E. Aldrich, M. J. Bronskill, R. K. Wolff, and J. W. Hunt, *J. Chem. Phys.*, **55**, 530 (1971).
- (6) O. Mičić, V. Marković, and D. Nikolić, *J. Phys. Chem.*, **77**, 2527 (1973).
- (7) Z. D. Draganić and I. G. Draganić, *J. Phys. Chem.*, **77**, 765 (1973).
- (8) B. M. Weeks, S. A. Cole, and W. M. Garrison, *J. Phys. Chem.*, **69**, 4131 (1965).
- (9) C. R. Maxwell, D. C. Patterson, and N. E. Sharpless, *Radiat. Res.*, **1**, 530 (1954).
- (10) J. V. Davies, M. Ebert, and A. J. Swallow, in "Pulse Radiolysis," M. Ebert, J. P. Keen, A. J. Swallow, and J. H. Baxendale, Eds., Academic Press, New York, N. Y., 1965, p 165; R. Brams, *Radiat. Res.*, **27**, 319 (1966).
- (11) E. Peled and G. Czapski, *J. Phys. Chem.*, **74**, 2903 (1970).

Thermodynamic Group Contributions from Ion Pair Extraction Equilibria for Use in the Prediction of Partition Coefficients. Correlation of Surface Area with Group Contributions¹

Sister Marie Joan Harris,² Takeru Higuchi,* and J. Howard Rytting

Departments of Chemistry and Pharmaceutical Chemistry, University of Kansas, Lawrence, Kansas 66044

(Received February 5, 1973; Revised Manuscript Received July 16, 1973)

The ion pair extraction constants for 26 alkyl sulfates have been determined at a minimum of nine temperatures from which the free energy, enthalpy, and entropy of transfer data were calculated for 18 different organic groups. The trends in the free-energy data are interpreted in terms of interfacial interactions, water structuring, and specific solvation in the aqueous phase. From correlations between the free energies of transfer for the hydrocarbon groups investigated and their respective van der Waals volumes and relative surface areas, it is demonstrated that interfacial solute-solvent interactions in the aqueous phase, as reflected by the relative surface areas, are of greater significance than the volume of the solute in determining the solution behavior of organic molecules. A simple method for measuring surface areas with molecular models is described and evaluated, and the areas thus determined are shown to correlate closely with free energies of transfer of saturated hydrocarbon groupings from water to a nonpolar phase. From the extraction data for a homologous series of alkyl sulfates, it was found that the transfer process was an entropy controlled one below 25° for the larger anions. It was also shown that, at 30°, there was a constant increment of -916 cal/mol in the free energy, -378 cal/mol in the enthalpy, and 1.77 eu in the entropy of transfer for each additional methylene group for those anions containing five or more carbons. The importance of the specific solvation of polar groups in the organic phase was evaluated for the halogen substituents and the ether group. Although the results indicated that the increase in the average solvation number is not large, the absolute magnitude of the thermodynamic data should be affected by the additional 0.25 and 0.50 molecules of chloroform found to be solvating the ion pairs containing the halide and ether groups, respectively.

Introduction

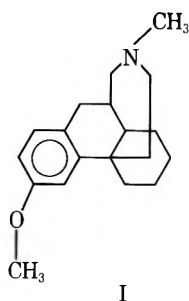
One of the major goals of research in the field of solution thermodynamics has been the development of *a priori* methods for the prediction of solution behavior and the utilization of these methods in various physical and biological studies. However, rigorous attempts to predict how a given solute will behave in a given solvent simply from the physical properties of the pure components have been limited almost entirely to mixtures of nonpolar species.³ The semiempirical group contribution approach is, however, an *a priori* method which has achieved a relative degree of success. In this approach a molecule is considered to be composed of groups which are associated with certain thermodynamic properties. Consequently, the activity coefficient, free energy, or partition coefficient can be found from the sum of the values for the different groups comprising the molecule. In contrast to the more theoretical approaches, this method is derived solely from an analysis of empirical data. However, the results frequently assume a form similar to those mathematically derived from statistical mechanics. This concept was first introduced by Langmuir⁴ as the "principle of independent surface action," and was verified and refined by Butler in his papers on the thermodynamics of hydration.^{5,6}

Since that time many investigators have applied the group contribution approach to the transfer of a whole molecule from one phase to another. Nevertheless, the application of this concept has been limited largely through lack of accurate data. At this time we wish to report some of the necessary data and also a relatively simple predictive approach which seems to yield numerical values for

free energies of such phase transfers from water to nonpolar solvents for various hydrocarbon groupings. The approach used permits accurate and ready estimation of partition coefficient values for these systems and also provides an additional insight into the nature of solute-solvent interactions in both aqueous and nonaqueous systems.

Various types of experimental data have been used to obtain values for the transfer of functional groups between phases.³ Measured partition coefficients have been particularly useful. However, the limited solubility of many organic molecules in water often presents difficulties in measuring partition coefficients. Thus, the use of ion pairs to facilitate the measurement of partition coefficients was considered. The feasibility of such an approach is supported by correlations reported by Schill and his coworkers^{7,8} between measured extraction constants and carbon number, and by the previous thermodynamic data obtained from the studies of ion pair extraction equilibria in this laboratory.⁹

In this study, the protonated form of dextromethorphan, *d*-3-methoxy-*N*-methylmorphinan (I), was chosen as the extracting cation to be paired with several inorganic anions and a series of alkyl sulfates. The organic phase consisted of chloroform or chloroform-carbon tetrachloride mixtures where the chloroform acted as a solvating agent to aid in the extraction process. A detailed investigation of the effects of such factors as pH, anion concentration, ion pair dissociation, and extraction procedures on the observed ion pair extraction constants was conducted also.¹⁰ In addition, a correlation was made between the corre-



sponding free-energy differences attributable to alkyl substituents and their effective surface areas. These differences were found to be essentially determined by the effective surface areas exposed by the hydrocarbon groups in the aqueous phase, and to a lesser degree by the surface interactions of the same solute groupings in the organic phase.

Experimental Section

Ion Pair Extraction Studies. Equipment and Reagents. All absorbance readings were made using a Cary Model 16 spectrophotometer and complete spectra were recorded on a Cary Model 15 spectrophotometer. Shaking was carried out on a Burrell Wrist-Action shaker and all pH measurements were determined with a Corning Model 12 research pH meter.

Dextromethorphan, obtained through the courtesy of Vick Divisions Research of the Vick Chemical Co., was found to be 99.75% pure by a nonaqueous titration.¹¹ All other chemicals used in the study were Analytical Reagent grade.

Solutions were prepared with water which had been distilled a second time from acid permanganate in an all glass apparatus. Reagent grade chloroform was shaken three times with distilled water to remove its preservative, dried over phosphorus pentoxide, and distilled immediately prior to its use. Reagent grade carbon tetrachloride was also distilled before use.

Phosphate buffers were prepared to contain 0.1 *M* NaH₂PO₄ and sufficient H₃PO₄ to adjust the pH to the desired value. A pH of 2.40 was most commonly employed. The buffer solutions were saturated with the organic phase prior to use.

Chloroform-carbon tetrachloride mixtures were prepared on a per cent volume basis and all organic phases were saturated with water prior to use.

Preparation of the Sodium Alkyl Sulfates. Equimolar amounts of the respective alcohol and concentrated sulfuric acid were mixed in an ice bath and allowed to react at room temperature for 48 hr. The mixture was diluted with water and was neutralized with sodium carbonate. After evaporating to dryness, at room temperature, the residue was extracted with hot methanol and the solution was again evaporated. This residue was recrystallized twice from hot methanol-2-propanol mixtures and the product was dried in a vacuum oven for 3 hr.

Procedure. Ten milliliters of the aqueous phase was placed with 10 ml of the organic phase in a sealed 25-ml volumetric flask. Twenty-five-ml flasks were used to reduce the amount of vaporization of the organic phase. The two phases were shaken for 2 hr in water baths held at constant temperatures controlled to $\pm 0.05^\circ$. A determination of extraction constants as a function of shaking time indicated that equilibrium is reached within 15 min. The shaker was stopped and the flasks were allowed to equili-

brate for at least 10 min. The contents of the flasks were transferred to separatory funnels equilibrated to the same temperature as the solutions. The two phases were separated with the aqueous phase being filtered through a small plug of glass wool. If readings were to be made on the organic phase, the ion pair was converted to the free base by shaking the organic phase in a volumetric flask at room temperature for 45 min with about 10 ml of 0.1 *M* NaOH which had been saturated with the respective organic phase. The contents were transferred to a separatory funnel and the organic phase was collected. Using data given in ref 10, the concentrations of dextromethorphan in the aqueous NaOH phase both in the protonated and free base form was found to be negligible (<0.1%) compared with dextromethorphan in the organic phase. In most cases, readings were made only on the aqueous phase, and the concentration of the ion pair in the organic phase was found by difference. However, readings were made on the organic phase for all of those anions exhibiting an interfering uv spectrum of their own. Aqueous solutions containing four to six different anion concentrations and approximately 5×10^{-4} *M* dextromethorphan were shaken at nine to ten different temperatures for each anion investigated. The overall range of anion concentrations was 9×10^{-4} – 7×10^{-2} *M*. For short-chain alkyl sulfates, the concentrations were about $(1.0\text{--}5.0) \times 10^{-2}$ *M*, while for the majority of the compounds, the anion concentration range was about $(1.0\text{--}5.0) \times 10^{-3}$. All data can be considered to be obtained under conditions of infinite dilution, so that the concentrations of the species under investigation are equal to their activities.

Surface Area Measurements. The relative surface areas of the group (*tert*-butyl being set equal to one) were estimated by covering CPK atomic models obtained from the Ealing Corp., Cambridge, Mass., with spheres approximately corresponding to hydrogen atoms in diameter and determining the average number of such contacting spheres. Spheres the size of hydrogen atoms were rather arbitrarily chosen to approximate the maximum possible surface area "seen" by the hydrogen atoms of a water molecule. Styrofoam balls having a diameter of 1 in. were attached to the models with rubber cement. Care was taken to get as many spheres around the model as possible while being certain that each sphere came into actual contact with the model. A plane formed by placing the model on a flat surface using the point of attachment of the group was used to define the surface to be measured. After all the spheres were in place, the number of spheres were counted and the average number of at least five determinations was used to calculate the surface area relative to the *tert*-butyl group. Often, more than five determinations were made, particularly in the cases where rotation and various conformations were possible. These were taken into account in arriving at the average number. Two individuals using styrofoam balls obtained from different sources (both labeled as 1 in. but having slightly different diameters) determined the areas reported here independently. Although the absolute number of spheres surrounding the groups differed significantly (*e.g.*, for the *tert*-butyl group the average values were 29 and 25.4) the relative surface areas showed good agreement.

Results and Discussion

Calculation of Group Contribution Data. The extraction of the protonated form of dextromethorphan paired with suitable anions seems to provide an ideal system for the

collection of thermodynamic data. In an attempt to ensure the accuracy of this data, an investigation of the ion pair extraction equilibria used in the study was undertaken. Three competing equilibria were found to interfere in the determination of true extraction constants: (1) the extraction of dextromethorphan as the free base; (2) the extraction of buffer anions; (3) the dissociation of the ion pair in the organic phase.

The extraction constant for the buffer ion (H_2PO_4^-) was measured between water and 100% CHCl_3 and found to be 4.76×10^{-2} at 25° . This small value should be even smaller in the 25% CHCl_3 in CCl_4 mixture used in this study. The amount of solvation of its ion pair by the chloroform molecules in the organic phase was relatively low. Such behavior is expected for large anions with dispersed charges.

The extent of dissociation of the ion pair in the organic phase was examined by making a series of measurements on dextromethorphan propyl sulfate into 25% chloroform in carbon tetrachloride at 25° . The dissociation constant was calculated to be 6.32×10^{-6} . Only at low anion concentrations, where the concentration of the ion pair in the organic phase approaches 10^{-6} or 10^{-5} M, is the ion pair dissociation significant. It was found that through proper control of pH (keeping the pH low) and the use of sufficiently large anion concentrations, interferences from 1 and 3 can be essentially eliminated.

Assuming that dissociation of the ion pair and extraction of the free base is negligible, the observed partition coefficient can be related to the anion concentration as follows

$$PC^{\text{obsd}} = K_{\text{DM}^+\text{X}^-}[\text{X}^-] + \text{constant} \quad (1)$$

at a constant pH, temperature, and buffer concentration where PC^{obsd} is the observed partition coefficient, $K_{\text{DM}^+\text{X}^-}$ is the true extraction constant, $[\text{X}^-]$ is the concentration of the anion, and the constant represents the extraction of the buffer anions. The true extraction constant was obtained by plotting PC^{obsd} vs. anion concentration and the slope becomes $K_{\text{DM}^+\text{X}^-}$. In all cases, a straight line with a positive nonzero intercept was obtained as predicted if dissociation is unimportant and the extraction of the other species occurs.

This part of the investigation served to emphasize the importance of thoroughly studying and understanding the factors affecting the efficient use of ion pair extractions. It further indicates that many interfering equilibria can be eliminated or adjusted for by simple variations in the extraction conditions. Details of this portion of the work can be found in ref 10.

Group contribution data can be obtained by an extrapolation procedure or by a difference method. In this study, the latter approach was adopted, and the thermodynamic data were collected by finding the difference between a substituted and unsubstituted parent compound, for example, $\Delta G_{30}(\text{3,3-dimethylbutyl sulfate}) - \Delta G_{30}(\text{ethyl sulfate}) = \Delta \Delta G_{30}(\text{tert-butyl})$. This method supplies true group contribution values provided the hydrogen atom which has been replaced makes an insignificant contribution to the thermodynamics of transfer. Nemethy and Scheraga¹² have pointed out that there is a significant difference in the number of water molecules around a methyl group, as compared to a methylene group, and various earlier extrapolation procedures have suggested that the contribution of a methyl group is about 1.06 kcal/mol greater than a methylene group.^{13,14} However, the validity

TABLE I: Thermodynamic Values for the Extraction Equilibria of Dextromethorphan Alkyl Sulfate Ion Pairs between Water and 25% v/v CHCl_3 in CCl_4

Alkyl sulfate	$\Delta G_{30},^a$ cal/mol	$\Delta H,$ cal/mol	$\Delta S_{30},$ eu
Ethyl	-190	-1258	-3.52
Propyl	-995	-2142	-3.78
Butyl	-1843	-3368	-5.03
Pentyl	-2806	-4155	-4.45
Hexyl	-3774	-4544	-2.54
Heptyl	-4633	-4960	-1.08
Octyl	-5575	-5281	0.97
3-Methylbutyl	-2697	-3035	-1.11
3,3-Dimethylbutyl	-3326	-3960	-2.09
Cyclohexylpropyl	-5409	-5422	-0.29
Cyclohexylethyl	-4595	-4919	-1.07
Phenethyl	-3166	-5006	-6.07
Phenylpropyl	-3823	-5578	-5.79
Phenylbutyl	-4715	-5641	-3.06
4-Pentene 1-sulfate	-1941	-3803	-6.14
5-Hexene 1-sulfate	-2538	-3048	-1.68
Cyclopentylethyl	-3889	-4384	-1.63
3-Bromo-1-propyl	-1802	-3931	-7.02
3-Methoxy-1-propyl	-629	-2229	-5.28
3-Methyl-1-pentyl	-3566	-3981	-1.37
2-Butoxy-1-ethyl	-2243	-1350	2.95
p-Fluorophenethyl	-3345	-4759	-4.66
3-Chloro-1-propyl	-1434	-3345	-6.30
Neooctyl	-5031	-4118	3.01
Phenoxyethyl	-3087	-4860	-5.85
Fluoroethyl	-228	-1707	-4.88

$$^a \Delta G = -RT \ln K_{\text{extraction}}$$

of extrapolation procedures is questionable, and no additional evidence for this end group effect has been presented. Consequently, the overall group contribution values obtained in this study probably include an end group contribution, the value of which is presently unknown.

Table I summarizes the thermodynamic data from which the group contribution data tabulated in Table II were calculated. The actual extraction constants for each alkyl sulfate are listed in ref 10. The π values are defined after the manner of Hansch¹⁵ (i.e., π is defined as $\pi = \log P_X - \log P_H$, where P_H is the partition coefficient of the parent compound and P_X is the value for a derivative). The F factors are the antilogs of the π values and represent the factor by which the partition coefficient changes when the group is substituted in a molecule. When several derivatives were investigated to find the thermodynamic properties of a single group, the alkyl derivative from which the data were derived is shown in parentheses in Table II.

The reproducibility of the free-energy data for nonpolar or slightly polar groups, together with their agreement with values obtained in earlier investigations, serves to emphasize the reliability of the results found in this study. The accuracy of the enthalpy and entropy data for these groups, however, is less reliable, inasmuch as the data were differentiated to obtain the ΔH values, and an assumption was made that the enthalpy change of transfer is temperature independent.

Solvation of Polar Groups. In interpreting the data listed in Table II, the fact that the organic phase in this study consisted of 25% chloroform in carbon tetrachloride

TABLE II: Thermodynamic Values for Various Organic Groups at 30°

Group	$\Delta\Delta G_{30}$, cal/mol	$\Delta\Delta H$, cal/mol	$\Delta\Delta S_{30}$, eu	π value	F factor
Neohexyl	-4831	-2860	6.53	3.49	3090
Cyclohexyl	-4405 (Et)	-3661	2.45	3.18	1510
	-4414 (Pr)	-3280	3.49	3.18	1510
Neopentyl	-4036	-1976	6.79	2.91	813
Cyclopentyl	-3699	-3126	1.89	2.67	468
sec-Butyl	-3376	-2723	2.15	2.43	269
tert-Butyl	-3136	-2702	1.43	2.26	182
Phenyl	-2872 (Bu)	-2274	1.97	2.07	118
	-2828 (Pr)	-3436	-2.01	2.04	110
	-2976 (Et)	-3748	-2.55	2.14	139
Phenoxy	-2897	-3602	-2.33	2.08	120
Isopropyl	-2507	-1777	2.41	1.81	64.6
Butoxy	-2053	-92	6.47	1.48	30.2
Ethylene	-947	-1891	-3.09	0.68	4.79
Methylene	-916	-378	1.77	0.66	4.57
Bromo	-807	-1789	-3.24	0.58	3.80
Chloro	-439	-1203	-2.52	0.32	2.09
4-Fluoro	-179	247	1.41	0.13	1.35
(aromatic)					
Fluoro	-38	-449	-1.36	0.03	1.06
(aliphatic)					
Methoxy	303	-87	-1.50	-0.26	0.55
-O-					
(MeOPr ⁻)	1214	1139	-0.25	-0.88	0.13
(BuOEt ⁻)	1541	3208	5.50	-1.11	0.08
(PhOEt ⁻)	79	146	0.22	-0.06	0.87

must be taken into consideration. Consequently, the thermodynamic values for the polar groups investigated reflect the specific solute-solvent interactions existing in both the aqueous and the organic phases. Behavior of this type is expected for the halogen substituents, the phenyl group, and groups with ether linkages. The average solvation number of the ion pair in the organic phase should be indicative of the extent of this interaction. The extent of solvation can be obtained from measurements of extraction constants as a function of chloroform concentration employing

$$\log K^{\text{obsd}} = \log K_{\text{DM}^+\text{X}^-} + n \log [\text{CHCl}_3] \quad (2)$$

where $K^{\text{obsd}} = \frac{[(\text{DM}+\text{X}^-)(\text{CHCl}_3)_n]/[\text{DM}][\text{X}^-]}{[(\text{DM}+\text{X}^-)(\text{CHCl}_3)_n]/[\text{DM}][\text{X}^-][\text{CHCl}_3]^n}$, and n = the average solvation number. The average solvation numbers for 3-chloropropyl sulfate, propyl sulfate, butoxyethyl sulfate, and hexyl sulfate were found from the slopes of the graphs shown in Figure 1. As expected, the normal alkyl sulfates exhibited approximately identical average solvation numbers of 2.76 and 2.82 for hexyl and propyl sulfates, respectively, while values of 3.26 and 3.08 were found for butoxyethyl sulfate and 3-chloropropyl sulfate. From the difference in the numbers found for the anions containing the polar groups and their corresponding alkyl sulfates, an additional 0.26 molecule of chloroform was shown to solvate the halogen-substituted ion pair, while the solvation number was increased by 0.50 for the molecules containing the ether linkage. Although these increases in the average solvation number are small, their effect on the thermodynamic values appears to be significant, and must be considered when using the data collected in this study.

Effect of the Surface Area of the Group. When examining theoretical explanations for solution behavior, it is found that the solution process is frequently divided into three steps: the removal of the solute molecule from its

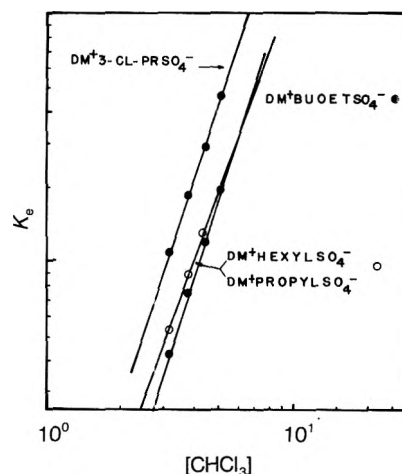


Figure 1. Determination of the average number of chloroform molecules solvating the ion pairs in the organic phase. Scale for K_e is 1-100 for 3-chloropropyl sulfate and propyl sulfate, 10-1000 for butoxyethyl sulfate, and 100-10,000 for hexyl sulfate.

environment; the formation of a cavity in the liquid to which it is being transferred; and the introduction of the solute molecule into the cavity. According to these considerations, the thermodynamic properties of a solute in solution ultimately depend on two factors (the size of the solute molecule and the magnitude of the molecular interaction energies). Using the free energy of transfer data obtained in this study, an attempt was made to clarify whether the effective surface area or the volume of the solute species is more important in determining its thermodynamic properties in solution.

The relative surface areas of a wide variety of saturated straight chain, branched chain, and cyclic hydrocarbon groups were measured as described in the Experimental Section and are reported in Table III.¹⁶ In columns SD,

TABLE III: Relative Surface Areas for Several Saturated Hydrocarbon Groups

Functional group	Relative surface ^a area		% ^b SD	% ^c SE	n
	A	B			
Methyl		0.51	0	0	6
Ethyl	0.70	0.74	2.2	0.9	6
<i>n</i> -Propyl	0.93	0.96	2.2	1.0	5
Isopropyl	0.88	0.90	3.7	1.6	5
<i>n</i> -Butyl	1.18	1.18	3.8	1.2	10
sec-Butyl	1.08	1.15	1.6	0.6	8
<i>tert</i> -Butyl	1.00	1.00	2.2	1.0	5
<i>n</i> -Pentyl	1.42	1.42	0.9	0.3	10
Neopentyl	1.29	1.29	1.5	0.5	7
Cyclopentyl	1.18	1.20	3.5	1.1	10
Cyclohexyl	1.38	1.33	3.4	0.6	33
<i>n</i> -Hexyl	1.70	1.64	3.6	1.2	9
sec-Hexyl		1.40	1.5	0.7	5

^a These are relative surface areas with the *tert*-butyl group set equal to one. Those values in column A were determined by one individual and those in column B by another. The statistical data refer to the values in column B. ^b This refers to the per cent standard deviation in the *n* values reported in column B for that group. ^c This refers to the per cent standard error for the values in column B.

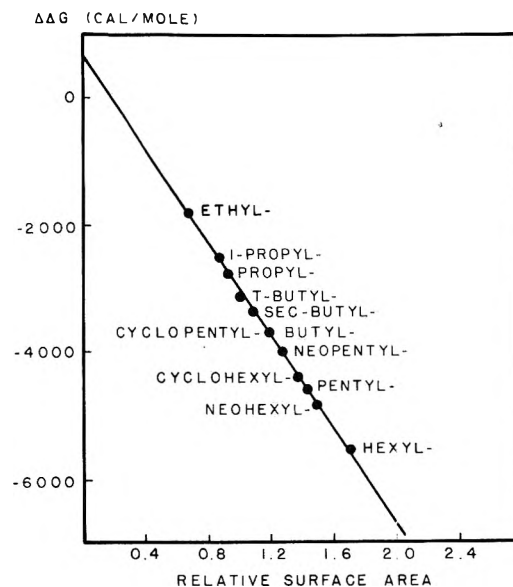
SE, and *n* are listed the standard deviations, standard errors, and number of measurements made in the determination of the values listed in column B. The average of the standard deviations for all groups measured¹⁶ is 1.6% and of the standard error, 0.6%. These values are quite good when one considers that a difference of one sphere will introduce from 2 to 6% difference in the value obtained for most of the molecules considered.

In Figure 2 is shown the correlation obtained between the free energies of transfer taken from Table II for a number of saturated straight chain, branched chain, and cyclic hydrocarbon groups and their relative surface areas in water.

It is evident from the plot that there is a direct relationship between the free energy of transfer and the relative surface areas of all of the groups. It may also be noted that despite the differences in molecular configuration, the butyl and the cyclopentyl groups are represented by the same data point. This behavior is also in line with Langmuir's suggested relationship between the activity coefficient of a solute and its interfacial energy of interaction,⁴ with Butler's interaction energies proposed to explain the thermodynamic data obtained for the hydration of alcohols and alkyl halides,^{5,6} and with recent correlations between the surface areas of solutes and their partition coefficients,¹⁷ solubilities,¹⁸ and complex formation constants.¹⁹

Interesting results were observed when the thermodynamic values for the pair, butoxy and pentyl, and the pair, phenyl and cyclopentyl, were compared. Each group within the respective pairs has the same relative surface area and differ only in that the first member of each pair can undergo specific solvation by the two phases. Table IV tabulates the data for comparison.

According to the above proposal, groups having the same relative surface areas should exhibit the same free energies of transfer. In both cases, the groups in Table IV which are capable of undergoing specific interaction with the two solvent phases have free energies of transfer which are more positive than predicted. Assuming that the solute-solvent interactions in the aqueous phase are stronger than those in the organic phase, the transfer of the

**Figure 2.** A correlation between the free energies of transfer at 30° and the relative surface areas of common organic groups.**TABLE IV: A Comparison of Enthalpies and Entropies of Transfer for Groups with Similar Relative Surface Areas**

Group	$\Delta\Delta G_{30}$, cal/mol	$\Delta\Delta H$, cal/mol	$\Delta\Delta S_{30}$, eu
Butoxy	-2053	-92	6.47
Pentyl	-4580	-1880	8.85
Phenyl	-2872	-2274	1.97
Cyclopentyl	-3699	-3126	1.89

group should require heat. As a result, the overall enthalpy of transfer should be more positive than that expected in the absence of specific solvation. Although the absolute values of the enthalpy data in Table IV are questionable, they do show the expected trends. It can also be assumed that interactions between water and a butoxy group should be stronger than between water and a phenyl group, and this seems to be reflected in the greater difference between the free energies of transfer for the butoxy and pentyl groups compared to that for the phenyl and cyclopentyl groups. Consequently, it would appear that the free-energy values for groups capable of undergoing specific solvation by either phase will be in direct proportion to the strength of the specific solute-solvent interactions involved.

Effect of the Volume of the Group. Contrary to the above proposal, some workers²⁰⁻²⁵ have postulated that the thermodynamic properties of a solute in solution are primarily determined by the volume of the solute molecule. Figure 3 shows the free-energy data obtained in this study correlated with the van der Waals volumes calculated from the values given by Bondi,²⁶ while Figure 4 is a graph published by McAuliffe²⁷ for the solubility of hydrocarbons in water as a function of their molar volumes. In both plots, there does not appear to be a similar dependence on volume for the straight chain compounds as compared to the branched chain and cyclic compounds. This is in direct contrast to the behavior observed in the relative surface area correlation of Figure 2.

It is suspected that previous volume correlations are the fortuitous result of several factors. In most studies, the physical significance of the volumes used is ambiguous, and their values are highly dependent on the method cho-

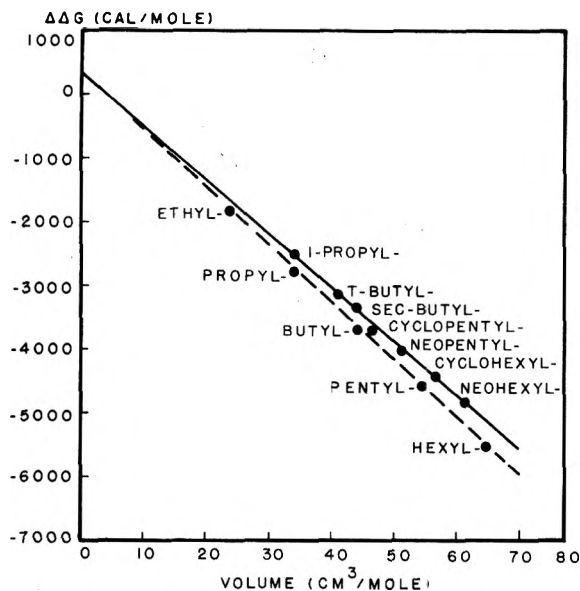


Figure 3. A correlation between the free energies of transfer at 30° and the van der Waals volumes of common organic groups.

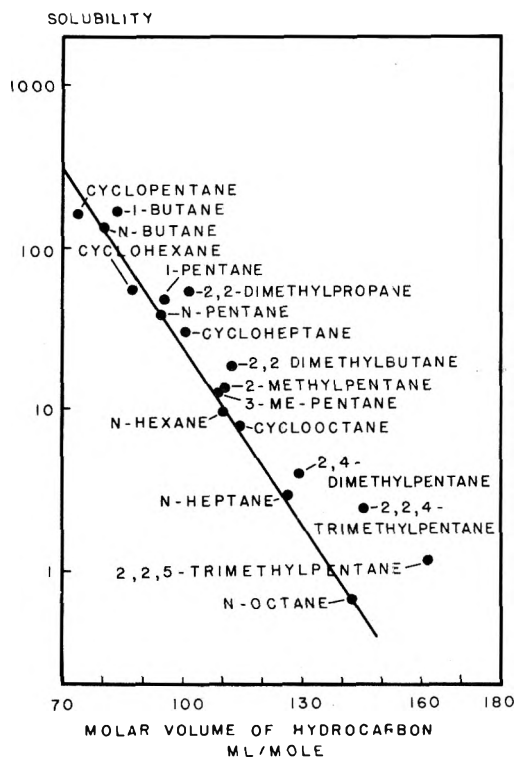


Figure 4. Solubility of hydrocarbons in water as a function of their molar volumes as reported by McAuliffe in ref 20.

sen to obtain them. Frequently, the compounds have been judiciously chosen so that only compact symmetrical molecules have been investigated. For such compounds, there appears to be a direct relationship between the volume and the effective surface area of the molecule, so that excellent correlations result with either property. In addition, many investigations have been limited to homologous series of compounds, which is, in effect, correlating the solution property with the volume of the methylene group.

It appears that in this study, many of these problems have been avoided through the investigation of a diverse selection of organic groups. The relative surface areas de-

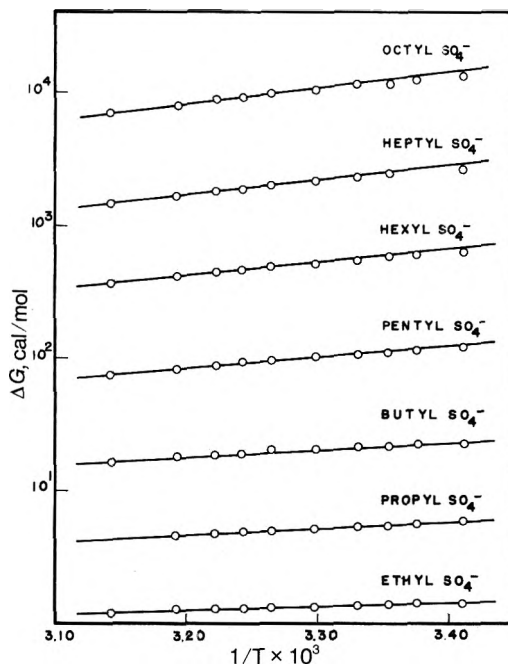


Figure 5. Van't Hoff plots for several alkyl sulfates extracted with dextromethorphan from pH 2.40 phosphate buffer ($\mu = 0.1$) into 25% CHCl_3 in CCl_2 .

termined by the method used in this investigation are independent of any volume measurements and should reflect the true values with a high degree of confidence. Subsequent to this work, a similar approach has been reported by Hermann,¹⁸ in which he calculated the surface areas of a number of hydrocarbon molecules and found that the areas were linearly related to the hydrocarbon solubility in water. Our studies confirm his results for functional groups, as well as whole molecules. A major difference between this study and Hermann's is that his surface areas are based upon calculations using bond lengths, atomic radii, and solvent molecule radii and solved by a computer, whereas, in this work, molecular models were used, and the relative surface area estimated from the number of spheres that one could place around the model. The excellent correlation obtained with the relative surface areas seems to indicate that although the volume of a molecule or group cannot be neglected, the interfacial interactions between water and the solute are of greater importance in explaining the thermodynamic behavior of organic molecules in aqueous solutions. Such a correlation further implies that it may be possible to predict partition coefficients for large hydrophobic molecules, which are difficult to obtain empirically, from a simple determination of their relative surface areas. Table III (microfilm edition)¹⁶ includes surface area measurements for a large number of saturated hydrocarbon groups which should prove useful in such predictions.

Methylene Group. By far, the greatest amount of group contribution data has been collected for the methylene group. Essentially this is due to the ease with which partition coefficient and solubility measurements can be made for a homologous series of compounds. In this study, the protonated form of dextromethorphan was paired with a series of alkyl sulfates from ethyl to octyl. Figure 5 shows the van't Hoff plots obtained for each homolog.

Figure 6 shows the relationship between the thermodynamic data of transfer and the number of carbons in the alkyl chains at 30°. Similar to the behavior reported for

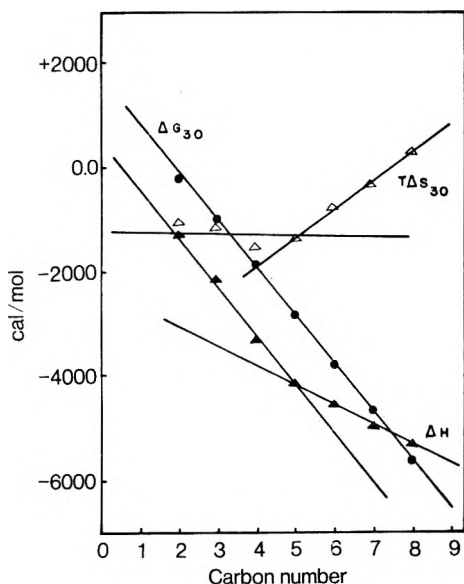


Figure 6. Thermodynamic properties as a function of carbon number for straight chain hydrocarbon groups at 30°.

the lower members of the alcohol and alkane series,²⁷⁻²⁹ ethyl sulfate is off the line due to the relative sizes and proximity of the ethyl and sulfate portions of the molecule. From the slope of the line, the free-energy increment per methylene group was found to be -917 cal/mol. This agrees quite well with reported values of -800 ,³⁰ -872 ,³¹ -850 ,^{3,32} and -988 cal/mol.³³ It appears that the enthalpic portion of Figure 6 is composed of approximately two straight lines. The transfer equilibrium for anions containing four or less methylene groups seems to be an enthalpy controlled process in which there is a constant increment of -992 cal/mol/ $-\text{CH}_2-$. Once the chain length reaches five or more carbons, both the enthalpy and entropy increase steadily by -378 cal/mol and 1.77 cal/mol/deg for each additional methylene group. Data for these alkyl sulfates between 20 and 30° yielded a similar plot except that for the larger aliphatic compounds, the transfer process appears to be entropy controlled. This is reflected in an apparent leveling of the enthalpy of transfer and a rapid increase in the entropy of transfer as the chain lengthens.

In recent years, although the additivity of the enthalpic and entropic portion of the solution process has been questioned, some investigators have shown that if the studies are extended to compounds with sufficiently long chains, a constant increment in the enthalpy is observed.³⁴⁻³⁶ However, it has also been observed that compounds with chains longer than C_8 no longer seem to exhibit a constant increment in their excess enthalpy values with carbon number.^{34,37} The change in the methylene group contribution at or around C_5 which is observed in Figure 6 for the enthalpy curve has previously been reported for measurements of the heat of micelle formation and for heats of solution studies³⁴⁻³⁷ and seems to be satisfactorily ascribed to a head group effect. The behavior observed in this study at temperatures greater than 30° agrees quite well with previous work, and it can be concluded that, although the excess enthalpy and entropy values for a group are much more sensitive to chain length than the free energy, all three thermodynamic properties for a methylene group are additive, and the surface area of the solute molecule is the important factor in determining the thermodynamic qualities.

Cyclic Hydrocarbons. Values of -4405 and -3699 cal/mol were found for the free energy of transfer associated with a cyclohexyl and cyclopentyl group, respectively. Using the value of -916 cal/mol/ $-\text{CH}_2-$ which was determined earlier, the values of the excess free energy found for the cyclohexyl and cyclopentyl groups are equivalent to acyclic compounds containing five and four carbons, respectively. Consequently, it appears that ring closure has the effect of raising the free energy to a value comparable to that of a normal alkyl chain containing one less methylene group than the cyclic structure.

The increased solubility of cyclic compounds in water seems to be due to both enthalpy and entropy effects, neither of which appears to be the controlling factor. It may be noted that both cyclic anions show more positive enthalpies and more negative entropies of transfer than the corresponding aliphatic ions. From an examination of Figure 2 and Figure 3, it can be seen that both the relative surface areas and the van der Waals volumes are greater for the normal alkyl chains. Since it has been shown earlier that the free energies of transfer for hydrocarbon groups are a function of the effective surface areas of the groups, a greater amount of interfacial interaction is expected between the normal alkyl anions and water. Therefore, it seems plausible to attribute the increased solubility of cyclic hydrocarbons to their compact structure. However, this does not seem to be reflected in the trends in the enthalpy values listed in Table I. Consequently, it appears that either due to the inaccuracy of the enthalpy data, or due to some effect peculiar to the systems investigated, it is impossible to support any particular explanation for the increased solubility of cyclic hydrocarbons with the thermodynamic data available.

Phenyl Group. The phenyl group is an important group because of the frequency with which it appears in so many compounds. However, it must be kept in mind that the thermodynamic values found in this study for this group are influenced by the specific interactions occurring between the π electrons of the phenyl group and the chloroform molecules in the organic phase. Consequently, the data for this group indicate a lower solubility in the aqueous than would have been obtained if a nonpolar organic phase had been employed, but the values can be of use to indicate obvious trends in comparisons to saturated hydrocarbons.

In order to verify the reproducibility of the data, the group contribution values of the phenyl group were determined from a study of the phenyl-substituted ethyl, propyl, and butyl ion pairs for which the free energies of transfer of the alkyl sulfates were found to be -3166 , -3823 , and -4715 cal/mol, respectively. The difference between each pair should be equal to the contribution of a methylene group. However, it can be seen that this is only true for phenylpropyl sulfate and phenylbutyl sulfate. The sensitivity of the phenyl group to the chain length of the parent compound probably arises from its ability to interact with the charge center since a comparison of cyclohexylethyl sulfate and cyclohexylpropyl sulfate, with free energy values of -4595 and -5408 cal/mol indicate approximately the correct contribution for a methylene group. This example serves to point out the importance of separating the group under study far enough from the sulfate portion of the anion, and renders questionable any data obtained from compounds with very short chains. It also indicates that *a priori* predictions using group contribution data most probably will require a correction term

if a molecule contains two polar groups sufficiently close to interact with each other.

It again appears that the group contribution to the free energy remains constant once the chain length is sufficiently long. Other workers have reported free-energy values of -2905^{38} and -4979 cal/mol.³⁹ On the other hand, it seems that the enthalpy and entropy values are very dependent on the compound used to obtain them, which could be an example of the compensation phenomenon described by Lumry and Rajender⁴⁰ that they attributed to some vague type of water interaction. In this study, however, it may also be possible that variations in the enthalpy and entropy data could arise from the method used to find them. When calculating thermodynamic properties from the difference in the data for a substituted and unsubstituted parent compound, an implicit assumption is made that the thermodynamic behavior of the alkyl chain in the parent compound and substituted compound is identical. Two factors may render this assumption invalid. First, if the substituent is a large bulky group, it may shield the alkyl chain from the surrounding water molecules. The shorter the chain, the more significant would be this effect. This would result in an overall decrease in the enthalpy and entropy values relative to the values expected if the group had no effect on the chain. Second, a large substituent on the end of an alkyl chain could also limit the number of configurations the chain could assume in comparison to the unsubstituted parent compound. This would imply that in the substituted compound a larger surface may be exposed to interact with water, and therefore, a greater amount of water structuring would occur relative to the normal unsubstituted alkyl sulfate. Consequently, the enthalpy and entropy of transfer would be higher than the expected values. It is impossible to definitively say which effect is more important, and the data in Table I could be interpreted either way, with the former effect dominating in the propyl derivative and the latter in the butyl derivative. It might be speculated that if the chain length were sufficiently long these effects would become negligible and a constant value for the enthalpy and entropy for each group would be observed.

It is interesting to compare the group contribution data listed in Table II for the phenyl group and the cyclohexyl group, both of which were calculated from their propyl derivatives. It can be seen that the substitution of a phenyl group on a compound renders it 14 times more water soluble than the use of a cyclohexyl group in this extraction system, and the effect would be even larger for extraction into a nonpolar organic solvent. The source of this effect seems to be the large positive entropy of transfer associated with the cyclohexyl group which probably arises from the significant amount of water structuring caused by this group relative to the phenyl group. Although the absolute values of the enthalpy and entropy data are questionable it appears from this preliminary data that the overall solubility of the compound in water is influenced to a much greater extent by this structuring effect than by the specific solvation of the phenyl group in the aqueous phase.

Ether Group. The presence of an oxygen atom with its lone pair of electrons should result in an increased water solubility due to interactions between the oxygen and the dipoles of the water molecules. Butler has calculated these interactions to be of the order of 5100 cal⁴¹ while McGowan has indicated that the actual values are highly

dependent on the molecules studied.⁴² Several other publications have listed free-energy data for aromatic and aliphatic alkoxy compounds,^{15,43-45} and all of these seem to reflect the strong interaction of the ether group with water. Similar findings have appeared in this investigation, but, once again, the values are altered, due to interactions between the group and the chloroform molecules in the organic phase. For anions containing an ether group, even the free energy of transfer, which has been independent of the compounds studied, for other groups, shows a wide variation. In addition, the values appear to be much lower than the 3000 cal/mol predicted from activity coefficient measurements. As indicated earlier, this is probably due to the nonideal behavior of the ether compounds in the organic phase in this study, in addition to the effect of the relatively small separation of the ether group from the sulfate portion of the anion. It may be noted, that the enthalpy values do reflect the specific solvation of the oxygen atom by water molecules. Of the groups studied, with the exception of the aromatic fluoro group, molecules containing an oxygen atom are the only ones showing positive enthalpy values. The drastic decrease in the contribution of the ether linkage derived from phenoxyethyl sulfate reflects both the electronic interactions of the phenyl group with the oxygen atom and the shielding effect of this bulky group, which prevents the oxygen from interacting with the water molecules. As a result, a comparison of the F factors in Table II indicates that the use of a phenyl group or a phenoxy group as a substituent will have approximately the same effect on the partition coefficient.

Halogen Groups. A scarcity of information exists for aliphatic substituents, but Hansch has reported⁴⁶ values of -532 cal/mol for chloro, -818 cal/mol for bromo, and 232 cal/mol for fluoro which are similar to the data observed in this investigation. Although the interaction between the organic phase and the halogen derivatives is not large, it must be kept in mind that the thermodynamic values for these groups are affected by this interaction. It appears that the free energy of transfer tends to become more negative as the size of the group increases. Since compounds containing halogen substituents exhibit a dipole, solvent-solute interactions are expected, and should be reflected in the enthalpy and entropy values. However, similar results should also arise from the disordering of water structure as the size of the group increases. Therefore, the gradual decrease in the enthalpy and entropy in the order $F^- > Cl^- > Br^-$ is probably due to both factors. The difference in the behavior of an aromatic fluoro group as compared to an aliphatic one is common to all halogen substituents.^{15,46} The fluoro group should act to withdraw electrons from the ring, allowing it to interact more strongly with nearby water molecules. This specific solvation effect is indicated in Table II by the positive enthalpy and entropy of transfer values listed for the aromatic fluoro group in comparison to the negative values for the group as an aliphatic substituent. It can be assumed that, in general, the halides decrease the water solubility of a molecule more as an aliphatic substituent than as an aromatic group and, in all cases, their effect on the partition coefficient is only slight.

Branched Hydrocarbons. It has long been observed that a branched isomer is more soluble in water than the straight chain one. This increased solubility can be predicted from a consideration of effective surface areas, since the isomer with the greater degree of branching

should also have the smallest effective surface area exposed to its aqueous surroundings. Consequently, the interaction energy should be less, and the branched compound should be more soluble in water.

Once again, the increase in water solubility with branching is reflected in the difference in the free-energy values for *tert*-butyl and *sec*-butyl. From the results obtained for neopentyl and neohexyl, it can be concluded that branching on nearby carbon atoms does not seem to influence to any large degree the contribution of a methylene group. It was previously found to be -916 cal/mol, and from these data, it is calculated as -800 cal/mol. The large positive entropies of transfer are indicative of the water structuring caused by these groups. Thus, it would appear that these substituents act to increase the partition coefficient of a given compound primarily through an entropy controlled process.

The value of the free energy of transfer again seems to be independent of the compound chosen to determine it, while the enthalpy and entropy of transfer are quite sensitive to their environment. It was found that the excess free energies for a *tert*-butyl group determined from 3,3-dimethylbutyl sulfate and neo-octyl sulfate were -3136 and -3188 cal/mol, while the enthalpy values were -2702 and -750 cal/mol and the entropy terms were 1.43 and 8.04 eu. Due to the bulky nature of the *tert*-butyl group, it seems probable that the effect of its shielding of the chain from water interactions, and the influence of its size on the average configuration of the alkyl chain, as described earlier for the phenyl group, are also applicable in this case. The importance of either is difficult to ascertain due to the lack of any previously published enthalpy and entropy data for these groups.

Ethylene Group. The validity of the group contributions for the ethylene group is highly questionable due to the difficulty encountered in isolating the unsaturated sodium alkyl sulfate together with the fact that it too can interact with the organic solvent phase. However, the data are included in Table II to indicate the trends expected. The value of -947 cal/mol for the free energy of transfer for the ethylene group agrees closely with that observed by other workers.^{17,47} It indicates that the effect of the presence of each isolated double bond in a compound is comparable to that due to the presence of a single methylene group. It is impossible to place much significance on the enthalpic or entropic data for this group. However, it is expected that both terms should reflect specific interactions with the water phase, and consequently, should show endothermic behavior accompanied by an increase in the entropy term upon transfer into the organic phase.

Conclusions

The data presented in this study show that, for saturated hydrocarbon groups, excellent correlation is found for the free energy of transfer from aqueous to nonpolar phases with the surface areas of the group. A relatively simple method for estimating surface areas is described and analyzed. A statistical analysis indicates that the measurements probably have an average uncertainty of about 2%. Group contributions are reported for 18 functional groups and are interpreted in terms of interfacial interactions, water structuring, and specific solvation.

From the consistency of the thermodynamic data collected in this study, it can be concluded that ion pair extraction equilibria provide a feasible method for the determination of group contributions. Although the free-energy

values appear to be highly reliable, the enthalpy and entropy data seem to be very sensitive to the compounds and the method used for their determination. However, such information does serve to indicate trends and to designate controlling factors in the solution process.

The data collected and evaluated in this investigation should be of use in the *a priori* prediction of partition coefficients and excess thermodynamic properties for organic molecules provided the species in question contains no groups capable of interacting with each other. These predicted values can be of great significance for large molecules of importance in biological systems whose partition coefficients are difficult to determine. Further studies in this area should clarify the role of steric and electronic effects on the group contributions, investigate the contribution of a methyl group in aliphatic compounds, and verify the apparent compensation phenomenon observed in the enthalpic and entropic portion of the solution process.

Acknowledgments. This work was supported in part by the Institute of Pharmaceutical Chemistry, Division of Alza Corporation, and the University of Kansas General Research Fund.

Supplementary Material Available. The complete Table III, including surface area data for 120 saturated hydrocarbon groups, will appear following these pages in the microfilm edition of this volume of the journal. Photocopies of the supplementary material from this paper only or microfiche (105 × 148 mm, 20× reduction, negatives) containing all of the supplementary material for the papers in this issue may be obtained from the Journals Department, American Chemical Society, 1155 16th St., N.W., Washington, D. C. 20036. Remit check or money order for \$3.00 for photocopy or \$2.00 for microfiche, referring to code number JPC-73-2694.

References and Notes

- (1) Taken in part from the Ph.D. Dissertation by M. J. H., University of Kansas, 1971.
- (2) Present address. Department of Chemistry, Avila College, Kansas City, Mo.
- (3) S. S. Davis, T. Higuchi, and J. H. Rytting, *J. Pharm. Pharmacol.*, **24**, 30P (1972).
- (4) I. Langmuir, *Colloid Symp. Monogr.*, **3**, 48 (1925).
- (5) J. A. V. Butler, D. W. Thomson, and W. H. MacLennan, *J. Chem. Soc.*, 674 (1933).
- (6) J. A. V. Butler and P. Harrower, *Trans. Faraday Soc.*, **33**, 171 (1937).
- (7) G. Schill, *Acta Pharm. Suecica*, **2**, 13 (1965).
- (8) R. Modin and G. Schill, *Acta Pharm. Suecica*, **4**, 301 (1967).
- (9) A. F. Michaelis and T. Higuchi, *J. Pharm. Sci.*, **58**, 201 (1969).
- (10) M. J. Harris, Ph.D. Dissertation, University of Kansas, 1971.
- (11) J. S. Fritz, "Acid-Base Titrations in Nonaqueous Solvents," The G. Frederick Smith Chemical Company, Columbus, Ohio, 1952, p 13.
- (12) G. Nemethy, I. Z. Steinberg, and H. A. Scheraga, *Biopolymers*, **1**, 43 (1963).
- (13) R. Aveyard and R. W. Mitchell, *Trans. Faraday Soc.*, **66**, 37 (1970).
- (14) P. Molyneux, C. T. Rhodes, and J. Swarbrick, *Trans. Faraday Soc.*, **61**, 1043 (1965).
- (15) C. Hansch and T. Fujita, *J. Amer. Chem. Soc.*, **86**, 1616 (1964).
- (16) See paragraph at end of paper regarding supplementary material.
- (17) F. M. Plakogiannis, E. J. Lien, C. Harris, and J. Biles, *J. Pharm. Sci.*, **59**, 197 (1970).
- (18) R. B. Hermann, *J. Phys. Chem.*, **76**, 2754 (1972).
- (19) R. W. Wildnauer and W. J. Canady, *Biochemistry*, **5**, 2885 (1966).
- (20) I. Hanssens, J. Mullens, C. Deneuter, and P. Huyskens, *Bull. Soc. Chim. Fr.*, 3942 (1968).
- (21) H. W. Smith, *J. Phys. Chem.*, **26**, 350 (1922).
- (22) A. E. Rheineck and K. F. Lin, *J. Paint Technol.*, **40**, 611 (1968).
- (23) J. C. McGowan, *J. Appl. Chem.*, **2**, 323 (1952).
- (24) A. B. Lindenberg, *C. R. Acad. Sci. Paris*, **243**, 2057 (1956).
- (25) N. C. Deno and H. E. Berkeheimer, *J. Chem. Eng. Data*, **5**, 1 (1960).
- (26) A. Bondi, *J. Phys. Chem.*, **68**, 441 (1964).

- (27) C. McAuliffe, *J. Phys. Chem.*, **70**, 1267 (1966).
(28) R. Archibald, *J. Amer. Chem. Soc.*, **54**, 3178 (1932).
(29) C. H. Deal, E. L. Derr, and M. N. Papadopoulos, *Ind. Eng. Chem., Fundam.*, **1**, 17 (1962).
(30) J. A. V. Butler, C. N. Ramchandani, and D. W. Thomson, *J. Chem. Soc.*, 280 (1935).
(31) R. S. Hansen, R. A. Miller, and S. D. Christian, *J. Phys. Chem.*, **59**, 391 (1955).
(32) T. Higuchi and S. S. Davis, *J. Pharm. Sci.*, **59**, 1376 (1970).
(33) M. S. Mamtora, MS Thesis, University of Kansas, Lawrence, Kan., 1969.
(34) R. Aveyard and R. W. Mitchell, *Trans. Faraday Soc.*, **64**, 1757 (1968).
(35) L. Benjamin, *J. Phys. Chem.*, **68**, 3575 (1964).
(36) J. M. Corkill, J. F. Goodman, and J. R. Tate, *Trans. Faraday Soc.*, **63**, 773 (1967).
(37) F. Franks, *Nature (London)*, **210**, 87 (1966).
(38) J. H. Clint, J. M. Corkill, J. F. Goodman, and J. R. Tate, *J. Colloid Interface Sci.*, **28**, 522 (1968).
(39) D. J. Currie, C. E. Lough, R. F. Silver, and H. L. Holmes, *Can. J. Chem.*, **44**, 1035 (1966).
(40) R. Lumry and S. Rajender, *Biopolymers*, **9**, 1125 (1970).
(41) J. A. V. Butler, *Trans. Faraday Soc.*, **33**, 229 (1937).
(42) J. C. McGowan, P. N. Atkinson, and L. H. Ruddle, *J. Appl. Sci.*, **16**, 99 (1966).
(43) E. Deutsch and C. Hansch, *Nature (London)*, **211**, 75 (1966).
(44) R. P. Quintana and W. R. Smithfield, *J. Med. Chem.*, **10**, 1178 (1967).
(45) J. Iwasa, T. Fujita, and C. Hansch, *J. Med. Chem.*, **8**, 150 (1965).
(46) C. Hansch and S. Anderson, *J. Org. Chem.*, **32**, 2583 (1967).
(47) D. J. Lamb and L. E. Harris, *J. Amer. Pharm. Assoc.*, **49**, 583 (1960).

Surface Tension of Saturated Anhydrous Hydrogen Sulfide and the Effect of Hydrogen Sulfide Pressure on the Surface Tension of Water

Carlyle S. Herrick* and George L. Gaines, Jr.

General Electric Corporate Research and Development, Schenectady, New York 12301 (Received April 26, 1973)

Publication costs assisted by the General Electric Research and Development Center

The surface tension of anhydrous liquid H₂S in the temperature range 25–40° varies from 11.3 to 8.7 dyn/cm. The Guggenheim equation fits these data precisely. Measurements of the surface tension of water in contact with H₂S at pressures up to 300 psi and from 25 to 40° show that H₂S causes a greater reduction in surface tension with pressure than any gases previously studied. The data for H₂S and for other gases suggest that the maximum lowering of surface tension corresponds to the adsorption of one close packed monolayer of gas molecules on the water surface. H₂S and CO₂ reach monolayer adsorption at about ½ saturation pressure. In general, this behavior may permit order-of-magnitude prediction of surface tension effects from values of the pressure required for phase change. We have also obtained an estimate for the contact angle of H₂S-saturated water on the solid H₂S hydrate.

Introduction

In the GS process for enriching the deuterium content of natural waters,¹ liquid water and gaseous H₂S under pressure are contacted on a large scale and surface properties probably play an important role. Slowinski, *et al.*,² have shown that pressurized gases may substantially reduce the surface tension of liquids. In a limited study (below 1 atm) Tamamushi³ found that for equal pressures hydrogen sulfide gas had a larger effect on surface tension than several other gases. Rough estimates by Heuer⁴ showed that additions of H₂S (up to 10 mol % in the gas) caused increased surface tension reduction in the methane-water system. The authors of ref 2 and 3 suggest that the more condensable or more soluble gases have the larger effect. Accordingly, there is both practical and scientific interest in the effect of pressurized H₂S on the surface tension of water. This report presents and discusses such measurements. We also present the results of surface tension determinations on liquid H₂S.

Experimental Section

Surface tension measurements were made using the differential capillary rise method. Two Pyrex glass capillary

tubes, of radius 0.025 and 0.0595 cm, were mounted side by side in a Teflon holder which could be inserted vertically in a two-window pressure vessel. This vessel consisted of a commercial liquid level gage with top and bottom valves and fittings suitable for sample manipulation and flow-through cleaning. Only Teflon, type 316 stainless steel, and Pyrex glass were used in the assembly. The completed vessel had a maximum working pressure of about 2000 psi. In operation it was immersed with the capillaries vertical in a 20-gal controlled-temperature water bath. A thermistor sensor working through a commercial narrow proportional band solid state controller to an electric immersion heater controlled bath temperature to ±0.01°. Bath temperature was measured using a mercury thermometer calibrated at the Bureau of Standards to 0.01°. Two centrifugal pumps circulated bath water around the pressure vessel at a total rate of about 10 gpm. The 22-lb mass of the pressure vessel constituted a large thermal inertia against small temperature changes so that satisfactory isothermal conditions were achieved.

Working surfaces were cleaned before use by a warm (heat of mixing) 2/1 mixture of 98% H₂SO₄ and 36% HNO₃. The capillaries were immersed in the acid for 16

hr and the pressure vessel was completely filled with the acid for the same time. Both were then rinsed ten times. Each rinse consisted of a complete filling with distilled water followed by complete emptying. The capillaries were emptied by wicking onto a mechanically pulped paper toweling which gave no evidence of back-contamination. In preliminary experiments, significant contamination was encountered from a presumed vacuum pump oil aerosol in the laboratory air which replaced the water during the emptying phase of each rinse. Accordingly, the replacement air was passed through an activated charcoal bed, and this eliminated the contamination.

After rinsing, the component parts were either filled with H_2S saturated distilled water and assembled if the succeeding measurement was to be $\text{H}_2\text{O}_{(l)}\text{-H}_2\text{S}_{(v)}$, or dried thoroughly with noncontaminating nitrogen and assembled if the succeeding measurement was to be $\text{H}_2\text{S}_{(l)}\text{-H}_2\text{S}_{(v)}$.

The cleaned capillaries were calibrated in six liquids, acetone, hexane, benzene, toluene, chloroform, and water, against air by determining the capillary constant C for the equation

$$\gamma = C(\rho_l - \rho_v) \left(\Delta h - \frac{r_2}{3} + \frac{r_1}{3} \right) \quad (1)$$

where γ is surface tension in dynes/cm, ρ_l and ρ_v are the densities of liquid and vapor phases, respectively, in grams/cm³, Δh is the difference between heights of liquid columns in the capillaries in cm, and r_1 and r_2 are the capillary radii in cm. The average value of C for all six liquids was 22.94 with a standard deviation of 0.17. Water-air surface tensions calculated in this way are slightly higher than published values demonstrating that the laboratory distilled water source was free of surface-contaminating agents.

Distilled water for use in H_2S measurements was degassed in a Pyrex vessel by boiling. While still boiling the liquid was transferred to a separate Pyrex storage vessel maintained under 1 atm of H_2S pressure by a continuous gas bubbler system leading to a flare. After the water cooled at room temperature under the H_2S atmosphere it was ready for experimental use.

The H_2S was Linde CP grade of 99.6% purity. This H_2S content was confirmed by gas chromatography on the gas actually used. CO_2 was the major contaminant. Since H_2S is stored as a liquid, a vapor take-off from the cylinder causes CO_2 enrichment resulting in variable gas composition. To maintain the rated purity it was necessary to remove H_2S from the storage cylinder as a liquid, then vaporize the entire sample removed. During the measurements on liquid H_2S , it was noted that the liquid, initially clear and colorless, slowly developed a light brown color in the experimental chamber. The cause of this change, which did not affect the surface tension readings, is unknown. (It is possible that it resulted from the formation of some colloidal sulfur, due to traces of residual oxygen.)

Pressure measurements were made using an Ashcroft 1082 test gauge with 0-300 psi range, 1 psi divisions, and accuracy 0.25% of full scale. Capillary column height measurements were made to 0.0001 cm using a Gaertner traveling microscope. Liquid and vapor densities given by Galley, *et al.*,⁵ based on the experimental data of Janik⁶ and Reamer, *et al.*,⁷ were used.

Surface tension values are estimated accurate to ± 0.25 dyn/cm.

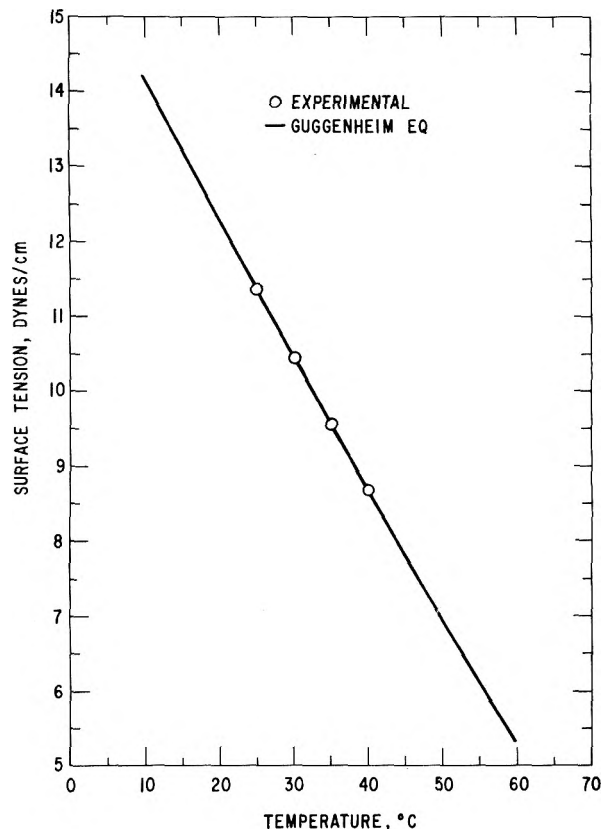


Figure 1. Surface tension of liquid H_2S against its saturated vapor.

Results

Surface Tension of Liquid Hydrogen Sulfide Against Its Vapor. Liquid H_2S was charged directly to the experimental vessel without a phase change. Surface tension values for liquid H_2S against its saturated vapor for temperatures from 25 to 40° are shown in Figure 1.

Surface Tension of Water Against Hydrogen Sulfide Vapor. The system was equilibrated at 1 atm H_2S pressure before each set of readings. After each increase in pressure the capillary rise equilibrated within 1 min, however, the liquid columns in the capillaries required weeks to equilibrate to the new density. Consequently measurements at pressures above 1 atm were made in rapid succession until the pressure excursion was completed. Then the 1 atm liquid density was used in eq 1 at all pressures. It was assumed that the surface tension was fully determined by the composition of a thin layer of liquid immediately below the surface and that when this thin layer was in equilibrium with the gas phase that equilibrium values of the surface tension were obtained. After completion of a pressure excursion the initial capillary rise value was reproduced upon reequilibrating the water surface at 1 atm for 60 hr.

Surface tensions of water against its own vapor were estimated by correcting the accepted values against air at 1 atm to zero pressure using the slope of the nitrogen pressure data measured by Slowinski, *et al.*,² and these values were used for zero pressure of H_2S . The experimental results are given in Figure 2. At each temperature a straight line is drawn through the zero pressure surface tension using the slope calculated by a least-squares fit of the experimental data taken in the presence of H_2S . The resul-

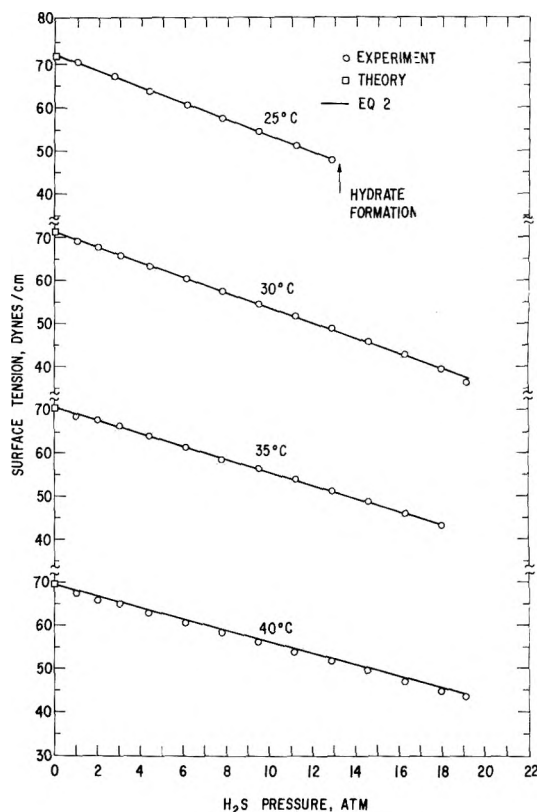


Figure 2. Surface tension of water saturated with H₂S against H₂S vapor.

tant fit is within experimental error at all temperatures. Values for the surface tensions indicated by the lines in Figure 2 can be calculated within 0.01 dyn/cm using

$$\gamma = 75.828 - 0.145t - 2.6 \times 10^{-4}t^2 + 6.38997P - 0.821572Pt + 2.62702 \times 10^{-2}Pt^2 - 2.6396 \times 10^{-4}Pt^3 \quad (2)$$

where γ is in dynes/cm, P is in atmospheres of H₂S, and t is in degrees centigrade.

At 25° and 12.25 atm a crystalline solid hydrate was observed. This temperature is about 0.5° above the position of the hydrate phase line at this pressure as derived from the data of Selleck, *et al.*⁸ Hydrate formation in the capillaries was accompanied by a large decrease in column height. By suitable repeated manipulation of the degree of supersaturation solid hydrate was formed on the inner walls of both capillaries in layers so thin that no change in diameter could be detected by the microscope. Capillary rise measured against the hydrate covered surface Δh_h compared with that against glass Δh_g permits an estimate of the contact angle between H₂S saturated water and the H₂S hydrate.

$$\cos \theta = \left(\Delta h_h - \frac{r_2}{3} + \frac{r_1}{3} \right) / \left(\Delta h_g - \frac{r_2}{3} + \frac{r_1}{3} \right) \quad (3)$$

The observations fell within the limits $62^\circ < \theta < 69^\circ$. Hydrate formation on the outside of the large capillary at the immersion line limited visibility and prevented a closer estimate.

Discussion

Surface Tension of Liquid H₂S. Prior determinations by Devyatikh, *et al.*⁹ appear to be limited to temperatures below the normal boiling point (-60°). The Guggenheim

equation¹⁰

$$\gamma = \gamma_0 \left(1 - \frac{T}{T_c} \right)^{11/9} \quad (4)$$

fits our data precisely, using the critical temperature $T_c = 373.6^\circ\text{K}$, and $\gamma_0 = 80$, as shown in Figure 1. Galley, *et al.*,⁵ estimated $\gamma_0 = 79.02$ from the critical constants.

Liquid H₂S surface tensions calculated from the parachor value of 80.1 recommended by Quayle¹¹ were about 20% smaller than the experimental values.

Surface Tension of Water Against H₂S Vapor. The effect of compressed gases on the surface tension of liquids has not received extensive study. Slowinski, *et al.*,^{2a} who measured the pressure effect for six gases other than H₂S interpreted their results in terms of the approximate Gibbs equation

$$\Gamma_2^{(1)} = - \frac{P}{RT} \frac{d\gamma}{dP} \quad (5)$$

They observed substantially linear variations of surface tension with pressure, as we have for H₂S. They pointed out that eq 5 then implies the surface excess of the gas $\Gamma_2^{(1)}$ is proportional to pressure. We have estimated in columns 1-5 of Table I the maximum values of $\Gamma_2^{(1)}$ from eq 5 evaluated at the pressure corresponding to the first pressure induced phase change, on the premise that $\Gamma_2^{(1)}$ cannot continue to increase beyond such a point. By applying the monolayer assumption (*i.e.*, $A = 1/\Gamma_2^{(1)}$), the surface area per adsorbed molecule was estimated in column 5. These estimated areas are close to molecular areas in close-packed monolayers and fall in the sequence expected for the gases studied. Clearly these calculations are only semiquantitative because of the long extrapolations required to extend the hydrogen, nitrogen, and methane data to a phase change point, the ideal gas approximation implicit in eq 5, and the observable small deviations from linearity in the data for some gases. In addition $\Gamma_2^{(1)}$ is less than the surface concentration of adsorbed gas by the bulk concentration of dissolved gas although the latter contribution is negligible in the cases treated here.

Both Masterton, Bianchi, and Slowinski^{2b} and Hough, Wood, and Rzasal¹² had concluded from similar analyses of their data that maximum surface excesses approximated monolayer coverage in nitrogen-, methane-, and argon-water systems. The experimental results of these two studies (ref 2 and 12) are in qualitative agreement for the systems and pressure range covered in both; at higher pressures, however, the experimental artifacts observed by Hough, *et al.*, make any conclusions doubtful.

Ericksson¹³ has analyzed the data of Slowinski, *et al.*,^{2a} in thermodynamic terms. He concluded that a monolayer model, with adsorbed gas molecule molecular areas similar to those observed in adsorption studies on solids, adequately fitted the data, but he did not consider the question of attainment of saturation adsorption.

Surface tension measurements on dilute solutions are generally analyzed by another approximate Gibbs equation

$$\Gamma_2^{(1)} = - \frac{1}{RT} \frac{d\gamma}{d \ln N_2} \quad (6)$$

where N_2 is the mole fraction of gas dissolved in the liquid. Equation 6 is equivalent to eq 5 when Henry's law is obeyed. Since the more soluble gases CO₂ and H₂S do de-

TABLE I: Surface Excess of Pressurized Gases at Water Surfaces^e

Gas	T, °C	$-d\gamma/dP$, erg/cm ² /atm	Limiting pressure, atm	Max $\Gamma_2^{(1)}/10^{14}$, molecules/cm ² /10 ¹⁴	Area per molecule, Å ²	Max $\Gamma_2^{(1)}$ (Figure 3), molecules/cm ²
H ₂	25	0.016	9200 ^b	35	2.8	
N ₂	25	0.068	1762 ^c	29	3.4	
CH ₄	25	0.106 ^d	432 ^c	11.1	9.0	
CO ₂	25	0.71	63.5 ^d	11.0	9.1	8.8 × 10 ¹⁴
C ₂ H ₆	25	0.49	41 ^d	4.9	20.4	
H ₂ S	25	1.86	13.7 ^c	6.2	16.1	4.9 × 10 ¹⁴
	30	1.74	22.3 ^d	9.4	10.6	
	35	1.50	25.1 ^d	9.1	11.0	
	40	1.33	28.1 ^d	9.1	11.0	5.1 × 10 ¹⁴

^a Slope at highest experimental pressure. ^b Formation of ice VI, P. W. Bridgeman, *J. Franklin Inst.*, **177**, 315 (1914). ^c Hydrate formation; N₂ and CH₄, D. R. Marshall, S. Saito, and R. Kobayashi, *AIChE J.*, **10**, 202 (1964); H₂S, ref 5 and 16. ^d Liquefaction: CO₂ and C₂H₆; S. S. Byk and V. I. Fomina, *Russ. Chem. Rev.*, **37**, 469 (1968). CO₂: "Handbook of Chemistry and Physics," 44th ed., Chemical Rubber Publishing Co., Cleveland, Ohio, p 2428. C₂H₆; D. R. Stull, *Ind. Eng. Chem.*, **39**, 517 (1947). H₂S; ref 5. ^e Surface tension data for H₂S, present work; all others, ref 2a.

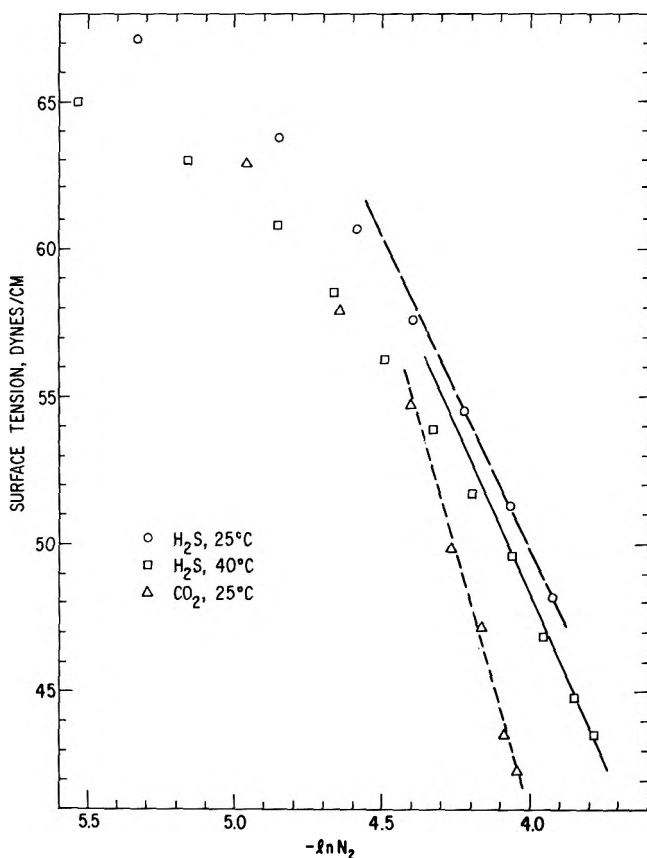


Figure 3. Surface tension of water as a function of mole fraction of gas in solution, illustrating the constant limiting values of $-d\gamma/d \ln N_2$. The CO₂ data are from ref 2a.

viate from Henry's law it is of interest to compare results based on eq 5 and 6.

Solubility data for H₂S in water have been obtained by Wright and Maass¹⁴ and Clarke and Glew¹⁵ at low pressures, and by Selleck, *et al.*,⁸ at higher pressures. While doubt has been expressed about some of the data,^{5,15} and extrapolation appears uncertain, we have extrapolated the data of Wright and Maass¹⁴ up to 5 atm, and used the equation fitted by Burgess and Germann¹⁶ to the Selleck, *et al.*,⁸ results to estimate solubilities at higher pressures. Figure 3 shows our surface tension values at 25 and 40° plotted against the logarithm of H₂S mole fraction in solution. Also shown are the data of Slowinski, *et al.*,^{2a} for the surface tension of water in the presence of CO₂, using

solubilities given by Stewart and Munjal.¹⁷ For pressures above 45 atm, their solubility data have been extrapolated by fitting an equation of the form suggested by Zel'venskii¹⁸

$$S = 0.1416P - 1.127 \times 10^{-3}P^2$$

for solubility in grams of CO₂ per 100 grams of H₂O and P in atm.

As the straight lines in Figure 3 indicate, in all three cases the surface excess appears to reach a constant maximum value at pressures above about half the phase change pressure. These constant maximum $\Gamma_2^{(1)}$ values (column 7 of Table I) are consistent with essentially close-packed gas molecules in a surface monolayer. For H₂S, compare the molecular area of 20 Å² (monolayer assumption) with the estimate of 17–17.5 Å² based on the $\frac{2}{3}$ power of the molecular volume obtained from the liquid density at 25–40° given in ref 6.

In summary, when the available data are analyzed by eq 5 one finds approximately a close-packed monolayer of gas adsorbed on the liquid surface at the gas pressure corresponding to the first pressure induced phase change. By eq 6 one finds that CO₂ and H₂S reach the close-packed adsorbed monolayer state at pressures considerably lower than the phase change pressure. Surface tension variations in other systems may be estimated by assuming a surface excess corresponding to monolayer coverage at phase change pressure. Conversely the phase change pressure may be estimated if the surface tension has been measured.

There is no adequate molecular theory for surface tensions of aqueous solutions to guide an extended analysis of the measurements. Attempts to calculate solution surface tensions from the values for H₂O and H₂S using the mole fraction average or several lattice-theory equations^{19–21} were unsuccessful.

Acknowledgment. We thank Mr. J. A. Murphy for assistance with a portion of the measurements.

References and Notes

- (1) W. P. Bebbington and V. R. Thayer, *Chem. Eng. Progr.*, **55**, (No. 9), 70 (1959).
- (2) (a) E. J. Slowinski, Jr., E. E. Gates, and C. E. Waring, *J. Phys. Chem.*, **61**, 808 (1957); (b) W. L. Masterton, J. Bianchi, and E. J. Slowinski, Jr., *J. Phys. Chem.*, **67**, 615 (1963).
- (3) B. Tamamushi, *Bull. Chem. Soc. Jap.*, **1**, 173 (1926).
- (4) G. J. Heuer, Ph.D. Dissertation, University of Texas, 1957; *Diss. Abstr.*, **17**, 2558 (1958).
- (5) M. R. Galley, A. I. Miller, J. F. Atherley, and M. Mohn, AECL-4255, Chalk River Nuclear Laboratories, 1972.

- (6) J. Janik, *Acta Phys. Polon.*, **23**, 487 (1963).
 (7) H. H. Reamer, B. H. Sage, and W. N. Lacey, *Ind. Eng. Chem.*, **42**, 140 (1950).
 (8) F. T. Selleck, L. T. Carmichael, and B. H. Sage, *Ind. Eng. Chem.*, **44**, 2219 (1952).
 (9) G. G. Devyatykh, A. D. Zorin, and I. V. Runovskaya, *Dokl Akad. Nauk SSSR*, **188**, 1082 (1969).
 (10) E. A. Guggenheim, *J. Chem. Phys.*, **13**, 253 (1945).
 (11) O. R. Quayle, *Chem. Rev.*, **53**, 439 (1953).
 (12) E. W. Hough, B. B. Wood, and M. J. Rzasas, *J. Phys. Chem.*, **56**, 996 (1952).
 (13) J. C. Ericksson, *Acta Chem. Scand.*, **16**, 2199 (1962).
 (14) R. H. Wright and O. Maass, *Can. J. Res.*, **6**, 94 (1932).
 (15) E. C. W. Clarke and D. N. Glew, *Can. J. Chem.*, **49**, 691 (1971).
 (16) M. P. Burgess and R. P. Germann, *AIChE J.*, **15**, 272 (1969).
 (17) P. B. Stewart and P. Munjal, *J. Chem. Eng. Data*, **15**, 67 (1970).
 (18) Y. D. Zel'venskii, *J. Chem. Ind. (USSR)*, **14**, 1250 (1937).
 (19) J. W. Belton and M. G. Evans, *Trans. Faraday Soc.*, **41**, 1 (1945).
 (20) I. Prigogine and J. Marechal, *J. Colloid Sci.*, **7**, 122 (1952).
 (21) G. L. Gaines, Jr., *Trans. Faraday Soc.*, **65**, 2320 (1969).

Thermochemistry of the Bromination of Carbon Tetrachloride and the Heat of Formation of Carbon Tetrachloride

G. D. Mendenhall,¹ D. M. Golden, and S. W. Benson*

Department of Thermochemistry and Chemical Kinetics, Stanford Research Institute, Menlo Park, California 94025
 (Received May 29, 1973)

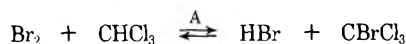
At 560°K the equilibrium constant for the reaction $\text{Br}_2 + \text{CCl}_4 \rightleftharpoons \text{BrCl} + \text{CBrCl}_3$ was determined as 0.0046 ± 0.001 by combined optical and chromatographic techniques. From this result and literature data we calculate the heat of formation difference $\Delta H_f^\circ(\text{CCl}_4, \text{g}) - \Delta H_f^\circ(\text{CHCl}_3, \text{g}) = 2.27 \pm 0.3$ kcal/mol at 298°, independent of calorimetry. Based on $\Delta H_f^\circ(\text{CHCl}_3, \text{g}) = -24.66 \pm 0.3$ kcal/mol, we obtain $\Delta H_f^\circ(\text{CCl}_4, \text{g}) = -22.4 \pm 0.4$ kcal/mol, a higher value than obtained from many earlier studies. The $\text{CCl}_3\text{-Cl}$ bond strength is estimated as 70.4 ± 1 kcal/mol.

Introduction

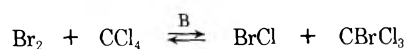
Values for the heat of formation of CCl_4 in the literature encompass an unfortunately wide range. Cox and Pilcher^{2a} and Stull, Westrum, and Sinke^{2b} have combined a number of calorimetric experiments with newer data and arrived at $\Delta H_f^\circ(298)(\text{CCl}_4, \text{gas}) = -25.2 \pm 1.5$ and -24.0 kcal/mol, respectively. Many of the early values depended on $\Delta H_f^\circ(\text{CHCl}_3)$.

Hu and Sinke³ recently reported results of rotating bomb calorimetry which lead to an assigned $\Delta H_f^\circ(\text{CCl}_4, \text{g}) = -22.9 \pm 0.5$ kcal/mol.⁴ Lord and Pritchard,⁵ however, arrived at a value of -27.4 kcal/mol from an equilibrium study of COCl_2 , CCl_4 , and CO_2 in the presence of excess Cl_2 . Their determination required a rather elaborate analytical procedure.

Sullivan and Davidson⁶ accurately measured the equilibrium constant for the reaction



and the thermochemistry of the system has been evaluated by Benson.⁷ We can estimate the heat of formation difference between CHCl_3 and CCl_4 from K_A and the equilibrium constant for



From a choice of $\Delta H_f^\circ(\text{CHCl}_3, \text{g})$ one obtains a precisely related $\Delta H_f^\circ(\text{CCl}_4)$.

Experimental Section

The spectrophotometric procedure and apparatus (a modified Cary Model 14) has been described previously.⁸

The Br_2 partial pressure was determined from the optical densities at 550 and 570 nm, while the OD (340 nm) gave the BrCl pressure after subtracting out the contribution from Br_2 at this wavelength. Mixtures of Cl_2 and Br_2 were added to the cell to obtain $\alpha \equiv P(\text{BrCl Torr})/\text{OD}$ (340 nm). In this calibration and in some of the reaction runs a correction was made for the presence of free Cl_2 from the equilibrium $2\text{BrCl} \rightleftharpoons \text{Br}_2 + \text{Cl}_2$, which has a value of 0.375 at 560°K.⁴

At the partial pressures of our experiments, pressure-independent α (λ nm) were Br_2 : 64.5 (550), 35.2 (570); BrCl : 48.6 (340); Cl_2 : 49.1 (340); CBrCl_3 : 174.4 (300). We did not relate these to published values because our instrument slit width varied over a wide range.

The corrosive nature of the halogens made special handling necessary. Bromine (and probably Cl_2) reacted with hot silicone grease, so all stopcocks in direct contact with the halogens were unheated and were lubricated with a silica gel-halocarbon mixture.⁹

The ratio $\text{CBrCl}_3/\text{CCl}_4$ was determined directly by condensing out the reaction mixture at -196° followed by vpc analysis by peak height ratio (F & M Model 720, thermal conductivity detector, 2 μl samples on a 10 ft \times 0.25 in. column of 20% di(2-ethylhexyl) sebacate on 60-80 m Chromasorb at 140°). Mixtures of known composition of the two halocarbons were injected for calibration, and it was shown that added Br_2 or Cl_2 did not effect the ratios from these standard mixtures. The partial pressures were obtained from the ratio and the relation

$$P^e(\text{CBrCl}_3) + P^e(\text{CCl}_4) = P^0(\text{CCl}_4)$$

The analytical procedure was tested by adding known pressure of CBrCl_3 and CCl_4 to the cell, condensing out as

TABLE I: Equilibrium Constants for the Reaction $\text{CCl}_4 + \text{Br}_2 \rightleftharpoons \text{CBrCl}_3 + \text{BrCl}$

Run	P^0 , Torr		P^e , Torr		Temp, °C (time, hr)	$\Sigma \text{Br}^e / \Sigma \text{Br}^{0a}$	K^e
1	CCl_4	57	53.7		(15)	1.03	0.0064
	Br_2	25	23		284 ± 1		
2	CCl_4	55	52.6		(17.5)	1.00	0.0045
	Br_2	20.5	18.3		285 ± 1		
			CBrCl_3	3.3			
			BrCl	2.4			
3	CCl_4	53.5	51.4		(8.5)	1.04	0.0045
	Br_2	23.4	22		287 ± 1		
			CBrCl_3	2.1			
			BrCl	2.4			
4	CBrCl_3	32	2.6		(13.5)	1.02	0.0054
	Cl_2	17	CCl_4	29.4	285 ± 1		
			Br_2	15.6			
			BrCl	0.95			
5	CCl_4	48.7	47.8		(41.5)	0.92	0.0038
	Br_2	4.8	3.55		287 ± 1		
			CBrCl_3	0.88			
			BrCl	0.73			
6	CCl_4	14.5	12.9		(18)	1.04	0.0032
	Br_2	46	46.5		287 ± 1		
			CBrCl_3	1.6			
			BrCl	1.2			
7	CCl_4	36.1	36.3		287	Av	0.0046 ± 0.001
	CBrCl_3	0.87	0.74		(22.5)		
8	CCl_4	44.7	44.4		287		
	CBrCl_3	2.8	3.1		(1.5)		

^a Equilibrium Br concentration/initial Br concentration calculated as Br.

TABLE II: Thermodynamic Properties of Species in Equilibria A and B^a

	$\Delta H_f^\circ(298^\circ)$	$S^\circ(298^\circ)$	$C_p(298^\circ)$	$C_p(400^\circ)$	$C_p(500^\circ)$	$C_p(600^\circ)$
Br_2^b	7.387	58.647	8.62	8.78	8.86	8.91
BrCl^b	3.50	57.337	8.36	8.61	8.74	8.83
HBr^b	-8.66	47.44	6.96	6.98	7.03	7.14
CHCl_3	-24.66 ± 0.3^b	70.66 ^c	15.71 ^c	17.83 ^c	19.34 ^c	20.44 ^c
CCl_4	-22.4 ± 0.4^d	74.12 ^c	20.02 ^c	22.04 ^c	23.28 ^c	24.07 ^c
CBrCl_3	-10.0 ± 0.3^d	79.8 ^e	20.42 ^f	22.25 ^f	23.40 ^f	24.00 ^f

^a Gas phase. ΔH_f° in kcal/mol, S° in gibbs/mol. ^b Reference 4. ^c Reference 2a. ^d This work. ^e Reference 7. ^f E. Gelles and K. S. Pitzer, *J. Amer. Chem. Soc.*, **75**, 5259 (1953).

before, and analyzing (Table I, runs 7 and 8). Mixtures of Br_2 and Cl_2 and of Br_2 , CCl_4 , and excess Cl_2 (and CBrCl_3 alone at 300 nm) were shown to undergo no significant change in OD at the three wavelengths tested under reaction conditions.

No significant peaks were seen in the vpc trace of the equilibrated reaction mixture other than those of CBrCl_3 and CCl_4 . (The halogens were probably destroyed on the column.) With Br_2 and CCl_4 mixtures above 360° , three additional peaks of longer retention times did appear successively in the vpc trace, and their intensities increased with reaction time. These were probably the polybromo products from CCl_4 .

Bromine (Mallinckrodt), CCl_4 (Mallinckrodt), and CBrCl_3 (Matheson Coleman and Bell) were of reagent grade and were degassed before use. CCl_4 was stored over molecular sieve (Linde 4A). About 20% of each Br_2 sample was distilled off to remove Cl_2 and other impurities. Chlorine (Matheson) was added to the vacuum system,

condensed out at -196° , and degassed several times before use.

Results and Discussion

Good agreement in K_{eq} values was found in six runs starting from both directions, and with final $\text{CCl}_4(\text{Br}_2)$ pressures covering a 4(13)-fold range (Table I). The error in the individual K 's was about ± 0.0020 , so all of them overlap the average. The error in K_{av} was assigned generously as ± 0.001 ; the standard deviation error is about half this.

Two internal checks are present in the data. Except for run 4, we expect $P^e(\text{BrCl}) = P^e(\text{CBrCl}_3)$, and this does obtain within error limits. The bromine balance at equilibrium was generally 2-4% too high. The delay in mixing reactants in the narrow inlet tube partly accounts for the discrepancy in some runs, but the errors are small and we neglected them.

For K_{av} we calculate

$$\Delta G^\circ(559^\circ\text{K}) = -RT \ln K_{av} = 5.98 \pm 0.3 \text{ kcal/mol}$$

$$\begin{aligned} \Delta G_B^\circ(559^\circ\text{K}) &= \Delta H^\circ(298) + \\ &\Delta \bar{C}_p(559 - 298)10^{-3} - 0.559[\Delta S^\circ(298) + \\ &\Delta \bar{C}_p \ln(559/298)] \cong \Delta H^\circ(298) - 0.559\Delta S^\circ(298) \end{aligned}$$

(Since $\Delta \bar{C}_p \sim$ only 0.03 gibbs/mol)

$$\begin{aligned} \Delta H_B^\circ(298^\circ\text{K}) &= 5.98 + 0.599\Delta S^\circ(298) \\ &= 8.84 \pm 0.3 \text{ kcal/mol} \end{aligned}$$

$$\Delta G_B^\circ(298^\circ\text{K}) = 7.15 \pm 0.3 \text{ kcal/mol}$$

An exactly similar treatment starting from Sullivan and Davidson's $K_A(442^\circ\text{K}) = 1.94 \pm 0.19$ gives

$$\Delta H_A^\circ(298^\circ\text{K}) = -1.41 \pm 0.1 \text{ kcal/mol}$$

$$\Delta G_A^\circ(298^\circ\text{K}) = -0.79 \pm 0.1 \text{ kcal/mol}$$

where we assigned $\Delta \bar{C}_p = 2.46$ gibbs/mol from 298 to 442°K. (The value of $\Delta H_A^\circ(298^\circ)$ calculated in ref 7 has an error of 0.6 kcal/mol.) It is easy to show that

$$\begin{aligned} \Delta H_A - \Delta H_B &= \Delta H_f^\circ(\text{HBr}) - \Delta H_f^\circ(\text{CHCl}_3) - \\ &\Delta H_f^\circ(\text{BrCl}) + \Delta H_f^\circ(\text{CCl}_4) \end{aligned}$$

therefore

$$\Delta H_f^\circ(\text{CCl}_4) - \Delta H_f^\circ(\text{CHCl}_3) = \Delta H_A - \Delta H_B -$$

$$\Delta H_f^\circ(\text{HBr}) + \Delta H_f^\circ(\text{BrCl}) = 2.27 \pm$$

$$0.3 \text{ kcal/mol at } 298^\circ$$

If $\Delta H_f^\circ(\text{CHCl}_3) = -24.66 \pm 0.3$ kcal/mol, the value derived⁴ from Hu and Sinke's data,³ then $\Delta H_f^\circ(\text{CCl}_4) = -22.4 \pm 0.4$ kcal/mol, in excellent agreement with the value of -22.9 ± 0.3 kcal/mol obtained by the same authors.^{3,4}

With the newer chloroform data and the correct ΔH_A , we obtain $\Delta H_f^\circ(\text{CBrCl}_3, 298^\circ) = -10.0 \pm 0.3$ kcal/mol,

and $\Delta H_f^\circ(\cdot\text{CCl}_3) = 19.0 \pm 1$ kcal/mol from Benson's analysis.⁷

We also find

$$\text{DH}^\circ(\text{CCl}_3\text{-Cl}) = 70.4 \pm 1 \text{ kcal/mol}$$

(DH° = dissociation enthalpy, 298°K)

$$\text{DH}^\circ(\text{CCl}_3\text{-H}) = 52.1 + 19 + 24.66 =$$

$$95.8 \pm 1 \text{ kcal/mol}$$

$$\text{DH}^\circ(\text{CCl}_3\text{-Br}) = 19 + 26.740 + 10.0 =$$

$$55.7 \pm 1 \text{ kcal/mol}$$

The latter two bond strengths are not changed from earlier estimates.⁷

The heats of formation of a number of halomethanes are also based on $\Delta H_f^\circ(\text{CCl}_4)$. Recently this situation was reviewed by Shaw,¹⁰ who assigned a number of heats of formation assuming $\Delta H_f^\circ(\text{CCl}_4) = -26.0$ kcal/mol. This value was chosen partly for self-consistency with equilibrium results, and we have not attempted to reevaluate his work.

References and Notes

- (1) Postdoctoral Research Associate.
- (2) (a) J. D. Cox and G. Pilcher, "Thermochemistry of Organic and Organometallic Compounds," Academic Press, New York, N. Y., 1970; (b) D. R. Stull, E. F. Westrum, and G. C. Sinke, "The Chemical Thermodynamics of Organic Compounds," Wiley, New York, N. Y., 1969.
- (3) A. T. Hu and G. C. Sinke, *J. Chem. Thermodyn.*, **1**, 507 (1969).
- (4) D. P. Stull, Ed., "JANAF Thermochemical Tables," Dow Chemical Company, Midland, Mich., 1963.
- (5) A. Lord and H. O. Pritchard, *J. Chem. Thermodyn.*, **1**, 495 (1969).
- (6) J. H. Sullivan and N. Davidson, *J. Chem. Phys.*, **19**, 143 (1951).
- (7) S. W. Benson, *J. Chem. Phys.*, **43**, 2044 (1965).
- (8) D. M. Golden, R. Walsh, and S. W. Benson, *J. Amer. Chem. Soc.*, **87**, 4053 (1965).
- (9) 25-5S grease from R. S. Hughes Co.
- (10) R. Shaw in S. Patai's, "Chemistry of the Carbon-Hydrogen Bond," Wiley, New York, N. Y., 1973, Chapter 16.

COMMUNICATIONS TO THE EDITOR

Definition of Volume Flow in the Kedem-Katchalsky Formulation of Electroosmosis

Publication costs assisted by the U.S. Public Health Service

Sir: We should like to point out a possible source of confusion in certain applications of the important and widely used equations of membrane transport formulated by Kedem and Katchalsky.¹⁻³ These equations, derived on the basis of nonequilibrium thermodynamics, describe an isothermal membrane system in which three processes may take place *within the membrane*: flow of water (J_w), flow of cations (J_1), and flow of anions (J_2). The conjugate forces are the electrochemical potential differences of the three species ($\Delta\mu_w$, $\Delta\tilde{\mu}_1$, $\Delta\tilde{\mu}_2$). The corresponding dissipation function is

$$\Phi = J_w\Delta\mu_w + J_1\Delta\tilde{\mu}_1 + J_2\Delta\tilde{\mu}_2 \quad (1)$$

All flows in this and subsequent expressions are considered positive if they proceed from side I to side II, the forces being defined as $\Delta X = X_I - X_{II}$. An alternative description of the same system¹ can be obtained by transforming this dissipation function into one involving the salt flux (J_s) and the electric current (I), the conjugate forces being the chemical potential difference of the salt ($\Delta\mu_s$) and the electromotive force (E)

$$\Phi = J_w\Delta\mu_w + J_s\Delta\mu_s + IE \quad (2)$$

In deriving eq 2 it is assumed that electrodes reversible to one of the ions are used both in passing electric current and in measuring electrical potential difference. Under the assumption that the electrodes are reversible to the anion, the flow of salt is identified with the cation flux according to the relation

$$J_s = J_1/\nu_1 \quad (3)$$

where ν_1 is the stoichiometric coefficient of the cation in the dissociation of the salt. Equation 2 is more useful than eq 1 in that its flows and forces are more readily measured. A still more useful form¹ is obtained for moderately dilute solutions by replacing water flow by volume flow (J_v)

$$\Phi = J_v(\Delta p - \Delta\pi) + J_s\Delta\mu_s^c + IE \quad (4)$$

Here Δp and $\Delta\pi$ represent hydrostatic and osmotic pressure differences, respectively, and $\Delta\mu_s^c$ represents the concentration-dependent part of $\Delta\mu_s$. In these transformations the following definitions, *inter alia*, were used

$$I = (z_1J_1 + z_2J_2)F \quad (5)$$

$$J_v = \bar{V}_sJ_s + \bar{V}_wJ_w \quad (6)$$

F is the faraday, z the charge number of an ion, and \bar{V} a partial molar volume. The electroneutrality condition requires that

$$\nu_1z_1 + \nu_2z_2 = 0 \quad (7)$$

It will be apparent that the flows in eq 1 represent material transport across the membrane. However, in eq 2 this is not the case unless $I = 0$. J_s is a virtual transfer of salt

which may include a component due to processes at the electrodes. Similarly volume flow, as defined in eq 6, will be a virtual flow under conditions of current passage, in that it contains J_s . Neglecting second-order effects due to changes in partial molar volumes, the actual transfer of volume across the membrane exactly equals the volume change observed in each compartment (including the volume change of the electrode), and can be expressed as

$$J_v^{\text{obsd}} = \bar{V}_1J_1 + \bar{V}_2J_2 + \bar{V}_wJ_w \quad (8)$$

If the partial molar volumes of the ions⁴ are assumed additive, then

$$\bar{V}_s = \nu_1\bar{V}_1 + \nu_2\bar{V}_2 \quad (9)$$

and combining eq 3 and 5-9 the following relation between J_v and J_v^{obsd} is obtained

$$J_v = J_v^{\text{obsd}} - \bar{V}_2I/z_2F \quad (10)$$

On the other hand, if volume changes could be measured after removal of electrodes, the flow observed would be equal to J_v .⁵

To take the most common example in which eq 10 may be important, suppose that silver|silver chloride electrodes are used. Again neglecting second-order effects, the volume changes associated with the electrode processes are expressed by the relation

$$\bar{V}_{Ag} + \bar{V}_{Cl} = \bar{V}_{AgCl} \quad (11)$$

Consequently

$$J_v = J_v^{\text{obsd}} + (\bar{V}_{AgCl} - \bar{V}_{Ag})I/F \quad (12)$$

Using the values $\bar{V}_{AgCl} = 25.8 \text{ cm}^3 \text{ mol}^{-1}$, $\bar{V}_{Ag} = 10.3 \text{ cm}^3 \text{ mol}^{-1}$, and $F = 9.65 \times 10^4 \text{ C mol}^{-1}$, we obtain the result that

$$J_v = J_v^{\text{obsd}} + 1.61 \times 10^{-4}I \quad (13)$$

where J_v is usually expressed as cm sec^{-1} and I as A cm^{-2} . Alternatively, the second term on the right-hand side of eq 13 can be expressed as a correction of 15.5 cm^3 per faraday of charge passed. A correction analogous to this (but different in form and intended for a different use) has been made by Mackay and Meares⁶ in calculating the electroosmotic transport of *water* (not volume) across an ideally permselective cation exchange membrane, given the observed volume changes.

The correction term in eq 13 may be important in measuring the electroosmotic coefficients of a membrane. For example, the electroosmotic permeability β is related to the streaming potential by an Onsager reciprocal relation of the form

$$\beta = (J_v/I)_{(\Delta p - \Delta\pi), \Delta\mu_s^c} = -(E/(\Delta p - \Delta\pi))_{\Delta\mu_s^c, I} \quad (14)$$

where the subscripts indicate flows and forces made to vanish. The relationship holds only if the observed volume flow has been corrected as indicated in eq 13. Similarly, in the relation between electroosmotic pressure P_E and streaming current

TABLE I: Difference between Observed and Corrected Volume Flows in Electroosmosis Experiments on Anion Exchange, Cation Exchange, and Charge-Mosaic Membranes^a

Membrane (Active area, cm ²) (Current I, mA/cm ²)	Solution concn. M	J _v ^{obsd} , cm/sec	J _v , cm/sec
Anion exchange	0.1	-9.7 × 10 ⁻⁷	-8.0 × 10 ⁻⁷
(0.094)	0.01	-11.8 × 10 ⁻⁷	-10.1 × 10 ⁻⁷
(1.06)	0.001	-12.4 × 10 ⁻⁷	-10.7 × 10 ⁻⁷
Cation exchange	0.1	+10.8 × 10 ⁻⁷	+12.5 × 10 ⁻⁷
(0.095)	0.01	+13.7 × 10 ⁻⁷	+15.4 × 10 ⁻⁷
(1.05)	0.001	+14.7 × 10 ⁻⁷	+16.3 × 10 ⁻⁷
Mosaic	0.1	+1.3 × 10 ⁻⁷	+3.0 × 10 ⁻⁷
(0.092)	0.01	+1.5 × 10 ⁻⁷	+3.3 × 10 ⁻⁷
(1.08)	0.001	+2.8 × 10 ⁻⁷	+4.6 × 10 ⁻⁷

^a From the data of Weinstein, *et al.*⁸

$$P_E \equiv ((\Delta p - \Delta\pi)/E)_{J_v, \Delta\mu_s^c} = -(I/J_v)_{\Delta\mu_s^c, E} \quad (15)$$

the observed volume flow must be corrected.⁷ Ion exchange membranes of relatively loose structure will tend to have high values of β, and consequently the correction will generally be negligible, but for tight membranes it may be significant.

The correction will be especially important in the study of charge-mosaic membranes, which consist of alternating anion and cation exchange regions. For such membranes β may be nearly zero since the electroosmotic flows through the two types of region are oppositely directed and tend to cancel. Table I contains data from experiments described by Weinstein, *et al.*⁸ on the electroosmotic coefficients of homogeneous and charge-mosaic membranes. Note that J_v is roughly double J_v^{obsd} in the case of the mosaics.

Acknowledgments. This study was supported by the Office of Saline Water (Contract No. 14-30-3145) and the U. S. Public Health Service (Grant No. HL 14322 to the Harvard-MIT Program in Health Sciences and Technology).

References and Notes

- (1) O. Kedem and A. Katchalsky, *Trans. Faraday Soc.*, **59**, 1918 (1963).
- (2) O. Kedem and A. Katchalsky, *Trans. Faraday Soc.*, **59**, 1931 (1963).
- (3) O. Kedem and A. Katchalsky, *Trans. Faraday Soc.*, **59**, 1941 (1963).
- (4) V₁ and V₂ are subject to the same thermodynamic questions of definition as Δμ₁ and Δμ₂.
- (5) Alternatively, the dissipation function could be written in terms of J_v^{obsd}. From eq 4 and 10

$$\Phi = J_v^{obsd}(\Delta p - \Delta\pi) + J_s \Delta\mu_s^c + IE'$$

where E' = E - V₂(Δp - Δπ)/z₂F.

- (6) D. Mackay and P. Meares, *Trans. Faraday Soc.*, **55**, 1221 (1959).
- (7) Three of the Kedem-Katchalsky coefficients (κ, P_E, τ₁) may be measured by the passage of current under conditions of zero volume flow. In practice such determinations are invariably carried out with J_v^{obsd} = 0 though the rigorously correct condition is J_v = 0.
- (8) J. N. Weinstein, B. M. Misra, D. Kalif, and S. R. Caplan, *Desalination*, **12**, 1 (1973).

Stanford University Medical Center
Palo Alto, California

John N. Weinstein

Biophysical Laboratory
Harvard Medical School
Boston, Massachusetts 02115

S. Roy Caplan*

Comments on the Paper by Weinstein and Caplan on the Definition of Volume Flow in the Kedem-Katchalsky Formulism of Electroosmosis

Sir: The correction given by Weinstein and Caplan is clearly justified and I would like to add a small reformulation.

The dissipation function for discontinuous systems is derived by calculation of the entropy changes in the compartments separated by the membrane. In the absence of an electric current, the flows J_i are given by the change of the amount of each species in the compartments, ±dn_i/dt. In order to pass an electric current, electrodes have to be introduced and their entropy changes must be included in the calculation; for the derivation of entropy production in the membrane the electrodes are assumed to be reversible. Mazur and Overbeek¹ emphasized that this leads to the simple form of the dissipation function generally used (eq 1 in Weinstein and Caplan,² and eq 1 in ref 1 therein), with the flows explicitly referring to the number of moles passing through the membrane and not necessarily to the changes of n_i in the solution compartments. Thus our statement that upon introduction of electrodes reversible to ion 2 we may identify the flow of ion 1 with the salt flow is inexact. It should have read J₁/ν₁ is equal to the flow of salt in the absence of electric current, and gives the composition changes in the solutions if current is passed through electrodes reversible to ion 2. In this case

$$-dn_s'/dt = dn_s''/dt = AJ_1/\nu_1$$

(A-membrane area)

Following the inexact definition, we wrote for the volume flow

$$J_v = J_s \bar{V}_s + J_w \bar{V}_w \quad J_s = J_1/\nu_1 \quad (14)$$

instead of the correct expression

$$J_v = J_w \bar{V}_w + J_1 \bar{V}_1 + J_2 \bar{V}_2 \quad (14, \text{cor})$$

counting the total volume of the species passing the membrane.

The corrected expression for J_v gives (with dilute solutions) for the transformed dissipation function

$$\Phi = (J_v - I\bar{V}_2/z_2F)(\Delta p - \Delta\pi) + J_s \Delta\mu_s^c + IE \quad (16, \text{cor})$$

As pointed out by Weinstein and Caplan,² with the other forces as defined here, J_v - I V₂/z₂F, and not J_v, is the flow conjugate to (Δp - Δπ). The correction is small in most cases, but may be very important in some systems.

I would recommend leaving the notation J_v for the total volume flow (J_v^{obsd} in ref 2, J_v according to eq 14, cor here) in accord with the literature and introduce, if necessary, another abbreviation for J_v - I V₂/z₂F.

References and Notes

- (1) P. Mazur and J. T. G. Overbeek, *Recl. Trav. Chim. Pays-Bas*, **70**, 83 (1951).
- (2) J. N. Weinstein and S. R. Caplan, *J. Phys. Chem.*, **77**, 2700 (1973).

Polymer Department
The Weizmann Institute of Science
Rehovot, Israel

O. Kedem

Received February 12, 1973

Received March 5, 1973

Electron Spin Resonance Study of Photoinduced Triplet States from Organic Dye Solutions

Publication costs assisted by the Air Force Materials Laboratory

Sir: The development of tunable organic dye lasers is proving to be a significant advancement in the field of photochemistry.^{1,2} A major difficulty of organic dye laser systems is that quenching of stimulated emission may occur when the singlet state undergoes intersystem crossing to a triplet state. The triplet state of dye molecules is detrimental to laser action because it depletes the population of the singlet lasing level, as well as allowing for the possibility of laser quenching arising from $T \leftarrow T$ absorption.^{3,4} We have undertaken an esr investigation of a number of dyes to determine the factors which affect intersystem crossing to a triplet state and to determine what class or type of dye gives a $\Delta M = \pm 2$ esr signal.

Glazkov, *et al.*,⁵ had looked at concentrated (10^{-2} M) solutions of some xanthene dyes and attributed a $\Delta M = \pm 2$ esr signal to a triplet of dye aggregates and not to the monomer. We have also obtained the esr spectra of these and other dyes in concentrated alcoholic solutions and have found the intensity of the half-field signal to be both concentration and wavelength dependent. A 5×10^{-5} M EPA solution of Rhodamine 6G also gave a signal at 1637 G, however, Selwyn and Steinfeld⁶ found no spectrophotometric evidence for aggregate formation at this concentration of Rhodamine 6G at 77°K in EPA. This shows that the triplet esr signal is due to the monomer rather than an aggregate of the dye.

Besides the xanthene dyes, Crystal Violet and Ethyl (Diquinoline) Red also gave strong esr signals between 1612 and 1637 G. The half-lives and zero-field splitting parameter D^* were measured and are listed in Table I.

Some oxazine dyes were also investigated and Oxazine 1, Cresyl Violet Chloride, Acetate, and Nitrate, and Nile Blue gave no triplet esr signal. No phosphorescence was observed for these oxazine dyes, indicating very little triplet formation and short lifetimes. The chloride and oxalate salts of Malachite Green also gave no triplet esr signal, although phosphorescence was detected. As shown in Table I, Fluorescein gave a signal at 1612 G but Erythrosin B with iodide substituents gave no esr signal and very weak phosphorescence. The lack of an esr signal for the $\Delta M = \pm 2$ transition is most likely due to the heavy atoms in which the triplet lifetime is too short and the steady-state concentration too low to detect a triplet esr signal.

TABLE I: ESR Data from Dye Molecules Giving a Triplet Signal

Dye ^a	$\Delta M = \pm 2$ G	ΔH_{pp} ^b	$t_{1/2}$, ^c sec	D^* , ^d cm ⁻¹
Rosamine	1634	28	0.7	0.0293
Rhodamine B				
Cl ⁻	1626	18	0.5	0.0336
OAc	1627	18	0.5	0.0315
Rhodamine 6G	1637	14	0.8	0.0244
Acridine Red	1628	26	0.7	0.0299
Fluorescein	1612	9	0.6	0.0478
Ethyl (Diquinoline)				
Red	1628	19	0.1	0.0324
Crystal Violet	1636	22	0.2	0.0208

^a The dyes (10^{-3} – 10^{-2} M) in ethanol-methanol (4:1) glass at 77°K were photolyzed in the cavity with an Ostram HBO-200 W mercury lamp. Degassing the sample had little effect on the signal. ^b Line width from peak to peak on derivative. ^c Half-lives were measured from the dark decay of the $\Delta M = \pm 2$ esr transition intensity. ^d Calculated from $D^* = \{3(h\nu)^2/4\} - 3(g\beta H_m)^2\}^{1/2}$ where ν is the klystron frequency and H_m is the field position of the low-field maximum of the $\Delta M = \pm 2$ esr transition derivative spectrum.⁸

Solvent radical signals at $g = 2.00$ were detected in all the dyes studied indicating dye sensitization of the solvent.⁷

As indicated in Table I, the anion has little effect upon the field position and intensity of the triplet signal for Rhodamine B. The anion also had no effect on producing a signal in the Cresyl Violet or Malachite Green cases.

Acknowledgment. The authors would like to acknowledge Dr. H. M. Rosenberg for helpful discussions and Dr. R. N. Steppel for providing purified samples of Cresyl Violet and Rhodamine dyes.

References and Notes

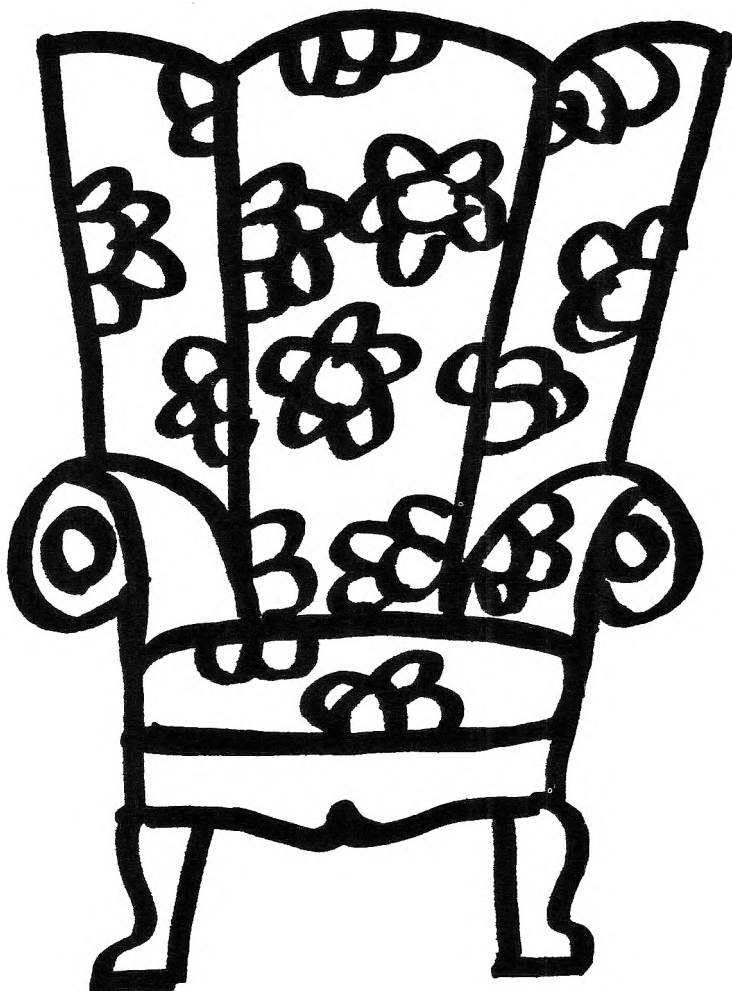
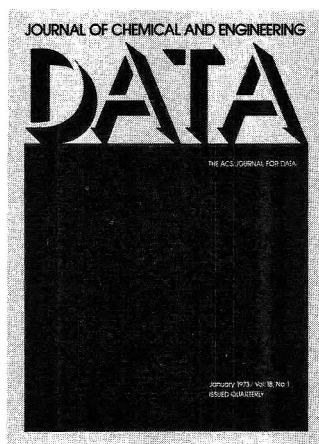
- (1) B. B. Snavely, *Proc. IEEE*, **57**, 1374 (1969).
- (2) K. H. Drexhage, *Laser Focus*, **9**, 35 (1973).
- (3) P. P. Sorokin, J. R. Lankard, V. L. Moruzzi, and E. C. Hammond, *J. Chem. Phys.*, **48**, 4726 (1968).
- (4) W. Schmidt and F. P. Schafer, *Z. Naturforsch.*, **22**, 1563 (1967).
- (5) Y. V. Glazkov, N. I. Zotov, and E. K. Kruglik, *Izv. Akad. Nauk SSR, Ser. Fiz.*, **32**, 1500 (1968).
- (6) J. E. Selwyn and J. I. Steinfeld, *J. Phys. Chem.*, **76**, 762 (1972).
- (7) S. Siegal and K. Eisenthal, *J. Chem. Phys.*, **42**, 2494 (1965).
- (8) C. Thompson, *J. Chem. Phys.*, **41**, 1 (1964).

Air Force Materials Laboratory
AFML/LPH
Wright-Patterson Air Force Base
Ohio 45433

F. R. Antonucci*
L. G. Tolley

Received August 10, 1973

**You
don't have
to search
the archives
for data . . .**



. . . because THE JOURNAL OF CHEMICAL AND ENGINEERING DATA will bring precise, reliable, useful technical information right to your fingertips quarterly! With a year's subscription, you'll receive a total of over 500 pages of valuable science and engineering data that are especially relevant now in light of today's new instrumentation. The information in JCED includes:

- experimental data relating to pure compounds or mixtures covering a range of states;
- manuscripts based on published experimental information which make tangible contributions through their presentation or which set forth a sound method of prediction of properties as a function of state;

- experimental data which aid in identifying or utilizing new organic or inorganic compounds; and
- papers relating primarily to newly developed or novel synthesis of organic compounds and their properties.

Start to benefit now from this "arm-chair" source of pertinent technical data—with your own personal

subscription to JCED . . . just complete and return the form below . . . get your data without the dust.



. . . another ACS service

**Journal
of Chemical
& Engineering
Data**

**Journal of Chemical & Engineering Data
American Chemical Society**

1155 Sixteenth Street, N.W.
Washington, D.C. 20036

Yes, I would like to receive the JOURNAL OF CHEMICAL & ENGINEERING DATA at the one-year rate checked below:

ACS Member Personal-Use	U.S.	Canada	Latin America	Other Nations
One-Year Rate	<input type="checkbox"/> \$15.00	<input type="checkbox"/> \$18.00	<input type="checkbox"/> \$18.00	<input type="checkbox"/> \$18.50
Nonmember	<input type="checkbox"/> \$45.00	<input type="checkbox"/> \$48.00	<input type="checkbox"/> \$48.00	<input type="checkbox"/> \$48.50
Bill me <input type="checkbox"/>	Bill company <input type="checkbox"/>	Payment enclosed <input type="checkbox"/>		

Name _____

Street _____

Home
Business

City _____

State _____

Zip _____

T-73

wiley

INVESTIGATION OF RATES AND MECHANISMS, Third Edition

Part II

Investigation of Elementary Reaction Steps in Solution and Very Fast Reactions

Edited by **Gordon G. Hammes**, *Cornell University*

Volume VI in *Techniques of Chemistry*, edited by A. Weissberger

Providing the concise information chemists need for application of fast reaction techniques to new problems, this volume, a complete up-dating of the previous edition, brings together recent international advances. It offers a comprehensive description of the modern fast reaction techniques used in studying elementary reactions in solution, the principles underlying the techniques, and illustrative examples of investigations of individual systems.

1973 688 pages \$27.50

GLASS SCIENCE

By **Robert H. Doremus**, *Rensselaer Polytechnic Institute*

A volume in the Wiley Series on the Science and Technology of Materials, edited by J. E. Burke, B. Chalmers, and James A. Krumhansl

Glass Science is an up-to-date, scientific presentation of the formation, structure, and properties of glass. Because it provides a separate discussion of glass structure and then relates it to the various properties of glass, this book is exceptionally valuable for anyone involved in the science of glass.

Treating nearly every topic in a new and original way, *Glass Science* covers both new (static fatigue) and old (molecular structure) research areas.

1973 352 pages \$17.95

ENERGY STRUCTURE AND REACTIVITY:

Proceedings of the 1972 Boulder Summer Research Conference on Theoretical Chemistry

Edited by **Darwin W. Smith** and **Walter B. McRae**, both of *University of Georgia*

Covering the main areas of current interest to researchers in theoretical chemistry, this book includes such topics as Atomic and Molecular Processes; Scattering; Theoretical Models for Chemistry; Semi-Classical Quantum Mechanics and Statistical Exchange; Electron Correlation; Ab Initio Methods; Density Matrices; Discussion: The Status of Many-Body Methods in Chemistry; Atom-Atom Interactions; Excited States and Electron Binding Energies; Large Molecules: Ab Initio Techniques; Discussion: The Status of Large Molecule Quantum Chemistry.

1973 432 pages \$14.95

MOLECULAR WAVE FUNCTIONS AND PROPERTIES:

Tabulated From SCF Calculations in a Gaussian Basis Set

By **Lawrence C. Snyder**, *Bell Telephone Laboratories*, and **Harold Basch**, *Bar Ilan University, Israel*

"The present volume fills a major need by presenting in easy to use tabular format SCF wave functions for 56 different molecules ranging from hydrogen with two electrons to tetrafluoroethylene with 48 electrons. . . . It is expected that this volume will play an important role in molecular quantum chemistry for a number of years to come."

—Lawrence L. Lohr, Jr., *University of Michigan*

1972 432 pages \$14.95

ELECTROKINETIC PHENOMENA

By **Egon Matijevic**, *Clarkson College of Technology*

A volume in the Wiley Series on Surface and Colloid Science, edited by Egon Matijevic

A theoretical and experimental discussion of electrokinetic phenomena, comprehensive in its coverage, this volume contains the most up-to-date information on applications of the phenomena. Chemists will find *Electrokinetic Phenomena* to be an essential reference for any problems of colloid stability.

1973 in press

ORGANIC MOLECULAR PHOTOPHYSICS, Volume 1

Edited by **John B. Birks**, *University of Manchester*

This is the first of two volumes of integrated articles that will provide a comprehensive coverage of organic molecular photophysics.

Contents: Spectroscopy of Aromatic Hydrocarbons. Fluorescence of Aromatic Molecular Vapors. Absorption and Fluorescence of Aromatic Molecules at High Pressures. Radiationless Transitions. Organic Dye Lasers. Triplet-Triplet Absorption Spectra of Organic Molecules. Intramolecular Excimers. Diffusion-Controlled Rate Processes. Electron Photo-Ejection From Aromatic Molecules in Condensed Media. Exciton Interactions in Organic Solids.

1973 592 pages \$37.50

Prices subject to change without notice.

Available at your bookstore or from Dept. 736

WILEY-INTERSCIENCE

A division of **John Wiley & Sons, Inc.**, 605 Third Avenue, New York, N.Y. 10016.

In Canada: 22 Worcester Road, Rexdale, Ontario.

WILEY-INTERSCIENCE, Dept. 736, 605 Third Avenue, New York, N.Y. 10016

Please send me the book(s) I have checked below—

- 0 471 93127-6—**Weissberger**: Investigation of Rates and Mechanisms, Third Edition Part II \$27.50
0 471 21900-2—**Doremus**: Glass Science \$17.95
0 471 80140-2—**Smith/McRae**: Energy Structure and Reactivity \$14.95
0 471 81012-6—**Snyder/Basch**: Molecular Wave Functions and Properties \$14.95
0 471 57636-0—**Matijevic**: Electrokinetic Phenomena
in press
0 471 07415-2—**Birks**: Organic Molecular Photophysics,
V.I. \$37.50

- My check (money order) for \$ _____ is enclosed.
 Please bill me.*

Name _____

Address _____

City _____

State/Zip _____

Please add state and local taxes where applicable. Prices subject to change without notice.

*Restricted to the continental United States.

093 A4241 WI